MICRORNA-215 REGULATES DIFFERENTIATION IN COLORECTAL CANCER STEM CELLS

MATTHEW FLETCHER JONES

New College

A thesis submitted to the Division of Medical Sciences, University of Oxford, in partial fulfillment of the requirements for the degree of Doctor of Philosophy in Oncology

Michaelmas Term, 2014

Weatherall Institute of Molecular Medicine

University of Oxford

This thesis is dedicated to the memory of Janet D. Rowley, my first mentor, role model, and inspiration.

ABSTRACT

Since the initial description of cancer stem cells (CSCs) as a self-renewing subpopulation of malignant cells with tumor-initiating capacity, a growing body of evidence has supported the existence of CSCs in virtually every tumor type. Our previous work in colorectal cancer has identified the transcription factor CDX1 as a key regulator of colorectal CSC differentiation. CDX1 expression is frequently lost in colorectal cancer, resulting in more aggressive, poorly differentiated tumors with higher proportions of CSCs. Many miRNAs have been implicated in tumor suppression and carcinogenesis, but the roles of miRNAs in differentiation, particularly in colorectal cancer, remain poorly understood. We began by identifying miRNAs downstream of CDX1 by using high-throughput small-RNA sequencing to profile miRNA expression in two pairs of colorectal cancer cell lines with stable CDX1 overexpression or knockdown. Validation of candidates identified by RNAseq in a larger cell line panel revealed miR-215 to be most significantly correlated with CDX1 expression. ChIP-qPCR and promoter reporter assays confirmed that CDX1 directly transactivates miR-215 transcription. MiR-215 is depleted in FACS-enriched CSCs compared to unsorted samples. Overexpression of miR-215 in poorly-differentiated, highly clonogenic cell lines causes growth arrest and a dramatic decrease in colony formation. miR-215 knockdown using a miRNA sponge causes an increase in clonogenicity and impairs differentiation in CDX1-high cell lines. Indeed, the effects of CDX1 expression on both gene expression and colony morphology can be attenuated by miR-215 inhibition, indicating that miR-215 is a functional mediator of CDX1. Microarray studies following miR-215 overexpression indicate that miR-215 induces terminal differentiation-associated growth arrest, due in part to direct silencing of BMI1 expression and de-repression of BMI1 target genes including CDKN1A. Our work situates miR-215 as a link between CDX1 expression and BMI1 repression that governs differentiation in colorectal cancer. We further characterize another miRNA-transcription factor axis in colorectal cancer, and we identify the novel miR-3189-3p as a potent effector of cell death with potential therapeutic implications.

[315 words]

ACKNOWLEDGEMENTS

I would like to thank my co-supervisors Professor Sir Walter Bodmer and Dr. Ashish Lal for their guidance and support throughout the course of my graduate studies. The rigor, clarity, and enthusiasm with which they approach their work has changed the way I understand the theory and practice of scientific research. I am particularly grateful for their assistance in navigating what has proven to be a fruitful and collegial collaboration, in which the unique resources, both technical and human, of each lab have propelled this project.

Furthermore, I would like to offer my thanks to the members of the Cancer and Immunogenetics Laboratory at Oxford and the Cancer Genetics Branch of the National Cancer Institute in Bethesda, Maryland. I am honored and grateful to have called them my colleagues and my friends. I owe Neil Ashley, Jenny Wilding, and Djamila Ouaret particular thanks, not only for their expertise in genetics and cell culture, but also for their invaluable levity in the face of trying circumstances. I am thankful for the help of Xiao Ling Li, Toshifumi Hara, and Murugan Subramanian at the NCI, who have taught me much about RNA biology. I would also like to thank Trevor Yeung and Shazad Ashraf for patiently indulging my curiosity in clinical practice and translational research. The other graduate students in the CIL, Ruchi Patel, Linting Hsia, and Mustak Ibn Ayub, have been excellent interlocutors, constant sources of advice and assistance, and worthy companions in the journey towards a D.Phil. Further thanks go to Professors Peter McHugh and Eric O'Neill for their careful examination of my work during my transfer of status.

Of course, no expression of thanks can fully express the depth of gratitude I have for the unflagging support of my parents, which has made everything possible.

Finally, I would like to thank the Marshall Aid Commemoration Commission, Cancer Research UK, and the National Institutes of Health Oxford/Cambridge Scholars Program for providing the funding for my research.

DECLARATION

I, Matthew Fletcher Jones, hereby declare that the work on which this thesis is based is my original work and that neither the whole work nor any part of it has been, is being, or will be submitted for another degree in this or any other university. The work is original, except where listed by reference in the text or listed as follows: stable transfection of HCT116 with pRC-CMV-CDX1 by David Bicknell; stable transfection of LS174T of with CDX1 shRNA by Ying Liu; microarray gene expression analysis by Laura Hollins (cell line panel) and Yuelin Zhu (miR-215 and miR-3189); xenograft experiments and miR-3189 growth curves by Xiao Ling Li; miR-215 promoter cloning by Toshifumi Hara; pri-miR-3189 cloning by Murugan Subramanian; and phyologenetic analysis of miR-3189 by Svetlana Shabalina.

SIGNED: ..... DATE: .....

TABLE OF CONTENTS

CHAPTER 1
GENERAL INTRODUCTION

CHAPTER 2
MATERIALS AND METHODS

CHAPTER 6

MIR-215 NEGATIVELY REGULATES CLONOGENICITY AND STEMNESS

CHAPTER 7
CHARACTERIZATION OF A NOVEL MIRNA IN THE P53 PATHWAY: THE KILLER MIRNA-3189

CHAPTER 8
GENERAL DISCUSSION & FUTURE DIRECTIONS

LIST OF FIGURES

LIST OF TABLES

LIST OF ABREVIATIONS

bp	Base Pairs
BSA	Bovine Serum Albumin
BMP	Bone Morphogenetic Protein
cDNA	Complementary DNA
ChIP	Chromatin Immunoprecipitation
CIL	Cancer and Immunogenetics Laboratory
CLIP	Cross-Linking Immunoprecipitation
CMV	Cytomegalovirus
CSC	Cancer Stem Cell
DNA	Deoxyribonucleic Acid
DMEM	Dulbecco's Modified Eagle Medium
DMSO	Dimethylsulfoxdie
dNTP	Deoxyribonucleotide Triphosphate
Dox	Doxorubicin
ECL	Enhanced Chemiluminescence
EDTA	Ethylenediaminetetraacetic acid
EMT	Epithelial to Mesenchymal Transition
FBS	Fetal Bovine Serum
FACS	Fluorescence-Activated Cell Sorting
GSEA	Gene Set Enrichment Analysis
HRP	Horseradish Peroxidase
IP	Immunoprecipitation
kb	Kilobase
LB	Luria-Bertani Broth
mAb	Monoclonal Antibody
MCS	Multiple Cloning Site
MET	Mesenchymal to Epithelial Transition
MSI	Microsatellite Instability
miRNA	microRNA
mL	Milliliter

μL	Microliter
μM	Micromolar
mut	Mutant
ng	Nanogram
NOD/SCID	Non-Obese-Diabetic/Severe Combined Immunodeficiency
nM	Nanomolar
ORF	Open Reading Frame
PAGE	Polyacrylamide Gel Electrophoresis
PBS	Phosphate Buffered Saline
PCR	Polymerase Chain Reaction
pM	Picomolar
PMSF	Phenylmethylsulfonyl Fluoride
PRC1, 2	Polycomb Repressive Complex 1, 2
PVDF	Polyvinylidene Difluoride
qRT-PCR	Quantitative Reverse-Transcription Polymerase Chain Reaction
RACE	Rapid Amplification of cDNA ends
RISC	RNA-Induced Silencing Complex
RNA	Ribonucleic Acid
RNAse	Ribonuclease
RPM	Reads Per Million
RPM	Revolutions Per Minute
RPKM	Reads Per Kilobase per Million mapped reads
RT	Reverse Transcription
SDS	Sodium Dodecyl Sulfate
s.e.m.	Standard Error of the Mean
SOC	Super Optimal Broth with Catabolite repression
siRNA	Small Interfering RNA
SNP	Single Nucleotide Polymorphism
TBS	Tris-Buffered Saline
TBST	Tris-Buffered Saline plus Tween-20
TEMED	N,N,N,N-Tetramethylethylene-diamine

UTR	Untranslated Region
UV	Ultraviolet
wt	Wild type

CHAPTER ONE

General Introduction

CHAPTER 1: GENERAL INTRODUCTION

1.1 The Colon

1.1.1 Anatomy and function

The colon and the rectum are segments of the large bowel, which comprises the final portion of the human digestive tract. The large bowel intersects the small intestine at the cecum. As solid waste is ushered through the large intestine via peristaltic smooth muscle contractions, water and salts are reabsorbed by the intestinal lining while gut flora carry out fermentation of undigested material. The stool proceeds through eight regions of the colon between its passage from the small intestine to its elimination from the body: from the ascending colon, right colic flexure, transverse colon, left colic flexure, descending colon, sigmoid colon, rectum and anal canal (Gray, 2010; Aigner and Fritsch, 2010). These distinct regions differ primarily in their position within the body, with the ascending colon traveling upwards from the cecum, the transverse colon passing latitudinally across the body above the small intestine, the descending colon then running downwards along the left side of the abdomen, and the sigmoid colon bending in an S-shape to connect the descending colon to the rectum (Gray, 2010). Although the distinction between the colon and rectum is largely anatomical rather than histological, there are macroscopic differences between the tissues, with the colon exhibiting regularly spaced haustra, or pouches, and further small folds within the haustra, while the lining of the rectum is comparatively smooth (Aigner and Fritsch, 2010). Furthermore, differences

in gene expression may underlie the histological similarities between the colon and the rectum (Sanz-Pamplona et al., 2011).

1.1.2 Micro-architecture and cell physiology

1.1.2.1 Composition of the colonic crypt

The colon is organized into basic functional subunits called crypts, which are structurally demarcated by invaginations of the colonic epithelial sheet. The apical surface of the colon itself is a simple, postmitotic epithelium, while the crypts are host to rapidly dividing epithelial cells (Clevers, 2013b). In addition to facilitating the self-renewal of the gut's epithelial lining, these pitted indentations ostensibly increase the functional surface area of the colon relative to a flat lining. The differentiated cells populating the crypt consist of three functionally distinct lineages: enteroendocrine cells, mucus-secreting goblet cells, and columnar epithelial cells (Geibel, 2005). The middle, proliferative compartment of an intestinal crypt is composed of progenitor, or "transit amplifying," cells, which divide approximately twice per day and exist in a state of intermediate differentiation and retain some plasticity in regard to the fates they may eventually adopt (Crosnier et al., 2006). Columnar epithelial cells and goblet cells make up roughly 95% of the total crypt cell population, while enteroendocrine cells account for the remaining proportion (Geibel, 2005). The differentiated cells of an individual crypt are the clonal descendants of a single stem cell, which lineage-tracing experiments have shown to reside at the crypt base (Ponder et al., 1985; Novelli et al., 1996; 2003) (**Fig 1.1**). Thus organized, the crypt consists of a proliferative hierarchy of cells with the crypt

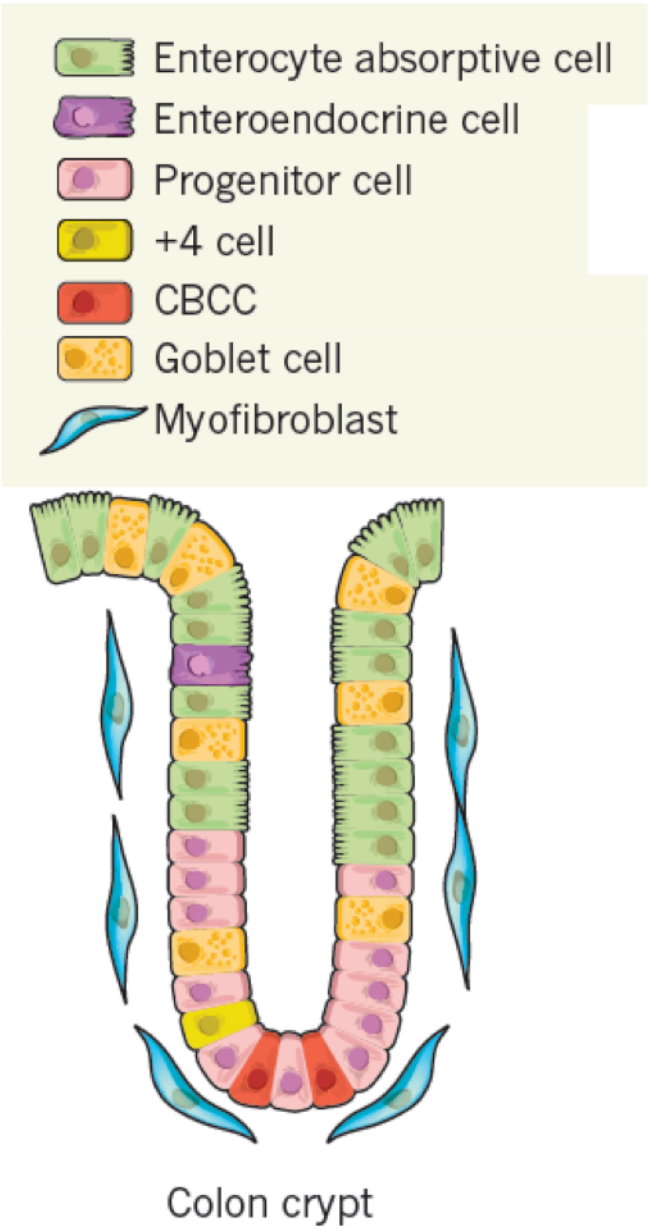

Figure 1.1
Structure and organization of the colonic crypt
The pit-like structure of the crypt is organized hierarchically such that crypt-base columnar cells (CBCC) proliferate and give rise to the other distinct lineages as they migrate upwards along the crypt axis. This figure is adapted from Medema and Vermeulen, 2011.

base stem cell at its apex. The crypt itself is surrounded by a sheath of pericryptal myofibroblasts, which are a specialized type of mesenchymal cells possessing characteristics of both smooth muscle and fibroblastoid cells, and which secrete hormones and growth factors to regulate the proliferation and differentiation of crypt epithelial cells (Humphries and Wright, 2008). These secreted factors are essential for the proper composition of the stem cell niche, as outlined below.

1.1.2.2 Crypt stem cells

There are thought to be at least two distinct subpopulations of multipotent stem cells within each intestinal crypt. Murine lineage re-tracing experiments have indicated that most, if not all of the mature cells of the epithelial sheet are derived from Lgr5+ crypt-base cells (Barker et al., 2007; Sato et al., 2009). However, there is also a discrete population of slowly dividing cells defined by expression of Bmi1 which reside at the "+4" position (**Fig 1.1**) above the bottom-most portion of the crypt (Sangiorgi and Capecchi, 2008). These cells are also believed to be marked by telomerase expression, which supports their classification as a persistent stem cell subpopulation(Montgomery et al., 2011; Itzkovitz et al., 2011). Under normal, homeostatic conditions, the Lgr5+ cells appear to give rise to the majority of mature, differentiated cells in the crypt, with the Bmi1+ cells acting as a presumably quiescent yet indispensible reserve population (Sangiorgi and Capecchi, 2008; Clevers, 2013a). When crypts are damaged, either by selective ablation of Lgr5+ cells or by irradiation, the Bmi1+ compartment expands to repopulate the crypt (Tian et al., 2011; Yan et al., 2012).

The current consensus regarding the balance between different stem cell populations holds that normal crypt dynamics are governed by neutral competition between several equipotent Lgr5+ stem cells. Analysis of the colonic crypts of a chimeric XY/XO patient revealed all crypts to contain either both X and Y or only X, indicating that mature crypts are monoclonal (Novelli et al., 1996). The balance between clonal populations in the developing crypt is stochastic, such that one clone comes to dominate an entire crypt by a process equivalent to neutral drift in population genetics[1] (Snippert et al., 2010; Lopez-Garcia et al., 2010). A recent study has characterized the Lgr5+ stem cells as a special type of secretory progenitor cell, which is presumably derived from the reserve Bmi1+ population (Buczacki et al., 2013). In sum, the normal gut lining consists of descendants of Lgr5+ crypt-base stem cells. However, the Lgr5+ population is dispensable, as it can be reconstituted by quiescent, indispensible Bmi1+ cells, which are thought to represent a pool of injury-inducible "reserve" stem cells.

The elegant spatiotemporal dynamics of proliferation and differentiation in the crypt are maintained by both crypt-intrinsic and –extrinsic morphogenetic signaling pathways. Along the crypt axis run opposing gradients of Wnt and bone morphogenetic proteins (BMPs) which are secreted by the stromal cells surrounding the crypt. These molecular gradients create different microenvironments favoring stemness at the crypt base and terminal differentiation at the apical surface of the colon, respectively. A high level of Wnt ligand exists at the crypt base, tapering along the crypt axis to a minimum at the apical surface (Gregorieff et al., 2005). The aforementioned Lgr5 stem-cell marker is a g-

[1] Neutral drift refers to the phenomenon in which a given genotype stochastically sweeps through an initially heterogeneous population in the absence of selective pressure (Kimura, 1968).

protein coupled receptor, which associates with the Wnt ligand receptors Frizzled/Lrp and mediates the response to the Wnt activator R-spondin (de Lau et al., 2012). Ligation of Wnt signaling receptors results in activation of the canonical Wnt pathway, and dissociation of β-catenin from the destruction complex via phosphorylation of the adenomatous polyposis coli (APC) protein. β-catenin is then free to translocate from the cytoplasm to the nucleus, where it recruits the TCF/LEF transcription factors to transactivate stem cell and proliferative genes including *MYC*, cyclin D1 (*CCND1*) and other Wnt pathway components such as *AXIN* and *LRP* (Clevers, 2006; Kim et al., 2005). The importance of Wnt signaling is illustrated by the restriction of nuclear β-catenin to cells at the crypt base, and nuclear β-catenin is considered a hallmark of intestinal stem cells (van de Wetering et al., 2002).

1.1.2.3 CDX1 and differentiation

There are several cellular signaling pathways purported to control intestinal epithelial differentiation, including Notch, BMP, and the caudal type homeobox transcription factors (CDX1/2/4). For the purposes of this thesis, we will focus on describing findings relating to *CDX1* and *CDX2*. The CDX family proteins are transcription factors that are expressed laterally along the developing mesoderm during embryogenesis, where they play important roles in patterning vertebrae by repressing HOX gene expression (van den Akker et al., 2002; Savory et al., 2009). In adult mammals, *CDX1* expression is restricted to the large intestine, where we have shown it to be expressed exclusively in the differentiated tissue along the apical epithelial surface of the colon (Chan et al., 2009). Expression of *CDX1* in the adult human colon is associated with differentiation of the

epithelial lineage and the direct transcriptional activation of structural enterocyte genes including *KRT20* (Chan et al., 2009), villin (Arango et al., 2012), and *FABP1* (Staloch et al., 2005). Mouse knockout models of *Cdx1* are viable and have normal digestive systems, which has been attributed to functional compensation by *Cdx2*, yet conditional intestine-specific double knockout of both *Cdx1* and *Cdx2* in mice results in exacerbated morphological defects relative to knockout of *Cdx2* alone (Verzi et al., 2011). Intestine specific *Cdx* double knockout mice have also been observed to develop metaplastic lesions in the colon in which the intestinal epithelium becomes gastric-like, suggesting that cooperation between *Cdx1* and *Cdx2* is necessary for intestinal homeostasis in mouse (Hryniuk et al., 2012). Both *CDX1* and *CDX2* have been implicated in inappropriate intestinal trans-differentiation of gastric epithelium, further indicating a significant role for the CDX family in regulating intestinal differentiation (Silberg et al., 1997; Mutoh et al., 2004; Wong et al., 2005).

1.2 Colorectal Cancer

1.2.1 Epidemiology

Colorectal cancer (CRC) is one of the most common types of human cancers and a cause of significant cancer-associated mortality and morbidity. Bowel cancer is the fourth most common type of cancer in the UK, and the third most common type of cancer in males and females separately, accounting for 41,581 new cases in 2011 alone (CRUK). Although some types of colon cancer are responsive to treatment when detected at an

early stage, it remains the second largest cause of cancer-related deaths in both men and women in the UK (Ferlay et al., 2013). Worldwide, colon cancer is the third most common type of cancer, with over 1,300,000 new cases diagnosed in 2012, accounting for over 10% of the total new cancer diagnoses in that year (CRUK). In general, colorectal cancer seems to afflict more men than women. A first-world diet high in red meat has also been implicated in increased colorectal cancer risk (Bingham and Riboli, 2004). As with many other cancers, age is one of the strongest risk factors, which is likely tied to the underlying biological fact that a longer life simply allows detrimental mutations to accumulate over a greater number of cell divisions (Armitage and Doll, 1954).

1.2.2 Molecular Etiology and Histopathology

During the process of carcinogenesis, gradual derangement of the glandular crypt architecture presages the development of gross malignancies. Transformation of the colonic epithelium is usually initiated by mutation of the tumor suppressor gene and key Wnt pathway component *Adenomatous Polyposis Coli* (*APC*) (Powell et al., 1992). Loss of functional APC leads to disassembly of the destruction complex and consequent nuclear accumulation of β-catenin, which in turn results in the abnormal activation of the TCF/LEF transcription factors and uncontrolled expression of many genes involved in proliferation and differentiation. It has been suggested that *APC* mutation initially occurs in the crypt stem cells, conferring upon them a selective advantage resulting in the repopulation of the crypt with the dysplastic progeny of the stem cell (Barker et al., 2009;

Huang et al., 2009). Mathematical models of adenoma development have demonstrated that the shift in the dynamic equilibrium between programmed cell death and proliferation in the crypt results in an altered set point rather than runaway growth, so that an adenoma initially reaches a stable size (Tomlinson and Bodmer, 1995; Johnston et al., 2007). Further mutations may accumulate in the dividing cells of the adenoma, and again natural selection drives the progression from stable adenoma to adenocarcinoma. This progression between equilibria is reflected by the typical time course of the progression from adenoma to carcinoma (**Fig 1.2**) (Vogelstein et al., 2013).

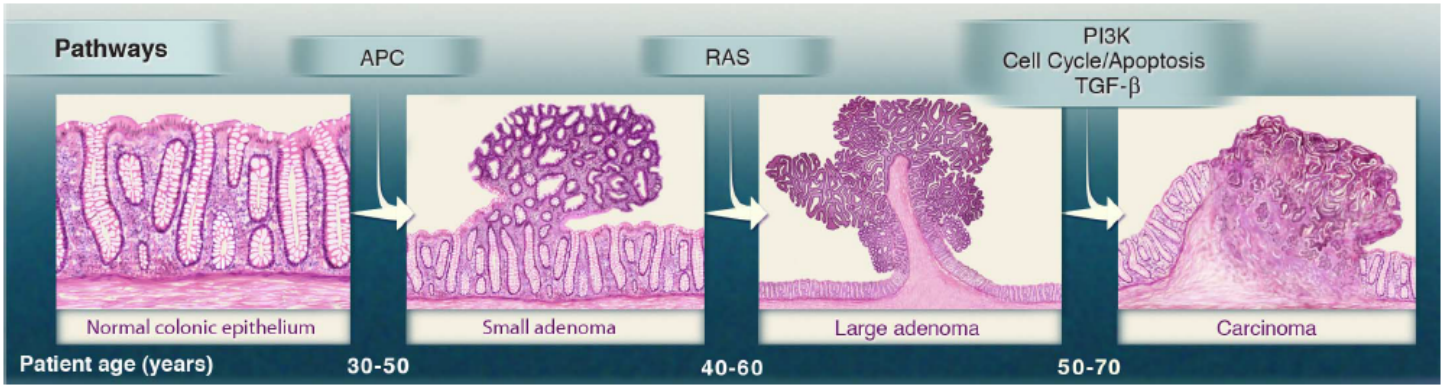

Figure 1.2
Fearon-Vogelstein model of colorectal tumorigenesis
The initial genetic event for the majority of colorectal tumors is an inactivating mutation in APC. As other mutations accumulate, the histology of the colonic mucosa becomes notably deranged. Though the sequence of mutations may vary between tumors, most bear mutations in APC, the KRAS pathway, and the p53 pathway. Patient age indicates the time intervals during which the driving mutations usually occur. This figure is adapted Vogelstein, *et al.*, 2013.

The progression from benign adenoma to invasive carcinoma is not inevitable, and in fact seems to be quite rare. For instance, patients with inherited *APC* mutations (familial adenomatous polyposis) display thousands of colorectal polyps yet develop frank carcinoma in comparatively few sites (Bodmer, 1999). The reason for this is the rate-

limiting requirement for mutations in other tumor suppressor genes and proto-oncogenes which are necessary for complete malignant transformation (Tomlinson et al., 1996). The most commonly seen mutations and their clinical frequencies in non-hypermutated tumors are *APC* (81%), *TP53* (60%), *KRAS* (43%), and *PIK3CA* (18%) but many other genetic and epigenetic alterations have also been described (Fodde et al., 2001; Fearon and Vogelstein, 1990).

1.3 Cancer stem cells

1.3.1 Definition

It is becoming increasingly clear that most, if not all, types of tumors are composed of a heterogeneous population of cells, of which only a subpopulation is capable of driving tumor growth and progression (Pierce and Speers, 1988). In this way, a tumor can be viewed as a dysfunctional, deranged organ, and the cells driving its growth are analogous, in many ways, to the normal stem cells responsible for creating and maintaining normal organs. These cancer stem cells (CSCs) are capable of long-term self-renewal and of differentiating into the diverse lineages that comprise the rest of the tumor (Medema and Vermeulen, 2011).

Because of their capacity to initiate a tumor *in vivo*, CSCs are often referred to as tumor-initiating cells, but this name can be misleading in its implication that CSCs are necessarily the cells of origin for autochthonous tumors, i.e. the first cells to undergo

malignant transformation in a tissue. Similarly, the name "cancer stem cell" can give the impression that CSCs arise from normal stem cells even though it is possible that CSCs are the progeny of progenitor cells that have escaped the controls that normally induce differentiation (Borovski et al., 2011; Johnston et al., 2007; Fevr et al., 2007). It is not clear that CSCs are always the first cells to undergo transformation nor that CSCs are derived from normal stem cells (Visvader, 2011). Rather, by the use of the term "cancer stem cell," we strictly adhere to the definition given by the AACR Workshop on Cancer Stem Cells: "a cell within a tumor that possess [*sic*] the capacity to self-renew and to cause the heterogeneous lineages of cancer cells that comprise the tumor" (Clarke et al., 2006).

1.3.2 Functional implications

1.3.2.1 Tumor heterogeneity

Just as cancer stem cells phenotypically mirror their normal counterparts in many important ways, the study of cancer stem cells has proceeded hand-in-hand with that of normal stem cells. The discovery of hematopoietic stem cells in mice by Till and McCulloch in 1961 was closely followed by studies that demonstrated stem-like populations of cells in hematopoietic malignancies (Till and McCulloch, 1961; Nicola et al., 1985; Sachs, 1987). A revival of interest in CSCs began in 1990s with the work of Bonnet and Dick, who showed that only leukemic cells bearing a specific surface marker signature (CD34+/CD38-) could initiate acute myeloid leukemia (AML) upon xenotransplantation into non-obese diabetic mice with severe combined

immunodeficiency (NOD/SCID mice) (Bonnet and Dick, 1997). As the hematopoietic system is one of the best-studied human tissues with regards to stem-progenitor-effector hierarchy, many of the original cnacer stem cell studies focused on identifying stem cells in hematological malignancies. However, according to the criterion of tumor initiation upon introduction to NOD/SCID mice, subpopulations of cancer stem cells have now been identified in many human malignancies.

The existence of stem cell subpopulations in cancers implies that tumors are phenotypically heterogeneous and hierarchical, like disorganized parodies of normal tissue. Indeed, it has been observed that cancer stem cells not only possess the capacity to engraft tumors in an immunodeficient host, but also to recreate a tumor containing the same diverse cellular lineages as the original lesion (Bonnet and Dick, 1997; Al-Hajj et al., 2003; Dalerba et al., 2007). The heterogeneity contributed by hierarchical differentiation may be viewed as an epigenetic layer atop the clonal, genetic heterogeneity known to exist in tumors.

As a tumor grows, it accumulates mutations. This process does not require genetic instability, as elegant mathematical models have demonstrated (Bodmer and Loeb, 2008), but many tumors do develop a “hypermutated” genome due to loss of DNA repair genes (Network, 2013). According to Darwinian selection, mutations that confer a growth or survival advantage are selected for, and the clonal descendants of the mutated cell expand. This is particularly evident in the emergence of tumor subclones resistant to targeted therapy, for example in the acquisition of Imatinib resistance (Shah et al., 2007).

This concept of clonal evolution was put forward in 1976 by Peter Nowell (Nowell, 1976), since which time an overwhelming amount of evidence has been gathered in its support (Shackleton et al., 2009). However, there has also been longstanding observation from light microscopic experiments of histopathologic diversity of cell types comprising a tumor (Clarke et al., 2006), for which clonal evolution cannot fully account. Cancer stem cell theory introduces the valuable concept that even among a genetically identical, clonal population, cells may occupy different positions within a hierarchy of differentiation similar, for instance, to the tension between clonality and functional heterogeneity within a normal colorectal crypt.

1.3.2.2 Resistance to treatment

Cytotoxic chemotherapy combined with surgical resection and radiotherapy has been a front-line treatment for most operable tumors for several decades, yet there are obvious shortcomings with these therapies in terms of both morbidity and mortality (Slevin and Payne, 2004). One of the greatest problems with these un-targeted treatment strategies is the high chance of disease recurrence. On a genetic level, this acquisition of resistance derives from the strong selective pressure imposed by therapy for randomly-occurring mutations that confer resistance. This phenomenon has been observed repeatedly in post-treatment tumor recurrences (Sakai et al., 2008; Ding et al., 2012; Marusyk et al., 2012). However, the problem of acquired resistance is compounded by the fact that different phenotypic cell lineages within a single tumor clone display differential sensitivity to treatment. This is supported by the observation that normal stem cells are relatively protected from molecular insult by several mechanisms, including the expression of ABC

drug transporters, upregulation of anti-apoptotic pathways, and resistance to DNA damage (Zhou et al., 2009). In this case, using clinical reduction of tumor mass as a metric of therapeutic success increases the chance of spurious "relapse," when in fact the tumor has merely been de-bulked of differentiated cells.

In some cases, there seems to be a correspondence between the proportion of cancer stem cells in a tumor and the likelihood of disease relapse. In colon cancer, for example, prevalence of a stem-cell like gene expression profile predicted likelihood of relapse after chemotherapy (Merlos-Suárez et al., 2011). Putative cancer stem cells in glioma (CD133+) and breast cancer ($CD44^{high}CD24^{low}$) are more resistant to ionizing radiation than the tumor bulk (Bao et al., 2006; Diehn et al., 2009). However, there are also counterexamples, such as the increased radiosensitivity of cancer stem cells in testicular germ cell tumors (Masters and Köberle, 2003). Further research into the balance between the stochastic acquisition and selection of therapy-resistant clones and intrinsic therapy resistance as a result of phenotypic tumor heterogeneity will be important for the development of new cancer treatments (Sikic, 2008).

1.3.2.3 Metastasis

Metastasis refers to the initiation of a secondary tumor in a tissue distant from the site of the primary tumor. The cancer cells that escape the primary tumor and colonize a metastatic site bear a fundamental similarity to cancer stem cells in their tumorigenic capacity. However, there are many steps that are necessary for metastasis to occur, and to claim that colonization is a direct result of primary cancer stem cells escaping into the

bloodstream would be an oversimplification of the multi-step metastatic cascade. In order to escape primary tumor, cancer cells are thought to undergo an epithelial-to-mesenchymal transition (EMT) which is necessary for carcinoma cells to survive outside of their epithelial niche and invade the circulation, and which involves down-regulation E-cadherin and upregulation of Vimentin and matrix metalloproteases (Yang and Weinberg, 2008). Furthermore, the circulating cell must possess or acquire the requisite traits to grow in the "foreign soil" of a distant tissue (Psaila and Lyden, 2009). Selection for the ability to grow in a new environment may result in a metastasis that is genetically distinct from the primary tumor, yet the cells initiating the metastasis must be the clonal descendants of cancer stem cell from the primary tumor. On the other hand, phenotypic plasticity and the evolution of metastatic traits within the primary tumor can result in metastases that are genetically very similar to subclones within the primary tumor (Navin et al., 2011).

Several lines of evidence point to the conclusion that stemness is a requirement of cells that colonize metastatic sites. The invasive front of pancreatic carcinoma was observed to be enriched with cancer stem cells; ablation of this subpopulation in pancreatic cancer cell lines abolished their invasiveness and metastatic potential (Hermann et al., 2007). Enrichment of breast cancer stem cells using the cell-surface marker aldehyde dehydrogenase (*ALDH1*) yielded a subset of cells with increased metastatic potential *in vivo* and which expressed a set of genes associated with metastasis (Charafe-Jauffret et al., 2009). Targeting prostate cancer stem cells by using siRNA and miRNAs to silence

expression of the prostate cancer stem-cell marker CD44 also reduced metastasis and invasion in mouse models (Liu et al., 2011).

1.3.2.4 Cancer stem cells in vitro

Although the current accepted standard for cancer stem cell characterization is the xenograft assay, the Cancer Immunogenetics laboratory and other groups have developed *in vitro* methods of modeling cancer stem cells (Charafe-Jauffret et al., 2009; Yeung et al., 2010). Cell lines isolated from colorectal cancer tumors and grown in Matrigel will exhibit distinct colony morphologies that reflect the clonogenicity of the cell line (Yeung et al., 2010). Cell lines that differentiate poorly *in vitro* can be compared to undifferentiated, aggressive tumors with a high proportion of cancer stem cells. Cell lines that form lumen-like structures in culture, on the other hand, are less clonogenic, contain a relatively lower proportion of CSCs, and have lower tumorigenic capacity after xenotransplantation into NOD/SCID mice (Yeung et al., 2010). We have found that cell lines and primary samples with high expression of differentiation markers such as villin and KRT20 and of the differentiation regulators CDX1 and CDX2 form organotypic structures in 3-dimensional cell culture systems (Yeung et al., 2010; 2011). These structures consist of well-organized colonies polarized around a central lumen, which recapitulates the apical-basal polarity of the normal colon and expresses genes associated with the intestinal brush border. Recent work by Ashley, *et al*. has shown the formation of lumens *in vitro* to be a key characteristic of well-differentiated colorectal cancer cell lines and primary tumors (Ashley et al., 2013; 2014).

These studies implicitly rely on the assumption of unidirectional stem-progenitor hierarchy, in which cancer stem cells differentiate and differentiated cells are fixed in that state. This idea was recently challenged by the observation that purified cultures of differentiated breast or colon cancer cells can, through a stochastic loss of differentiation, reconstitute the original population equilibrium between stem and differentiated cell states (Gupta et al., 2011; Kai et al., 2009).

Some disagreement exists as to the reliability of different markers for stem cell enrichment from cell lines or patient samples. Colorectal cancer cell populations enriched for the cell surface markers CD44 and CD24 are more clonogenic and form complex, lumen-containing megacolonies in vitro, differentiating into each of the three distinct lineages of the colonic crypt, proving that the functional characteristics of CSCs can be reliably detected *in vitro* (Yeung et al., 2010). Other putative stem cell markers include CD133, CD55, Lgr5, ALDH1, OLFM4, and EPHB2 (Vermeulen et al., 2012). Increased expression of the transcription factors CDX1 and CDX2 has been shown to play a key role in driving the process of differentiation *in vitro* (Chan et al., 2009; Lorentz et al., 1997). *In vitro* models of differentiation provide excellent systems not only for the study of mechanisms controlling cancer stem cell dynamics but also for screening potential cancer treatment in a realistic, phenotypically heterogeneous population of cells.

1.3.3 Genetic characteristics

1.3.3.1 Control of stemness

In addition to their functional similarity to normal stem cells, colorectal cancer stem cells share many molecular traits with normal adult colorectal stem cells. Here, we restrict our perspective to the genetic pathways important for colorectal cancer stem cells. Cancer stem cells can be enriched in a given population of cells by sorting for cell-surface markers associated with normal stem cells. In colorectal cancer, recent efforts to characterize the genes associated with stemness indicate that the cancer stem cell relies on Wnt and Notch signaling, with cancer stem cells showing high levels of nuclear β-catenin localization—a striking parallel with normal intestinal stem cells (Fevr et al., 2007; Vermeulen et al., 2010). Additionally, maintenance of stemness in both CSCs and normal intestinal stem cells depends on the expression of the polycomb group protein BMI1 (Sangiorgi and Capecchi, 2008; Yeung et al., 2011), which is responsible for maintaining gene silencing associated with DNA methylation. It is thought that one of the crucial requirements for maintaining stemness is evasion of replicative senescence, as stem cells are continually dividing subpopulations. *BMI1* expression has been reported to be necessary for this process by maintaining silencing of the senescence mediators encoded by the *CDKN2A* locus: $p15^{INK4A}$ and $p16^{ARF}$ (Bruggeman et al., 2007; van Lohuizen et al., 2000). The 7-transmembrane receptor Lgr5, recently discovered to potentiate Wnt signaling (de Lau et al., 2012), has also been associated with both normal and cancer stem-cell phenotypes (Barker et al., 2009).

A major difference between the normal colon stem cell and the colorectal cancer stem cell is that the niche for the normal colon stem cell has been quite well defined, while it is still unclear how a salutary microenvironment is maintained in support of the cancer stem

cell. Recent work by Yeung, *et al*. has shown that cancer stem cells infiltrating lymph nodes activate myofibroblasts to maintain a stem cell niche (Yeung et al., 2013). This result suggests that cancer stem cells retain some of the niche-dependency of their normal counterparts, yet it also implies that successful metastases undergo selection for the ability to recreate their niche in a new tissue. It seems clear that colon cancer stem cells rely on Wnt signaling and the activation of stem cell genes in much the same way as normal colon stem cells.

1.3.3.2 Control of differentiation

As mentioned above, cancer stem cells have been observed to differentiate into functionally distinct lineages in both *in vitro* and *in vitro*. This capacity for differentiation indicates that, in spite of their unchecked proliferative ability and malignant characteristics, cancer stem cells retain some of the impetus for differentiation present in their normal counterparts. Multilineage differentiation of cancer stem cells is observed *in vitro* when cell lines are cultured with the extracellular matrix components collagen, fibronectin, and serum growth factors present in Matrigel^{TM} (Yeung et al., 2010; 2011). The widely varying differentiation patterns observed across a large panel of colorectal cancer cell lines indicate that cell-intrinsic factors are also responsible for the balance between differentiation/proliferation and stemness in a cancer cell line.

Much work in the Cancer Immunogenetics Laboratory has been focused on understanding the mechanisms by which cancer stem cells give rise to well-differentiated or poorly differentiated tumors. Microarray gene expression profiling of a panel of over

100 colorectal cancer cell lines combined with analysis of the *in vitro* differentiation patterns, as determined by 3-dimentsional colony morphology, lines has revealed a significant correlation between expression of *CDX1* and differentiation, which parallels its reported roles in the normal colon described above. *CDX1* expression is not only a negative marker of stemness, but is also central to the capacity of a colorectal cancer cell line to differentiate (Ghandi's thesis, 2011) (Chan et al., 2009; Yeung et al., 2010; Ashley et al., 2013). In 19% of colorectal cancer cell lines assayed in a large study, *CDX1* expression was completely lost due to promoter methylation and was downregulated in a further 13% due to hemimethylation of the promoter (Wong et al., 2004). In another study, comparison of *CDX1* expression in colorectal adenocarcinoma versus matched normal tissue showed downregulation of *CDX1* in 73% of tumors, which was also attributable to promoter methylation (Pilozzi et al., 2004). Expression of *CDX1* also correlates inversely with that of *BMI1*, though the mechanism underlying this relationship has not yet been elucidated (Yeung et al., 2010; Yeung et al., 2011). In addition to this correlative data, CDX1 has also been shown to directly promote the expression of a structural protein important for epithelial differentiation, cytokeratin 20 (*KRT20*) (Chan et al., 2009). Introduction of *CDX1* into poorly-differentiated, non-lumen forming cell lines that do not express endogenous *CDX1* induces lumen formation in 3-dimensional cell culture (Yeung et al., 2010). These data are consistent with the previously noted role for CDX1 in regulating differentiation in the normal colon and in intestinal metaplasia. Though several transcriptional targets and functional effects of *CDX1* have been identified, there remains much to learn about the mechanisms by which it promotes differentiation and, in particular, those by which it inhibits stemness.

1.4 MicroRNAs

In the above sections, we have discussed some of the important genetic factors that contribute to the somatic evolution of colorectal cancer and to the cancer stem cell phenotype. This discussion has, so far, only dealt with protein-coding genes, yet recent advances in the study of non-coding RNAs demand that we consider the roles of microRNAs (miRNAs) in cancer, as well. MicroRNAs are an abundant class of small, gene regulatory RNAs which have been shown, over the past decade, to be intimately involved in normal physiological function, and their dysregulation has pathological consequences (Hermeking, 2012). In the following sections, we present an overview of the existing literature on microRNA function and microRNA involvement in human cancer.

1.4.1 Biogenesis and function

MiRNAs are 18-22nt RNA molecules that act as regulators of gene expression (Kim et al., 2009). MiRNAs were originally described in *c. elegans* as regulating the timing of gene expression during development (Lee et al., 1993; Pasquinelli et al., 2000; Reinhart et al., 2000). In humans, they are transcribed by RNA polymerase II (Lee et al., 2004) from predominantly intragenic loci, although intronic and intergenic miRNAs also exist, to generate a primary transcript, or pri-miRNA. MiRNA loci are often clustered together, in which case transcription occurs in a polycistronic manner (Ventura et al., 2008). In the nucleus, the pri-miRNA is processed by the so-called microprocessor complex, consisting

of the nuclease Drosha and the RNA binding protein DGCR8 (**Fig 1.3**) (Denli et al., 2004). Alternately, miRNAs that occur within the intron of an mRNA sufficiently close to either the 5' or 3' splice site may be so-called "mirtrons," which are processed to yield precursor miRNAs during the intron lariat debranching step of pre-mRNA splicing (Westholm and Lai, 2011). Although initially believed to be rare, recent analysis of high-throughput RNA-sequencing data has indicated that mirtrons may be more widespread than initially supposed (Ladewig et al., 2012). Whether produced via the microprocessor or the spliceosome, the products of nuclear processing are pre-miR hairpins, which are exported from the nucleus in a GTP-dependent manner by exportin 5 in association with the cofactor Ran (Lund, 2004; Bohnsack et al., 2004). In the cytoplasm, the pre-miRNA is further cleaved by the nuclease Dicer, generating a ~22nt miRNA duplex consisting of a mature miRNA and a miRNA* (miRNA star) strand (Hutvagner, 2001; Khvorova et al., 2003). The mature strand is incorporated into the RNA-induced silencing complex (RISC), while the star strand is generally degraded. There is no uniform rule as to

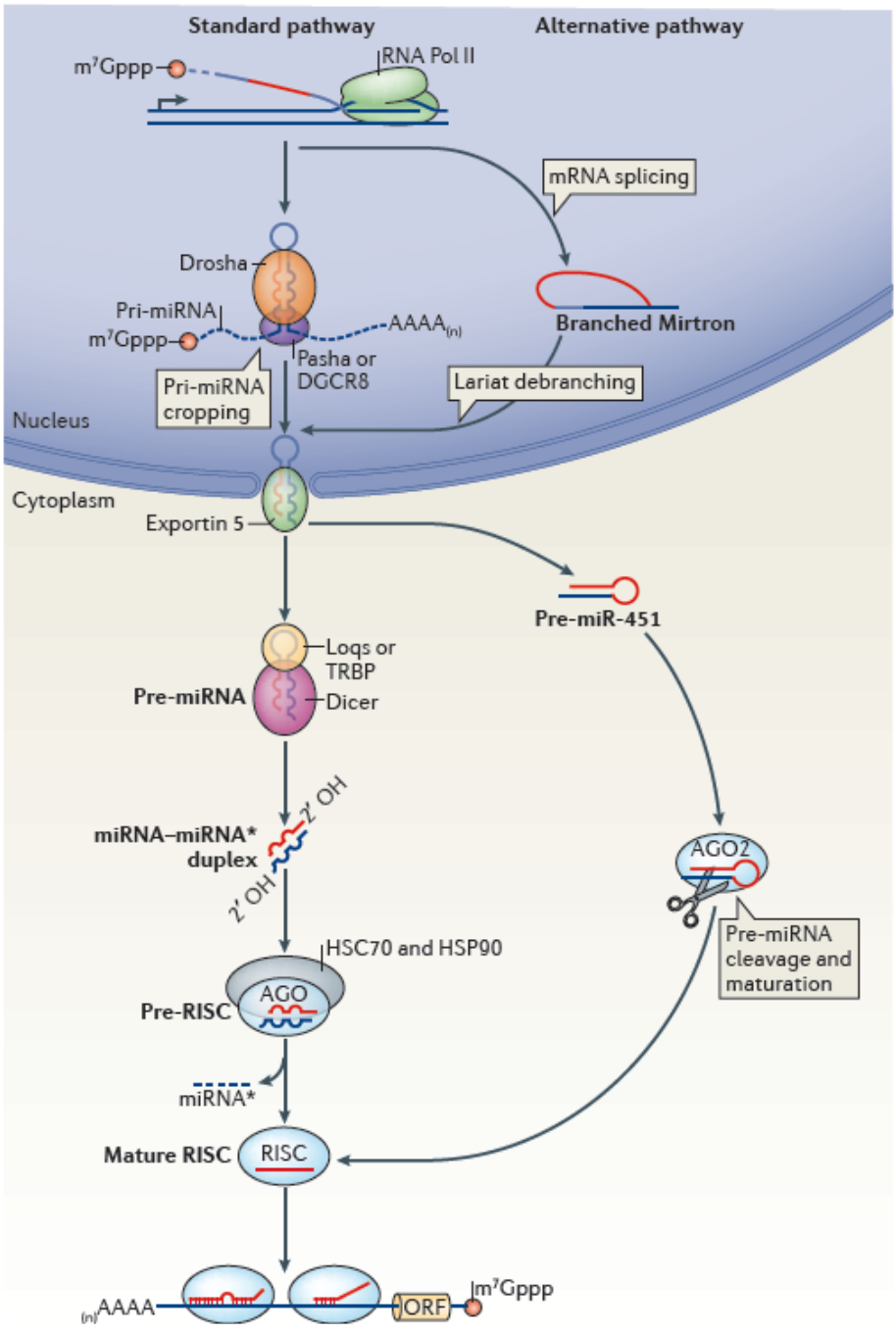

Figure 1.3
Canonical miRNA biogenesis pathway
miRNAs transcribed from traditional loci are processed in the nucleus by the Drosha/DGCR8 "microprocessor" complex, while "mirtrons" are initially processed during mRNA splicing. These two pathways converge at the stage of nuclear exportation. miRNA precursors are further cleaved in the cytoplasm by Dicer, and are incorporated into RISC, which they guide to semi-complementary sites in the 3'UTRs of target mRNAs. This figure is adapted from Ameres and Zamore, 2013.

which strand of the duplex is preferred, and there may be some degree of tissue or context specificity that determines whether one strand or the other—or both— is functional (Kim et al., 2009). The miRNA-RISC complex targets regions in the 3'-untranslated region (3'UTR) of mRNA transcripts, where the miRNA binds to sequences complementary to its 2^{nd}-8^{th} nucleotides. This sequence between positions 2 and 8 is called the seed sequence and is critical for specific binding (Filipowicz et al., 2008). Although miRNAs can decrease the translation of an mRNA transcript by several distinct mechanisms, the Bartel and Rajewski labs recently showed that miRNAs act to decrease the stability of their target mRNAs through rapid deadenylation (Guo et al., 2010; Selbach et al., 2008; Baek et al., 2008). Repression of mRNA translation through miRNA-mediated inhibition of the EIF4F translation initiation complex has been shown to be a necessary step prior to mRNA degradation (Meijer et al., 2013).

1.4.2 Nomenclature

As a relatively new class of genetic product, miRNAs adhere to a different nomenclature scheme than protein-coding genes. This terminology may be confusing to non-specialists, and it is briefly outlined here as a guide to the reader.

MicroRNA will hereafter be abbreviated to "miRNA." When referring to a specific miRNA, it is shortened further to "miR," although this may only be used in conjunction with the miRNA's designated number, e.g. miR-215 or miR-3189. MiRNAs are numbered roughly according to the order that they were discovered (Ambros et al., 2003;

Kozomara and Griffiths-Jones, 2014), and many high-numbered miRNAs are poorly conserved or expressed at low levels compared to the low-numbered miRNAs such as miR-9 or miR-34. The only departure from this nomenclature is let-7, which takes its name from an abbreviation of *lethal-7*. *Lethal-7* was the name of one of the two miRNAs first discovered as a regulator of heterochronic gene expression in *C. elegans* (Reinhart et al., 2000), and was the first miRNA discovered in humans (Pasquinelli et al., 2000). Due to its special significance in the history of the field, let-7 has kept its original name.

The unprocessed nuclear miRNA transcript is called the primary or pri-miRNA. The miRNA hairpin prior to Dicer processing is termed the precursor miRNA, or pre-miRNA. A miRNA listed without either pri- or pre- as a prefix is assumed to refer to the mature, single stranded product. Two mature miRNAs may be produced from a given pre-miRNA, one from the 5' arm of the hairpin structure and one from the 3' end. These mature miRNAs are distinguished by the suffixes -5p and -3p, such that pre-miR-3189, for example, yields both miR-3189-5p and miR-3189-3p (Kozomara and Griffiths-Jones, 2014). In many cases, one of these products is non-functional, and where such strand-preference has been well established, the mature product is referred to without a suffix.

Finally, many miRNAs share the same seed sequence, though they may differ in sequence outside of the seed region. These miRNAs are said to be "related," and are usually distinguished by alphabetical suffixing, e.g. miR-34b and miR-34c are seed relatives. Other mature miRNA sequences have been exactly duplicated in one or more regions across the genome, and are identified by numerical suffixes, e.g. miR-194-1 and

miR-194-2 (Ambros et al., 2003; Kozomara and Griffiths-Jones, 2014). Note that both seed relatives and paralogs may differ in their primary or precursor sequences.

1.4.3 MiRNAs in cancer

1.4.3.1 Global dysregulation of the miRNA-ome

There are currently over 1400 confidently identified human miRNAs in the miRNA database (www.mirbase.org) (Kozomara and Griffiths-Jones, 2014; Griffiths-Jones, 2004), and more will surely continue to be discovered as more deep sequencing data accumulates. MiRNAs are thought to exert some degree of direct control on the expression of over 60% of all genes (Friedman et al., 2008). When we consider that many genes under the regulation of miRNAs are, themselves, transcription factors or other regulatory proteins, miRNAs have some amount of indirect control over the expression of virtually every gene in the genome. As cancer is a disease of dysregulation—from cell intrinsic control of proliferation to secreted growth factors, oncogenic pathways are derangements of normal ones—it has become increasingly clear that miRNAs can play a pivotal role in the development and progression of cancer. Many cancers exhibit a global down-regulation of miRNA expression (Lu et al., 2005; Dvinge et al., 2013), often mediated by under-expression of Dicer or other genes involved in miRNA biogenesis (Kumar et al., 2009). miRNAs are also frequently located near fragile sites in the genome, as well as commonly amplified regions or common breakpoints, indicating that genomic instability can also result in miRNA dysregulation (Calin et al., 2004). Several miRNAs have been implicated in tumorigenesis, CSC self-renewal, and metastatic

progression. For example, miR-200c expression is lost as a result of p53 mutation in mammary epithelial cells, which results in upregulation of stem-cell markers and downregulation of epithelial markers (Chang et al., 2011).

In addition to the regulation of miRNAs themselves, it has also been noted that the availability of miRNA targets is altered on a transcriptome-wide level. Several groups have shown that differential preference for alternative polyadenylation sites in cancer compared to normal tissue results (Wang et al., 2008), resulting in the ablation of miRNA-seed complements in the 3'UTRs of pro-proliferative genes, such as *cyclin D1*, *cyclin D2*, and *IGFBP1* (Mayr and Bartel, 2009; Liaw et al., 2013). Furthermore, point mutations in miRNA-responsive 3'UTR elements may disrupt miRNA-mRNA interactions or even introduce new miRNA binding sites, resulting aberrant gene repression (Ziebarth et al., 2012; Thomas and Sætrom, 2012). Perhaps the most notable example of this de-repression is the activation of *KRAS* by a single-nucleotide polymorphism (SNP) in its 3'UTR which disrupts a let-7 binding site. This SNP has been shown to confer an increased risk of lung cancer (Chin et al., 2008), ovarian cancer (Ratner et al., 2010), triple-negative breast cancer (Paranjape et al., 2011) and is associated with decreased survival in oral cancer (Christensen et al., 2009).

1.4.3.2 Oncogenic miRNAs

Despite the global down-regulation of miRNAs observed in many cancers, it would be incorrect to draw the general conclusion that all miRNAs act broadly as tumor suppressors. In fact, there are several specific miRNAs that exhibit oncogenic effects.

Generally, these oncogenic miRNAs promote cell growth, invasiveness, metastasis, or angiogenesis by inhibiting the expression of a negative regulator of one or more of those processes. Although the analogy to oncogenes should not be overstated- for instance, it is rare to find a mutation in a miRNA which affects miRNA function (Wu et al., 2008; Diederichs and Haber, 2006; Ryan et al., 2010)- the inappropriate expression of some miRNAs is definitively associated with malignancy.

miR-155 is, perhaps, the prototypical oncogenic miRNA, or "oncomiR." Initial reports on miR-155 function focused on concurrent expression patterns with known oncogenes such as *MYC* and *BIC* in various malignancies including Hodgkin lymphoma and breast cancer (Tam and Dahlberg, 2006; Jiang et al., 2010). miR-155 has since been implicated in a wide range of oncogenic processes, including metastasis, migration, and angiogenesis (Kong et al., 2008; 2010; 2014), which emphasizes the general principle of miRNA function that miRNAs have far-reaching effects on gene expression, and their effects cannot be narrowly assigned to the regulation of a single gene or even a single pathway. miRNAs with pronounced effects on the cell typically achieve these effects by regulating many genes from diverse pathways (Le et al., 2011).

The miR-17-92 cluster encodes 6 miRNAs, most of which have been attributed oncogenic effects. The cluster itself is located near a fragile site, which is subject to rearrangements in some cancers (Calin et al., 2004), and is under the transcriptional control of the proto-oncogene *MYC* (He et al., 2005; Mestdagh et al., 2010). Activation of this miRNA cluster mediates the widespread downregulation of gene networks associated

with MYC-induced apoptosis(Mestdagh et al., 2010; Chen et al., 2011; Mu et al., 2009). Mechanistically, miR-17-92 upregulation by MYC promotes tumorigenesis by attenuating the apoptotic response to MYC overexpression.

1.4.3.3 MiRNAs in the p53 network

As mentioned in §1.2.2, mutation of the tumor suppressor gene p53 is a genetic characteristic of many colorectal adenocarcinomas and is thought to be a key step in the progression from adenoma to carcinoma. A majority of the downstream effects of p53 activation are mediated through its intrinsic function as a transcription factor that regulates the expression of a wide variety of genes (Menendez et al., 2009; Riley et al., 2008). The cellular effects of p53 are partly mediated by its ability to upregulate antiproliferative and proapoptotic genes such as p21 (G1 arrest), 14-3-3σ (G2 arrest) and PUMA (apoptosis). Interestingly, p53 also suppresses the expression of numerous genes (Menendez et al., 2009) including those involved in regulation of cell proliferation (McKenzie et al., 2010; Spurgers et al., 2006) and apoptosis (Murphy et al., 1999). At the transcriptomic scale, the p53 transcriptional response involves both activation and repression of hundreds of genes. In addition to direct effects of p53 on the promoters of protein-coding genes, p53 activation has recently been shown to modulate the expression of miRNAs, which in turn, can dampen the expression of hundreds of proteins (Hermeking, 2012; Jones and Lal, 2012). The miRNAs upregulated by p53 could provide an attractive mechanism to explain post- transcriptional inhibition of gene expression upon p53 activation. Such a mechanism may be particularly important during the stress response since it does not require the translation of effector proteins and may facilitate

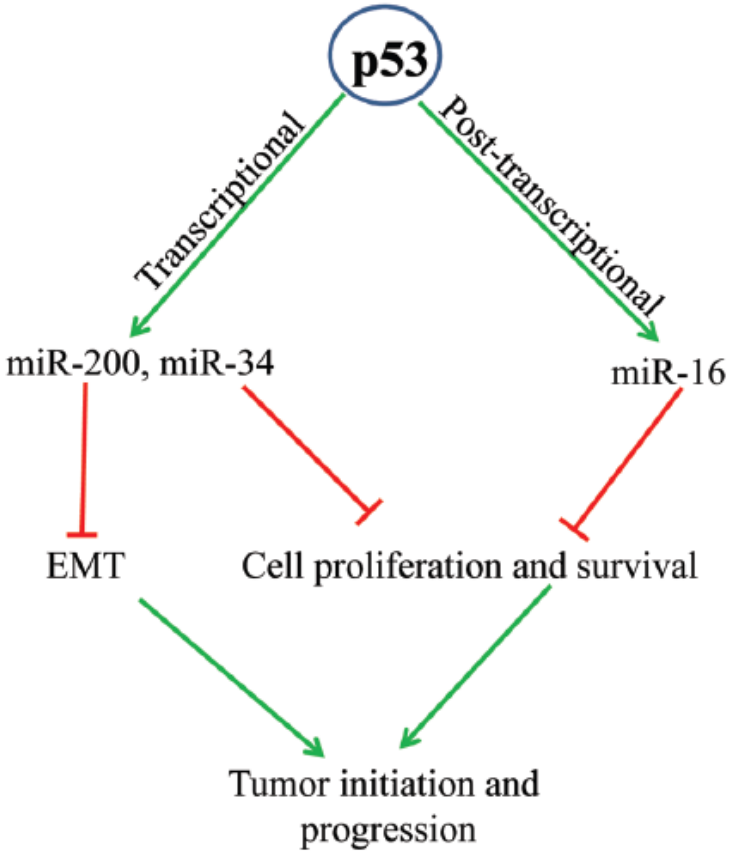

Figure 1.4
Regulation of miRNA biogenesis by p53
p53 enhances the expression of miRNAs including miR-200, miR-34 and miR-16. During DNA damage, p53 transcriptionally activates miR-34 family and post-transcriptionally upregulates miR-16. These miRNAs, inhibit the expression of several genes involved in cell proliferation and survival. Basal p53 levels can also regulate miRNAs such as the miR-200 family to inhibit EMT. By inducing miRNAs, p53 can exert its tumor suppressive function to inhibit tumor initiation and progression. This figure is adapted from Jones and Lal, 2012.

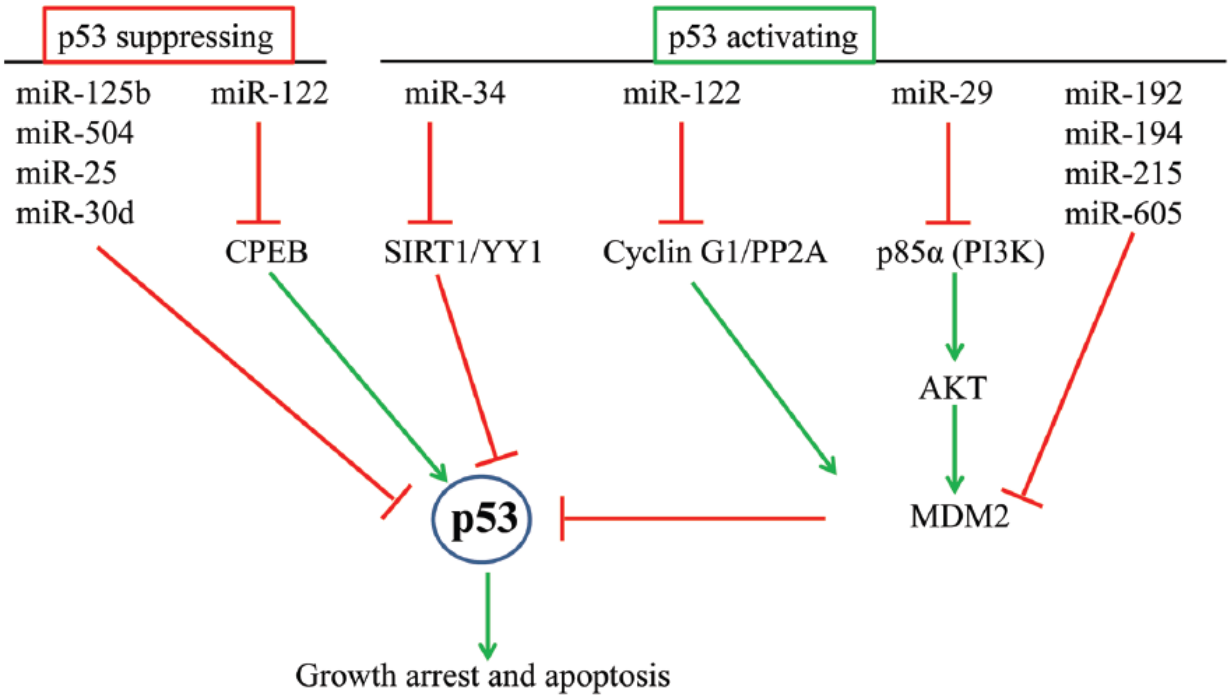

Figure 1.5
Post-transcriptional regulation of p53 by miRNAs
p53 is, itself, regulated by several miRNAs. miR-125b, miR-504, miR-25 and miR-30d directly bind to the 3'UTR of p53 mRNA and inhibit its expression. In fibroblasts, miR-122, inhibits CPEB leading to decreased p53 mRNA translation. In liver cells, miR-122 inhibits cyclin G1 3'UTR and upregulates p53 levels via decreased MDM2. miR-34, miR-192, miR-194, miR-215, miR-605 and miR-29 regulate the regulators of p53 to indirectly activate p53. This figure is adapted from Jones and Lal, 2012.

regulation of numerous processes by p53. There is an extensive literature on the roles of p53 in regulating miRNA expression and the contribution of miRNAs to tumor suppression and carcinogenesis. We illustrate several prominent examples in **Figure 1.4**. and **Figure 1.5**. For further information regarding these pathways and other cancer-associated miRNAs, the reader is referred to several excellent reviews on the topic: Hermeking, 2012; Ameres and Zamore, 2013; Kasinski and Slack, 2011; as well as the author's own review, Jones and Lal, 2012.

1.4.4 Experimental tools for the study of miRNAs

1.4.4.1 Synthetic miRNA mimics

A common approach for studying miRNA is to conduct gain-of-function experiments using transient transfection of synthetic miRNA mimetic molecules consisting of RNA with proprietary chemical modifications improve stability in the cell. These so-called miRNA mimics are transiently transfected into cells using simple cationic lipid chemistry (Luo and Saltzman, 2000). Some recent developments have even allowed this technique to be used to introduce mimics into mouse tissues *in vivo* by injection of a mimic:lipid emulsion (Trang et al., 2011). These methods allow for rapid assessment of transcriptomic and proteomic alterations in response to miRNA overexpression by targeted qRT-PCR or western blot or by high-throughput transcriptomic or proteomic profiling methods such as microarray or stable isotope labeling by amino acids in cell culture followed by mass spectrometry (SILAC-MS). Moreover, these methods can be combined with common functional assays to inform conclusions about the effects of

expression of a given miRNA on cellular processes such as proliferation, invasion, apoptosis, clonogenicity, etc.

However, there are several caveats that must be applied to studies undertaken with miRNA mimics: the level of mimic present in a cell after transfection may not accurately recapitulate physiological levels of miRNA expression (Thomson et al., 2013), and miRNAs often have acutely context dependent functions and operate in certain stimulus-response (e.g. following DNA damage or hypoxia) systems which are not easily captured by a simple over-expression experiment (Leung and Sharp, 2010). Experiments using miRNA mimics should be carefully controlled to ensure that these methodological shortcomings to not lead to spurious conclusions(Barreau et al., 2006). Furthermore, transfection of double-stranded miRNA mimics or siRNAs into human cells can have the unintended consequence of activating interferon signaling, as dsRNA is sensed by the cell as a sign of viral infection (Karpala et al., 2005). Care must be taken that biological miRNA mimics and non-specific mimics are of the same size and are both double stranded to control for non-specific interferon responses.

1.4.4.2 miRNA target identification

Integrative analysis of transcriptomic and proteomic profiling following miRNA overexpression combined with bioinformatics analysis of miRNA-mRNA seed matches may be used to predict potential direct targets of miRNA-mediated repression (Thomas et al., 2010). One of the most commonly used miRNA target prediction algorithms is TargetScan, which weights miRNA-mRNA seed matches according to their evolutionary

conservation, under the assumption that well-conserved matches imply functionally relevant target pairings (Lewis et al., 2005). Although TargetScan is notorious for the number of false positives it yields, the frequency of false negative results is more troubling. Other algorithms may be used to supplement TargetScan predictions, foremost among them RNA22 and PITA (Kertesz et al., 2007; Miranda et al., 2006). These programs predict the thermodynamic favorability of the formation of a given miRNA-mRNA duplex, and comparison of their predictions with those of TargetScan often gives a more realistic, though still imperfect, set of prospective miRNA targets which may then be biochemically validated.

When a list of candidate miRNA-mRNA target pairs has been generated, it is necessary to confirm that the repression of the mRNA target is due to a direct seed interaction between the miRNA and the mRNA 3'UTR. The standard method to test this interaction involves creating a chimeric luciferase mRNA containing the 3'UTR of interest downstream of the luciferase open reading frame. Using standard dual-luciferase reporter techniques, repression of the 3'UTR by a miRNA is then read out as repression of luciferase activity (Thomas et al., 2010).

1.4.4.3 AntagomiRs and miRNA sponges

Conversely, the effects of miRNA loss of function may be assayed by knockdown using antisense oligonucleotides or with a so-called miRNA 'sponge' construct, consisting of a repeating array of miRNA-complementary sequences designed to specifically bind and sequester miRNA molecules. Antisense oligonucleotides, or 'AntagomiRs' operate by a

principle similar to that of siRNA (Horwich and Zamore, 2008), yet in practice they often result in insignificant reduction of mature miRNA levels. Sponges, on the other hand, aim to stably sequester mature miRNA molecules, or "sponge" them away from their mRNA targets (Ebert et al., 2007). The principle of the sponge is described in greater depth in chapter 4 of this thesis.

There is thought to be considerable redundancy in miRNA networks. This redundancy, combined with the relative inefficiency of the available knockdown methods, means that strong loss-of-function effects remain elusive for many miRNAs. There exist knockout mice for several miRNAs (Park et al., 2010), and new targeted genome editing methods such as TALENs and CRISPR are beginning to be employed to knock out miRNAs in cell lines (Kim et al., 2013). Whether these deletion models for loss-of-function yield more pronounced effects, on aggregate, than post-transcriptional knockdowns remains to be seen.

1.4.4.4 Argonaute immunoprecipitation

A crucial assumption of the forgoing methods is that any exogenous miRNAs experimentally introduced into a cell are incorporated into the proper cellular compartments and participate in the RNA induced silencing pathway in the same manner as endogenous miRNAs. One method that we and others have used to test this assumption is pulldown of the miRNA-RISC complex through the immunoprecipitation of Argonaute 2 (AGO2). Enrichment of the transfected miRNA in the immunoprecipitate implies physiological incorporation of the mimic into RISC. This method has been

expanded to sequence all RISC-associated miRNAs, via high-throughput sequencing after cross-linking immunoprecipitation (HITS-CLIP), which provides a snapshot of all active functionally active miRNAs at a given time point. An exciting new improvement on the HITS-CLIP technique was recently reported, in which an intermolecular ligation step covalently joins miRNA-mRNA duplexes. Sequencing these miRNA-mRNA chimeras allows for unambiguous, high-throughput identification of miRNA target interactions (Grosswendt et al., 2014).

1.5 Summary and Aims

Recent studies have used high-throughput RNAseq or microarrays to identify miRNAs with heterogeneous expression patterns among tumor cell subpopulations (Zhang et al., 2011). The functional relationship between miRNAs and cancer stem cells however, remains unexplored, especially in the context of colorectal cancer. By identifying the miRNAs involved in cancer stem cell biology and the genes and pathways they regulate, we hope to gain new insights into the molecular mechanisms that govern the initiation and progression of colorectal cancer itself.

In colorectal cancer, CDX1 expression is often lost due to promoter methylation (Pilozzi et al., 2004; Suh, 2002; Wong et al., 2004), and substantial *in vitro* evidence indicates tumors expressing CDX1 are more well-differentiated and less aggressive than tumors with silenced CDX1 expression (Yeung et al., 2010; Chan et al., 2009). Previous research

suggests that CDX1 directly regulates the expression of a number of factors involved in intestinal development and is important for patterning of the differentiated epithelium well as mediating intestinal metaplasia in other tissues (Meyer and Gruss, 1993; Mutoh et al., 2004; Wong et al., 2005). However, there is very little information regarding the miRNAs regulated by CDX1 and how miRNAs contribute to the effects of CDX1 on differentiation in the normal colon or in colorectal cancer.

Broadly put, the goal of the research set out in this thesis is to characterize transcription factor-miRNA networks in colorectal cancer and how they regulate cancer stem cells, proliferation, and differentiation. Specifically, we have pursued the following projects to further this investigation:

1. Profile differential expression of miRNAs in response to CDX1 to identify CDX1-regulated miRNAs.

2. Identify miRNAs directly regulated by CDX1.

3. Elucidate the transcriptomic effects of the CDX1-regulated miRNA miR-215.

4. Evaluate the contribution of miR-215 to differentiation in colorectal cancer cell lines and mechanistically connect the functional consequences of miRNA expression downstream of CDX1 to specific miRNA-mRNA target interactions.

5. Characterize the phylogenetic conservation, upstream regulation, and downstream function of a novel miRNA in the p53 network: miR-3189.

CHAPTER TWO

Materials and Methods

CHAPTER 2: MATERIALS AND METHODS

2.1 Reagents and Suppliers

Chemicals and reagents not included in a standard kit or protocol were obtained from Sigma Aldrich (UK and US) unless otherwise indicated. Cell culture flasks and dishes were supplied from Corning (USA). Tissue culture medium and supplements, including antibiotics, were supplied from Gibco Invitrogen (USA), unless otherwise stated. Restriction enzymes and buffers and ligation reagents were supplied from New England Biolabs (Ipswich, Massachusetts, USA). When a pre-assembled kit was used for a method, all subsequently referenced materials were contents of the kit provided by the named manufacturer unless specifically noted otherwise.

2.2 Cell Culture Methods

2.2.1 Cell lines

The human colorectal cancer cell lines C10, C80, COLO201, DLD1, HCT116, HCT116-CDX1, HCT116-Vec, HCT116-p53KO, LIM1863, LS174T, LS174T-siCDX1, LS174T-Vec, LS180, SW480, SW620, and SW1222 were, for the purposes of this thesis, obtained from cryogenic storage of the Cancer and Immunogenetics laboratory (CIL) at the Weatherall Institute for Molecular Medicine (WIMM), Oxford, UK. The C80 cell line was originally established by David Bicknell of the CIL. The HCT116-CDX1, HCT116-

Vec, LS174T-siCDX1, and LS174T-Vec stable cell lines were derived from the parental cell lines HCT116 and LS174T, respectively, by Carol Chan during her doctoral work at the CIL. The SW1222 cell line was originally a gift from Meenhard Herlyn of the Wistar Institute. The remaining cell lines were originally procured from the American Type Culture Collection (ATCC) (Manassas, Virginia, USA), the Deutsche Sammlung von Mikroorganismen und Zellkulturen, GmbH (DSMZ) (Braunschweig, Germany), or the European Collection of Cell Cultures (ECACC) (Salisbury, UK).

2.2.2 Two-dimensional cell culture conditions

All cells were grown in regular-attachment, cell-culture-treated, vented 75cm^2 Corning flasks or 10 cm dishes with 10mL medium. Although tradition holds that some cell lines require specialized media, unpublished work from the CIL has shown that, with very few exceptions, maintaining cell lines in uniform conditions does not noticeably affect their growth or behavior. Therefore, all cell lines were grown in Dulbecco's modified Eagle medium (DMEM), supplemented with 10% fetal calf serum, 1% L-glutamine, and 1% Penicillin/Streptomycin. The stably transfected HCT116-vector, HCT116-CDX1, LS174T-shRNA, and LS174T-vector cell lines were the product of previous work in the Bodmer lab, and were maintained in DMEM with 1mg/mL Geneticin (G418) selection. HCT116 p53-/- was obtained from Bert Vogelstein. LIM1863 grew as a cell suspension. All other cell lines mentioned here grew adhering to the cell culture surface.

2.2.3 Cell culture maintenance

All cells were maintained in culture at 37˚ and 5% CO_2. When adherent cells reached 70%-80% confluence as determined by visual inspection under a light microscope, they were washed with sterile PBSA, trypsinized with 1x trypsin/EDTA, resuspended in 10mL DMEM, and split into a new flask between 1:10 and 1:20 ratio depending on the cell line and purpose. The suspension cell line LIM1863 was passaged at such times as clumps of cells visible to the naked eye appeared in the medium. The clumps were disaggregated by vigorous pipetting with a 10 mL serological pipette, the cells were centrifuged for 5 minutes at 500 x g, the pellet was washed, and the cells were resuspended in 10 mL DMEM. 1 mL of the resuspended cells was then diluted into 10 mL of DMEM in a flask for continued culture.

2.2.4 Cell counting

Cells were routinely counted for experiments that demanded precise numbers of cells, such as colony formation, flow cytometry, or chromatin immunoprecipitation. Briefly, cells were washed, trypsinized, and resuspended in DMEM. 100 µL of cell suspension was mixed with 10 µL of trypan blue dye to exclude dead cells from the count. 20 µL of the cell-trypan blue mixture was then loaded into a disposable plastic cell-counting chamber, and inserted into a Cellometer Auto T4 (Nexelcom Biosciences, USA) or TC20 Automated Cell Counter (Bio-Rad, USA). Images were then taken from eight areas

across the cell counting chamber, averaged, and the number of cells was calculated as cells per milliliter.

2.2.5 Cryopreservation and retrieval of cell lines

Cell cultures were routinely frozen and stored in a cryogenic freezer in the gas-phase of liquid nitrogen at -150˚C. After standard washing and trypsinization, 1 million cells were resuspended in freezing medium (fetal bovine serum, 10% dimethyl sulfoxide) and dispensed into a cryopreservation vial. The vial was then frozen for 1 hour on dry ice or submerged in isopropanol (2-propyl-acohol) and cooled at -80˚C for 1 hour, after which the frozen vial was transferred to a CBX 40 cryogenic freezer (Wessington Cryogenics, Houghton le Spring, UK) for long-term storage. Cells were retrieved from cryogenic storage and transported on dry ice. They were rapidly thawed in a 37˚ water bath, then diluted 1:10 with DMEM and incubated overnight in a T75 flask (Corning). Medium was changed the following day and cells were cultured as described above.

2.2.6 Three-dimensional cell culture

Colorectal cell lines were cultured in three dimensions in a 1:1 mixture of growth-factor reduced Matrigel^{TM} Basement Membrane Matrix (Corning, Tewksbury, Massachusetts, USA) and DMEM. Matrigel is a gelatinous mixture of collagen, laminins, various basement membrane proteins and growth factors secreted by the Engelbreth-Holm-

Swarm (EHS) mouse sarcoma cell line that is thought to recapitulate the composition of the extracellular matrix(Kleinman and Martin, 2005).

Matrigel was thawed and divided into 1 mL working aliquots. Aliquots of Matrigel were thawed at 4˚C overnight before seeding for 3-D culture. On the day of the experiment, prior to any cell manipulation, the 3-D culture vessel was pre-coated with Matrigel to prevent cells from sinking to the bottom and adhering to the surface of the plastic. 25 μL of undiluted Matrigel was dispensed and spread across the wells of a cell-culture-treated, normal attachment 96-well plate (Corning, USA) and incubated at least 30 minutes at 37˚C. Cells to be seeded were then washed, trypsinized, resuspended in DMEM and counted. Cell suspensions were then diluted to contain $2x10^4$ cells/mL. 80 μL of this cell dilution was mixed with an equal volume of Matrigel , and 50 μL aliquots of the 1:1 cell-Matrigel dilution were plated in triplicate into the pre-coated wells. The cell suspensions were allowed to solidify for 30 minutes at 37˚C, and then 150 μL DMEM were added atop the solidified Matrigel in each well. The 3-D cultures were incubated for two weeks in standard conditions, and the medium was changed every three days.

After two weeks, the colonies were fixed in 4% formaldehyde for 15 minutes, then the cells were permeableized with a 1% Triton-X100 (Fisher, USA) detergent solution. The colonies were washed three times with PBS and 150 μL of a 1:1000 dilution of phalloidin-TRITC conjugate (Life Technologies, USA) in PBS was added to the cells. In addition, 10 μL of DAPI was added to stain the nuclei. The cells were then incubated

overnight at 4˚C in the dark. After another wash with PBS, the cells were imaged on an Axio Vert inverted fluorescent microscope (Zeiss, Oberkochen, Germany).

2.2.7 5-Aza-2'deoxycytidine treatment

The DNA-methyltransferase inhibitor 5-aza-2'deoxycytidine was dissolved in a 1:1 mixture of acetic acid and water to a stock concentration of 5mM. The stock solution was filtered through a 0.22µm filter and stored at -20˚. Cells were seeded in a 75cm^2 flask with complete medium one day before 5-aza treatment. On day 2, the medium was removed, cells were washed with PBSA, and the medium was replaced with complete medium + 5µM 5-aza. The control flask was treated with an equal volume of acetic acid/water. This was repeated for 3 days, after which the cells were grown in complete medium without 5-aza for 24 h. The cells were then washed with PBSA and harvested using trypsin/EDTA.

2.2.8 Transient plasmid transfection

Plasmids were transiently transfected using the Lipofectamine LTX Plus reagents and protocol. 24 h prior to transfection, cells were seeded in a 24-well plate at a density between 1x10^5 and 3x10^5 cells/mL, depending on the cell line. DNA was diluted in 100µL/sample of serum-free OptiMEM medium. For the 2-vector promoter luciferase-reporter assay, 100ng reporter vector was co-transfected with 10ng control *Renilla* vector. For the single-vector psiCHECK2 3'UTR assay, 100ng was used per well. CDX1 and

miR-215 sponge transfections were routinely done scaled up to 6-well plates, where 1 μg of each was used per well. 1μL per sample of Plus reagent was added to diluted DNA. The DNA was then added to an equal volume of OptiMEM with Lipofectamine reagent added in a 1:20 ratio to the final volume. DNA/Lipofectamine complex was incubated for 5 minutes at room temperature, after which 100μL of DNA/Lipofectamine were added to each sample. Transfectants were incubated at 37˚ and 5% CO_2 for 24-72 h, depending on the downstream application.

2.2.9 Luciferase reporter assay

Luciferase reporter assays were carried out using the Dual-Luciferase® Reporter Assay System kit (Promega, USA). The work in this thesis makes use of three different reporter plasmids: pGL3 and pRL for promoter luciferase, and psiCHECK2 for 3'UTR luciferase. The construction of these plasmids is described below, and the protocol of the downstream assay is identical regardless of which plasmid set is used. The cell lines DLD1, HCT116, and HCT116 p53-/- were transiently transfected with the constitutively active *Renilla* luciferase-expressing vector pRL to control for transfection efficiency, and one of the 1.6, 1.0, 0.6, 0.4 and 0.2 kb miR-215 promoter constructs in the pGL3 Firefly luciferase-expressing vector, and the constitutively active CDX1-expressing vector pRC/CMV-CDX1. Alternately, chimeric *Renilla* luciferase-human 3'UTR construct in the psiCHECK2 vector was transiently transfected into HCT116.

24 h after transfection, media were aspirated, cells were washed with PBSA, and cells were lysed for 20 minutes, rocking at room temperature with 1x Passive Lysis Buffer. 20μL of lysate per sample were transferred to an opaque NUNC 96-well plate. The automated injection and detection system of the Fluostar Optima 2000 (BMG Labtech, Ortenberg, Germany) luminometer was used to inject 50μL of Luciferase Assay Reagent II into each well and detect firefly luminescence over the subsequent 13 seconds. The firefly reaction was quenched by addition of 50 μL Stop&Glo buffer, which concomitantly activates a *Renilla* luciferase reaction. *Renilla* luminescence was measured for a further 13 seconds. Finally, in the case of the pGL3-pRL system, firefly luminescence was normalized to *Renilla* for each sample to generate relative luminescence values. For psiCHECK2, *Renilla* is the reporter luciferase while firefly is the control, so the *Renilla* luminescence was normalized to firefly.

2.2.10 Transient miRNA mimic and siRNA transfection

Short RNA molecules, be they miRNA mimics or siRNAs, were typically introduced into cells *in vitro* by reverse transfection using Lipofectamine RNAiMax (Life Technologies, USA). Mimics were exclusively ordered from Dharmacon (GE Healthcare, USA). SiRNAs were ordered with pre-designed sequences from Eurofins (Eurofins MWG Operon, Luxembourg) or Qiagen (Qiagen, USA). The final concentration of each miRNA or siRNA transfection was 20nM in a total volume of 3mL per well in a 6-well plate. Starting with a 10 μM stock of miRNA mimic or siRNA, we diluted 1.5 μL into 150 uL serum-free Opti-MEM® (Life Technologies, USA). Meanwhile, 5 μL RNAiMax reagent

per well were diluted in 150 µL Opti-MEM per sample. Then 150 µL of the RNA-Opti-MEM solution was mixed 1:1 with the Lipofectamine RNAiMax solution in the cell culture vessel (6-well plate). After 5 minutes at room temperature, 500,000 cells were seeded into each well, and the final volume was adjusted to 3 mL with DMEM + 10% FBS.

2.2.11 Transwell Migration Assay

Following 24 h of transfection with miRNA mimics as described elsewhere, cells were washed and harvested by trypsinization. A Transwell insert (Corning, USA) consisting of a permeable membrane coated in a thin layer of Matrigel was submerged in 1mL complete DMEM+10% serum in the wells of a 12-well plate. After counting as described above, 1000 transfected cells were seeded in onto the upper surface of the Transwell insert in serum-free DMEM to induce migration to the bottom of the membrane.

2.2.12 Soft Agar Colony Formation Assay

After 48 h of transfection with miR-3189-3p, -5p, or control mimics, transfected cells were seeded in soft agar to assay tumorigenicity. Briefly, a 0.5% agar base layer was prepared by mixing molten 1% agar with an equal volume of complete DMEM+10% serum. The 0.5% agar was then added to the bottom of a 12 well plate and allowed to solidify at room temperature. Meanwhile, transfected cells were washed with PBS,

harvested with trypsin, counted and diluted to yield a suspension of 1000 cells/mL. 500 μL of this cell suspension were then mixed with 500 μL of molten 0.7% agar (temperature of molten agar should not exceed 40˚C to preserve cell viability), and 1 mL of the resulting mixture was added to each well coated with base layer. The agar was allowed to solidify at room temperature, and 0.5 mL of DMEM were overlaid on top of the agar. The cells were cultured in standard conditions for 2 weeks, and the medium overlay was changed every 3 days.

2.3 Animal methods

2.3.1 Xenograft assays

Animal protocols were approved by the National Cancer Institute Animal Care and Use Committee following AALAAC guidelines and policies. HCT116-p53WT and HCT116-p53KO cells were transfected with CTL or miR-3189-3p mimic for 36 h, then trypsinized and washed with PBS. $1x10^6$ cells were mixed with 30% Matrigel in PBS on ice and the mixture was injected into the flanks of 6-8 week old female athymic nude mice (Animal Production Program, Frederick, MD) (each group N = 10). Tumor volume was measured twice weekly after two weeks of injection and mice were sacrificed after 4 weeks.

2.4 DNA Methods

2.4.1 DNA cloning

2.4.1.1 Primer design

Primers for cloning were exclusively designed using NCBI PrimerBlast (http://www.ncbi.nlm.nih.gov/tools/primer-blast/) using standard settings. Specificity checking was set to query against the *Homo sapiens* genomic reference assembly. Quantitative real-time PCR primers were designed using the Integrated DNA Technologies (IDT) Real-Time PCR primer design tool (https://www.idtdna.com/scitools/Applications/RealTimePCR/). The specificity of the output primers was then confirmed using NCBI PrimerBlast.

2.4.1.2 Polymerase chain reaction

Standard end-point PCR was conducted in a total volume of 50 µL unless otherwise specified. The reaction mixture was composed of 25 µL Phusion Hi-Fidelity 2X Master PCR mix (New England Biolabs, Ipswich, Massachusetts, USA), 100ng template DNA, and 1 µL each 10 µM forward and reverse primer solutions. Standard PCR conditions involved an initial 3 minute denaturation step at 98˚C, then 30 cycles of the 3-step incubation: 98˚C for 10 second, 60-70 degrees for 30 seconds (annealing temp set 5 degrees below the primer melting temperature), and 72˚ for 30 seconds per kilobase of amplicon. Finally, the reaction was incubated at 72˚C for 10 minutes to ensure complete amplicon extension.

2.4.1.3 Restriction enzyme digestion

CDX1 promoter fragments and the pGL3 luciferase reporter vector backbone were digested with HindIII and Xho1 in NEB Buffer 2 plus bovine serum albumin (BSA) overnight at 37˚C. 3'UTR PCR products and the psiCHECK2 vector were digested with XhoI and NotI in NEB Buffer 3 plus BSA overnight at 37˚C. The miR-215 sponge insert was designed with SanDI complementary sticky ends that formed after oligonucleotide annealing, but the pMSCV-PIG-EV-PURO-IRES-GFP vector (Addgene, Cambridge, Massachusetts, USA) was digested with XhoI and EcoRI in NEB buffer 3 overnight at 37˚C to insert a SanDI linker. Then, the pMSCV-PIG-SandI construct was digested with SanDI (Thermo Scientific, Pittsburgh, Pennsylvania, USA) for 15 minutes at 37˚C in Fast Digest buffer (Thermo Scientific, USA). Unless otherwise noted, all enzymes and buffers were purchased from New England Biolabs (NEB), USA.

2.4.1.4 DNA Gel electrophoresis

After PCR and restriction enzyme digestion, DNA products were electrophoresed on 1-2% Agarose + Tris-Borate-EDTA Buffer (TBE), depending on the size of DNA fragments. The DNA samples were mixed with an appropriate amount of 6X orange loading dye and pipetted into the wells of the agarose gel. 10 μL of a 100 bp or 1 kb ladder was loaded as a reference (NEB, USA). The gel was then immersed in TBE buffer and subjected to a 100 volt electrostatic potential for 45 minutes, then stained in a solution of ethidium bromide diluted 1:1000 in TBE. The gel was imaged under *trans*-ultraviolet light.

2.4.1.5 DNA recovery and purification from agarose gel slices

After separation by agarose gel electrophoresis, DNA fragments were purified using the QiaQuick Gel Extraction Kit (Qiagen, USA). Briefly, the bands corresponding to the desired product were excised from the stained gel under UV light. The gel slices were weighed and immersed in a volume of the kit-supplied Buffer QG corresponding to 3 gel volumes (1mg gel = 3 µL buffer) and then incubated at 50˚C for 10 minutes or until the gel was completely dissolved. A volume of 100% isopropanol equivalent to the gel mass (1mg gel = 1 µL isopropanol) was then added to the solution. The gel-DNA solution was then applied to the upper chamber of a kit-supplied QiaQuick Spin Column and centrifuged for 30 seconds at maximum speed. The column was washed twice with Buffer PE and finally eluted in 35 µL of either water or Buffer EB. The concentration of DNA was then quantified on a Nano-Drop 2000 spectrophotometer (Thermo Scientific, USA).

2.4.1.6 DNA ligation

Gel purified, digested PCR products and vectors were ligated at a 3:1 molar ratio, as calculated using an online tool from the University of Dusseldorf (http://www.insilico.uni-duesseldorf.de/Lig_Input.html). The ligation reaction was performed in a 10 µL volume and was catalyzed by 1 µL T4 DNA Ligase in 1 µL 10XLigase Buffer (NEB, USA). The reaction was incubated for 8 h at room temperature.

2.4.1.7 Bacterial transformation

MAX Efficiency® DH5α™ chemically competent *E. coli* bacteria (Life Technologies, USA) were transformed according to supplier's instructions. 10 ng of plasmid DNA was mixed with 50 µL competent cells and incubated on ice for 30 minutes. The cell-DNA mixture was then heat-shocked in a 42˚C water bath for 45 seconds, followed by 3 minutes on ice. The cell-DNA mixture was then diluted into 250 µL Super Optimal broth with catabolite repression (SOC) medium (Life Technologies, USA) and transferred to a 37˚C shaking incubator for 1 hour. 200 µL of the diluted cell-DNA mixture was then spread on pre-warmed Luria Broth (LB)-Agar plates (made in-house) containing 100 µg/mL Ampicillin or 50 µg/mL Kanamycin, depending on the resistance cassette in transformed plasmid. Plates were then stored overnight at 37˚C. A toothpick was used to inoculate overnight LB-Ampicillin or LB-Kanamycin cultures with the resulting colonies.

2.4.1.8 Small scale plasmid purification

For diagnostic PCR, restriction analysis and sequencing, plasmids were purified using the Qiagen Miniprep kit (Qiagen, USA). Briefly, bacterial cell cultures were pelleted by centrifugation at 5000 x g for 5 minutes. Pellets were resuspended in 250 µL buffer P1 plus RNase A. The bacterial suspension was then lysed by addition of 250 µL buffer P2 and mixed by rapid inversion. The lysis reaction was neutralized after no longer than 5 minutes by the addition of 350 µL buffer N3, and cell debris was pelleted by centrifugation at 12,000 x g for 10 minutes. The supernatant was then applied to the upper chamber of a kit-supplied purification column followed by brief centrifugation at

maximum speed. The column was washed with 750 µL wash buffer PE, and the plasmid DNA was finally eluted in 35 µL water or EB elution buffer (tris-EDTA).

2.4.1.9 Large scale plasmid purification

For constructs needed in large quantities, or free of bacterial endotoxin for sensitive assays, the PureLink® HiPure Plasmid Midiprep kit was used (Life Technologies, USA). First, 200 mL of overnight bacterial culture was pelleted by centrifugation at 4000 x g for 10 minutes. The cell pellet was resuspended and homogenized in 10 mL R3 buffer with RNase A. The bacterial suspension was lysed by the addition of 10 mL lysis buffer L7 and mixed by inversion. After no longer than 5 minutes, the lysis reaction was neutralized by the addition of 10 mL precipitation buffer N3, and mixed by inversion. The cell lysate was then transferred to an equilibrated purification column and allowed to drain by gravity flow. The column was washed 50 mL wash buffer W8, and finally the DNA was eluted in 15 mL elution buffer E4. The eluate was then subjected to isopropanol precipitation.

2.4.1.10 Isopropanol precipitation of DNA

To a solution of DNA or RNA, 1 volume of 100% isopropanol was added. The solution was then centrifuged at max speed for 30 minutes at 4˚C. The supernatant was discarded and the DNA or RNA pellet washed with 70% ethanol. The pellet was allowed to air-dry for 10 minutes, and finally resuspended in EB buffer (DNA) or nuclease-free water (RNA).

Name	Sequence
RUNX1_UTRF1	TTAACTCGAGGGATCTCGCTGTAGGTCAGG
RUNX1_UTRR1	AATTGCGGCCGCAACACCTTGGAGAGAGGGTTC
EGR1_UTRF1	TTAACTCGAGCTTCCCCTTCCCCAATTACT
EGR1_UTRR1	AATTGCGGCCGCCCCAATCGCAGCTACTTTATTT
EFNB2_UTRF1	TTAACTCGAGGGACCCTGGTGGTACCTGT
EFNB2_UTRR1	AATTGCGGCCGCTTTTTAAGCGCTGAGCATTG
EREG_UTRF1	TTAACTCGAGCAAGTGCAGATTTGCTAGTGGA
EREG_UTRR1	AATTGCGGCCGCAGACGGAGTCTCGCTGTGTT
Dicer1_UTRF1	TTAACTCGAGTGACCAGTTAAAACAAAGCAATTC
Dicer1_UTRR1	AATTGCGGCCGCTTTACAGCAGAAAAGCCAGAAA
HOXA10_UTRF1	TTAACTCGAGCTGGTCCCCTCCCTCTGT
HOXA10_UTRR1	AATTGCGGCCGCGGTTTGACCCTTTTATGCATGT
BMI1_UTRF	GCATCTCGAGATGCCATTACAGCTTTCTAGATGC
BMI1_UTRR	GATGCGGCCGCCATCTTTCAATGGGCTTTCAAGC
215_pre_F1	TTCTAGAATTCCTT GGA CTC TCA TTT GAT TCC AGC
215_pre_F1	TTCTAGAATTCGTG GTC ACT TGG ACT CTC ATT TG
215_5RACE_GSP	TGGGATGACAGCAGTCGTTTCTTTGTTG
Human-pri-miR-3189 FPEcoR1	ACGTGAATTCAGAAGGTAAGTGAAATCTTAGA
Human-pri-miR-3189 RPNot1	ACTAGCGGCCGCTGTGCACATTCAGGAGGGTCCC

Table 2.1
Primer sequences used for cloning and 5' RACE

2.4.1.11 Sanger sequencing

The nucleotide sequence of cloned DNA was confirmed by Sanger DNA sequencing. Where applicable T7 sequencing primers were used to sequence from the vector backbone through the insert. Otherwise, the original PCR primers used to clone the insert were used as sequencing primers. Both forward and reverse reactions were routinely run for each clone. All sequencing was performed by the in-house Sanger Sequencing core facility at the Weatherall Institute for Molecular Medicine (Oxford, UK) or at the Center For Cancer Research Cancer Genomics Core at the National Cancer Institute (Bethesda, Maryland, USA).

2.5 RNA Methods

2.5.1 RNA isolation

Total RNA was isolated from cells using the MiRNEasy (Qiagen, USA) kit according to the manufacturer's instructions. RNA isolation was performed 1 doubling time after cells were seeded or 48 h following transfection. Cells were lysed in the culture dish (6-well plate) by the addition of 700 µL Qiazol lysis reagent. The lysate was then scraped into a microcentrifuge tube using a rubber policeman. The lysate was homogenized by vortexing for 1 minute and nucleoprotein complexes were allowed to dissociate by incubating at room temperature for 5 minutes. 140 µL chloroform were added to each sample and mixed by shaking for 15 seconds. After a 3 minute room-temperature incubation, samples were centrifuged at maximum RPM for 30 minutes at 4˚C to separate

organic and aqueous phases. The upper aqueous phase was removed and added to 550 µL 100% isopropanol. This mixture was then applied to the upper chamber of a kit-supplied spin column and centrifuged for 30 seconds at 12000 x g. The column was then washed sequentially with 750 µL buffer RWT and twice with 500 µL buffer RPE. Finally total RNA was eluted in 35ul of nuclease-free H_2O, aliquoted, and stored at -80˚. After each thaw, concentration and quality were assessed by Nano-Drop spectrophotometry.

2.5.2 RNA sequencing

After obtaining high-quality (determined by spectrophotometric ratios of 260 nm/280 nm and 260 nm/230 nm≥1.8 and validated on the Agilent Bioanalyzer platform) total RNA, RNA quality was further evaluated by the Agilent Bioanalyzer 2100 (Agilent, Santa Clara, California, USA). The 18-30 nt small RNA fraction was enriched from 10 µg total RNA by denaturing poly-acrylamide gel electrophoresis (PAGE). The gel-purified small RNA fraction was then ligated to 3' and 5' Illumina sequencing adapters. The adapter sequences were used as templates for reverse-transcription cDNA library synthesis. The cDNA library was then amplified by PCR for 12 cycles using adapter-specific primers, and the PCR products were purified by denaturing PAGE elution. Libraries were diluted to 8pM and washed over an Illumina Genome Analyzer II chip for cluster generation, and sequencing was carried out on the Illumina GAII platform (Illumina, San Diego, California, USA). The sequences of the ligated adapters were clipped from the reads and the subsequent trimmed data were analyzed using Burrows-Wheeler Aligner software package (http://bio-bwa.sourceforge.net/) (Li and Durbin, 2009). The coordinates of

known mature miRNAs were downloaded from miRBase (volume 18), and tag densities were counted and normalized over length of the mature miRNAs. RNAseq was performed in collaboration with Ashish Lal at the National Cancer Institute and Paul Meltzer at the National Human Genome Research Institute, both in Bethesda, Maryland.

2.5.3 miRNA Quantitative RT-PCR

For miRNA quantitation, 10ng of high-quality total RNA was reverse transcribed using the Applied Biosystems TaqMan (Life Technologies, USA) protocol and reagents. qPCR was performed using pre-designed, manufacturer-validated TaqMan probes for the given miRNA. For each sample, we prepared 1.2 volumes of RT master mix, consisting of 0.15 μL 100 mM dNTPs, 1 μL (50 Units) MultiScribe^{TM} Reverse Transcriptase, 1.5 μL 10x Reverse Transcription Buffer, 0.19 μL RNase Inhibitor, and 4.16 μL Nuclease-free water. We then combined 7 μL master mix with 5 μL of 2 ng/μL total RNA and 3 μL 5X TaqMan RT primer mix. The samples were incubated in a thermal cycler programed for 16˚C for 30 minutes, 42˚C for 30 minutes, and finally 85˚C for 5 minutes. cDNA was used directly for qRT-PCR by adding 1.33 μL RT product to a PCR mix containing 1.00 μL TaqMan Small RNA Assay (20X), 10 μL TaqMan Universal PCR Master Mix II 2X, and 7.67 μL nuclease-free water. The samples were loaded in triplicate into a 96-well plate, and the plate was sealed with optical adhesive film (Life Technologies, USA). Real-time PCR was then performed on an Applied Biosystems 7500 thermal cycler (Life Technologies, USA) using pre-programed TaqMan conditions. Ct data were analyzed using the ΔΔCt method to calculate an RQ (relative quantity) value relative to some

reference sample(s). For miRNA quantitation, samples were normalized to U6 snRNA expression.

2.5.4 mRNA quantitative RT-PCR

mRNA quantitation was performed using 1 µg of total RNA as input, and reverse transcription was carried out using the iScript™ Reverse Transcription Supermix (Bio-Rad, Hercules, California, USA) kit with oligo-dT primers. The mixture was incubated in a thermal cycler using the protocol: 25˚C for 5 minutes, 42˚C for 30 minutes, and 85˚C for 5 minutes. First strand cDNA was used for qPCR with specific custom-designed primers for the gene of interest using SYBR® Green Master Mix (Life Technologies, USA). 0.1 µL of RT-reaction product was added to 3 µL of 2.5 µM forward and reverse primer mixture, 4.8 µL nuclease-free water, and 7 µL SYBR Green Master Mix. The samples were then loaded into a 96-well qPCR plate (Life Technologies, USA) and sealed with optical adhesive film (Life Technologies, USA). qRT-PCR was then performed on an StepOnePlus™ thermal cycler (Life Technologies, USA) using standard 2-step SYBR Green qPCR settings. Automated primer melting curve analysis was also performed to verify primer specificity. mRNA Ct values were normalized to *UBC* or *GAPDH* expression and fold change was calculated relative to a reference sample using the ΔΔCt method.

Name	Sequence
BIRC5_RTF	CTTCATCCACTGCCCCAC
BIRC5_RTR	ACTTTCTCCGCAGTTTCCTC
CCNB1_RTF	GGCTTTCTCTGATGTAATTCTTGC
CCNB1_RTR	GTATTTTGGTCTGACTGCTTGC
CCNB2_RTF	CAAAAGCCGTCAAAGACCTTG
CCNB2_RTR	GGTTTCATGAGATAGACCAGAGG
CDKN2A_RTF	GATGTCGCACGGTACCTG
CDKN2A_RTR	TCTCTGGTTCTTTCAATCGGG
CDKN3_RTF	ACAATATCACCAGAGCAAGCC
CDKN3_RTR	GCAGCTAATTTGTCCCGAAAC
RUNX1_RTF	CCAGGTTGCAAGATTTAATGACC
RUNX1_RTR	TTTTGATGGCTCTGTGGTAGG
CDC20_RTF	GATGTAGAGGAAGCCAAGATCC
CDC20_RTR	AAGGAATGTAACGGCAGGTC
CDC25A_RTF	TGTTGAAGAGACCAGAACGATC
CDC25A_RTR	GGGAAGATGCCAGGGATAAAG
CENPA_RTF	CAAAGGATGTGCAACTGGC
CENPA_RTR	CATTGGATCTAGTCATGGCTCTG
CENPN_RTF	AGTTCAGCACTTGATCCATCTG
CENPN_RTR	CACCTGGTCCTTTACTCATCTG
JUND_RTF	CCTCAGCCACGTCAACAG
JUND_RTR	CACCCTCTCCAAGTCCG
EFNB2_RTF	GAATTCAGCCCTAACCTCTGG
EFNB2_RTR	ATCTTCATGGCTCTTGTCTGG
CEACAM1_RTF	ACAAACCCTCAGTCTCCAAC
CEACAM1_RTR	TTTCTGTGGCTGTTAGGGATG
CDX1_RTF	AGCCGTTACATCACAATCCG
CDX1_RTR	GTTCACTTTGCGCTCCTTTG
BMI1_RTF	CTTTCATTGTCTTTTCCGCCC
BMI1_RTR	AAGTACCCTCCACAAAGCAC
ERBB3_RTF	ACTTTTCTCTACTGGCGTGG
ERBB3_RTR	TTCCTTAGCTCTGTCTCTTTGAAG
p21 FP	GACTCTCAGGGTCGAAAACG
p21 RP	GGATTAGGGCTTCCTCTTGG
RCHY1 FP	TTTGACAAAGATAAGAAGCAGTATCA
RCHY1 RP	TCGGGACACATTTTCAATACA
p53R2 FP	CAAGGACGACGCTTGGAG
p53R2 RP	ACCGGCGAGAACTCTTTCTT
GADD45G FP	CTCACTGCCGGCGTCTAC
GADD45G RP	GATGTCGCCCTCGTCCTC
Scotin FP	CTCCTTACAACCCGGCCTAC

Scotin RP	ACTCACGCACACACACAACA
NOXA FP	AAGAAGGCGCGCAAGAAC
NOXA RP	TTCTGCCGGAAGTTCAGTTT
CD44 FP	ACTGCAAATCCAAACACAGG
CD44 RP	TGTCAGAGTAGAAGTTGTTGGATG
GNAI2 FP	CATCATGGCCATTGTCAAA
GNAI2 RP	GGTGCAGGACAGTGCAAATA
LANCL1 FP	TCCCGAATCCTTATGCTGAT
LANCL1 RP	GAAGCTCCCGAATCTTATTGG
CDC23 FP	CTCTCCCTGCATTGCCTCT
CDC23 RP	GTGCTGCCCGATCATACTCT
CDC25A FP	TTTCATACAGTTGCTGGGAAAC
CDC25A RP	GATGTGGCCTCCCTCGTAT
RAD21 FP	CCTCAGGGAGTTAAGCGAAA
RAD21 RP	TGGCAGAAGTTCTAACTCTGGTATT
BTRC FP	TGACAAGTACATTGTTTCTGCATC
BTRC RP	ATGCCTCGTTTGTGTCCATT
FOXM1 FP	GCCAACCGCTACTTGACATT
FOXM1 RP	GATTCGGTCGTTTCTGCTGT
UBE3A FP	GCACTTGTCCGGCTAGAGAT
UBE3A RP	CTCCCTCATCAACTCCTTGTTC

Table 2.2
Primer sequences used for qRT-PCR

2.5.5 Microarray gene expression analysis

HCT116 cells were reverse transfected in triplicate with miR-215, miR-3189-3p or control (cel-miR-67) mimics (Dharmacon, USA) as described above. After 48 h, total RNA was isolated as described above. Microarray samples were labeled using the Illumina® TotalPrep™ RNA amplification kit (Ambion, USA). All steps were performed with reagents included in the kit, and the lengthy protocol is summarized here.

2.5.5.1 In vitro transcription

First ten micrograms of RNA are diluted into 11 µL nuclease-free water. Then 9 µL of Reverse Transcription Master Mix are added and the mixture is incubated 2 h at 42˚C. Then, second strand cDNA is synthesized by adding 80 µL Second Strand master mix to each sample, and the samples are incubated for 2 h at 16˚C. The cDNA is then purified by mixing with 250 µL cDNA Binding Buffer and passing the diluted cDNA through a cDNA filter cartridge. The filter is washed with 500 µL wash buffer and the cDNA is then eluted in 20 µL nuclease-free water. To synthesize biotinylated cRNA by *in vitro* transcription, 7.5 µL of IVT Master Mix is added to each sample, and the samples are incubated overnight at 37˚, then 75 µL water is added to each sample. Finally, the cRNA is mixed with 250 µL ethanol and 350 µL cRNA Binding Buffer and passed through a cRNA filter cartridge. The filter is washed and the cRNA is eluted with 200 µL Nuclease-free water.

2.5.5.2 Direct Hybridization Assay

Gene expression was determined from comparative cRNA hybridization using the Illumina Direct Hybridization assay. First, the cRNA is heated to 65˚ for 5 minutes, then combined with 10 μL HYB buffer. The BeadChip Hyb Chamber (hybridization chamber) is then assembled according to manufacturer's instructions. The samples are then loaded into the inlet port of the BeadChips. The chips are then hybridized by incubation at 58˚ for at least 14 h but not longer than 20 h. After this incubation, the bead chips are removed from the hybridization chamber and washed sequentially in 55˚C wash buffer, room-temperature E1BC buffer, 100% ethanol, and finally E1BC again. The chip is dried and blocked with Block E1 buffer for 10 minutes. Finally, the signal is detected by the addition of Cy3-Streptavidin followed by scanning on the Illumina iScan Reader (Illumina, USA).

2.5.5.3 Data analysis

Low-level microarray analysis was performed in collaboration with Yeulin Zhu in Paul Meltzer's laboratory at the National Cancer Institute. Data were analyzed using the Bioconductor package in the R statistical programing environment (Bioconductor, Seattle, USA).

2.5.6 5' Rapid amplification of cDNA ends (RACE)

In order to prolong the half-life of primary miRNA transcripts, before conducting the RACE experiment we began by knocking down Drosha in LS174T using small-

interfering RNA transfection (see section 2.2.10). 48 h after siDrosha transfection, total RNA was isolated per standard protocol (see section 2.4.1), and 5'RACE was carried out using the SMARTer RACE kit (Clontech Laboratories, Mountain View, California, USA). See **Figure 2.1** for a schematic of the proprietary SMARTer RACE workflow. Briefly, first-strand cDNA was synthesized using kit-provided oligo-dT primers, SMARTScribe Reverse Transcriptase, and the SMARTer IIA oligo. Reactions were incubated at 42˚C for 90 minutes followed by 70˚C for 10 minutes. The cDNA samples were then diluted into 200 µL tricine:EDTA buffer.

To amplify the 5' cDNA end, 2.5 µL cDNA was used as template for a 50 µL PCR reaction using the supplied UPM universal primer mix and a gene specific primer (**Table 2.1**). The remainder of the reaction mix was composed of the components of the Advantage 2 Polymerase kit (Clontech, USA). PCR products were electrophoresed on a 2% agarose gel and bands were excised, purified, and sequenced directly without cloning using the internal gene specific primer (GSP).

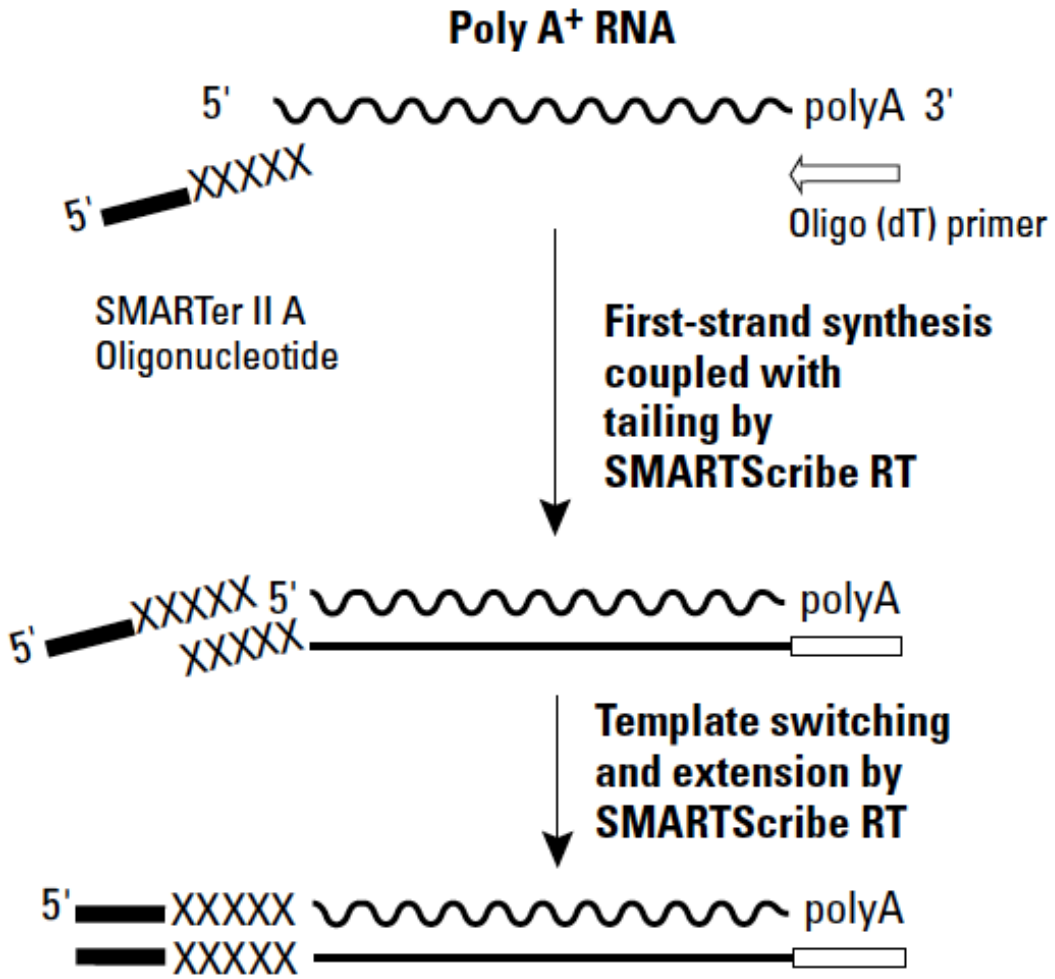

Figure 2.1
Outline of the SMARTer™ RACE system
Figure adapted from SMARTer RACE cDNA Amplification Kit User Manual, Clontech 2012.

2.6 Protein methods

2.6.1 Preparation of protein lysates

Cells were manipulated as necessary for transfection, doxorubicin treatment, etc. and cultured in 6-well plates. After the desired time course, usually 48 h after treatment, medium was aspirated and cells were placed on ice. The cells were then washed twice with cold PBSA. During the wash steps, lysis buffer was prepared by diluting 10x radioimmunoprecipitation assay buffer (RIPA) (Millipore, Billerica, Massachusetts, USA) into water and adding an appropriate amount of 100x protease inhibitor cocktail (Sigma Aldrich, St. Louis, Missouri, USA). To each well, 125 µL diluted lysis buffer was added, and the cells were scraped into a microcentrifuge tube using a rubber policeman. The lysates were incubated on ice for 30 minutes, then centrifuged at maximum speed in a bench-top microcentrifuge for 30 minutes at 4˚C. The supernatant was transferred to a fresh tube and the pellet was discarded.

2.6.2 BCA assay

Protein concentration of cell lysates was determined using a bicinchoninic acid colorimetric assay (Thermo Scientific, Rockville, Illinois, USA). In principle, peptide bonds reduce a cupric sulfate solution, from which the resultant cuprate cations chelate bicinchoninic acid to yield a vividly purple compound. The intensity of the color is directly related to the amount of protein in the solution. To calibrate the assay, a standard

curve is prepared by serially diluting kit-supplied pure bovine serum albumin. In the wells of a transparent 96-well plate, either 20 μL of each standard concentration or sample were dispensed in duplicate. A BCA™ working reagent was then prepared by combining 50 parts of BCA™ solution A with 1 part of BCA™ solution B. To each standard or sample well, 200 μL of working reagent was added. The plate was then incubated at 37˚C for 30 minutes, and absorbance at 562 nm was measured by a spectrophotometric plate reader (μQuant, BioTek Instruments, USA). The absorbance values were plotted against the concentration of the BSA standards and fitted by least-squares linear regression. The protein concentration of unknown samples were then calculated from the standard curve.

2.6.3 Antibodies

Dilutions and sources of antibodies are listed in **Table 2.3**. Secondary antibodies were purchased from Dako (USA) or Cell Signaling (USA). Antibody dilutions and blocking media were optimized as needed.

Antibody	Source	Dilution	Secondary Antibody	Secondary dilution
CDX1 mAb	In house	1:2,000	RAM	1:5,000
Ago2 mAb	Cell Signaling	1:5,000	RAM	1:5,00
p53(DO-1) mAb	Santa Cruz	1:10,000	RAM	1:10,000
CCNB1(1B10) mAb	Sigma Aldrich	1:5,000	RAM	1:5,000
p21(C19) mAb	Santa Cruz	1:10,000	GAR	1:5,000
GAPDH(14C10) mAb	Cell Signaling	1:10,000	GAR	1:10,000
β-Actin(4967) mAb	Cell Signaling	1:1,000	GAR	1:1,000
β-Tubulin(6046) mAb	Cell Signaling	1:2,000	GAR	1:5,000
BMI1(2830) mAb	Cell Signaling	1:20,000	GAR	1:10,000

Table 2.3
Antibodies and dilutions
RAM= Rabbit-anti-mouse, GAR= Goat-anti-rabbit; mAb= monoclonal antibody

2.6.4 Western immunoblot

2.6.4.1 SDS poly-acrylamide gel electrophoresis

The Bio-Rad Mini-PROTEAN® Tetra Cell electrophoresis unit (Bio-Rad, USA) was used to separate and analyze proteins. To denature protein samples, 10 µg protein was mixed with 2X Protein Loading Buffer (National Diagnostics, Charlotte, North Carolina, USA) and incubated at 98˚C for 10 minutes. The denatured samples and 6 µL pre-stained rainbow size marker (Bio-Rad, USA) were loaded into the wells of a 4% acrylamide stacking gel cast atop a 10% acrylamide resolving gel. The samples and standard were electrophoresed for 90 minutes under an electrical potential of 100 V or until the bromophenol blue loading dye had reached the bottom of the gel. After electrophoresis, the gel was removed and briefly rinsed in transfer buffer.

2.6.4.2 Immunoblotting

For immunoblotting, the proteins were transferred from the polyacrylamide gel to a Hybond-P PVDF membrane (GE Healthcare, Little Chalfont, UK). The membrane was activated in 100% methanol for 1 minute and then submerged in transfer buffer for 15 minutes. Transfer was carried out under semi-dry conditions for 1 hour at 15 V using a Trans-Blot® SD semi-dry transfer cell (Bio-Rad, USA). The membrane was then blocked in 5% milk or BSA in TBST for 1 hour at room temperature. Primary antibody incubation was carried out with the dilutions specified in **Table 2.3** overnight at 4˚C. The membrane was then washed thrice with TBST for 10 minutes, followed by incubation with the appropriate secondary antibody-HRP conjugate. Generally, secondary antibody

incubation was carried out with a 1:5000 dilution in TBST+5% milk for 1 hour at room temperature. After a 3X wash with TBST, the membrane was developed using enhanced chemiluminescence via an ECL Prime Western Blotting Detection kit (GE Healthcare, UK). Briefly, a 1:1 mixture of solutions 1 and 2 was added to the membrane and incubated at room temperature for 5 minutes under protection from sunlight. Finally, autoradiography film was exposed to the membrane to reveal protein bands.

2.6.5 Immunoprecipitation

For immunoprecipitation of Ago2 ribonucleoprotein complexes, we used a modified version of the protocol described by Easow, *et al*. (Easow et al., 2007) and elsewhere. Cells were washed and lysed in a similar manner to §2.5.1, except that RIPA buffer was prepared using nuclease-free water. Lysis proceeded as described in §2.5.1, and lysate concentration was determined as described in §2.5.2. As cells were spinning, 25 µL Pierce Protein G Magnetic Beads (Thermo Scientific, USA) were washed 3 times with 300 µL nuclease-free lysis buffer. 2 µL anti-Ago2 (Abcam, Cambridge, UK) monoclonal antibody or IgG isotype control was added to the bead suspension and incubated with rotation at 4˚C for 4 h. The antibody-coated beads were then washed 3 times with 300 µL nuclease-free lysis buffer, and 300 µg lysate was added to the beads and incubated overnight with rotation at 4˚C.

After the overnight incubation, the beads were washed again 3X with nuclease-free lysis buffer and divided into two aliquots. From one, protein was eluted by boiling for 10

minutes with SDS-PAGE loading buffer and Ago2 enrichment was confirmed by western blot. From the other, RNA was isolated by phenol:chloroform extraction. Briefly, RNA was eluted by digestion with Proteinase K (Millipore, USA) in 100 µL lysis buffer at 55˚C for 15 minutes. The supernatant was then combined with 300 µL acid phenol:chloroform (Ambion, USA), vortexed for 1 minute, and centrifuged for 1 minute. The supernatant was collected and subjected to standard ethanol precipitation. RNA quantity was assayed by Nano-Drop and miRNAs enrichment was quantitated by qRT-PCR.

2.6.6 Chromatin Immunoprecipitation (ChIP)

2.6.6.1 In vitro *crosslinking*

CDX1 ChIP was carried out with using the reagents and protocol included in the ChIP-IT® Express kit (Active Motif, USA). The general scheme is outlined in **Figure 2.2**. To begin the ChIP protocol, cells were grown in 4 15cm dishes, to yield approximately 50 million cells when 70-80% confluent. To the culture medium, 0.55 mL 37% v/v formaldehyde was added and incubated with agitation at room temperature for 5 minutes. The plates were washed with PBSA and then the crosslinking reaction was quenched with the addition of 10 mL Glycine Stop-Fix solution. Each plate was then placed on ice and washed twice with 10 mL of ice-cold PBSA. 5 mL of Cell Scraping solution was added and cells were scraped into 15 mL conical tubes using a rubber policeman. The cells were then centrifuged for 10 minutes at 720 x g, 4˚C. The pellet was resuspended in 1mL lysis buffer supplemented with 1 µL PMSF and 1 µL protease inhibitor cocktail.

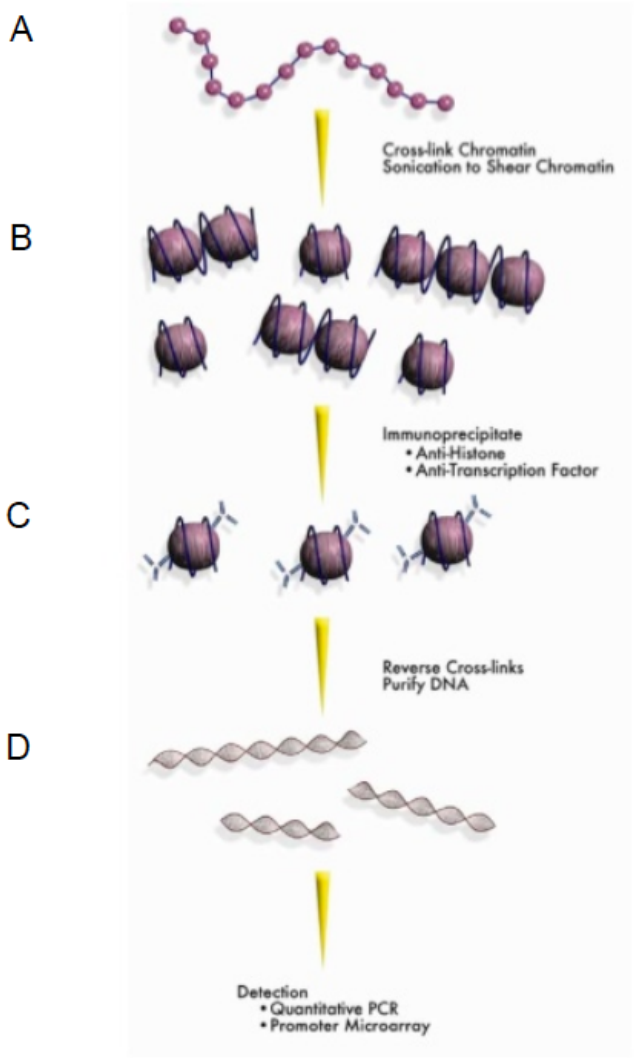

Figure 2.2
Chromatin immunoprecipitation workflow
Figure adapted from Millipore EZ-ChIP Manual (Millipore, USA). A) Cells are fixed in formaldehyde to cross-link proteins and chromatin. B) Chromatin lysate is sheared by sonication. C) Protein-chromatin complexes are precipitated using antibody-conjugated magnetic beads. D) Cross links are reversed and DNA is purified for downstream analysis.

2.6.6.2 Sonication

The cell lysate was then sheared with Biorupter® Sonicator (Diagenode, Liege, Belgium). The lysates were transferred to microcentrifuge tubes and placed in the water-submerged sonication rotor of the Bioruptor. The cells were then pulsed with 30 seconds of maximum intensity and 90 seconds rest. This cycle was repeated 10 times. The size range of DNA fragments was checked by reversing the crosslinks in sodium chloride at 65˚ overnight and running the DNA on a 1.5% Agarose gel.

2.6.6.3 Immunoprecipitation

100 µL of sheared chromatin was combined with the 25 µL of the kit component protein G magnetic beads, 20 µL ChIP buffer 1, 2 µL protease inhibitor cocktail, and 3 µg of CDX1 monoclonal antibody (Chan's Thesis, 2010) or IgG isotype control. 10 µL of sheared chromatin was set aside as input. The IP reactions were incubated overnight at 4˚C with rotation.

2.6.6.4 Elution and DNA purification

After the overnight incubation at 4˚C, beads were sequentially washed with 800 µL each Wash Buffer 1 and Wash Buffer 2. The beads were then pelleted and resuspended in 50 µL Elution Buffer AM2 and incubated with rotation at room temperature for 15 minutes. The supernatant was transferred to a fresh tube, and the crosslinks were reversed by addition of 50 µL Reverse Cross Link Buffer and incubation overnight at 65˚C. The input samples were treated in parallel. After the crosslinks were reversed overnight, all samples and inputs were treated with 2 µL proteinase K and incubated at 37˚C for 1 hour. The

DNA was then purified using the kit-supplied filter columns. 2 µL of DNA was then used as template for qPCR analysis of promoter enrichment. Values were normalized to enrichment of the GAPDH promoter and fold enrichment was calculated relative to the input samples.

2.7 Flow Cytometry

2.7.1 CD24/CD44 Immunofluorescence

Cells were grown under standard conditions for 1 doubling time before harvesting with trypsin/EDTA for flow sorting. Trypsinized cells were washed with PBSA, filtered through a CellTrics® 20µm filter and resuspended in flow buffer (PBSA + 10% fetal calf serum) to a density of 10^7 cells/mL. 200µL of cell suspension were aliquoted per sample and incubated for 30 minutes at 4˚ with 1:200 dilution of either Alexa488-Anti-CD24 or Alexa647-Anti-CD24 (Invitrogen, USA). Immunostained samples were then washed with 1mL ice-cold flow buffer and spun down in a refrigerated centrifuge at 4˚ and 400 x g for 5 minutes. Cells were resuspended in 200µL flow buffer and either stained according to the same procedure with an appropriate secondary antibody and used directly for FACS.

Cells were sorted by FACS on a MoFlo™ cell sorter (Beckman Coulter, Pasadena, USA) using the integrated Summit data collection software (Beckman Coulter). Gain and voltage settings were adjusted depending on sample composition. Forward and side scatter parameters were used to exclude doublets and debris. The remaining cells' fluorescence was detected by 488-nm blue laser excitation for Alexafluor-488 conjugated

antibodies and 633-nm red laser excitation for Alexafluor-647 conjugated antibodies. Emission was plotted logarithmically to identify positive and negative staining populations. The top 10% of the positive-stained cells were gated and collected in 200 µL DMEM for further experiments.

2.7.2 Propidium Iodide Cell Cycle Analysis

HCT116 and HCT116 p53-/- cells were reverse transfected with miR-215, miR-3189-3p, or control mimics (Dharmacon, USA) for 48 h, then washed twice with PBSA, then trypsinized. Cells were fixed with ice-cold 70% ethanol and stained with 10 µL propidium iodide (Sigma Aldrich, USA) in the presence of RNase A overnight at 4˚C. The cells were then washed with PBSA, resuspended in 500 µL PBSA, and filtered through a 30 micron mesh to eliminate multicellular aggregates. The PI staining in the resulting cell suspension was measured on a FACSCalibur (BD Biosciences, USA). The data were exported and analyzed manually using FlowJo v10. (Tree Star, Inc., Ashland, Oregon, USA).

2.8 Statistical Methods

2.8.1 Gene Set Enrichment Analysis

GSEA was performed using the Broad Institute GSEA software (MIT, Cambridge, USA) (Subramanian et al., 2005). Briefly, all miRNAs in the sequenced pair of HCT116 lines were ranked and listed by difference between normalized read counts in –CDX1 and –

vector. Using the top 100 differentially expressed miRNAs in the LS174T pair as a gene set, the ranked list was queried for presence of miRNAs in the gene set. The significance of the enrichment score is evaluated by the frequency of obtaining a similar score in 1000 random permutations of gene-list labels.

2.8.2 t-Test

Unless specifically noted, all experiments were performed in triplicate biological replicates, and error bars represent the standard error of the mean for these replicates. p-values are computed using a two-tailed student's t-test using the values from the biological replicates. In some experiments where the magnitude of the readout was variable but the relevant comparisons were consistent, representative data are shown.

2.8.3 Hypergeometric probability analysis

For the analysis of microarray data, it was useful to compare the similarity of genes differentially expressed in different microarray experiments (e.g. miR-215 and CDX1 arrays). As a heuristic illustration, these data are plotted in a Venn diagram. To calculate the p-value of the intersection between two microarray data sets, we used an algorithm for sampling from a hypergeometric probability distribution. Calculations were performed in the R programming environment using the `phyper` function.

2.8.4 Analysis of phylogenetic conservation

Pairwise conservation between human and mouse for miR-215 was determined using the mVista algorithm using standard settings (Frazer et al., 2004). Multiple alignments of mammalian orthologous regions for human miR-3189 precursor were created using the Muscle sequence alignment software (Edgar, 2004). MiRNA-3189 candidates were mapped to mammalian genomes using BLAST (Altschul et al., 1997) or LiftOver (Karolchik et al., 2014). On the basis of the reciprocal BLAST hits and analysis of syntenic regions, we identified 14 orthologous candidates for miR-3189 precursors in different mammalian genomes. Phylogenetic analysis was conducted using MEGA5 and RAxML software (Tamura et al., 2011; Stamatakis et al., 2012). RNA secondary structures for single sequences and for multiple alignments were predicted by Afold and Alifold respectively (Ogurtsov et al., 2006; Lorenz et al., 2011).

CHAPTER THREE

Identification of CDX1-Regulated MiRNAs by Small RNA Sequencing

CHAPTER 3: IDENTIFICATION OF CDX1-REGULATED MIRNAS BY SMALL RNA SEQUENCING

3.1 Introduction

The transcription factor CDX1 is an important regulator of both intestinal development and homeostasis (Park et al., 2009; Lynch et al., 2000). In colorectal cancer, CDX1 expression is related to the grade of the tumor, i.e. the degree to which the malignant tissue exhibits characteristics of normal, differentiated colonic epithelium (Pilozzi et al., 2004). Furthermore, aberrant CDX1 expression drives inappropriate trans-differentiation in the case of Barrett's metaplasia, in which the squamous epithelium of the esophagus is converted to intestine-like columnar epithelium in response to gastro-esophageal reflux (Wong et al., 2005). The *CDX1* promoter is hypermethylated in the colorectal cancer cell line HCT116, leading to low levels of CDX1 protein; conversely, LS174T expresses CDX1 at high levels relative to a panel of 110 CRC cell lines and has an unmethylated *CDX1* promoter (see **Appendix II**) (Wong et al., 2004; Chan et al., 2009). Due to their differential CDX1 expression, the colorectal cancer cell lines HCT116 and LS174T occupy different ends of the clonogenicity-differentiation spectrum. Previous work from our lab has demonstrated that HCT116 forms a high number of small, undifferentiated colonies *in vitro*, and colonizes a high number of tumors in NOD/SCID mice; LS174T, on the other hand, forms comparatively fewer large, well-differentiated colonies with lumens *in vitro*, and is less efficient at *in vivo* tumor initiation (Yeung et al., 2010). While previous work in the Cancer and Immunogenetics laboratory, including the theses of

N.A.C.S. Wong, Trevor Yeung, Carol Chan, and Shaan Ghandi, has extensively characterized the role of CDX1 in regulated cancer stem cells and differentiation in the colon (Yeung et al., 2010; 2011; Chan et al., 2009; Wong et al., 2004), it remains unclear how and to what extent miRNAs are involved in regulating the broad transcriptomic changes associated with differentiation.

MicroRNAs are small, non-coding RNAs that have been extensively implicated in transcriptomic regulation, both as large-scale effectors (Choi et al., 2011; Cheung et al., 2013) and fine-tuners of gene expression (O'Loghlen et al., 2012; Bu et al., 2013), over the past ten years. Drawing on the precedent for uncovering miRNAs embedded in transcription factor pathways set by studies on p53, we hypothesize that miRNAs are essential effectors of CDX1 function and mediate gene expression changes necessary to bring about the phenotypic changes associated with stem cell differentiation. To identify such miRNAs, we have used high throughput small RNA sequencing to measure changes in global miRNA expression in response to CDX1 expression in a CDX1-negative (CDX1(-)) background or CDX1 knockdown in a CDX1-expressing (CDX1(+)) background.

High throughput RNA sequencing (hereafter referred to as RNAseq) has recently emerged as a cost-effective alternative to microarray hybridization for gene expression profiling. In addition to the improved sensitivity and dynamic range of RNAseq relative to microarray, sequencing platforms offer several advantages for miRNA expression profiling (Linsen et al., 2009). Many miRNA are expressed from paralogous genomic

loci, so miRNA families consist of many miRNAs with high degrees of sequence similarity. Sequencing can accurately distinguish between similar miRNA relatives and isoforms whereas these distinctions may be elided by microarray. Moreover, sequencing does not require prior knowledge of miRNA sequences, so new miRNAs or miRNA isoforms may be measured or even discovered in the process (Git et al., 2010).

3.2 Results

3.2.1 Differential CDX1 expression underlies phenotypic differences between HCT116 and LS174T

In order to understand the effects of CDX1 on differentiation, we have previously developed variants of the HCT116 and LS174T cell lines with stable alterations in CDX1 expression. HCT116 has been stably transfected with the constitutively active pRC-CMV-CDX1 plasmid (designated HCT116-CDX1) or the pRC-CMV empty vector (HCT116-Vec). Conversely, LS174T was stably transfected with the pSilence-siCDX1 vector, expressing a short-hairpin RNA against CDX1 (designated LS174T-siCDX1) or the pSilence empty vector (LS174T-Vec). These constructs were created by N.A.C.S. Wong and described in his thesis work (2006), and the stable cell lines were made by Carol Chan and described in her thesis (2010) and in Chan, *et al*., 2009.

HCT116-CDX1 robustly expresses CDX1 protein, while CDX1 is expressed at undetectable levels in HCT116-Vec. The baseline CDX1 expression of LS174T-Vec is

reduced to levels below the sensitivity of western immunoblot in LS174T-siCDX1, as shown in **Figure 3.1**. The differences in differentiation and clonogenicity caused by overexpression or knock-down of CDX1 have been extensively characterized *in vitro* by 3-dimensional cell culture in Matrigel. HCT116-CDX1 forms some lumens and a greater number of complex, differentiated colonies in Matrigel, whereas HCT116-Vec forms few, if any (**Fig 3.2 A, B**). The lumen-forming capacity of LS174T-Vec is significantly reduced after stable CDX1 knockdown (**Fig 3.2 C**) (Yeung et al., 2011; 2010).

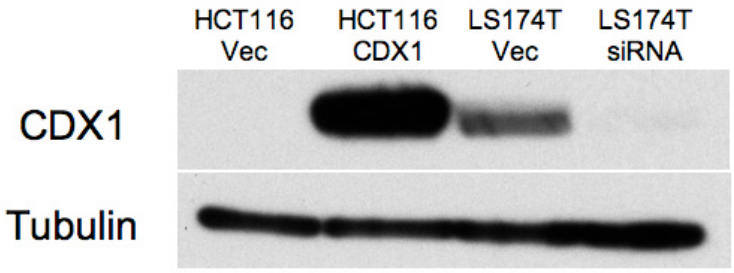

Figure 3.1
Immunoblot for CDX1 in stably transfected HCT116 and LS174T cell lines
Protein lysate from the indicated stable transfectants was probed with anti-CDX1 monoclonal antibody or anti-β-Tubulin as a loading control. Stable pRC-CMV-CDX1 transfection clearly and significantly results in increased CDX1 protein levels in HCT116. Stable shRNA knockdown of CDX1 in LS174T results in nearly complete abrogation of CDX1 protein expression. This figure is adapted from Chan's thesis (2010).

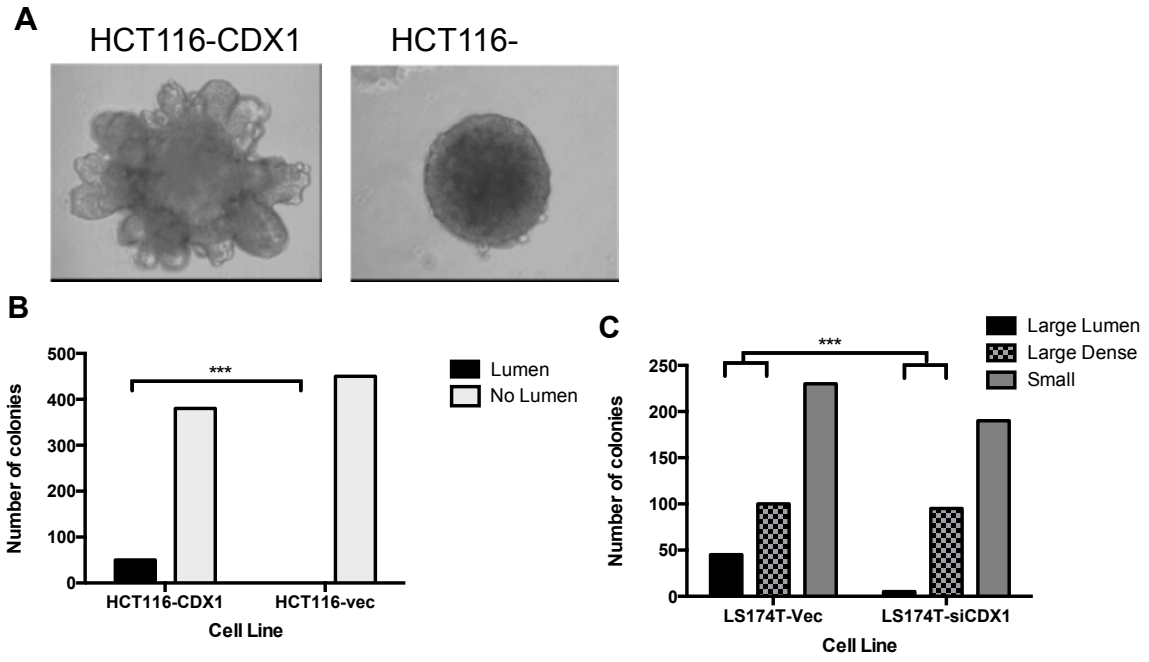

Figure 3.2
***In vitro* morphology of HCT116-CDX1 and LS174T-siCDX1**
A) Transmitted light micrographs of HCT116-CDX1 and –Vec colonies after 3 weeks growth in Matrigel. (B,C) Tally of lumen containing vs. dense colonies in stable HCT116 and LS174T transfectants 3 weeks after initial seeding as single-cell suspensions in Matrigel. This figure is adapted from Yeung, *et al.*, 2011

3.2.2 High throughput small RNAseq of cell lines with stably modified CDX1 expression

In order to identify potential miRNA targets of the CDX1 transcriptional program, we undertook high-throughput sequencing of small RNAs isolated from the four cell lines HCT116-vector, HCT116-CDX1, LS174T-vector, and LS174T-shRNA. We hypothesized that CDX1 overexpression or knockdown would result in patterns of differential miRNA expression, and by comparing two pairs of isogenic cell lines, we hoped to obtain a profile of CDX1-induced changes in the small RNA transcriptome with minimal background noise. With the assistance of Paul Meltzer's lab at the National Cancer Institute in Bethesda, MD, we sequenced the small RNA (18-33nt) fraction of the aforementioned cell lines. The complete normalized RNA sequencing data are presented in **Appendix I**.

Sequencing reads were mapped to the annotated miRNAs present in miRBase, v19, which listed 2104 human miRNAs in its latest available release. Due to the quasi-stoichiometric mechanism of miRNA action, in which a miRNA with a greater number of copies in the cell is able to repress a greater number of mRNAs, miRNAs with fewer than 50 normalized mapped reads per million total reads (reads per million, or RPM) were excluded from subsequent analyses as they were deemed unlikely to be physiologically significant (Creighton et al., 2009). 314 miRNAs passed this cutoff in LS174T-Vec, with 1587 normalized reads mapping to the most abundant miRNA, miR-387a. 357 significantly expressed miRNAs were detected in LS174T-siCDX1, with 1343 reads

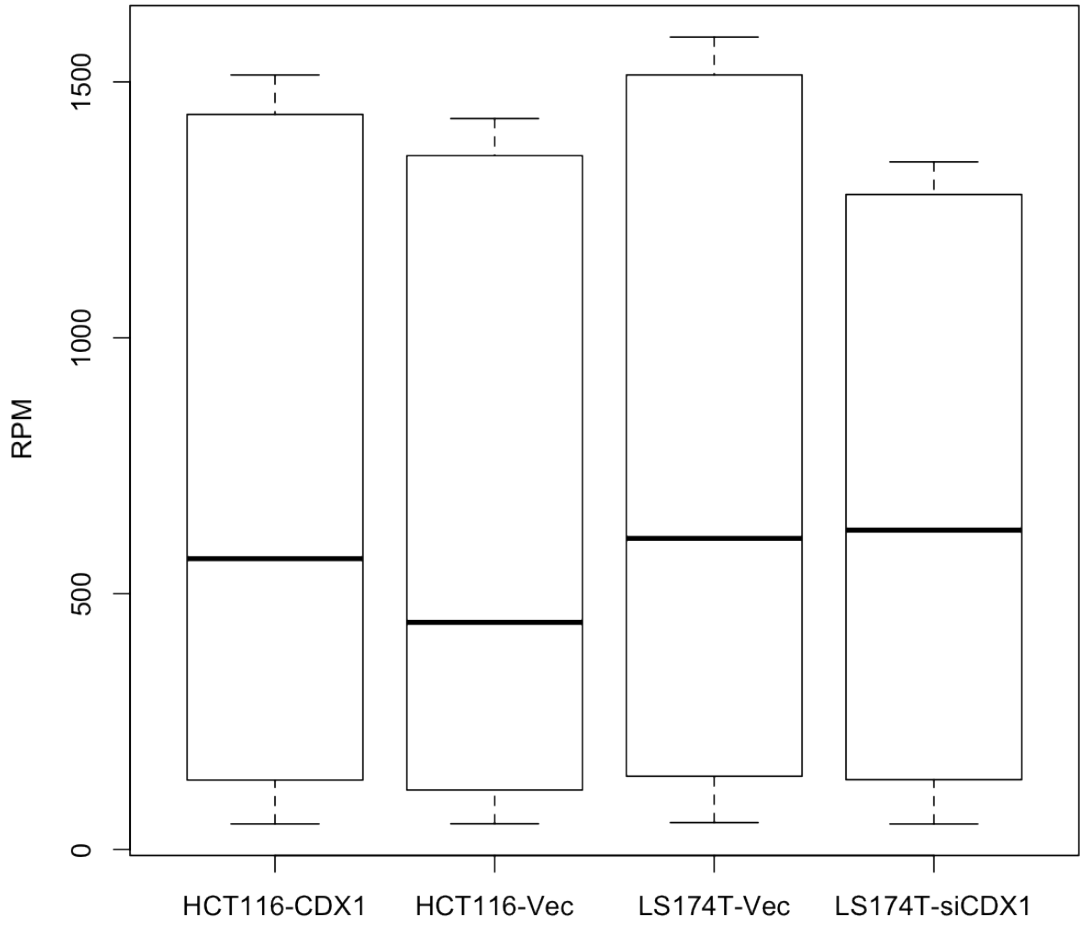

Figure 3.3
Distribution of small RNAseq reads amongst HCT116 and LS174T samples
Box plots showing mean, maximum, minimum, and interquartile range of read counts per miRNA for the four cell lines subjected to small RNAseq.

mapping to the most abundant miRNA, which was also miR-387a. In HCT116-CDX1 and HCT116-Vec, 363 and 396 miRNAs passed the 50-read cutoff, respectively. Interestingly, miR-378 was also the most abundantly expressed miRNA in HCT116-CDX1 and HCT116-Vec, with 1513 and 1428 normalized reads, respectively. These data are summarized in depicted in **Figure 3.3** and summarized in **Table 3.1**.

To asses the differential expression of miRNAs relative to CDX1 status, the fold changes for each miRNA in each pair of isogenic cell lines were calculated as the ratios between HCT116-CDX1(RPM)/HCT116-Vec(RPM) and LS174T-Vec(RPM)/LS174T-siCDX1(RPM). These fold changes are compared in **Figure 3.4**. miRNAs with ≥1.5 fold difference between CDX1(+) and CDX1(-) samples were considered as candidate targets of CDX1, with preference being given to miRNAs with higher read counts (**Fig. 3.4 and Table 3.2)**. miRNAs highlighted in red and labeled on Figure 3.4 were selected for validation by TaqMan quantitative reverse transcription-PCR (qRT-PCR). We chose to validate the results for a group of 8 miRNAs with robust levels of expression and large fold-differences relative to CDX1, with predicted 5' CDX1 sites, and with functionally interesting predicted targets **(Table 3.3)**. The Transcription Element Search System (TESS) algorithm was used to search for predicted CDX1 binding sites within 2kb upstream of the miRNA transcription start site. Potential mRNA seed matches suggesting miRNA-mRNA target interactions were detected using the TargetScan algorithm, which weights seed complementary regions in mRNA 3'UTRs according to their degree of phylogenetic conservation to evaluate the likelihood that a given miRNA-mRNA interaction is physiologically important. Rather than only validate the sensitivity of

Cell Line	miRNAs above cutoff	mean read count	median read count	most abundant miRNA	maximum read count
HCT116-CDX1	363	748.7	568.3	miR-378a-3p	1513
HCT116-Vec	396	684.8	443.8	miR-378a-3p	1428
LS174T-Vec	357	790.5	608.2	miR-378a-3p	1587
LS174T-siCDX1	314	694.4	624.1	miR-378a-3p	1343

Table 3.1
Summary statistics for small RNAseq samples

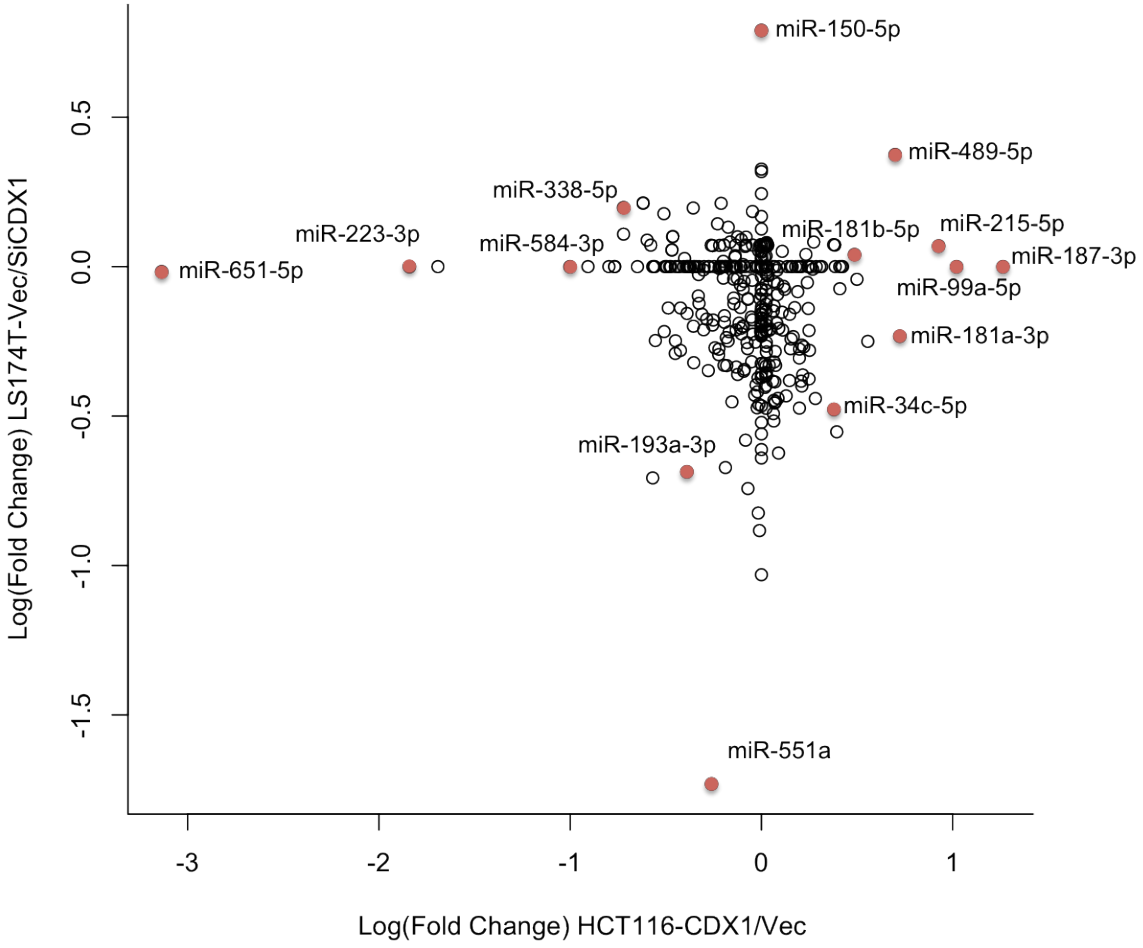

Figure 3.4
Differential expression of known miRNAs relative to CDX1 status
The $\log_2$ fold change between CDX1(+) and CDX1(-) samples was calculated for each miRBase-annotated miRNA with RPM≥50 in at least one of the four cell lines subjected to small RNA-seq (i.e. HCT116-CDX1, HCT116-Vec, LS174T-siCDX1, LS174T-Vec). Highly expressed miRNAs with large fold changes are labeled and highlighted in red.

sequencing to detect miRNAs that are strongly upregulated by CDX1, for instance, this validation approach ensures that the sequencing has equal ability to detect down-regulated miRNAs and that differences detected in only one of the cell line pairs are not sequencing artifacts. It also allows us to investigate miRNAs that are directly or indirectly down-regulated by CDX1, which may be as important as the miRNAs that are up-regulated. A new batch of total RNA was isolated from the same cell lines used for RNAseq, and pre-designed TaqMan primers were used to reverse transcribe and quantitatively amplify eight miRNAs: miR-34c, miR-99a, miR-150, miR-181a, miR-181b, miR-193a-3p, miR-215, and miR-584 **(Fig. 3.6)**. Most of the candidate miRNAs assayed displayed similar fold changes in both RNAseq and qRT-PCR, with the notable exceptions of miR-193a-3p in HCT116-CDX1/Vec and miR-99a in LS174T-Vec/siCDX1.

miRNA	HCT116-CDX1 reads	HCT116-vector reads	HCT116 fold change	LS174T-shCDX1 reads	LS174T-vector reads	LS174T-fold change
let-7a-2-3p	707.2	269.8	2.6	0	0	NA
miR-22	113.0	447.3	0.3	1286.5	1519.0	1.2
miR-34c-5p	640.9	267.7	2.4	588.6	195.9	0.3
miR-95	266.2	1008.6	0.3	1285.0	1516.3	1.2
miR-99-5p	651.5	62.2	10.5	1.7	5.1	3.0
miR-125a	103.4	65.5	1.6	1016.2	837.9	0.8
miR-125b-1-3p	992.3	513.1	1.9	0	0	NA
miR-181a-1-5p	1445.4	597.4	2.4	1519.1	1286.8	0.8
miR-181a-2-5p	1434.3	600.9	2.4	1519.0	1282.8	0.8
miR-181b-1-5p	485.6	153.7	3.2	1158.6	1277.3	1.1
miR-181b-2-5p	582.3	190.0	3.1	1284.2	1408.7	1.1
miR-181c-3p	75.1	36.4	2.1	13.2	0	NA
miR-215	1447.8	171.3	8.5	1265.8	1484.6	1.2
miR-223	1.1	76.9	0.01	0	0	NA
miR-338	39.6	208.1	0.2	83.9	136.3	1.6
miR-365a	298.5	841.9	0.4	0	0	NA
miR-584	106.9	862.9	0.1	27.8	40.3	1.4
miR-651	0.2	247.4	0	176.7	169.9	1.0
miR-671	355.2	1090.6	0.3	609.5	43.2	0.7
miR-3065	31.2	69.8	0.4	36.0	32.1	0.9
miR-3158	138.2	402.6	0.3	68.1	85.8	1.3

Table 3.2
Normalized read counts and fold changes for a subset of sequenced miRNAs
An extended view of data presented graphically in Figure 3.4. Read counts are shown as RPM, and fold changes for the two pairs of cell lines are calculated as HCT116-CDX1/HCT116-Vec and LS174T-Vec/LS174T-siCDX1, respectively. A full tabulation of read counts is presented in **Appendix I.**

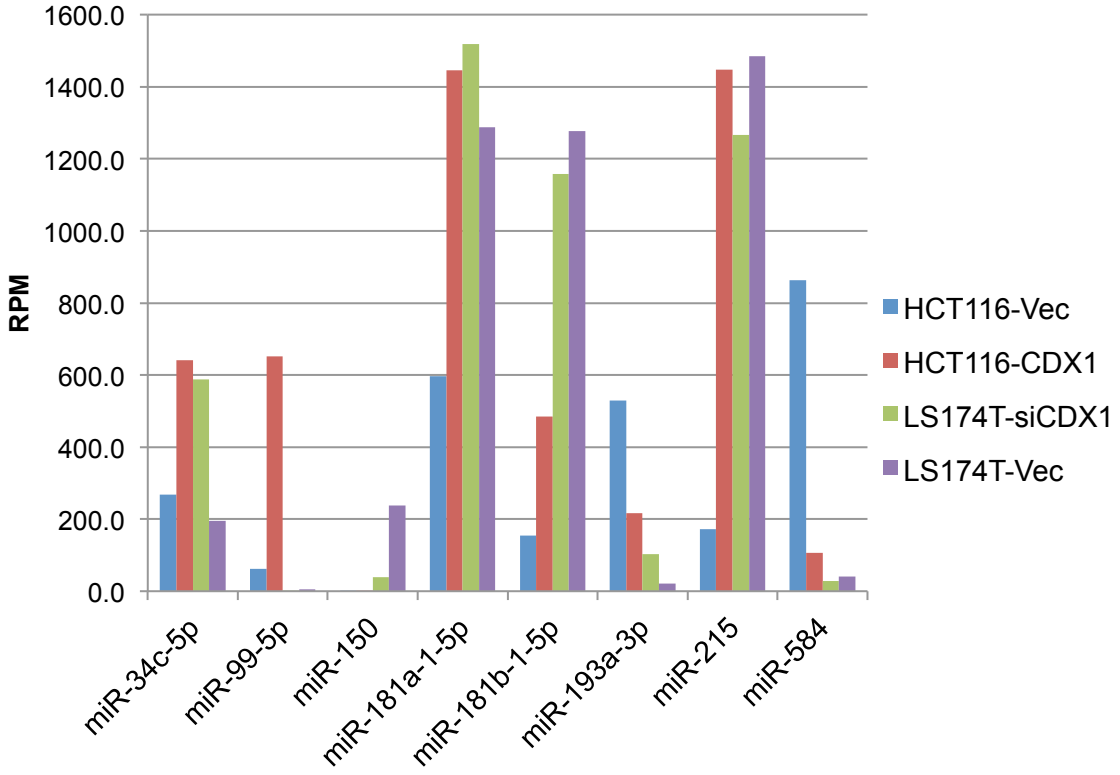

Figure 3.5
Normalized RNAseq read counts of candidate CDX1-regulated miRNAs
Many miRNAs were expressed at very low levels in all 4 cell lines or did not exhibit significant changes in response to CDX1 modulation. At least 50 reads in one or more cell lines and 1.5-fold change were detected for each of the plotted miRNAs. This is a graphical representation of a subset of data presented in Table 3.1 and is meant to illustrate the variation in abundance between candidate miRNAs which is not apparent in Figure 3.4. These same miRNAs are further described in Table 3.3.

miRNA	Fold Change HCT116	Fold Change LS174T	# CDX1 sites	Predicted targets
miR-34c	2.4	0.3	0	*MET, MYB, E2F3, MYC, CDK4*
miR-99-5p	10.5	3.0	7	*HOXA1, MTOR, IGF1R*
miR-150	N/A	6.2	0	*MYB, VEGFA*
miR-181a-2-5p	2.4	0.8	1	*BCL2, CDX2, NOTCH2, SPRY2*
miR-181b-2-5p	3.1	1.1	1	*BCL2, CDX2*
miR-193a-3p	0.4	0.2	0	*E2F6*
miR-215-5p	8.5	1.2	5	*DICER1, ZEB2, EREG, IGF1, RUNX1*
miR-584-3p	0.1	1.4	0	*HOXA11*

Table 3.3
Candidate miRNAs selected for qRT-PCR validation, predicted upstream CDX1 binding sites and predicted mRNA targets
The TESS algorithm was used to search the 2-kilobase genomic region 5' to the transcription start site for each miRNA in order to find putative CDX1 binding sites. mRNA targets were predicted using the TargetScan algorithm.

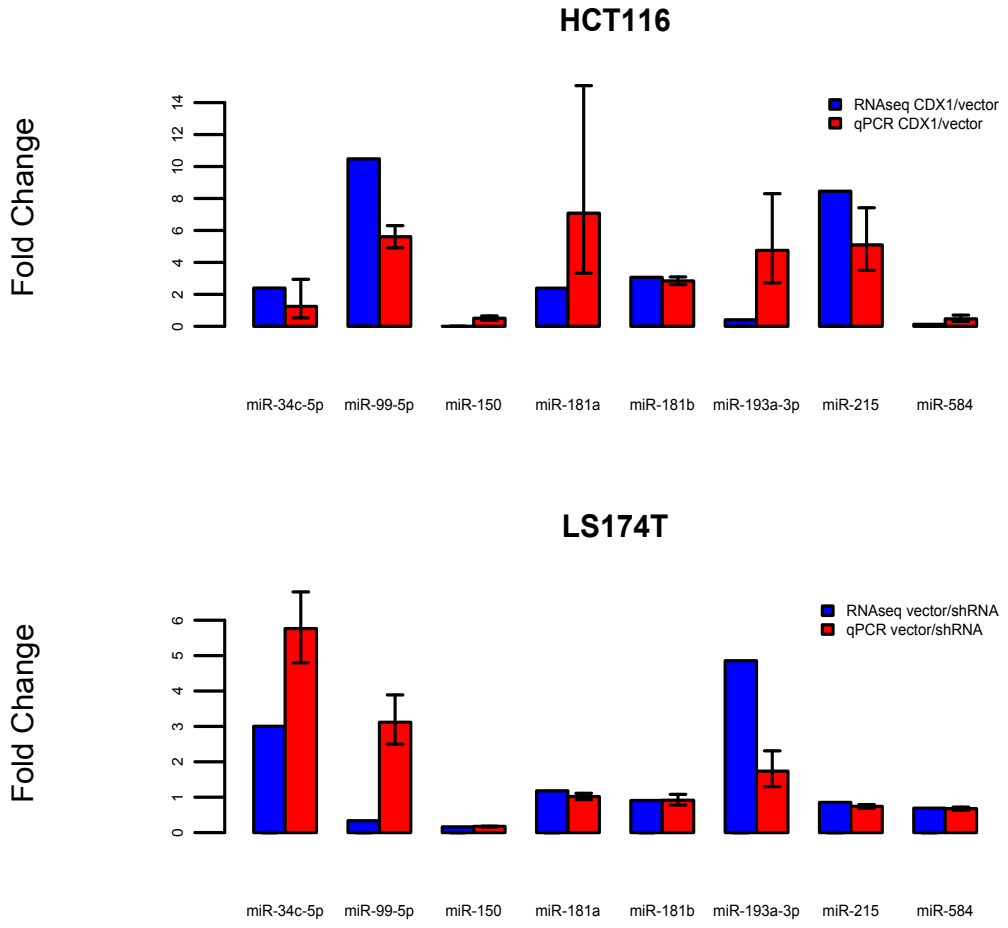

Figure 3.6
qRT-PCR validation of small RNAseq results
RNA from the sequenced samples was further assayed by qRT-PCR to validate the relative expression of candidate miRNAs. Most candidate miRNAs exhibited similar relative expression in both qRT-PCR and RNAseq experiments. Raw Ct values were normalized to the U6 snRNA, and candidate miRNA fold changes were calculated via the ΔΔCt method relative to HCT116-vector or LS174t-shRNA, respectively.

3.2.3 CDX1 induces concerted changes in global miRNA expression

In order to asses the signal-to-noise ratio of our small RNA-seq data, we sought to compare quantitatively the differential expression of miRNAs between the isogenic LS174T and HCT116 variants. The miRNA expression profiles of CDX1(+) and (-) samples were compared using Gene Set Enrichment Analysis (GSEA) using the top 100 differentially expressed miRNAs between LS174T and LS174T-shRNA as a "gene set," and all sequenced miRNAs ranked in descending order by differential expression between HCT116-CDX1 and HCT116-vector as a "gene list" **(Fig. 3.4).** The GSEA algorithm is then used to compute a running rank-sum statistic modeled on the Kolmogorov-Smirnov test, such that each time a miRNA in the gene set also occurs in the gene list, the running sum in increased by an amount proportional to the ranked position of that miRNA in the set. GSEA yielded a normalized enrichment score of 1.33 and a family-wise error rate (FWER) p-value of 0.028, indicating that the list of differentially expressed miRNAs in HCT116 samples was significantly enriched for miRNAs with large differential expression in LS174T samples

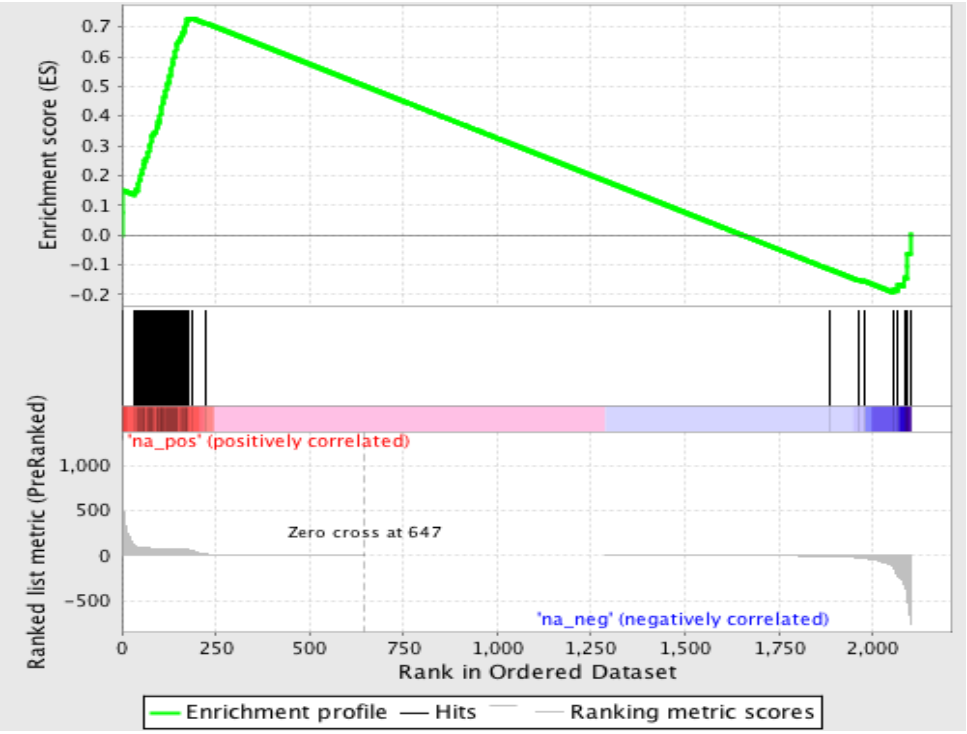

Figure 3.7
miRNAs with increased expression after CDX1 overexpression are enriched among the set of miRNAs with decreased expression after CDX1 knockdown.
GSEA was used to calculate the enrichment of miRNAs differentially expressed between HCT116-CDX1 and HCT116-vec in the set of miRNAs downregulated by CDX1 knockdown in LS174T. GSEA shows a significant enrichment of the 100 most down-regulated genes in LS174T-siCDX1 at the top of the ranked list of miRNAs up-regulated in HCT116-CDX1. The upper panel shows the running-sum enrichment score. The bottom panel shows the weight of the sum statistic as it varies with the list rank position. More weight is given to genes at the top and bottom of the list as enrichment for extreme up- or down-regulated genes are a more robust markers of profile similarity.

3.2.4 *In silico* transcription factor binding prediction for CDX1

The results of GSEA suggest that CDX1 acts in a concerted manner to regulate a subset of the miRNA-ome, but the RNAseq data do not reveal whether the effects of CDX1 on miRNA expression are directly due to CDX1 transactivating miRNAs at their promoters or to indirect mechanisms. CDX1 is known to bind to several consensus sequences (C/TATAAAT/G, in direct or reverse orientation) (Gautier-Stein et al., 2003) in regulatory regions of DNA . To investigate the potential for direct regulation of miRNA transcription by CDX1, we searched for CDX1 binding sites upstream of candidate miRNAs *in silico* (Schug, 2008). The TESS transcription factor binding prediction algorithm indicates that the genomic regions 1kb upstream from the transcription start sites of the top 10 miRNAs upregulated by CDX1 overexpression in HCT116 are significantly enriched for CDX1 binding sites relative to 10 randomly selected miRNAs **(Fig. 3.8).**

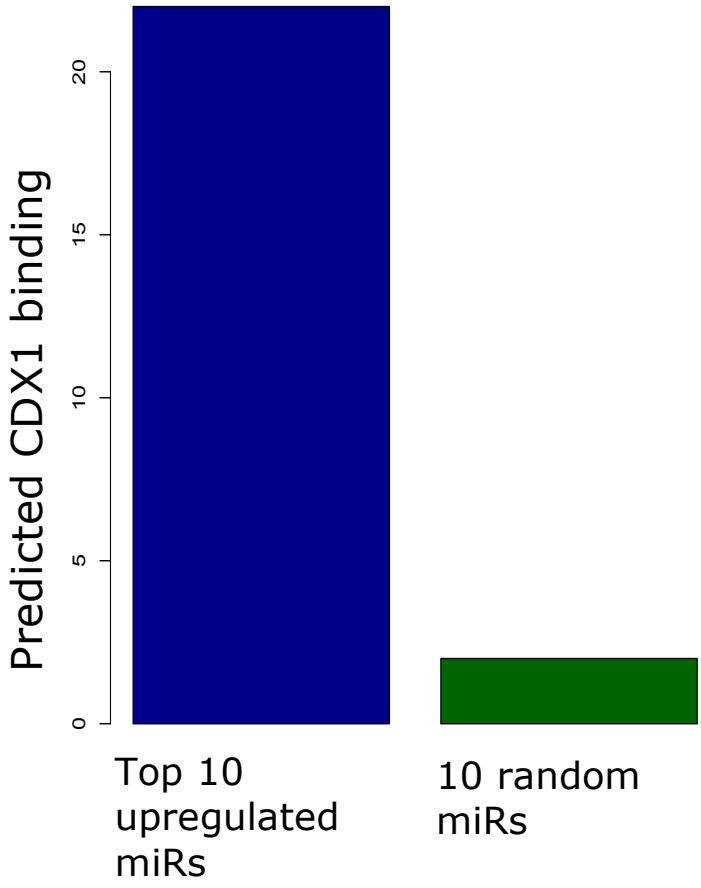

Figure 3.8 Promoter regions of candidate miRNAs are enriched for CDX1 binding sites
The genomic regions 1kb upstream of the mature sequences of the top 10 CDX1-associated miRNAs identified by RNAseq and 10 randomly selected miRNA promoters were examined for the presence of predicted CDX1 binding sites. 22 CDX1 sites were found in the top 10 candidate promoters, while only 2 were found in the random 10. The y-axis shows the total number of binding sites for the top or bottom 10 miRNAs. As determined by a two-tailed student's T-test, p=0.015.

3.3 Discussion

We first approached the unknown quantity represented by miRNAs in colorectal cancer by focusing on a master transcriptional regulator of differentiation in the colon, namely CDX1. miRNAs have been shown to be potent downstream mediators of differentiation-inducing factors in systems as diverse as quiescent muscle stem cells (Cheung et al., 2013) and induced pluripotent stem cells (Anokye-Danso et al., 2011). Therefore, it seemed likely that one of the important transcription factors in colon stem cell differentiation would also regulate some miRNAs in order to carry out its downstream functions. Although we and others have identified protein coding genes regulated at the transcriptional level by CDX1 (Chan et al., 2009; Verzi et al., 2011), there are no existing records in the literature of any previous attempts to identify miRNA regulated by CDX1. Our approach offers a novel and comprehensive insight into the effects of CDX1 on global miRNA expression in colorectal cancer cell lines.

We began investigating the effects of CDX1 on miRNA expression by sequencing small RNAs from a quartet of stably-transfected cell lines. Each sample displayed comparable numbers of total miRNAs expressed as well as similar mean, median, and maximum levels of expression. This suggests that library preparation and sequencing methods performed equally well with all 4 samples, and any systematic biases were reproduced consistently between samples. Ideally, more biological replicates could be performed to control for intra-cell line variation. Moreover, the experiment could be repeated on a greater number of cell lines to refine the association of miRNAs with CDX1 expression.

Interestingly, miR-378a was the most abundant miRNA in each cell line, and its expression level displayed little variation between samples. However, a better approach to compare variation between samples might have spiked-in a standard curve of varying concentrations of a synthetic RNA for normalization (Jiang et al., 2011). Previous reports have suggested that high throughput sequencing library preparation may introduce biases towards abundant miRNAs (Linsen et al., 2009), so it is possible our RNA sequencing method did not faithfully capture biological variation in very abundant miRNAs. A recent study has suggested that miR-378a is significantly downregulated in colorectal cancers relative to adjacent normal colonic epithelium, yet little is known about its function (Li et al., 2014). It is possible that this miRNA plays important roles in the biology of the colorectal epithelium, and these physiological functions must be maintained in cancer, albeit at an attenuated level. The results of Li, et al., may also be confounded by the well-known phenomenon of global miRNA downregulation, usually by loss of *DICER1* expression, in cancer cells relative to normal cells (Kumar et al., 2009; Lu et al., 2005). The small RNA seq data presented in this chapter raise several such questions beyond the scope of this thesis, but they may prove a fruitful resource for other investigators.

By imposing a few simple criteria (>50 reads in at least one sample samples, at least 1.5-fold change after CDX1 modulation, consistent fold change across both cell line pairs) we were able to identify a handful of promising candidate miRNAs. The expression levels of these candidate miRNAs as measured in miRNA seq were validated by qRT-PCR, but a more comprehensive validation might have been accomplished by using microarrays to measure miRNA expression. Many of the most upregulated miRNAs in

HCT116 contained CDX1 consensus binding sequences in their upstream promoter regions, indicating that these miRNAs may be upregulated due to direct transactivation by CDX1 rather than indirectly through some related factor or pathway. It should be noted that HCT116-CDX1 expresses CDX1 at a much higher level than LS174T-Vec, as shown in figure 3.1, so it is possible that some miRNAs are up-regulated due to non-specific activity of supra-physiological levels of CDX1. Although many miRNAs were also down-regulated by reintroduction of CDX1 into HCT116, or correspondingly upregulated by CDX1 knockdown in LS174T, the regulatory regions of at least a subset of these miRNAs were comparatively depleted of CDX1 binding sites. However, this does not eliminate the possibility that CDX1 may, in some instances, act to directly repress the expression of certain miRNAs by recruiting co-repressors or occluding the binding site of a necessary transcription factor.

From a global perspective, CDX1 modulation caused a consistent change in the expression profile of a subset of all annotated miRNAs. Using GSEA, we showed that miRNAs with the top differential expression values between LS174T-vector and –shRNA were significantly enriched at the top of a list of all miRNAs ranked according to their differential expression between HCT116-CDX1 and HCT116-vector. As we would expect from a master regulator of differentiation, CDX1 not only regulates individual miRNAs, but it also indirectly brings about broad changes in the transcriptome at the level of miRNAs.

The results of small RNAseq were successfully validated by independent qRT-PCR experiments on freshly isolated RNA. The data from these two orthogonal assays agree quite well within the bounds of the statistical errors inherent in the measurements from the respective assays. The few miRNAs (miR-193a in LS174T and miR-99a in HCT116) that could not readily be validated by qRT-PCR may be due to noise in one or both assays. It may be that faulty qRT-PCR probes resulted in unequal error in the measurement of the expression levels of different miRNAs. However, in most cases, the direction and significance of differential expression for a given miRNA was faithfully reproduced in qRT-PCR validation. In the following chapters, we employ an extended qRT-PCR screen for candidate miRNA expression in a wider panel of cell lines to identify more robust correlations with CDX1 expression across a greater variety of genetic backgrounds.

CHAPTER FOUR

Characterization of MiR-215 as a Direct Target of CDX1

CHAPTER 4: CHARACTERIZATION OF MIR-215 AS A DIRECT TARGET OF CDX1

4.1 Introduction

As discussed in the previous chapter, a population of colorectal cancers will tend towards a bimodal distribution of CDX1 expression due to categorical on/off control of the activity of the CDX1 promoter by CpG methylation. This is not to claim that the number of CDX1(+) and CDX1(-) tumors is evenly distributed, but rather that two distinct classes of CDX1 expression exist. The Cancer Immunogenetics Laboratory and others have established that a sufficiently large panel of cancer cell lines can accurately recapitulate the intertumoral genetic variation of colorectal cancers (Wilding and Bodmer, 2014; Barretina et al., 2012). By assaying the expression of candidate miRNAs identified by miRNAseq in Chapter 3 across a panel of 10 colorectal cancer cell lines, we have refined their associations with CDX1 expression and controlled for a number of confounding factors that arise from different mutation and gene expression landscapes in different cell lines. Measuring the correlation between CDX1 and candidate miRNAs across a range of cell lines averages across the background.

The work presented in this chapter first leverages the diversity of a panel of cell lines to identify miR-215 as the candidate miRNA with the most robust correlation with CDX1. Subsequently, a handful of standard molecular genetic techniques are used to interrogate the regulatory relationship between CDX1 and miR-215. We identify miR-215 as a novel, direct target of CDX1 transactivation. Although previous work on miR-215 has

focused almost exclusively on its upstream regulation by p53 (Braun et al., 2008; Georges et al., 2008), our data suggest that there may be some synergy between CDX1 and p53 in the regulation of miR-215 expression.

4.2 Results

4.2.1 Evaluation of candidate miRNA expression in 10 colorectal cancer cell lines

4.2.1.1 Microarray expression levels of CDX1 in a panel of colorectal cancer cell lines

In the previous chapter, 8 miRNAs identified as candidates downstream of CDX1 by RNA seq were validated using qRT-PCR. Both the RNA seq and subsequent qRT-PCR validation were carried out in cell lines with forced CDX1 modulation, either by stable overexpression or knockdown. In order to better understand the effects of endogenous variation in CDX1 expression, we expanded the scope of the qRT-PCR experiment to quantify the expression of these 8 miRNAs in a panel of 10 cell lines. As established in Wong, *et al.*, variation in CDX1 amongst colorectal cancer cell lines is entirely due to hypermethylation of CpG sites within the CDX1 promoter, resulting in a roughly bimodal distribution of CDX1 expression across CRC cell lines. A great effort has been made in the Cancer and Immunogenetics laboratory to characterize the transcriptome-wide gene expression and 3D-culure morphology of a wide panel of over 100 cell lines. These results are described in the theses of Ghandi (2011), Chan (2009), and Wong (2006) as well as in Chan, *et al*., 2010, Yeung, *et al*., 2011, and Ashley, *et al*. 2014, yet due to the

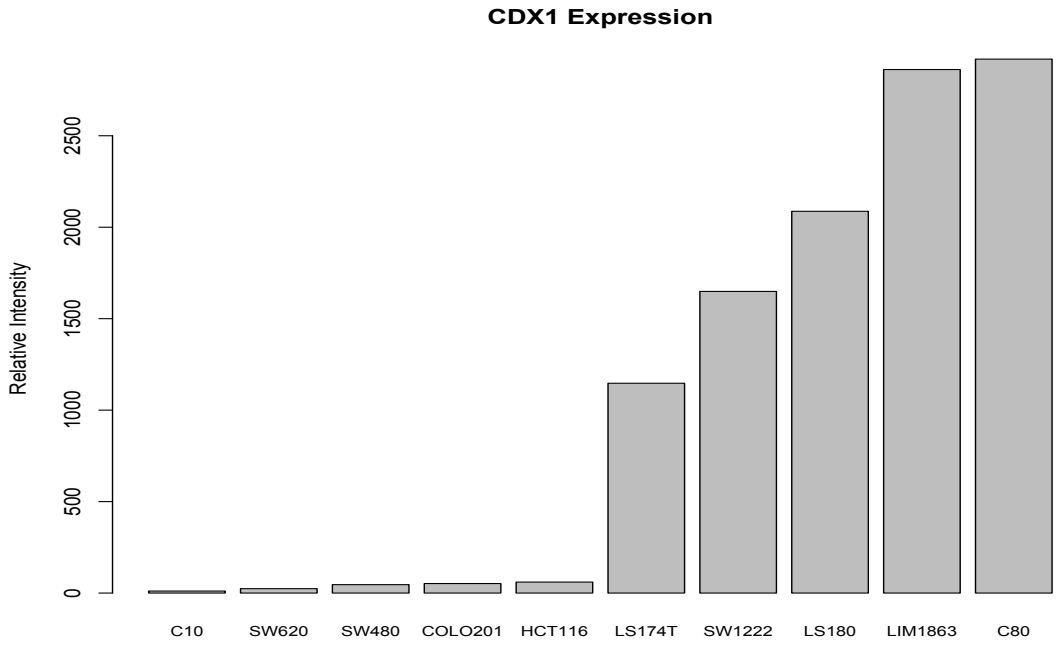

Figure 4.1
Relative CDX1 mRNA expression in 10 colorectal cancer cell lines
CDX1 expression in 10 cell lines measured by Affymetrix Human Genome U133 Plus 2.0 microarray. 5 Cell lines (C10, SW620, SW480, COLO201, HCT116) have very little CDX1 expression due to promoter hypermethylation and are classed as CDX1(-). The five cell lines classed as CDX1 (LS174T, LS180, C80, LIM1863), have at least ~20-fold higher CDX1 expression levels than the CDX1(-) cell lines.

continued growth of the lab's cell line panel, much of the work remains unpublished. For the measurement of candidate miRNA expression, we chose 5 cell lines with hypermethylated CDX1 promoters: C10, SW620, SW480, COLO201, and HCT116; and 5 cell lines with hypomethylated CDX1 promoters: LS174T, SW1222, LS180, LIM1863, and C80 (Wong et al., 2004). The relative levels of CDX1 expression had previously been determined by AffyMetrix microarray gene expression profiling and are listed in **Figure 4.1**. Although this panel of cell lines straddles the divide in CDX1 expression, it encapsulates the inherent intertumoral variation in other genetic characteristics of colorectal cancers such as genomic instability type and driver mutations (**Table 4.1**).

4.2.1.2 Candidate miRNA expression in a panel of colorectal cancer cell lines

The expression levels of the 8 miRNAs miR-34c, miR-99a, miR-150, miR-181a, miR-181b, miR-193a-3p, miR-215, and miR-584 were assayed from total RNA extracted from the 10 aforementioned cell lines using manufacturer-designed TaqMan qRT-PCR primer and probe-sets. Fold change in expression for a given miRNA was calculated relative to the average normalized Ct for that miRNA across all 10 cell lines **(Fig 4.2)**. The qRT-PCR data were used to further analyze the relationship between expression of the 8 candidate miRNAs and CDX1 by Spearman's rank correlation, in which each cell line was ranked according to its expression levels for CDX1 and each candidate miRNA. The rank statistics for a given miRNA were then correlated with the ranks corresponding to CDX1. This approach showed significant positive correlations between miR-215 and CDX1 and miR-193a-3p and CDX1 **(Table 4.2)**.

Cell line	*CDX1*	RER status	*TP53* mutation	*KRAS* mutation	*BRAF* mutation	*CTNNB1* mutation	*APC* mutation
C10	low	-	Mut	WT	WT	WT	WT
C80	high	-	Mut	mut	WT	WT	Mut
COLO201	low	-	Mut	WT	Mut	Mut	Mut
HCT116	low	+	WT	Mut	WT	Mut	WT
LIM1863	high	-	Mut	WT	WT	WT	Mut
LS174T	high	+	WT	Mut	WT	Mut	WT
LS180	high	+	WT	Mut	WT	Mut	WT
SW480	low	-	Mut	Mut	WT	WT	Mut
SW620	low	-	Mut	Mut	WT	WT	Mut
SW1222	high	-	Mut	WT	WT	WT	Mut

Table 4.1
Genetic characteristics and mutational status of 10 colorectal cancer cell lines
Cell lines are listed alphabetically. RER = Replication error. WT= wild type. Mut= Mutation. Mutations are highlighted in blue.

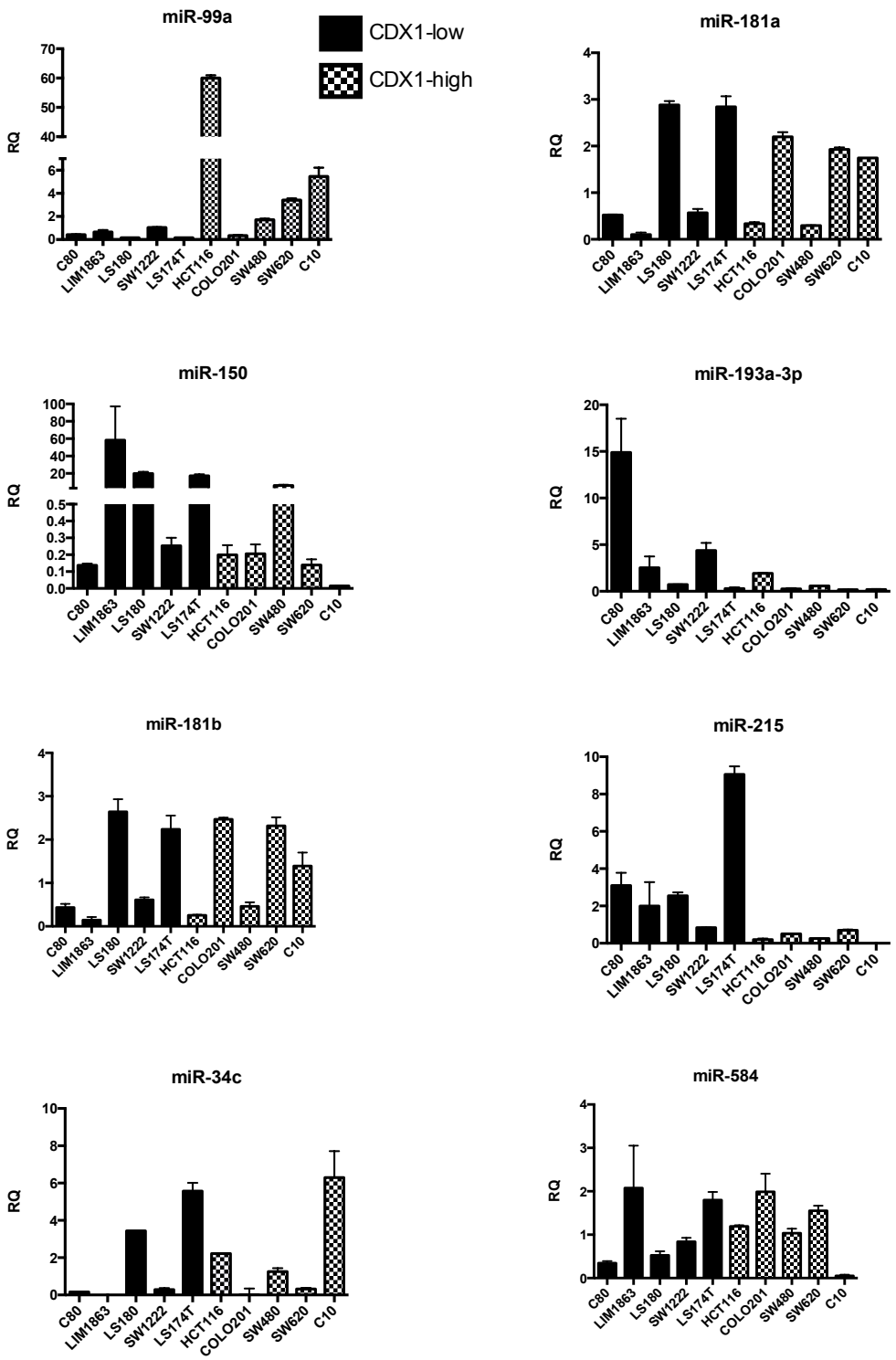

Figure 4.2
Candidate miRNA expression in 10 cell lines with differential CDX1 status
The relative expression of 8 candidate miRNAs in 5 CDX1(+) lines and 5 CDX1(-) lines. Ct values were normalized to U6 snRNA and fold change was calculated relative to the average for a given miRNA across all 10 cell lines. RQ= relative quantity, i.e. fold change relative to average across all cell lines

Cell Line	miR-215	miR-193a-3p	CDX1
SW1222	5	2	4
SW620	6	10	9
SW480	8	6	8
LS180	3	5	3
HCT116	9	4	6
LS174T	1	7	5
COLO201	7	8	7
C80	2	1	1
C10	10	9	10
LIM1863	4	3	2
Spearman's ρ	0.758	0.855	
p-value	0.0159	0.0035	

Table 4.2
Spearman's rank correlation of miRNA and CDX1 expression levels in 10 colorectal cancer cell lines

4.2.1.3 Categorical analysis of candidate miRNA-CDX1 contingency

Because of the bimodal distribution of CDX1 in this panel of 10 cell lines, we were also able to use a categorical approach to hypothesis testing. The 10 cell lines were grouped into two categories: CDX1-high and CDX1-low, as is clearly appropriate from figure 4.1. The CDX1-high group comprised LS180, C80, LIM1863, SW1222, and LS174T, while the CDX1-low group comprised HCT116, COLO201, SW480, SW620, and C10. The expression data for a given miRNA was categorized as "high" in a particular cell line if it exceeded the mean expression level across all 10 cell lines (RQ >1) and "low" if it was below the mean (RQ<1). Expression data for each candidate miRNA were thus arranged in 2x2 contingency tables and evaluated with Fisher's Exact Test (**Table 4.3)**. This more stringent statistical approach winnowed our pool of 8 candidates down to 1: miR-215. The significance of the miR-215 association only narrowly passes the arbitrary cutoff of $p<0.05$, and repeating this experiment in more cell lines would not only strengthen this association, but it may also result in the inclusion of other miRNAs as significantly associated with CDX1.

miRNA	miRNA-HIGH	miRNA-LOW	Fisher's Exact p-value
miR-215			
CDX1 high	4	0	
CDX1 low	1	5	0.04762
miR-193-3p			
high	3	1	
low	2	4	0.5238
miR-99a			
high	1	4	
low	4	1	0.2063
miR-150			
high	3	1	
low	2	4	0.5238
miR-584			
high	2	4	
low	3	1	0.5238
miR-181a			
high	2	3	
low	3	2	1
miR-181b			
high	2	3	
low	3	2	1
miR-34c			
high	2	2	
low	3	3	1

Table 4.3
Categorical analysis of miRNA-CDX1 correlations

4.2.2 Characterization of the miR-215 primary transcript

Although further study may have revealed meaningful connections between other candidate miRNAs and CDX1, we chose to focus our efforts on the miR-215, which was identified through the most conservative screening approaches, deeming it least likely to be the product of a chance association.

4.2.2.1 CDX1 transfection induces miR-215 expression but not miR-194

Many miRNAs are frequently transcribed polycistronically with "clustered" neighboring miRNA sequences (Altuvia et al., 2005). miR-215 is clustered with miR-194, although these two miRNAs have little sequence homology and are predicted to target distinct sets of mRNAs (data not shown). The miR-215-194 cluster locus on chromosome 1q41 is flanked by a 5' region with DNAse hypersensitivity, H3K27-acetylation, and is enriched for ENCODE Transcription Factor ChIPseq reads. This region is, like the miR-215 coding sequence, conserved down to *Xenopus* while the surrounding genomic regions are not **(Fig 4.3A, Fig 4.5A)**. These data indicate the presence of a significant regulatory element immediately upstream of the miR-215-194 cluster. The miR-215-194 primary transcript, however, remains uncharacterized. Because miR-215 is transcribed as a polycistron with miR-194, we might expect to see coordinate regulation of these two miRNAs by CDX1, yet differential miR-194 expression was not detected by small RNA seq in chapter 3. In order to validate this asymmetrical response to CDX1 expression at the miR-194-215 locus, we transiently transfected either pRC-CMV-CDX1 (the CDX1 construct used in chapter 3) or empty vector into parental HCT116 (i.e. the cell line from

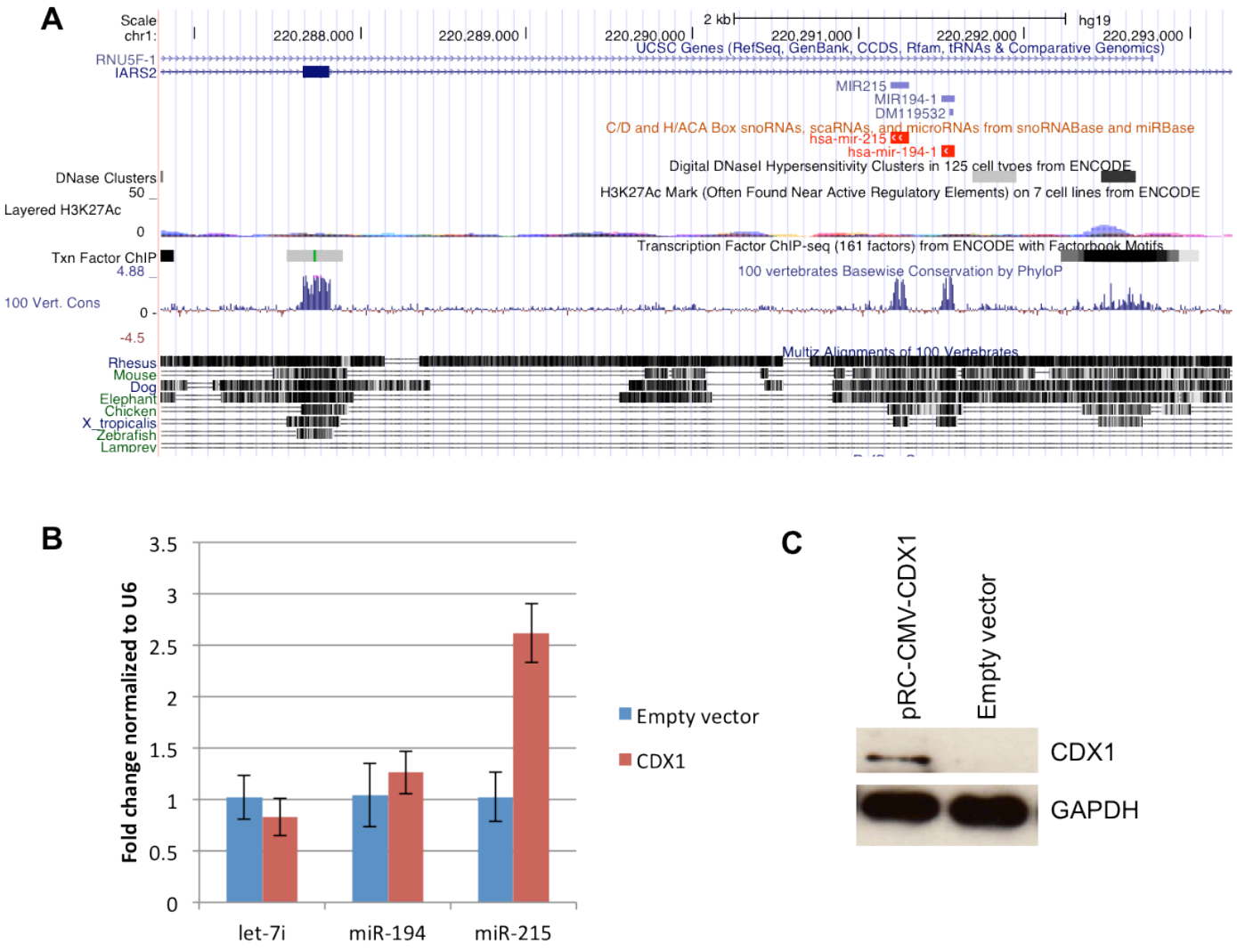

Figure 4.3
Transient CDX1 transfection specifically increases miR-215 expression
(A) UCSC genome browser depiction of the miR-194-215 cluster locus on chromosome 1. (B) Transient transfection of pRC-CMV-CDX1 into HCT116 for 48 hours strongly induces miR-215 expression, but not the clustered miR-194, as determined by TaqMan qRT-PCR normalized to U6 snRNA. The unrelated miRNA let-7i is shown as a negative control. (C) Protein lysates from transfectants in (B) were immunoblotted for CDX1 to confirm overexpression after transient transfection. GAPDH is shown as a loading control.

which the two stably transfected clones described in Chapter 3 were derived) and measured the expression of miR-215 and miR-194 after 48 hours. Consistent with the results of RNA seq and earlier qRT-PCR experiments, miR-215 was robustly up-regulated ~3.5 fold, yet miR-194 expression was unaffected **(Fig 4.3)**.

4.2.2.2 Identification of the pri-mir-194-215 transcription start site

Although miR-215 has been studied in the context of colorectal cancer, and several groups have identified transcription factors other than CDX1 responsible for controlling the upstream regulation of miR-215, there has been no successful identification of the transcription start site of the miR-215 primary transcript. In order to understand the regulation of miR-215 expression, we set out to characterize the 5' end of the miR-215 primary transcript using 5' rapid amplification of cDNA ends (RACE) (**Fig 4.4A**). This experiment was conducted in LS174T cells, which displayed the highest level of miR-215 expression (**Fig 4.2**). In order to prolong the half-life of the normally short-lived primary miRNA transcript, we used small interfering RNA (siRNA) to transiently knock down the primary miRNA processing enzyme Drosha (**Fig. 4.4B**). The products from RACE PCR were then gel purified and directly sequenced (**Fig. 4.4C, D)**. The sequence aligned perfectly with the miR-194-215 locus and located the 5' end of the pri-mir-194-215 transcript 972 base pairs upstream of the miR-194 stem-loop sequence **(Fig. 4.5A)**

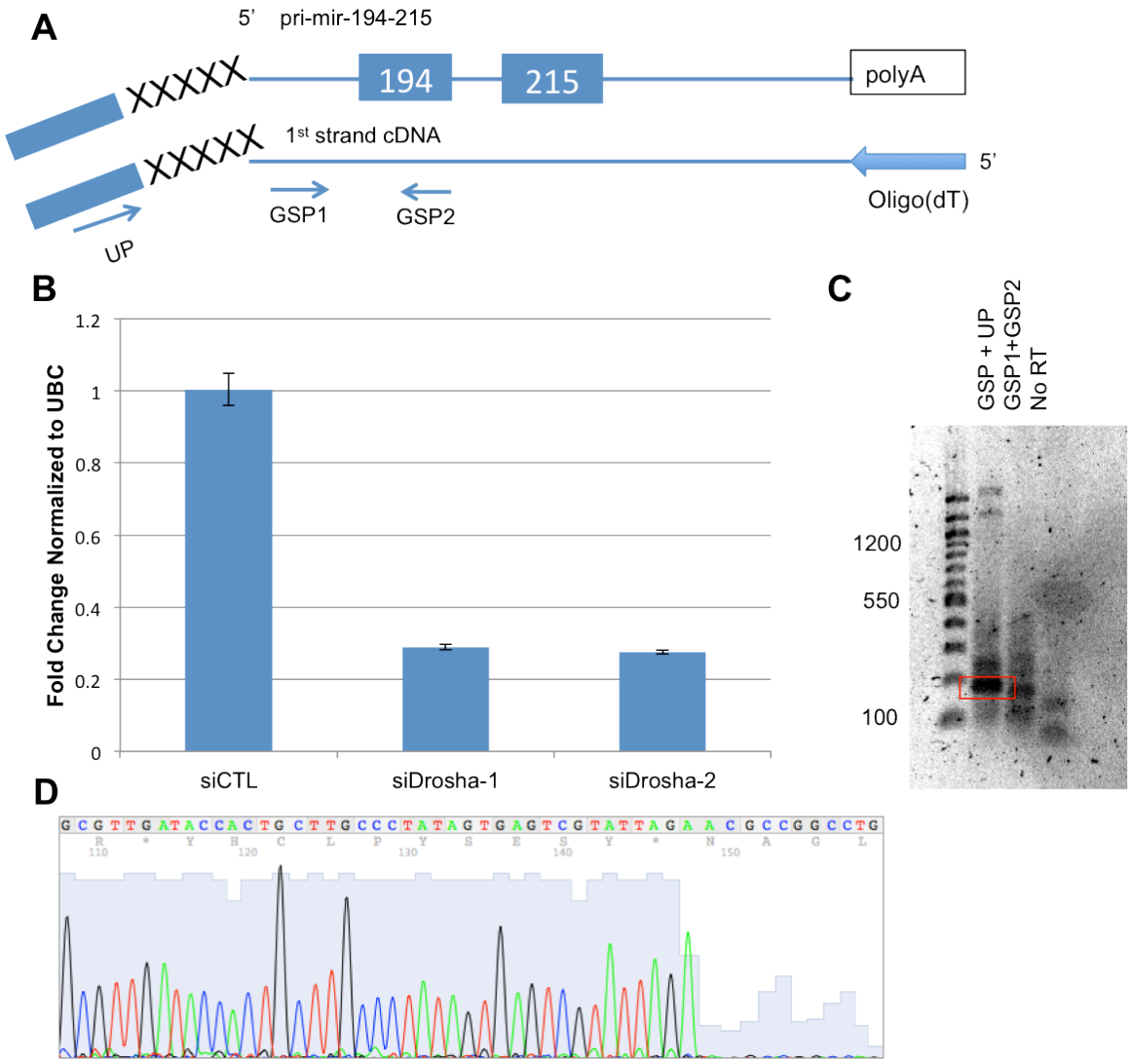

Figure 4.4
Drosha knockdown facilitates pri-mir-194-215 characterization by 5'RACE
(A) Schematic of 5'RACE for the miR-194-215 primary transcript. GSP1 and GSP2= Gene specific primer sets. UP= Universal primer, specific to RACE adapter. Not to scale, as the 3' end of the transcript remains uncharacterized. (B) Relative Drosha mRNA expression was measured by TaqMan qRT-PCR following siRNA knockdown in the cell line LS174T. Two different siRNa sequences were used, each yielding about 70% knockdown. (C) Agarose gel electropherogram of 5'RACE products. Total RNA was isolated from LS174T transiently transfected with siDrosha-2 for 48 hours. 5'RACE was carried out as shown in (A). (D) The band highlighted in (C) was excised, purified, and subjected to Sanger sequencing using the primer GSP2. The sequence ends abruptly at after 148 bases, indicating the 5' end of the transcript.

4.2.3 Transactivation of the miR-215 promoter

4.2.3.1 Heterologous luciferase reporter assay for CDX1 activity at the miR-215 promoter

An interesting consequence of the identification of the miR-194-215 transcription start site is that 4 of the 5 predicted CDX1 binding sites upstream of miR-215 occur *downstream* of the transcription start site, with only 1 occurring in an untranscribed upstream region. However, the CDX1 binding sites within the primary transcript are also highly conserved, suggesting they may play some role in transcriptional regulation. (**Fig 4.5**). With the aid of Toshifumi Hara in the Lal lab at the National Cancer Institute, we cloned genomic segments 200, 400, 600, 1.0kb and 1.6kb upstream of the 5' end of the miR-194 mature sequence into the pGL3 vector upstream of the firefly luciferase gene. Using a dual-luciferase reporter system with *Renilla* luciferase as a transfection control, we assayed transactivation of the miR-215 promoter region by CDX1. Luciferase experiments were conducted in the CDX1(-) background of HCT116, and co-transfection of pRC-CMV-CDX1 significantly induced luciferase activity in all constructs. The magnitude of the response to CDX1 co-transfection was directly, although non-linearly, related to the length of the heterologous promoter (**Fig 4.6)**. Although the 200bp construct which lacked any CDX1 sites showed the weakest activity, the 400 and 600bp constructs did not differ in their responses despite their difference in number of CDX1 binding sites. Apparently the distal CDX1 binding site was most important for promoter activity, as the 1.0kb and 1.6kb constructs showed the strongest activity in response to CDX1 (**Fig 4.6)**.

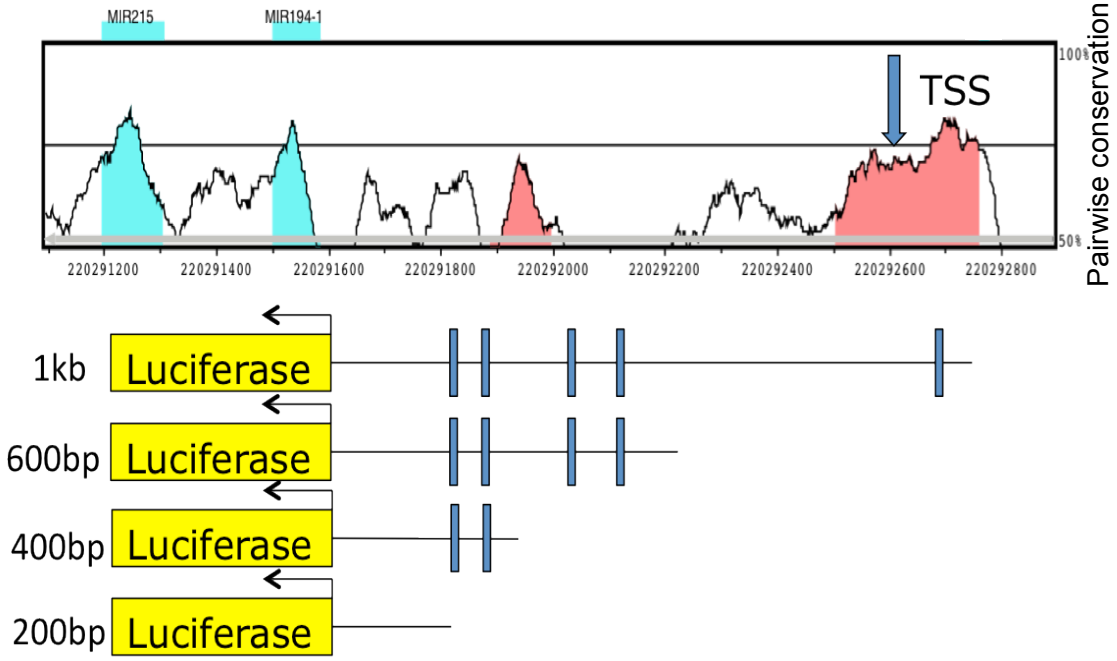

Figure 4.5
Human-mouse pairwise conservation of the mir-194-215 cluster and promoter reporter constructs
Top panel: Vista conservation plot showing a sliding window average of the percentage of pairwise sequence conservation between human and mouse and the miR-194-215 locus. Blue regions indicate predicted coding sequences and salmon regions indicate predicted regulatory sequences. The blue arrow labeled TSS indicates the position of the transcription start site identified by 5'RACE.
Bottom panel: Drawn to the same scale as the vista plot, the four luciferase reporter constructs created to test the CDX1 responsiveness of the miR-215 promoter. The blue bars indicate the positions of TESS-predicted CDX1 binding sites.

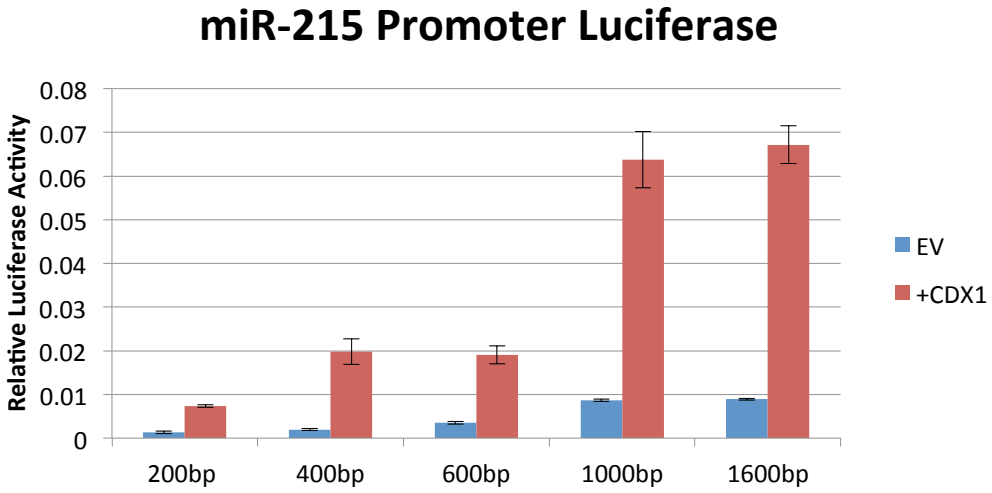

Figure 4.6
CDX1 directly transactivates the mir-215 promoter
pGL3 constructs containing miR-215 promoter fragments of the indicated length were co-transfected into HCT116 cells with either pRC-CMV-Empty Vector or pRC-CMV-CDX1 and pRL constitutive *Renilla* luciferase plasmid as a transfection control. Luminescence was measured after 24 hours. Co-transfection significantly increased luminescence in for all constructs, but the 1000bp and 1600bp constructs increased most profoundly with CDX1 co-transfection.

4.2.3.2 The effect of p53 status on of CDX1 transactivation of the miR-215 promoter

Luciferase experiments were conducted in cell lines with a CDX1(-) background as a matter of course, yet we noticed a clear difference in relative luminescence between HCT116 and DLD1, despite their similar endogenous CDX1 expression levels **(Fig. 4.7)**. A clear and significant difference in luminescence was observed when either of the 1.0kb or 1.6kb promoter constructs were co-transfected with a constitutively active pRC/CMV-CDX1 construct in HCT116, yet this effect was much less pronounced in DLD1.

DLD1 and HCT116 differ most notably in their p53 status: HCT116 is p53-wild type while DLD1 carries a S241F p53 mutation. Additionally, induction of miR-215 by p53 has been previously reported (Braun et al., 2008; Georges et al., 2008). To investigate the potential interplay between p53 status and CDX1-mediated transcriptional activity, we repeated the miR-215 promoter luciferase assay in an HCT116 line in which the p53 locus had been deleted by homologous recombination **(Fig. 4.7)**. There was a significant difference in CDX1-mediated luminescence between the parental HCT116 and HCT116p53-/- lines. More work will be necessary to fully understand the relationship between p53 and CDX1, both in the specific case of miR-215 and in activating a concerted transcriptional program.

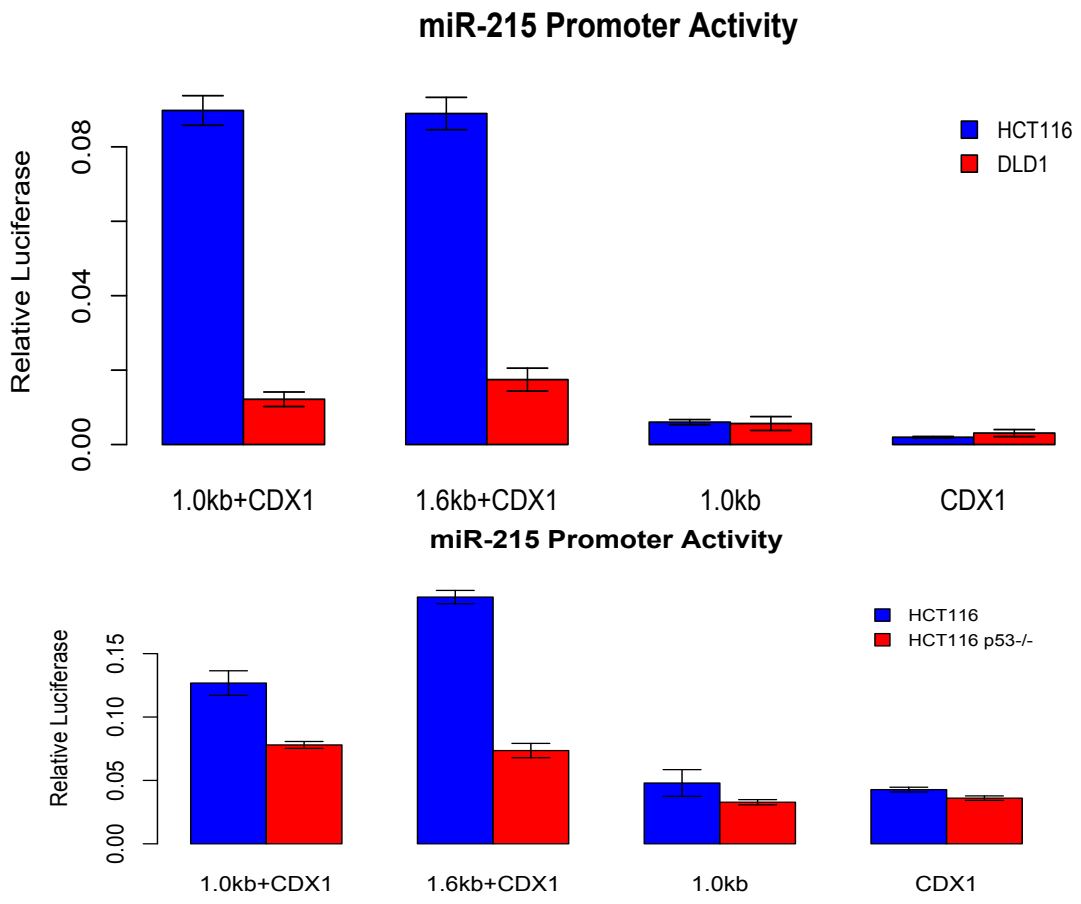

Figure 4.7
Wild type p53 is potentiates CDX1 transactivation of the miR-215 promoter
Upper panel- DLD1 and HCT116 cells were transiently transfected with luciferase reporter constructs containing either the 1.0kb or 1.6kb region upstream of the miR-194 mature sequence. When cotransfected with CDX1, HCT116 cells showed a nearly 50-fold increase in firefly luciferase activity compared to transfection with either the reporter or CDX1 alone. The response to CDX1 was also 7-fold greater in HCT116 than in DLD1 (Student's t p-value=0.0006).
Lower panel- The same assay conducted in HCT116 and HCT116 p53-/-. Firefly luciferase activity driven by the 1.0kb promoter was 160% higher in the HCT116 parental than p53-/- (p=0.008), and firefly activity driven by the 1.6kb promoter was 260% higher (p=0.002).

4.2.3.3 5-Aza-2'-Deoxycytidine induces miR-215 expression in a CDX1-dependent manner

Because CDX1 expression is controlled by methylation of CpG sites in its promoter, treatment of CDX1(-) cell lines with the DNA-methyltransferase inhibitor 5-aza-2'-deoxycytidine (5-aza) results in increased CDX1 expression. Using the protocol developed in Chan's thesis (2009) and Chan, *et al.,* 2010, treatment of the CDX1-methylated cell line HCT116 with 5-azaC results in an approximately 4-fold increase in CDX1 expression, and a corresponding 4-fold increase in mir-215 expression. With our prior knowledge of the regulatory relationship between CDX1 and miR-215, this result suggests an indirect effect of 5-aza on miR-215 through de-repression of the upstream regulator CDX1. However, it may also be due to the activation of a different regulatory factor or de-methylation of the miR-215 promoter itself. To test the CDX1-dependence of the effects of 5-aza on miR-215, we transiently transfected HCT116 with siRNA against CDX1 (siRNA sequence taken from Chan's thesis (2009) or scrambled siRNA before treating with 5-aza. The CDX1 siRNA completely abolishes the effect of 5-aza on both CDX1 and miR-215 expression, which further supports the conclusion that CDX1 directly regulates miR-215 (**Fig 4.8).**

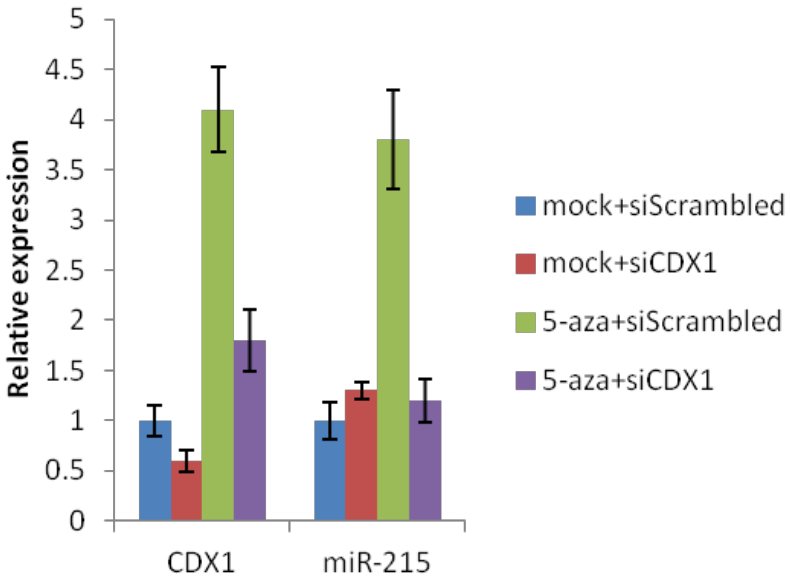

Figure 4.8
5-Aza-2'-Deoxycytidine treatment increases miR-215 expression in a CDX1-dependent manner
After 5-aza treatment, both CDX1 and miR-215 expression in the normally CDX1-methylated line HCT116 increased by approximately 4-fold compared to mock-treatment. Transfection with siRNA against CDX1 prior to 5-aza treatment abolished upregulation of both CDX1 and miR-215. As determined by Student's T-test, p=0.001

4.2.3.4 CDX1 chromatin immunoprecipitation enriches for the miR-215 promoter

Chromatin immunoprecipitation for CDX1 was performed in order to measure the occupancy of the miR-215 promoter by CDX1 in standard cellular conditions. We have substantial evidence correlating miR-215 expression to CDX1, and ectopic CDX1 expression induces miR-215 and activates a heterologous miR-215 promoter, but ChIP remains to best method to demonstrate a direct, molecular interaction between endogenous CDX1 and the miR-215 promoter. We chose to perform this experiment in SW1222 cells, despite their relatively lower levels of miR-215 expression, because they express high levels of CDX1 (**Fig 4.9)** and because they grow in a mostly regular monolayer on plastic, which has methodological advantages for ChIP. After fixing the cells in formaldehyde and lysing the nuclei, the chromatin was sheared by sonication to a size range of 200-600 bp. Equal volumes of sheared lysate were then incubated with either monoclonal CDX1 antibody, non-specific mouse IgG as a negative control, or monoclonal RNA polymerase II antibody as a positive control (data not shown). After reversing the crosslinks, digesting away the protein, and purifying the DNA, we used SYBR-Green qPCR to assay for enrichment of several promoter regions. KRT20 has been extensively validated as a target of CDX1, and Chan's thesis (2009) demonstrated CDX1 binding through ChIP. Primer sequences for the *KRT20* promoter were taken from Chan's thesis (2009), while miR-215 promoter primers were designed to flank the putative CDX1 binding site immediately 5' of the transcription start site. Primers flanking the core GAPDH promoter were used as an internal control. The promoters of *KRT20* and miR-215 were enriched in CDX1 ChIP samples, normalized to the GAPDH

promoter and compared to input. As we would expect, the CDX1 ChIP from the CDX1(+) cell line SW1222 resulted in much stronger enrichment than from the CDX1(-) cell line HCT116 (**Fig 4.9**). Collectively, these results confirm the binding of CDX1 to the miR-215 promoter at levels comparable to that of a well-characterized, protein-coding CDX1 target gene.

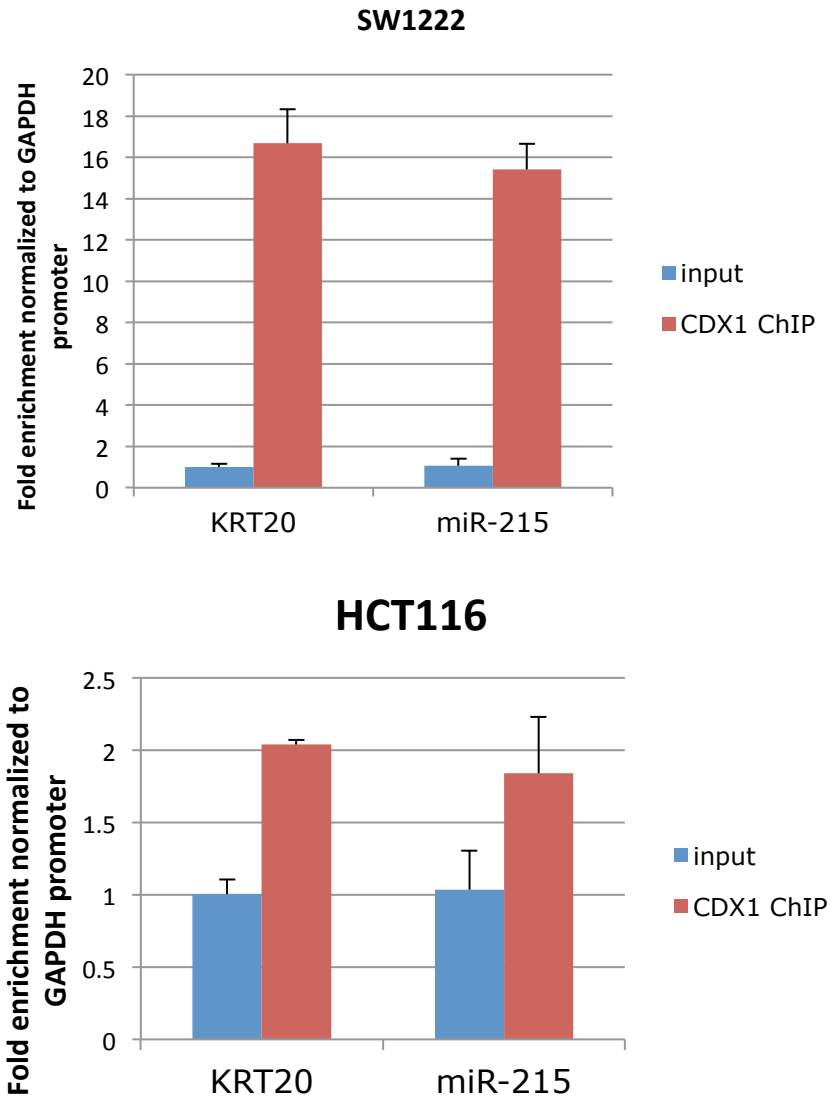

Figure 4.9
CDX1 ChIP-qPCR shows similar enrichment for *KRT20* and miR-215 promoters
Upper panel: ChIP-PCR from the CDX1-high SW1222 cell line showed similar levels of enrichment for the miR-215 and *KRT20* promoters. miR-215 primers were designed to amplify the putative CDX1 binding site ~1.0kb upstream of miR-194. The KRT20 primer sequences were taken from Chan's thesis (2009).
Lower panel: ChIP-PCR from the CDX1-low HCT116 also showed enrichment of KRT20 and mir-215 promoters, though the degree of enrichment was much less pronounced. In both cell lines, *KRT20* and miR-215 promoter enrichment was calculated normalized to the *GAPDH* promoter and calculated relative to the input (no IP) sample.

4.3 Discussion

After using qRT-PCR to validate the relative expression of the candidate miRNAs identified by small RNA sequencing, we proceeded to evaluate their expression in a larger cohort of samples with a bimodal distribution of CDX1. Of the 8 previously identified candidate miRNAs, only miR-193a-3p and miR-215 displayed a significant correlation with CDX1. However, analysis by Pearson's correlation presupposes a smoother variation in CDX1 levels across the ten samples than was actually the case. Because the samples could easily be grouped into two categories based on CDX1 levels, we performed an analysis of 2x2 contingency tables using Fisher's exact test. Samples were grouped according to their miRNA expression in the following manner: those with fold change greater than 1 relative to the average normalized cycle threshold for a given miRNA across all 10 samples were placed into the "high" category, and those with a fold change less than 1 were placed into the low category. By this measure, only miR-215 is significantly associated with CDX1 expression (see table 2).

MiR-215 is well-conserved across animal phyla (Frazer et al., 2004; Karolchik et al., 2014), indicating a significant, functional role in the regulation of gene expression. Unlike other miRNAs that have been implicated in cancer, such as let-7 or miR-34, comparatively little is known about the pathways that interact with miR-215, but there are some hints in the literature that miR-215 is, indeed, an important mediator of differentiation waiting to be characterized. A study on the miRNA expression profile of Barrett's esophagus revealed miR-215 to be significantly upregulated in esophageal metaplasia (Wijnhoven et al., 2010). Barrett's metaplasia is a condition in which the

normal squamous epithelium of the esophagus is replaced by intestine-like columnar epithelium in response to chronic acid reflux. A previous finding from Wong, *et al*. also showed that demethylation of the CDX1 promoter and the consequent increase in CDX1 expression is a major driver of the metaplastic response in Barrett's esophagus (Wong et al., 2005). Given that miR-215 is over-expressed in a disease involving abnormal differentiation into gut lineages in association with CDX1, it seems theoretically plausible that miR-215 is involved in CDX1-mediated multilineage differentiation in colorectal cancer.

The only genetic factor currently known to regulate miR-215 expression is the seemingly omnipresent tumor suppressor p53. A pair of *Cancer Res*. papers showed that miR-215 and its homolog on chromosome 11, miR-192, are upregulated by p53 response to genotoxic stress, and that these miRNAs are capable of inducing cell-cycle arrest via a p21-dependent mechanism (Braun et al., 2008; Georges et al., 2008). p21-mediated growth arrest has long been thought to play a role in terminal differentiation (Macleod et al., 1995; Evers et al., 1996; Topley et al., 1999), so it may be the case that miR-215 effects the differentiation-related program of CDX1 by upregulation of p21. However, the mechanism by which miR-215 influences p21 accumulation is not clear. It is also interesting to note that Braun, *et al*. claimed that although miR-215 could effectively induce growth arrest, it did not trigger an increase in cell-death via apoptosis. This observation is consistent with a model in which miR-215 expression is involved with the processes of growth arrest and differentiation rather than apoptosis and cell death, and it may also help to explain the high level of miR-215 expression in some CRC cell lines.

Rather than functioning as a *bona fide* tumor suppressor as previously claimed (Song et al., 2010; Karaayvaz et al., 2011; White et al., 2011), miR-215 may be responsible for variation in grade and aggressiveness between tumors, i.e. tumors with low miR-215 expression (and hence, low CDX1 expression) are more likely to be more poorly differentiated and aggressive than tumors with high miR-215 expression.

Furthermore, Braun, *et al*., and Georges, *et al*., observed co-regulation of miR-215 and 194 by p53, and functionally grouped these miRNAs with their paralogous cluster on chromosome 11 consisting of miR-194-2 and miR-192. However, our results in this chapter and chapter 3 show no indication that CDX1 regulates the expression of any of miR-194-1, miR-194-2, or miR-192. It may be the case that the CDX1 binding sites we have identified downstream of the miR-194-215 transcription start site are necessary for specific induction of miR-215 expression via some post-transcriptional regulatory mechanism, although further site-directed mutagenesis experiments would be needed to confirm this theory. Further study of transactivation of miR-215 expression could also be carried out by using a CDX1 construct with a mutated DNA-binding domain. We would hypothesize that transfection of this mutant would not result in miR-215 upregulation.

To establish a direct, causal relationship between CDX1 and miR-215, we created luciferase constructs in which the expression of the firefly reporter was driven by the putative miR-215 promoter. These constructs contained different lengths of promoter sequence upstream of miR-194-215. When these reporter constructs were co-transfected into HCT116 cells along with a constitutively active CDX1-expressing vector,

luminescence was detected at a level significantly above that observed with either the reporter or CDX1 vector alone, and the amount of luminescence varied directly with the number of CDX1 binding sites present in the heterologous promoter. However, even the shortest promoter induced some luciferase activity in the presence of CDX1, so a gel-shift assay could be conducted to determine whether there is a cryptic CDX1 binding site in this region. Additionally, mutation of the distal CDX1 binding sites would strengthen the conclusion that the activity of the miR-215 promoter is directly dependent on CDX1.

Interestingly, the induction of the miR-215 promoter by CDX1 was mitigated in p53mt or p53-null cell lines, which suggests that the transcriptional activity of CDX1 may depend on p53 status. As discussed above, miR-215 has been shown to be a direct target of p53, but the potentiation of CDX1 transactivation does not depend on activation of p53, but rather baseline p53 status. CDX1 ChIP in both the p53 mutant cell line SW122 and the p53-wild type cell line HCT116 enriched for the miR-215 promoter region, so apparently p53 is not necessary for the binding of CDX1 to the DNA, but perhaps instead for subsequent steps in transcriptional activation. This indicates a permissive role for p53 in regulating miR-215, and further strengthens the hypothesis that miR-215 functions as an effector of CDX1 rather than as a classical tumor suppressor whose primary function is to suppress growth and cell survival. In the context of cancer, this function does not necessarily contravene the growth and survival imperatives of tumor cells, but it does, perhaps, account for the phenotypic heterogeneity seen in some tumors. miR-215 as differentiation-mediator may, in fact, help us to understand the relationship between the

tumor bulk, which often consists of terminally differentiated cells, and the cancer stem cell compartment.

In addition to the *in vitro* data we present here, it would be valuable to investigate the nature of miR-215 regulation by CDX1 in primary tumor samples. We had attempted to analyze this by mining The Cancer Genome Atlas data, but there appear to be annotation flaws in the raw data files that prevent retrieval of CDX1 expression values for certain samples. This issue would need to be addressed by a bioinformatics specialist before such analysis could proceed.

The results of this chapter indicate that miR-215 is a novel transcriptional target of CDX1. An interesting implication of this work is that CDX1 regulates only one member of a polycistronic miRNA cluster. CDX1does not appear affect the expression of miR-215 relatives on other chromosomes. In subsequent chapters, we explore the effects of miR-215 on the regulation of gene expression, as well as functional phenotypes such as proliferation, and differentiation.

CHAPTER FIVE

Identification of MiR-215 targets

CHAPTER 5: IDENTIFICATION OF MIR-215 TARGETS

5.1 Introduction

In the previous chapters, we have established miR-215 as a direct target of CDX1 using a combination of systems and molecular biology methods, including RNA seq, promoter reporter assays, and chromatin immunoprecipitation. However, none of these techniques have explicitly allowed us to predict the effects of miR-215 on gene expression or cellular phenotype. MiRNAs canonically function to repress the expression of target genes (Kim et al., 2009), so identifying the genes that are targeted by miR-215 will allow us to generate hypotheses regarding the functions effected by miR-215. We can then design the appropriate experiments to test these functional hypotheses.

Early studies suggested that miRNAs decreased the expression of their target genes by inhibiting mRNA translation without affecting mRNA stability (Filipowicz et al., 2008; Ameres and Zamore, 2013; Muramatsu et al., 2013). However, recent high-throughput studies that analyzing global changes in miRNA target expression at both mRNA and protein levels suggest that mammalian miRNAs predominantly act by promoting mRNA degradation (Selbach et al., 2008; Baek et al., 2008; Guo et al., 2010). High throughput transcriptome profiling remains simpler, faster, and less expensive than high-throughput proteomics so the assumption that miRNAs act predominantly to decrease the mRNA levels of their target genes greatly simplifies the process of target identification. Indeed, these paradigm shifting observations have allowed us and others to identify the genome-wide targets of specific miRNAs by simply interrogating changes in mRNA levels using

microarrays or RNAseq after over-expressing or antagonizing the miRNA of interest (Li et al., 2014; Subramanian et al., 2014; Jahid et al., 2012; Korpal et al., 2008). By performing microarray gene expression profiling in combination with bioinformatic miRNA target prediction, we have been able to generate lists of candidate targets for a given miRNA. In general, the workflow first identifies mRNAs that are significantly downregulated by the introduction of a synthetic miRNA mimic using mRNA microarrays, then examines these differentially expressed transcripts for the presence of seed matches to the miRNA of interest using an algorithm that weights matches according to their phylogenetic conservation (TargetScan) (Lewis et al., 2005), thermodynamic favorability (PITA) (Kertesz et al., 2007) or other ancillary factors. Finally the candidate miRNA targets are confirmed using the 3'UTR luciferase assay, which remains the accepted standard for inferring direct repressive relationships between a miRNA and a 3'UTR (Thomson et al., 2011).

In this chapter, we present data following the workflow outlined above. In addition, we make substantial efforts to validate the methodologies used to perturb miR-215 expression. The mimic transfection approach is compared at length with vector-driven miR-215 overexpression, and the physiological incorporation of miR-215 mimic is assessed by quantitative RNA immunoprecipitation of the RNA-induced silencing complex. We also detail the construction of a novel miRNA "sponge" construct, which is thoroughly validated and subsequently used to soak up endogenous miR-215. Finally, we identify a particularly provocative direct target of miR-215, namely the polycomb

repressive complex I (PRC1) component *BMI1*, and we confirm its downregulation by miR-215 as part of the CDX1 axis.

5.2 Results

5.2.1 Impact of miR-215 overexpression on the transcriptome

5.2.1.1 Physiological validation of miR-215 mimetic through Argonaute-RNA immunoprecipitation

Transfection of synthetic miRNA mimetic molecules, hereafter referred to as miRNA mimics, is a convenient and efficient method for introducing exogenous miRNAs into cells both *in vitro* and *in vivo* (Thomson et al., 2011). A standard method to identify miRNA targets involves transfecting a mimic of the miRNA of interest into cells that normally express low levels of that miRNA and assaying the resulting changes in the transcriptome using microarray gene expression profiling. However, this method presupposes that transient transfection of synthetic miRNA mimics will faithfully recapitulate the physiological expression levels and functions of the endogenous miRNA. Before we proceed to interrogate the effects of miR-215 on the transcriptome, we must first validate the physiological relevance of miR-215 mimic transfection. In order to accomplish this, we and others have used a method whereby miRNA-RISC complexes are quantitatively captured via immunoprecipitation of Argonaute 2 (AGO2) following mimic transfection (Thomson et al., 2013; Subramanian et al., 2014; Li et al., 2014).

We conducted this experiment by transfecting HCT116 cells with 20 nM of miR-215 mimic or control mimic (cel-miR-67, hereafter referred to as CTL). RNA was then purified from the immunoprecipitate, and the relative RISC-associated quantity of the miR-215 mimic was assayed by qRT-PCR. By comparing the enrichment of the mimic in the AGO2 IP fraction to that of an unrelated, endogenous miRNA, we determined that the amount of miR-215 mimic incorporated into the RNA-induced gene silencing machinery was within physiological levels. The unrelated endogenous miR-200a is robustly expressed in HCT116 (see RNA seq data, Appendix I), and it was enriched some 50-70 fold in AGO2 immunoprecipitate (**Fig 5.1 A, Top Panel)**. This enrichment was not affected by transfection with miR-215 mimic nor by transfection with a control mimic. Although miR-215 was overexpressed by 120 fold after miR-215 mimic transfection compared to transfection with a control mimic as measured by standard qRT-PCR (**Fig 5.1A, Middle Panel**), the amount of miR-215 present in the AGO2 IPs was only 35-fold greater than control (**Fig 5.1 A, Bottom Panel**). This is consistent with the relative amount of a highly-expressed endogenous miRNA present in the RISC, as shown by comparison with the enrichment levels of miR-200a. The efficacy of AGO2 immunoprecipitation was confirmed by western immunoblot for AGO2 (**Fig 5.1 B)**. AGO2 protein was specifically enriched in the IP samples incubated with anti-AGO2, while AGO2 was not detectable in the IgG control IP samples.

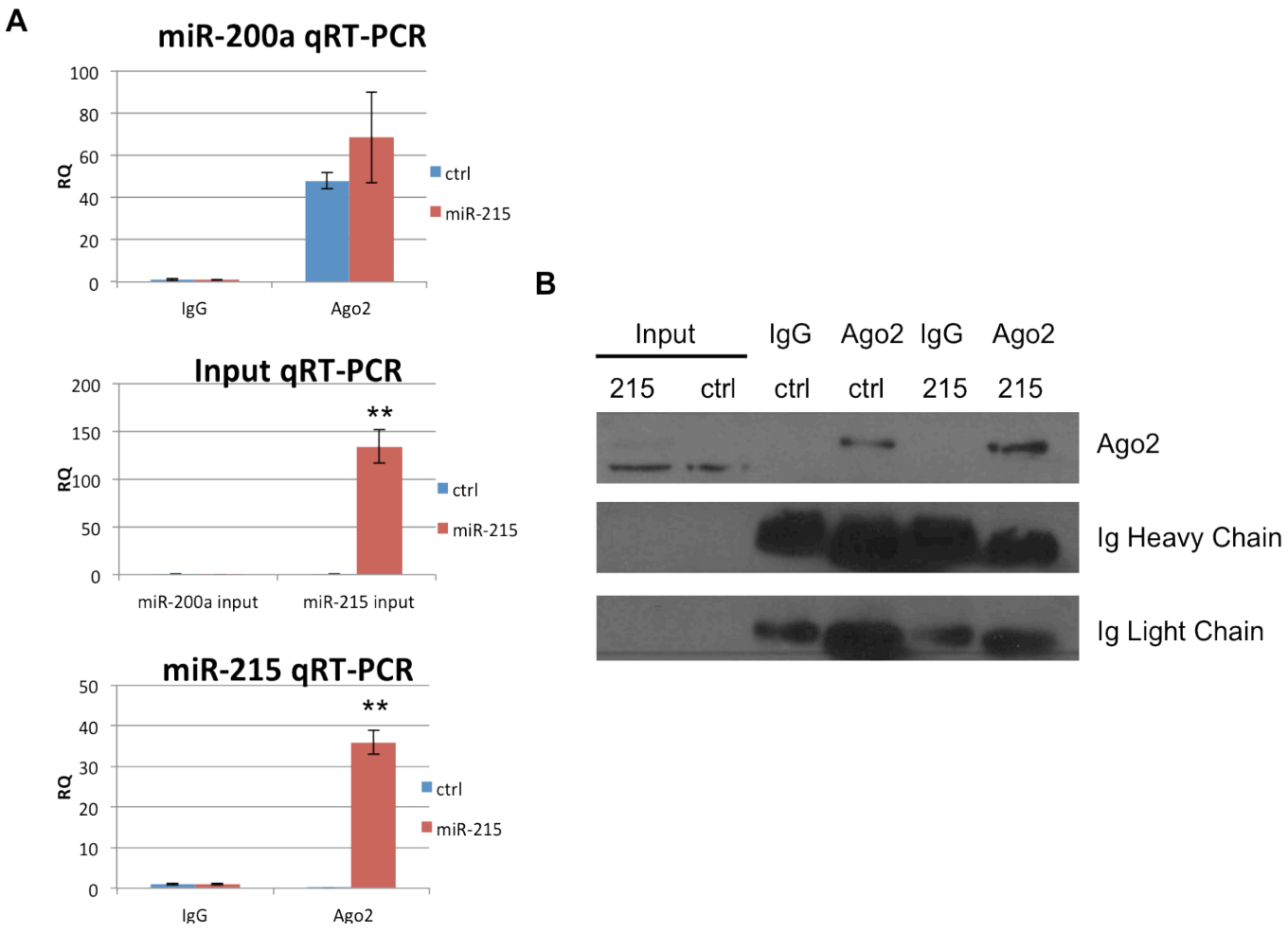

Figure 5.1
miRNA mimic transfection results in physiological levels of miRNA overexpression
(A) HCT116 cells were transiently transfected for 48-hours with miR-215 mimic or control. The cells were then lysed and subjected to RNA immunoprecipitation with anti-Ago2 or IgG as a negative control. RNA was isolated from Ago2 and IgG immunoprecipitates and an equal volume of input and subjected to qPCR for miR-215. The unrelated miR-200 was also quantified to demonstrate the expected amount of Ago2 enrichment for an endogenously expressed miRNA and to show the specificity of the miR-215 mimic. B) Western immunoblot analysis of the lysates used for RNA isolation in (A). The IP samples show intense bands corresponding to immunoglobulin heavy and light chains. Ago2 was successfully recovered in immunoprecipitations from both the control and miR-215 transfected samples.

5.2.1.2 Microarray gene expression profiling following miR-215 mimic transfection

Having validated the physiological levels of miR-215 overexpression following miR-215 mimic transfection, we used microarray gene expression profiling to identify genes whose expression changed significantly after the introduction of miR-215 to HCT116 cells. HCT116 was transfected in triplicate with 20nM miR-215 mimics, total RNA was purified, and hybridized to the Illumina Human HT-12-v4 Expression BeadChip. Differential expression was calculated using a student's t-test between control- and mimic-transfected replicates. P-values were adjusted for multiple hypothesis testing using the Bonferroni correction. Using an arbitrary fold-change cutoff of 0.6-fold downregulation relative to control and an adjusted p-value cutoff of adj. $p<0.05$, we obtained a list of 1642 mRNAs significantly downregulated by miR-215. Similarly, we imposed an arbitrary fold change cutoff of 1.5-fold and a significance requirement of adj. $p<0.05$ to identify 1674 mRNAs significantly upregulated by miR-215. It is likely that many of the changes in both of these lists are due to indirect effects, especially in the case of the upregulated genes, because miRNAs are known to act primarily by reducing the expression of their target genes. Further microarray data are listed in **Appendix II**.

As mentioned in Chapter 4, prior work in the Cancer and Immunogenetics lab has characterized the gene expression profiles of over 100 colorectal cancer cell lines. Because we are interested in miR-215 as a downstream effector of CDX1, we compared the list of genes downregulated in the miR-215 microarray with those downregulated in the HCT116-CDX1 microarray relative to HCT116-vec. We reasoned that genes in the intersection between these two lists would reflect the most physiologically relevant

targets of miR-215 vis-à-vis CDX1. We found 530 genes appearing in both miR-215 and CDX1 downregulated lists (**Fig 5.2 A**). We used the hypergeometric probability distribution to evaluate the likelihood that such a degree of overlap could occur by chance, and we found that this intersection is highly significant, with a p-value ~ 10^{-27}. We further compared the list of significantly down-regulated genes in the miR-215 microarray with the complete list of computationally predicted miR-215 targets obtained from the TargetScan algorithm to roughly estimate the extent to which the transcriptomic changes pursuant to miR-215 mimic transfection result from direct targeting of mRNAs by miR-215. We found 253 genes in common between these lists (**Fig 5.2 A**), which is also a highly significant intersection ($p = 3.7x10^{-14}$).

A manually selected subset of differentially expressed genes from the miR-215 microarray were validated by SYBR-Green qRT-PCR using input RNA from an independent set of miR-215 mimic transfections. These genes were chosen to represent both ends of the array's dynamic range, from the strongly downregulated to the strongly upregulated, as well as to represent diverse and well-studied cellular pathways. The cell cycle genes *CDC20, CDKN2A, CDKN3,* and *CCNB2* were downregulated in both the array and qRT-PCR while *CDKN1A* (p21) was strongly upregulated. The negative regulator of apoptosis *BIRC5,* a.k.a. Survivin, was robustly down-regulated, as were the stemness-promoting genes *EFNB2* and *RUNX1*. The epithelial surface protein *CEACAM1* was also strongly up-regulated. The only gene in our sample that was not successfully validated was *JUND* (**Fig 5.2 B**). These data are not intended to suggest coherent

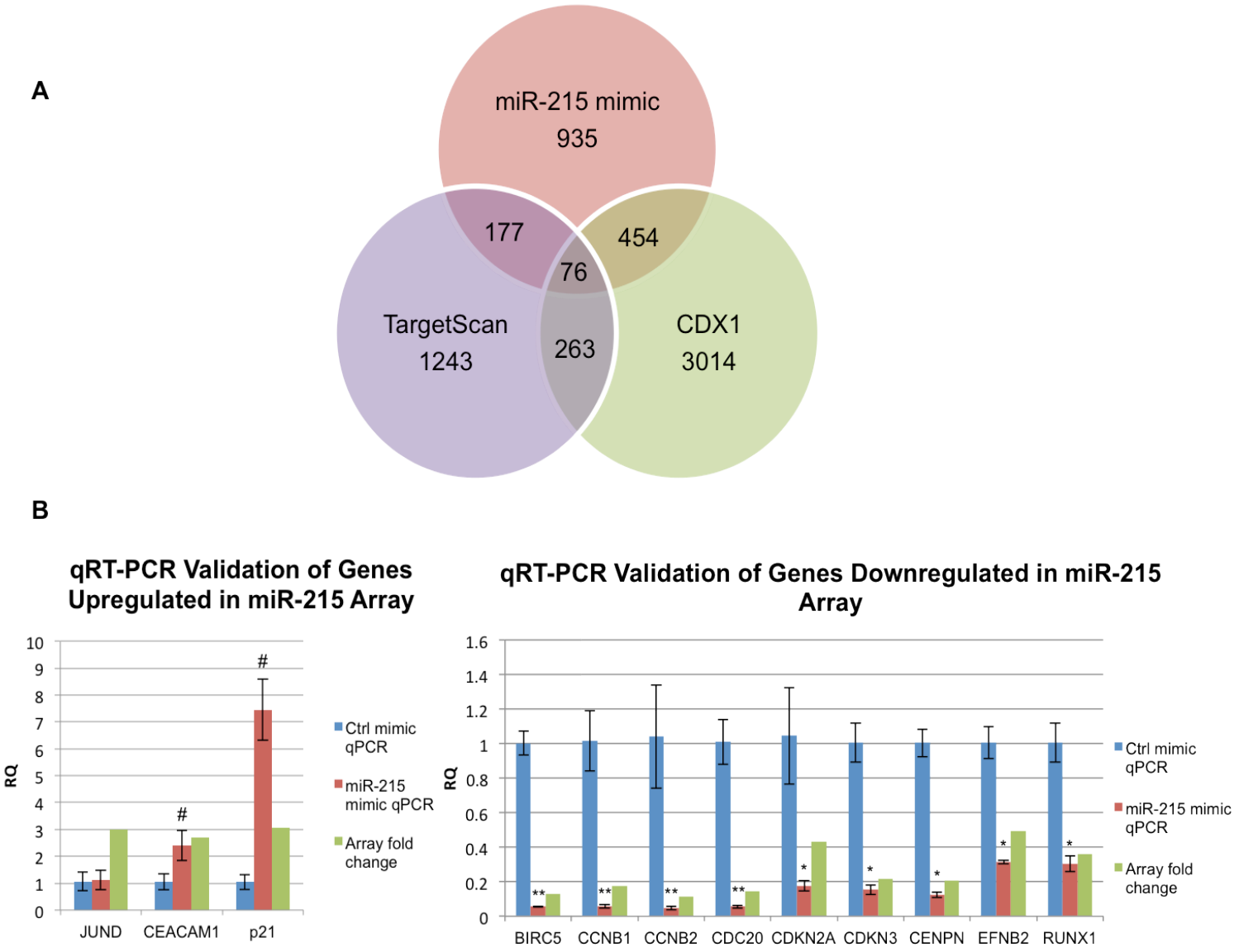

Figure 5.2
Regulation of the transcriptome by miR-215
A) Venn diagram showing the intersection between the genes significantly downregulated in the miR-215 microarray, the genes significantly down-regulated in the CDX1 microarray, and the mRNAs predicted to be direct miR-215 targets by TargetScan. Note that for this preliminary analysis, TargetScan prediction was made irrespective of seed-match conservation to provide a less conservative picture of miR-215 3'UTR seed matches. Venn diagram is not drawn to scale B) HCT116 was transfected with miR-215 mimic or control, RNA was isolated after 24 hours, and mRNA expression levels of genes identified as differentially expressed in the microarray was measured using SYBR Green qRT-PCR. Blue and red bars represent expression levels following independent transfection of ctrl or miR-215 mimics; green bar represents fold change miR215/control measured in the microarray. Of the 12 genes assayed, only JUND was not observed to be differentially expressed in both the array and qRT-PCR experiments. RQ= Relative quantity; Comparisons between blue and red bars: #p<0.05, *p<0.01, **p<0.001

regulation of the aforementioned pathways by miR-215, but rather to support the validity and accuracy of the results of microarray gene expression profiling, shown graphically by the similarity between the heights of the green and red bars in **Figure 5.2 B**.

5.2.1.3 Validation of the effects of synthetic miR-215 mimics

Prior to conducting the microarray study of miR-215 mimic-transfected HCT116 cells, we confirmed that mimic transfection resulted in physiological levels of active exogenous miR-215. However, after characterizing the transcriptomic effects of miR-215 mimic transfection, it is important to confirm that these effects are not somehow artifacts caused by transfection of synthetic mimic molecules and that the synthetic miR-215 mimic does not have different effects than endogenously expressed miR-215. We therefore cloned the precursor miR-215 stem-loop sequence (pre-miR-215) as predicted by miRBase v. 20 (mirbase.org) (Kozomara et al., 2014) into the pCDH4-CMV vector using primers flanking the miR-215 precursor and excluding the neighboring miR-194. Transfection of this construct results in overexpression of pre-miR-215, which is processed by the endogenous miRNA biogenesis pathway.

The resulting pre-miR-215 constructs were tested for their capacity to express mature miR-215 and for the differential expression of genes previously identified as differentially expressed after miR-215 transfection. We transfected HCT116 cells with either pCDH4-empty vector (pCDH4-EV) or pCDH4-pre-miR-215. After 48 hours, total RNA was isolated and miR-215 expression was measured by TaqMan qRT-PCR, with all three constructs displaying >500-fold increases in miR-215 expression (**Fig 5.3 A**). The

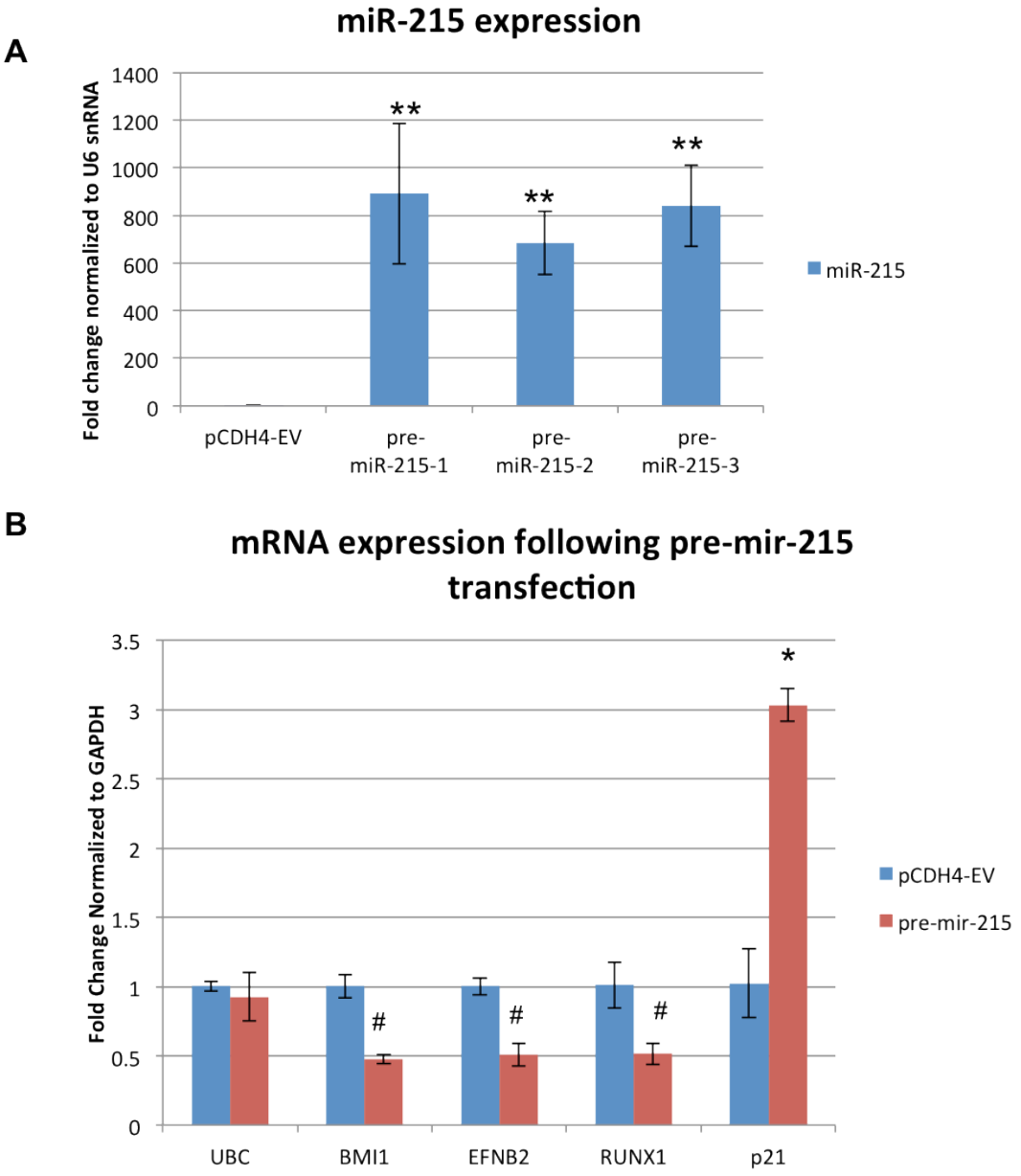

Figure 5.3
Vector driven miR-215 overexpression targets the same genes as synthetic miR-215 mimics
A) The miR-215 precursor sequence was cloned into the MCS of the pCDH4 vector downstream of the constitutive CMV promoter. HCT116 was transfected in duplicate with DNA isolated from 3 different bacterial clones of either pre-miR-215 or the empty vector control (pCDH4-EV). RNA was isolated after 48 hours, and mature miR-215 expression was measured by TaqMan qRT-PCR. B) mRNA expression of a subset of candidate miR-215 targets was assayed by SYBR-Green qRT-PCR from the total RNA isolated in (A). Error bars represent average of three transfections. #p<0.05, *p<0.01, **p<0.001

same batches of RNA were then subjected to SYBR-Green qRT-PCR to assay the expression of a subset of candidate miR-215 targets. Expression of the housekeeping gene *UBC* was unaffected by pre-mir-215 transfection, while *BMI1*, *EFNB2*, and *RUNX1* were all decreased to a similar extent as in the microarray. p21 mRNA was also strongly upregulated as in the miR-215 microarray(**Fig. 5.3 B**). These results suggest that vector-driven miR-215 expression has the same gene-regulatory effects asmimic transfection. Due to the relative ease of using miRNA mimics, subsequent experiments were performed using miR-215 mimics rather than the pre-miR-215 vector.

5.2.1.4 Validation of transcriptomic effects of miR-215 in other cell lines

Although the mechanism for miRNA-mediated repression of gene expression is predicated on sequence specific interactions between miRNA and mRNA molecules, it is possible that some unforeseen factors may privilege certain of these interactions in one cell line while interfering with them in another(Erhard et al., 2014). To wit, it is unreasonable to assume that because miR-215 downregulates a set of genes in HCT116, it would also downregulate the same set of genes in every other colorectal cancer cell line. To verify the robustness of the effects of miR-215 on the transcriptome, we transfected three additional cell lines with miR-215 mimic or control and assayed the mRNA expression levels of a subset of genes identified as differentially regulated in the HCT116 miR-215 microarray (**Fig. 5.4**).

For this experiment we used the CDX1-low cell line DLD1, which is similar to HCT116 with respect to CDX1 and miR-215 expression levels, and the CDX1-high cell lines

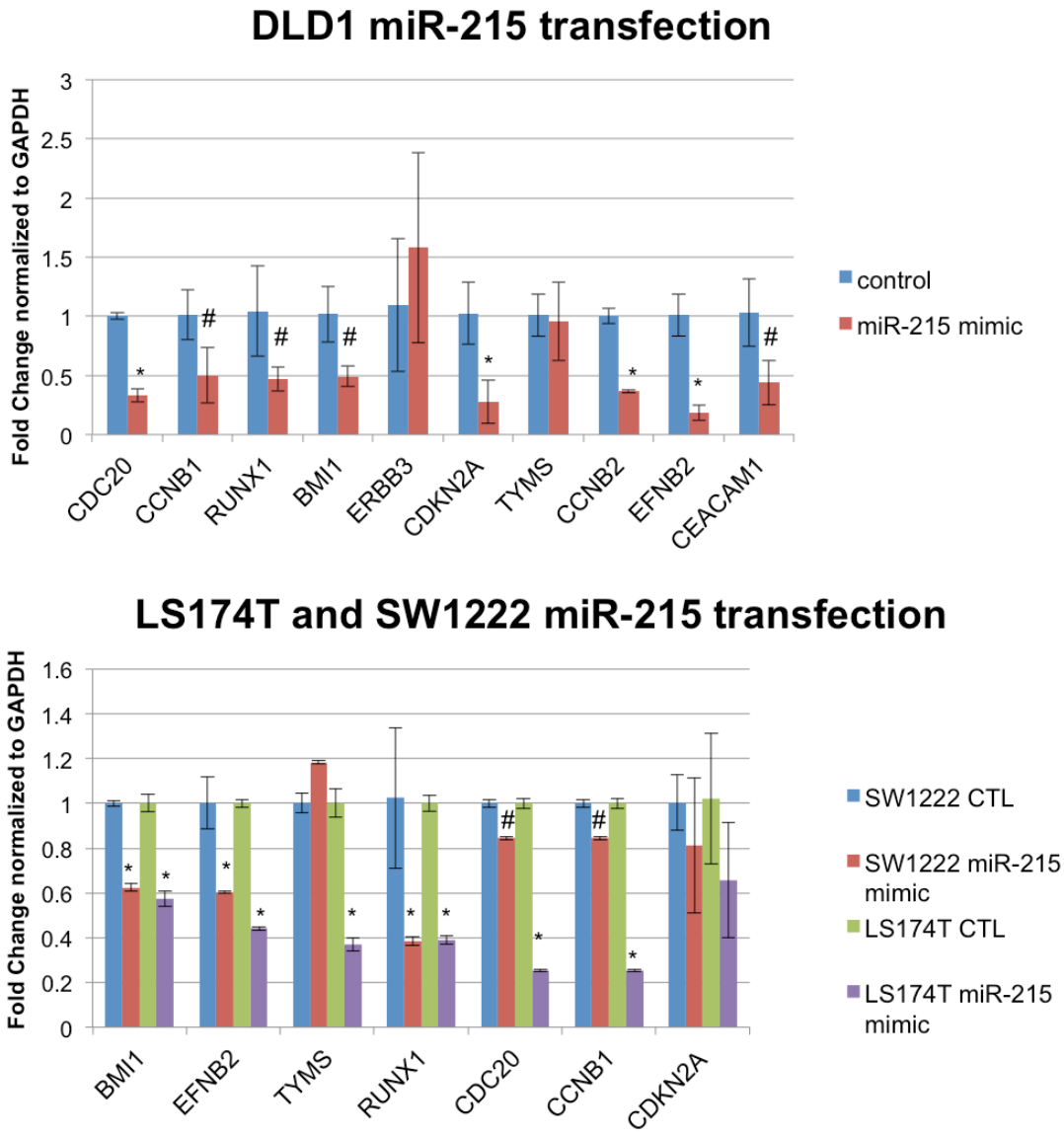

Figure 5.4
Evaluation of miR-215 cell line specificity
Top-The CDX1-low cell line DLD1 was transiently transfected with miR-215 mimic or control for 48 hours, total RNA was isolated and expression of miR-215 regulated transcripts was evaluated by SYBR-Green qRT-PCR, normalized to GAPDH.
Bottom- The CDX1-high cell lines LS174T and SW1222 were transfected with miR-215 and gene expression was measured as above. #p<0.05. *p<0.01

LS174T and SW1222. Though it may seem redundant to introduce exogenous miR-215 into cell lines that already express it, transfection of LS174T and SW1222 with miR-215 mimic in fact informs us as to the extent of saturation by endogenous miR-215 in these cell lines. In all three cell lines transfected with miR-215 mimic and subjected to qRT-PCR, we observed a high level of concurrence with the results from HCT116 (**Fig 5.4**). Moreover, the effects of miR-215 on gene expression in SW1222 and LS174T were very similar, with the exceptions of CDC20 and CCNB1. Taken together, these results show that the effects of miR-215 on gene expression are largely preserved between cell lines.

5.2.1.5 miR-215 expression activates the p53 signaling pathway

In order to gain a global perspective on the effects of miR-215 on the transcriptome, we interrogated the sets of significantly up- and downregulated genes identified from the microarray experiment using Ingenuity canonical pathway analysis. The Ingenuity software searches through each list of differentially expressed genes and tabulates the number of genes that occur in its curated, canonical pathways. The ratio to number of genes in the gene set to number of genes in the pathway is computed and assigned a p-value using the student's t-test with the Benjamini-Hochberg correction for multiple hypothesis testing.

The set of miR-215 upregulated genes was revealed by ingenuity analysis to be significantly enriched for members of the canonical p53 pathway (**Fig 5.5 A**). Our previous, manual inspection of the upregulated gene set supported this conclusion. We confirmed this bioinformatic prediction by assaying the protein expression of key p53 pathway genes by western immunoblot following miR-215 mimic transfection in

HCT116 for 48 hours. The levels of p53 protein increased slightly, yet there was a dramatic increase in the levels of p21 protein, a well-studied downstream effector of p53. Cyclin B1 (CCNB1) associates with CDK1, a target of the cyclin-depending kinase inhibitor activity of p21 and was consequently downregulated in miR-215 mimic transfected HCT116 (**Fig 5.5 B)**.

However, the usefulness of Ingenuity and other such bioinformatic analysis may be limited by the subtlety and diversity of some transcriptomic changes which may, nonetheless, prove biologically meaningful. Although some genes from several canonical pathways were statistically over-represented in the set of miR-215 downregulated genes, there were no clear outliers as was the case for the p53 pathway in the upregulated gene set. The canonical pathway data for down-regulated genes was, therefore, adjudged to be uninformative (data not shown).

5.2.1.6 miR-215 is not induced by p53 activation

Previous studies have shown that expression of the miR-194-215 cluster is induced by p53(Braun et al., 2008; Georges et al., 2008). In particular, Pichiorri, *et al*., suggested that p53 and miR-215 constitute an auto-regulatory feedback loop, in which p53 induces miR-215, and miR-215, in turn, represses *MDM2*, which is a negative regulator of p53 (Pichiorri et al., 2010). Because our microarray results clearly support the induction of the p53 pathway by miR-215, we sought to test whether we could confirm the other p53-related claims surrounding miR-215. However, MDM2 was neither down-regulated in the microarray nor in a separate transfection of HCT116 with miR-215 mimic (**Figure 5.5**

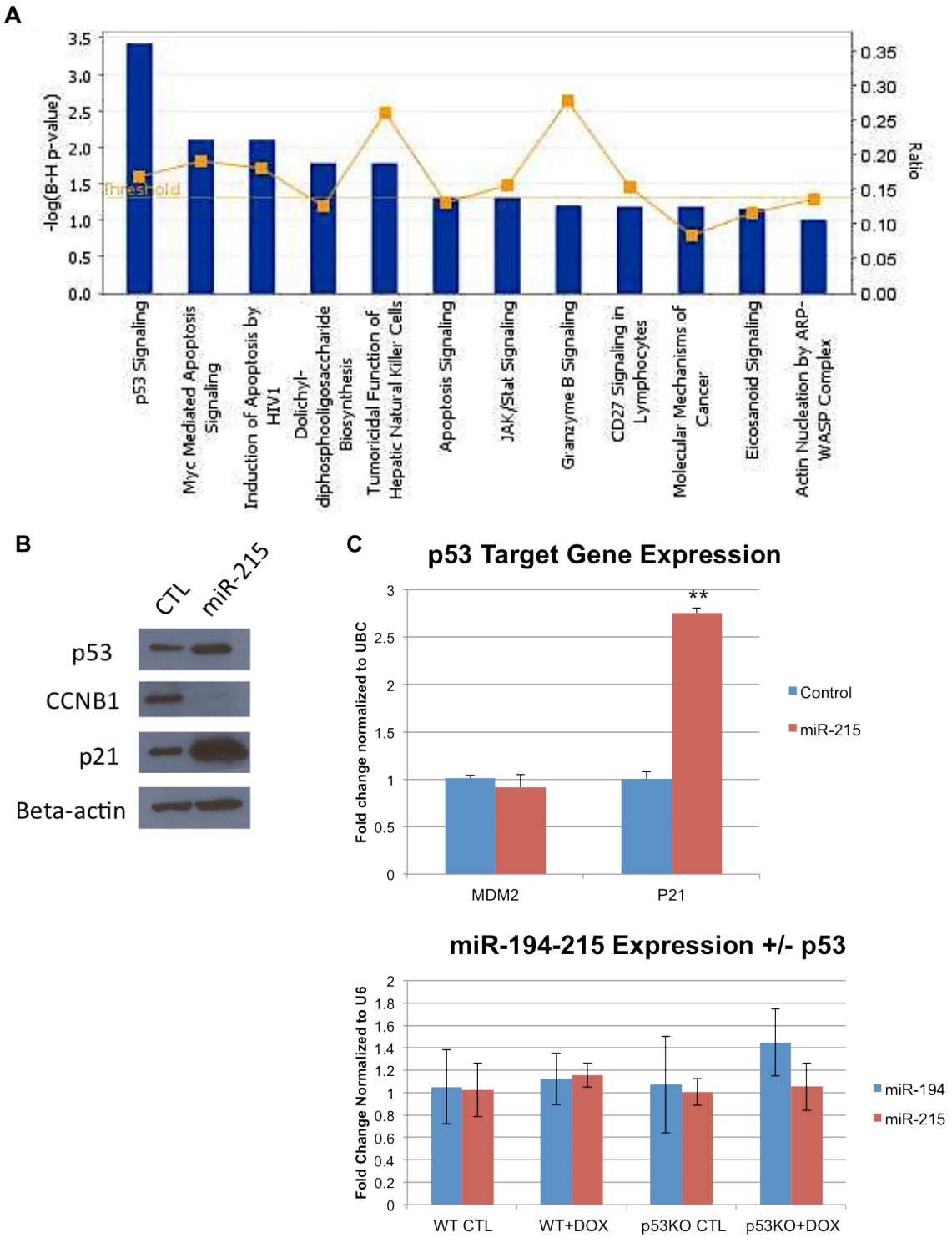

Figure 5.5
miR-215 expression activates the p53 signaling pathway
Legend next page

Figure 5.5 (*previous page*)
miR-215 expression activates the p53 signaling pathway
A) Ingenuity pathway analysis was conducted on the set of genes significantly upregulated in the miR-215 microarray. The p53 tumor suppressor pathway was the most over-represented canonical pathway in the up-regulated gene set, with a Benjamini-Hochberg corrected p-value of <0.0003. The height of the blue bars represents the significance of the enrichment for a given pathway (X-axis= -log B-H p-value). The orange points represent the ratio of genes involved in a given canonical pathway present in the upregulated gene list divided by the total number of genes in that canonical pathway B) Immunoblot for p53 pathway genes was performed 48 hours after transfecting HCT116 cells with miR-215 mimic or control (CTL). A slight increase was observed in p53 protein levels, but there was a dramatic increase in p21 and a corresponding decrease in cyclin B1 (CCNB1). Beta-actin is shown as a loading control. C) *Top*- mRNA expression levels of the p53 target and negative regulator *MDM2* and the p53 downstream effector p21 measured by SYBR-Green qRT-PCR following miR-215 mimic transfection. *Bottom*- miR-194 and miR-215 expression were measured by TaqMan qRT-PCR following p53 activation by treatment with 300nM Doxorubicin for 6 hours. WT= HCT116-p53 wild type, p53KO= HCT116 p53-/- (knockout), DOX= Doxorubicin. **p<0.001

C), as determined by qRT-PCR. Furthermore, neither miR-215 nor its clustered neighbor miR-194 were upregulated by the known p53-activating genotoxic poison doxorubicin. In fact, miR-215 expression following 12h of treatment with 300nM doxorubicin was no higher in p53 wild-type HCT116 than in an isogenic p53-knockout variant of HCT116. (**Fig. 5.5 C**).

5.2.2 Identification of direct targets of miR-215

Although there are several reports in the literature detailing the effects and upstream regulation of miR-215 (albeit not in relation to CDX1), there is a comparative lack of knowledge surrounding the genes that it directly represses through seed-sequence interactions. Characterization of the transcriptomic effects of miR-215 along with our prior knowledge of the transcriptomic effects of its upstream regulator CDX1 and bioinformatic predictions regarding seed-sequence complementarity allows us to begin to posit mRNAs as direct targets of miR-215. However, it is first necessary to describe several molecular tools used in the process of identifying and validating the miR-215 target mRNAs.

5.2.2.1 miR-215 loss of function: the miRNA sponge approach

Mature miRNAs are notoriously difficult to knock down via conventional antisense RNA approaches (Ebert et al., 2007). Although genome-editing methods are becoming faster, cheaper, and easier, they still require extensive validation and suffer from greater off-target effects than frequently realized. We therefore elected to use a miRNA-sponge

approach, which was originally developed in the Phillip Sharp lab (Ebert et al., 2007), in which a repeating array of sequences with partial complementarity to miR-215 are expressed from a vector construct, such that a given sponge transcript contains at least 5 binding sites for miR-215. The repeats are designed with a "bulge" in positions 9-12 of the miRNA (**Fig 5.6 A)**, to prevent cleavage by RNaseA, which would otherwise result in the degradation and subsequent depletion of miRNA-bound sponge RNA molecules. The partial complementarity scheme allows the sponge RNA to effectively bind and stably sequester miR-215 away from its mRNA targets, thereby creating a loss-of-function without necessarily eliminating miR-215 from the cell. MiRNA sponges have been successfully used for loss of function bot *in vitro* and *in vivo* (Subramanian et al., 2014; Bu et al., 2013). Due to the sequence homology between miR-192 and miR-215, it is likely that the miR-215 sponge would also have some effect on miR-192 activity (**Fig 5.6 A)**.

Although an important aspect of the miRNA sponge mechanism lies in the inclusion of multiple microRNA binding sites (MBS), the optimal number of MBSs is not apparent *a priori*, and indeed it may vary depending on the miRNA, its expression level, the expression of its target mRNAs or other factors altogether. To avoid using an inefficient, time consuming process of sequential ligation to incorporate MBS sequences into the vector backbone one-by-one, we utilized a rapid, stochastic ligation protocol initially developed by Kluiver, *et al*. This method relies on the non-palindromic activity of the SanDI restriction endonuclease to introduce an asymmetrical overhang. As the SanDI restriction site rarely occurs naturally in plasmid sequences, we inserted a short linker

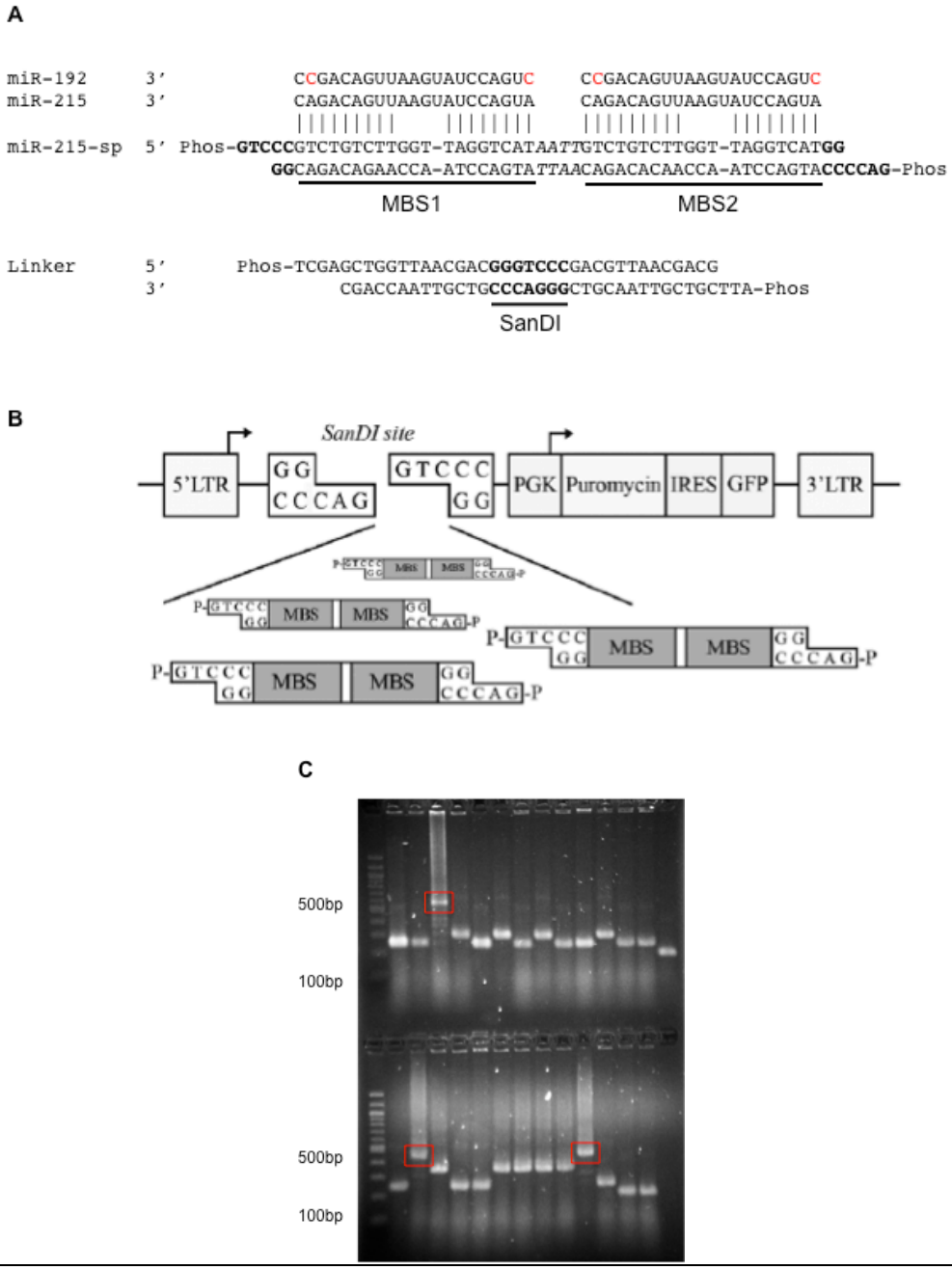

Figure 5.6
Creation of a miR-215 sponge construct
A) Oligonucleotide sequence used to design a miR-215 seed-family sponge. This figure displays the complementarity between the sponge, miR-215 and miR-192 as well as the SanDI linker sequence used to modify the pMSCV-PIG vector backbone. B) Schematic for stochastic, uni-directional concatemerization of sponge repeats allowed for by use of non-palindromic SanDI digestion of the linker-modified pMSCV-PIG. Adapted from Kluiver, *et al.* (2012). C) Colony PCR of miR-215 sponge clones shows a distribution of insert lengths. The colonies corresponding to the three highlighted bands included 3 or 4 copies of the sponge repeat and were purified, sequenced, and used for downstream functional studies. MBS= miRNA binding sequence, Phos=phosphate group.

derived from synthetic oligonucleotides containing the SanDI site into the multiple cloning site of the vector pMSCV-PIG-puro-IRES-GFP. Synthetic oligonucleotides with the sequence shown in **Fig. 5.6A** were annealed and ligated with the SanDI-digested, dephosphorylated backbone (Kluiver et al., 2012a; b).

The number of insert fragments ligated into the vector is stochastic and depends only on the relative ratio of insert:vector. The asymmetrical sticky ends ensure that insert concatemerization preserves the desired 5'-3'directionality (**Fig 5.6 B**). Following transformation, a number of clones were screened by colony PCR with primers flanking the MCS to determine the number of MBSs incorporated. Most colonies contained one copy of the insert, while several also contained two copies. Two colonies contained 3 copies and one contained 4 (i.e. 8 MBSs total, as each insert molecule is a dual repeat) (**Fig 5.6 C**). These longer constructs were purified and sequenced to confirm their size.

5.2.2.2 miR-215 sponge effectively de-represses miR-215 targets

There are longstanding challenges involved in assessing the effectiveness of miRNA loss-of-function approaches. Simple antisense RNA knockdown can confound qRT-PCR because the miRNA primers often have the same or similar sequence as the antisense RNA used for the knockdown. Even if the sponge approach is effective, there may be little or no detectable change in miRNA expression by qRT-PCR, because the sponge is specifically designed to sequester, not destroy, miRNA molecules. These sequestered miRNAs may still be detected by qRT-PCR (Thomson et al., 2013).

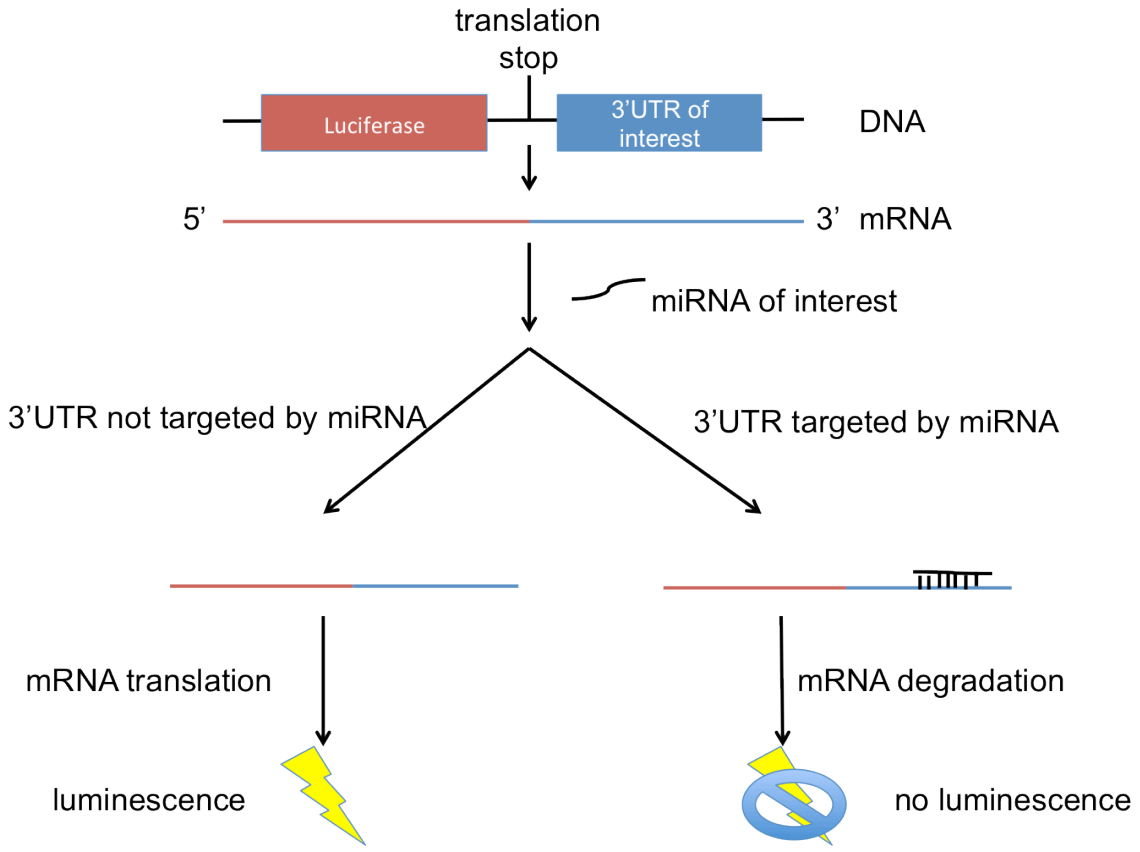

Figure 5.7
Principle of 3'UTR luciferase system
A schematic illustrating the utility of 3'UTR luciferase reporter constructs to test miRNA-3'UTR interactions *in vitro*. The 3'UTR of interest is cloned at the 3' end of the human codon-optimized *Renilla* luciferase ORF, such that a chimeric transcript encoding the luciferase protein and the 3'UTR is expressed after transfection into a human cell line. In the presence of a miRNA targeting the 3'UTR of the chimeric transcript, the luciferase mRNA will be degraded, causing a reduction in bioluminescence in the presence of luciferin relative to a non-targeted luciferase transcript.

To truly assess the efficacy of the miR-215 sponge in disrupting miR-215 function, it is necessary to determine whether the targets that miR-215 would normally repress are de-repressed by sponge-mediated miR-215 sequestration. This is, of course, complicated by the fact that a functional sponge would greatly facilitate the discovery of the targets of miR-215, and without confirmation of sponge function, it remains difficult to know which targets to assay for de-repression. To circumvent this dilemma, we created a synthetic miR-215 target and assayed for the de-repression of an artificial 3'UTR reporter. **Figure 5.7** outlines the principles of the 3'UTR luciferase reporter assay, whereby the 3'UTR of a gene of interest is inserted downstream of a luciferase ORF in the psiCHECK2 vector. miRNA targeting of this chimeric transcript then results in an easily detectable reduction in luminescence.

Our synthetic miR-215 target consisted simply of the sequence antisense to the entire mature length of miR-215. We then cloned this synthetic target into the psiCHECK2 dual luciferase reporter vector (**Fig 5.8 A**) and co-transfected the resulting construct (215AS) into LS174T along with either the miR-215 sponge or the empty sponge vector (pMSCV-PIG-EV). Endogenous miR-215 expression in LS174T was sufficient to reduce the luciferase activity of 215AS by nearly 100-fold relative to the empty reporter vector (psiCHECK2-EV). Cotransfection with the miR-215 sponge, however, rescued luciferase activity by de-repressing the 215AS synthetic target (**Fig 5.8 B**). This result indicates that the miR-215 sponge successfully inhibits miR-215 by sequestering it away from its targets.

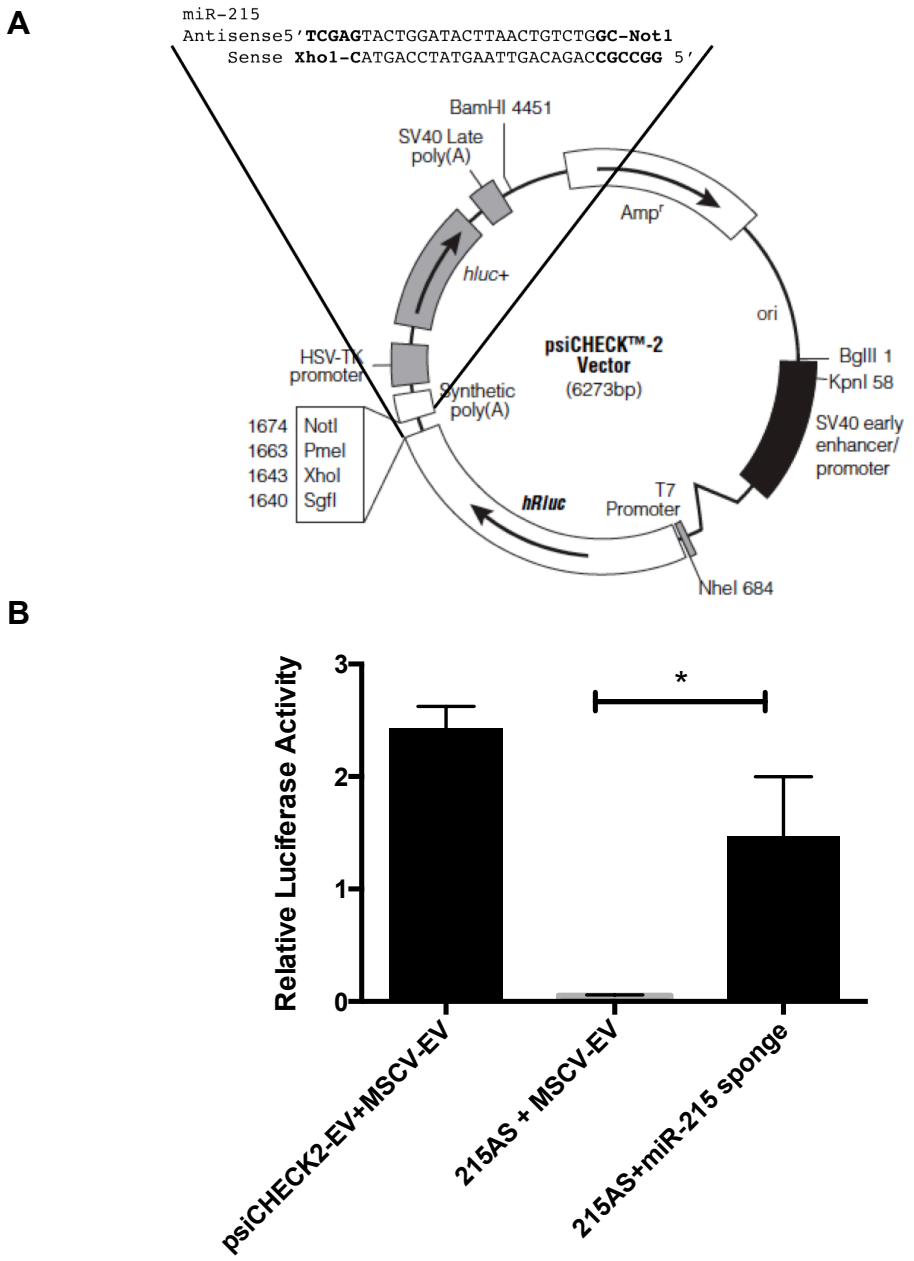

Figure 5.8
Validation of miR-215 sponge efficacy
A) An oligonucleotide duplex with sequence exactly antisense to mature miR-215 (in contrast to the bulged complement of the miR-215 sponge) was phosphorylated and cloned into the psiCHECK2 vector between the XhoI and NotI restriction sites and downstream of the luciferase ORF (hRluc). This construct is hereafter denoted as 215AS B) The miR-215 sponge described in Fig. 5.5 de-represses the 215AS construct. 215AS was co-transfected with the miR-215 sponge or the sponge empty vector (pMSCV-PIG-EV) into LS174T. Transfection of 215AS without the sponge (middle bar) resulted in robust repression of reporter luminescence. Co-transfection of 215AS with miR-215 sponge (right bar) rescued luminescence to nearly 70% of dual-EV control. *Renilla* luciferase activity was normalized to constitutively expressed firefly luciferase encoded by the *hluc+* cassette in psiCHECK2. * $p<0.05$ determined by 2-tailed student's t-test.

5.2.2.3 miR-215 sponge rescues a subset of genes indirectly repressed by CDX1

Having established the efficacy of the miR-215 sponge, we set out to use the sponge in order to establish miR-215 as a mediator of CDX1-associated transcriptional regulation. CDX1 is a well-documented regulator of gene expression, but we hypothesized that many of its effects, especially the negative regulation of the expression of certain genes, are carried out by miR-215 as a downstream effector. If this is the case, miR-215 knockdown using the miR-215 sponge should antagonize the repression of those genes inversely correlated with CDX1 expression. We selected several genes that occur in the middle portion of the Venn diagram in Figure 5.2 A and which are therefore likely to be regulatory targets of CDX1 via miR-215. We then measured there expression in RNA isolated from HCT116 cells 48 hours after transfection with miR-215 sponge and pRC-CMV-CDX1 or a combination of empty vector controls.

The expression of *RUNX1*, *BMI1*, *EFNB2*, and *CCNB2* significantly reduced by transfection of CDX1 and MSCV-PIG-EV relative to pRC-CMV-EV+MSCV-PIG-EV (dual empty vector control), which was to be expected from the results of gene expression profiling of HCT116-CDX1. We included *TYMS* in this analysis because despite its absence in the set of CDX1-downregulated gene because it is one of the handful of previously reported miR-215 targets (Song et al., 2010). We reasoned that because CDX1 reliably induces miR-215 expression, a focused look at genes downstream of miR-215 may reveal correlations with CDX1 that narrowly escaped the significance cutoff in the high-level analysis of CDX1 microarray data. GAPDH is included as a negative control, and its expression does not change significantly in response to CDX1

transfection. Co-transfection of CDX1 and the miR-215 sponge rescued the expression of all genes downregulated by CDX1to within 15% of the levels in the dual-empty vector control sample (**Fig. 5.9**). The implications of these data are twofold: firstly that the mRNA expression of mRNA targets of miR-215 can be de-repressed by miR-215 sponge transfection, and secondly that miR-215 knockdown antagonizes the transcriptional effects of CDX1.

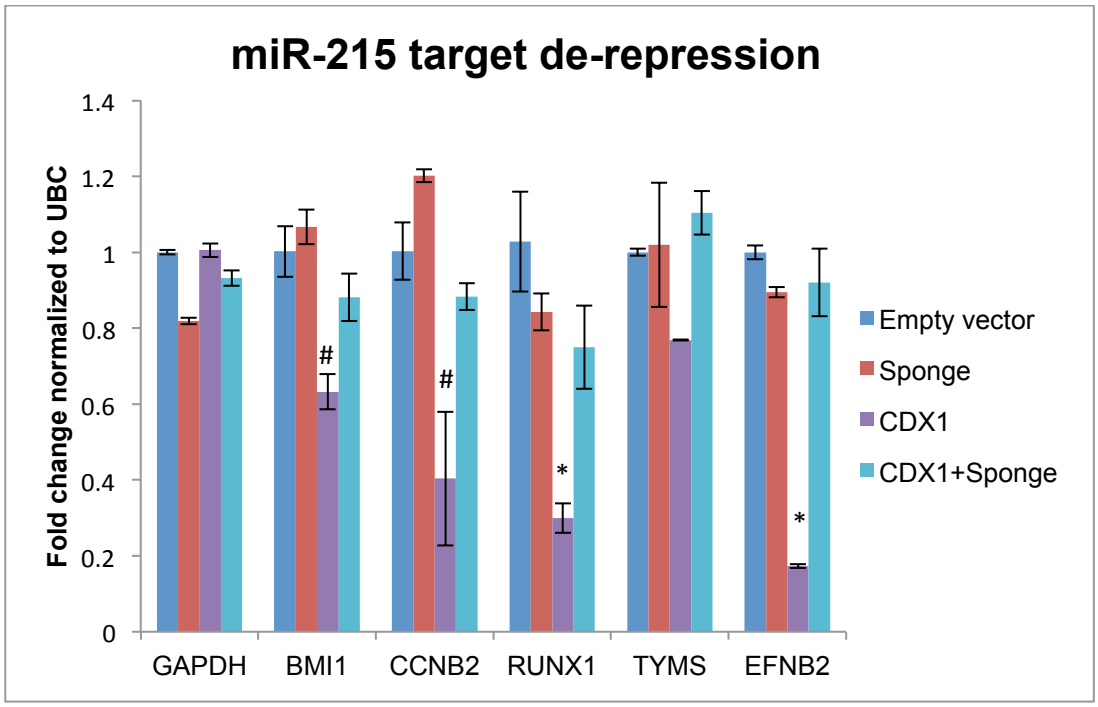

Figure 5.9
A mir-215 sponge construct antagonizes the effects of CDX1 on gene expression
HCT116 cells were co-transfected with the miR-215 sponge and pRC-CMV-CDX1, either construct alone, or an empty vector for 48 hours. RNA was isolated and the mRNA expression levels of 5 genes downregulated in both the CDX1 and miR-215 microarrays were assayed by SYBR-green qRT-PCR. Results are normalized to UBC, and GAPDH is presented as a negative control. All comparisons made relative to the empty vector control. #$p<0.05$, *$p<0.01$

Using the CDX1+sponge co-transfection approach in HCT116, we saw that miR-215 is necessary for CDX1-associated downregulation of several genes. We wanted to confirm that this phenomenon occurs in cell lines with high endogenous expression levels of CDX1 and miR-215. Therefore, we transfected LS174T and SW1222 with the miR-215 sponge or empty vector (pMSCV-PIG-EV), and after 48 hours we measured the expression levels of 9 genes that were downregulated in the miR-215 microarray experiment. *TYMS* was included as a positive control, due to previous reports of it being regulated by miR-215, and *GAPDH* and *UBC* were included as endogenous controls. The two cell lines differed somewhat in the number of genes de-repressed and in the extent of that de-repression. Notably, *BMI1* in LS174T was the most strongly up-regulated gene in either of the cell lines (**Fig 5.10**).

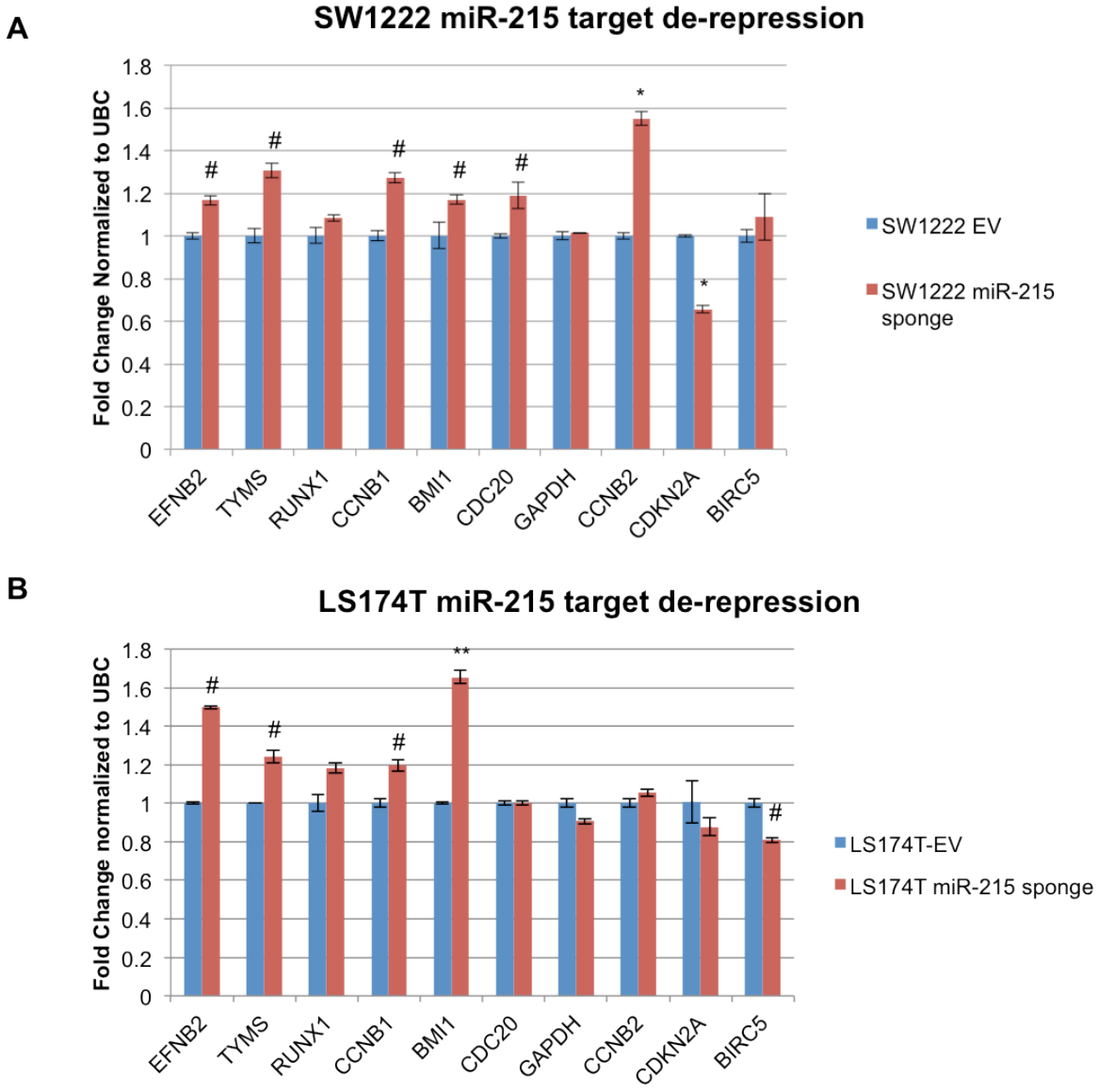

Figure 5.10
De-repression of miR-215 targets in cell lines expressing high levels of endogenous CDX1
A-B) SW1222 and LS174T were transiently transfected with the miR-215 sponge construct or pMSCV-PIG-EV for 48 hours, total RNA was isolated, and the expression of a subset of miR-215 target genes was assayed by SYBR-Green qRT-PCR. Ct values are normalized to the endogenous control UBC, and the housekeeping gene GAPDH is shown as an internal control. #p<0.05, *p<0.01

5.2.3.4 3'UTR luciferase reporter assay of miR-215 targets

The 3'UTR luciferase reporter assay, described in Figure 5.7 and utilized in a special case above, remains a definitive assay for the verification of the direct targeting of an mRNA 3'UTR by a given miRNA. We selected 5 mRNAs on the basis of the following criteria: significantly down-regulated in the miR-215 microarray, significantly down-regulated in the CDX1 microarray, contains a miR-215 seed match, has been previously reported to be involved in processes related to differentiation and/or colorectal cancer biology. These data are compiled in **Table 5.1** Although most of the miR-215 seed matches were detected using the TargetScan algorithm, BMI1 was not predicted by TargetScan. Because this gene has been of particular interest to the Bodmer lab, and was reliably down-regulated at the mRNA level by miR-215 and CDX1, and was de-repressed by the miR-215 sponge, we took a deeper look at the BMI1 3'UTR. The PITA algorithm queries 3'UTR sequences for miRNA seed matches and scores them on the basis of thermodynamic favorability. BMI1 was revealed by PITA to contain a miR-215 seed matching octamer with 1 mismatch and 1 guanosine-uracil wobble base pair (**Table 5.1**). It is difficult to predict how subtle differences in miRNA seed matches impact gene repression, so on the strength of this bioinformatic prediction and our previous data, we included BMI1 in the list of genes to be tested by 3'UTR luciferase reporter assay.

The full-length 3'UTR sequences of the genes shown in table 5.1 were cloned by standard methods into the multiple cloning site of the psiCHECK2 vector, as described in figures 5.7 and 5.8. The 215AS construct described above was included as a positive

Gene	miR-215 array FC	CDX1 array FC	miR-215 seed match	Reported role and citations
BMI1	0.38	0.69	**5′–AUGACCUAUGAAUUGACAGAC** **|{ ||||||** UGGUGGAUA–5′ pos.1150	Promotes stemness in colon (Sangiorgi and Capecchi, 2008; Tian et al., 2011; Yeung et al., 2011)
EFNB2	0.49	0.94	**5′–AUGACCUAUGAAUUGACAGAC** **||||||** AACUGGA–5′ pos. 1217 **5′–AUGACCUAUGAAUUGACAGAC** **|||||||** ACUGGAU–5′ pos. 1280	Secreted factor important for mesenchymal stem cell maintenance, possibly pro-metastatic (Ji et al., 2013)
EGR1	0.19	1.71	**5′–AUGACCUAUGAAUUGACAGAC** **|||||||** ACUGGAU 5′ pos. 97	Modulates Wnt signaling through *TCF4*, positive regulator of *PTEN* (Saegusa et al., 2008; Sarver et al., 2010)
EREG	0.22	1.40	**5′–AUGACCUAUGAAUUGACAGAC** **|||||||** AACUGGAU–5′ pos.95	Associated with resistance to anti-*EGFR* therapy (Takahashi et al., 2014; Jacobs et al., 2009)
HOXA10	0.28	1.12	**5′–AUGACCUAUGAAUUGACAGAC** **||||||** AACUGGA–5′ pos. 419	Oncogene, reported to be antagonistic with CDX2 (Rawat et al., 2008)

Table 5.1
Candidate miR-215 targets selected for 3'UTR luciferase assay
Array FC denotes the mean fold change detected in the miR-215 and CDX1 microarray experiments, respectively. The mature miR-215 sequence is shown in bold text, and the position and complementarity of corresponding 3'UTR seed matches are shown below the miR-215 sequence. "|" denotes a perfect nucleotide match while "{" denotes a G:U wobble base pair. Many mRNA seed matches end in adenosine, which is important for mechanistic reasons that remain unclear. Where relevant, the 3'- adenosine anchor is shown.

control, as it had previously been observed to be robustly repressed by miR-215. Each 3'UTR construct was transfected into HCT116 along with either miR-215 mimic or a *C. elegans* miRNA mimic as a negative control (CTL mimic). Cells were lysed, and the *Renilla* luciferase activity was measured after the addition of luciferin substrate and normalized to constitutively active firefly luciferase as a transfection control.

The positive control 215AS was repressed by a factor of 5 when co-transfected with miR-215 mimic. None of the 3'UTR constructs were repressed to such an extent, yet all 5 of them were significantly repressed by miR-215 mimic about 2-fold compared to CTL mimic. Interestingly, there was little difference between the efficiency of repression of the different seed-matches. As shown in table 5.1, *EREG* and *HOXA10* had the preferred 3'-A anchor, while *EFNB2* had two sites. *BMI1*, on the other hand, had an imperfect seed match with a G:U wobble base pair. However, all of these 3'UTRs were repressed to similar degrees (**Fig 5.11**). We can conclude, on the basis of this evidence, that *EREG, EFNB2, BMI1, HOXA10,* and *EGR1* are direct targets of miR-215.

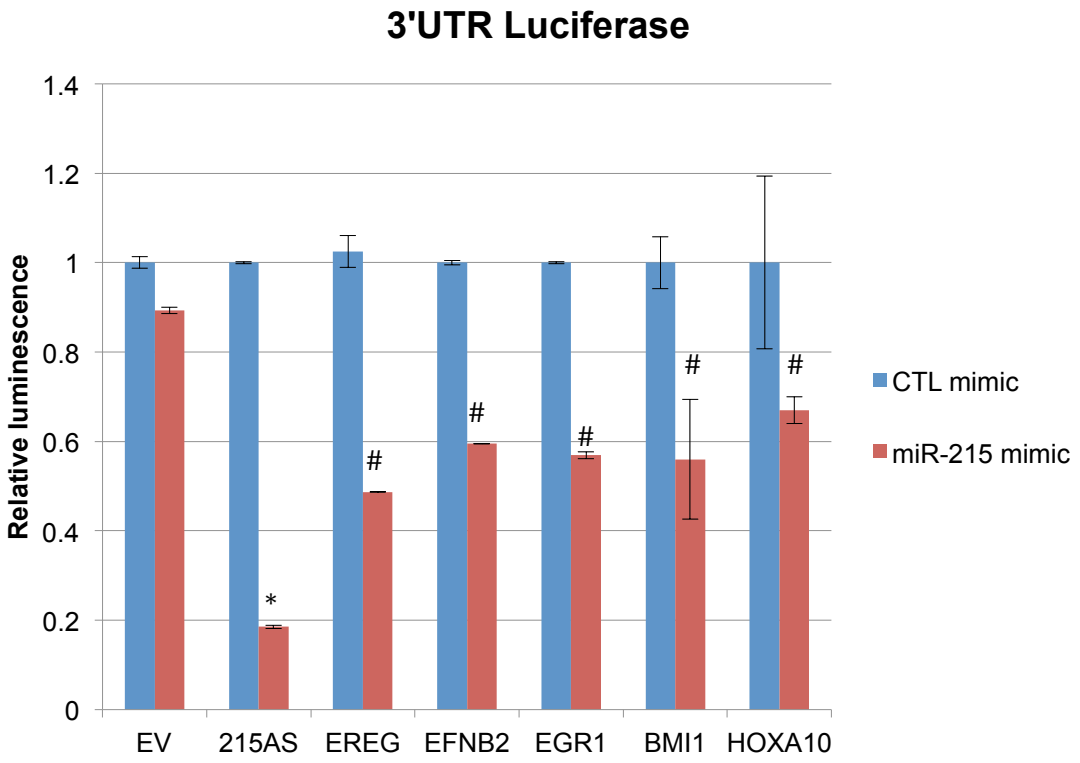

Figure 5.11
miR-215 directly represses the 3'UTR sequences of a set of target genes
The complete 3'UTR sequences of 5 bioinformatically predicted miR-215 target genes were cloned into the of the psiCHECK2 vector at the 3' end of an open reading frame encoding the *Renilla* luciferase protein. The 3'UTR constructs were transiently co-transfected into HCT116 for 24-hours along with miR-215 or control mimics. A repeating array of sequences antisense to mature miR-215 was cloned into psiCHEKC2 as a positive control (215 AS). Cells were lysed and *Renilla* luminescence was normalized to the signal from a constitutively active firefly luciferase cassette in psiCHECK2. *p<0.01, #p<0.05

5.2.3.5 miR-215 inhibits BMI1 protein production

Although the work presented in this chapter builds to a compelling case that miR-215 regulates the expression of a set of genes involved in controlling cell growth and differentiation, it is important to verify that these genes are, indeed downregulated at the protein level. Of the direct targets of miR-215, the Cancer and Immunogenetics laboratory has most extensively studied *BMI1* in relation to CDX1 and differentiation in colorectal cancer. It has been observed in the theses of Chan (2009) and Ghandi (2011) that CDX1 expression correlates negatively with BMI1. This relationship was confirmed by transiently transfecting pRC-CMV-CDX1 or empty vector into HCT116 and assaying for BMI1 expression at the mRNA level by qRT-PCR and the protein level by western immunoblot (**Fig 5.12 A, B**). This effect is phenocopied almost exactly by transient transfection of miR-215 mimic, which causes a very similar reduction in BMI1 mRNA and protein level (**Fig 5.12 A, B**). MiR-215 mimic transfection also significantly reduces BMI1 protein levels in the poorly-differentiated cell lines SW620 and CC20 (**Fig 5.12 C**).

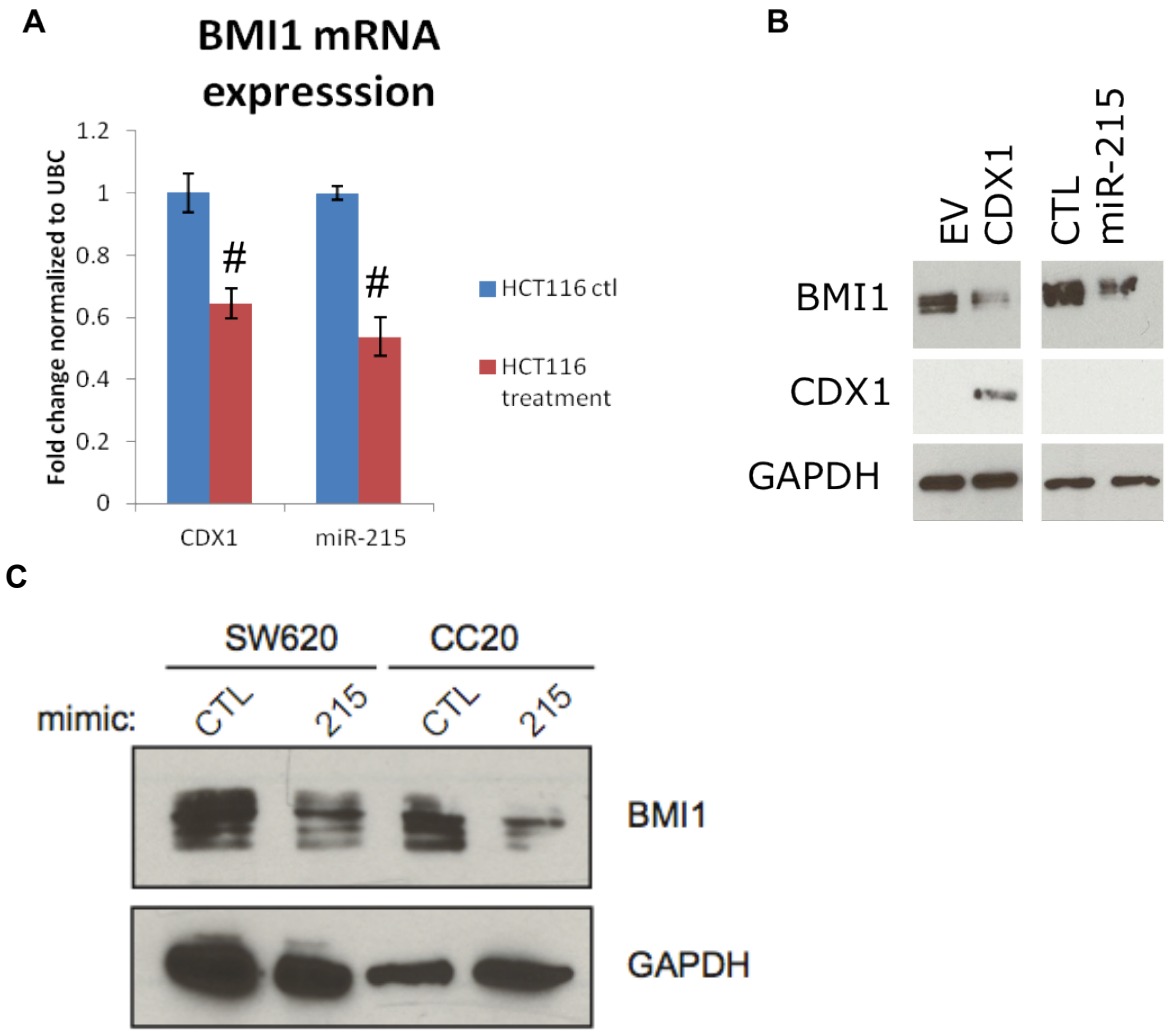

Figure 5.12
miR-215 recapitulates CDX1-mediated repression of BMI1 expression
A) RNA was harvested 48 hours after transfection of HCT116 with either pRC-CMV-CDX1, empty vector, miR-215 mimic, or control mimic. SYBR-Green qRT-PCR was used to quantitate BMI1 expression, which was found to be significantly down-regulated to similar extents in both CDX1- and miR-215-transfected cells. The red bars correspond to transfection of CDX1 or miR-215 mimic, while the blue bars correspond to empty vector or mimic control. B) HCT116 cells were transfected with pRC-CMV-CDX1 or miR-215 mimic as in (A). Whole cell lysates were then immunoblotted using monoclonal antibodies against BMI1, CDX1, and GAPDH as a loading control. CDX1 expression was only detected in the pRC-CMV-CDX1 transfectant, while BMI1 expression was clearly reduced in both –CDX1 and miR-215 transfectants. C) CC20 and SW620 were transiently transfected with miR-215 mimic or CTL. Whole cell lysate was immunoblotted for BMI1 expression. GAPDH shown as loading control.

5.3 Discussion

In this chapter we have investigated the effects of miR-215 on global RNA levels in colorectal cancer cell lines. Although our analysis here was restricted to HCT116 transcriptome, we have validated a subset of the differentially expressed genes in HCT116. These genes are also downregulated in response to miR-215 in DLD1, LS174T, and SW1222. We are primarily concerned with characterizing miR-215 as an effector of the gene expression changes indirectly associated with CDX1 expression, i.e. those not directly caused by CDX1 binding to a genomic element, so we then sought to identify which candidate miR-215 targets are inversely related with CDX1.

The results of the microarray experiment were consistent with previous reports of transcriptomic changes brought about by miRNA mimic transfection (Gottwein et al., 2007; Schultz et al., 2008; Subramanian et al., 2014; Li et al., 2014). The intersection between the gene set downregulated by miR-215 and the gene set predicted to contain miR-215 seed matches by TargetScan was highly significant, which indicates that many of the transcriptomic changes observed in the microarray experiment were due to direct repression by miR-215. Furthermore, the intersection between the gene set downregulated in the miR-215 array and the genes significantly downregulated in a separate experiment comparing HCT116-CDX1 and HCT116-Vec showed significant overlap. This suggests that CDX1 enlists miR-215 to mediate the repression of a large number of genes and that many of the hits in the miR-215 microarray are functionally relevant to the biology of CDX1.

Many genes are downregulated by CDX1, yet CDX1 is canonically a transcriptional activator, so it is tempting to suppose that a miRNA activated by CDX1 indirectly carries out this gene repression at a post-transcriptional level. We tested this hypothesis by using a miR-215 sponge construct to prevent miR-215 upregulation in response to CDX1 transfection. This, in turn, prevented the down-regulation of genes negatively associated with CDX1 expression, suggesting that these genes are downstream targets of a CDX1-miR-215 regulatory axis.

We also observed potent activation of the p53 pathway in response to miR-215 overexpression, with p21 upregulation occurring in response to both mimic and vector-based overexpression systems. Bioinformatic pathway analysis of the microarray results suggested that members of the p53 pathway were the most overrepresented category among upregulated genes. This is consistent with previously reported roles for miR-215 and its relatives in regulating p53 signaling (Georges et al., 2008; Braun et al., 2008; Pichiorri et al., 2010). However, all of these papers also noted the induction of miR-215 and miR-194 by p53 in response to DNA damage. As a measure of due diligence, we tested this claim and found neither miR-215 nor miR-194 to be upregulated after a doxorubicin treatment of standard dosage and duration. Pichiorri, *et al*. also propose that miR-215 targeting of the p53-inhibitor *MDM2* constitutes a feedback link between p53 and miR-215, however we found no evidence that miR-215 expression reduces the levels of *MDM2* mRNA. The study by Pichiorri*, et al*., was conducted chiefly in multiple myeloma cell lines, which may explain the discrepancy in *MDM2* targeting. However, the authors of that paper claim their finding to be of sufficient generality to explain the

previous observation that miR-215 activates p53, made by Georges, *et al*., and Braun, *et al*., using colorectal cancer cell lines. The results of this chapter refute that claim. Although it is outside the main focus of this thesis, there will need to be serious re-examination of the relationship between miR-215 and p53, as the experiments demonstrating both the upstream regulation of miR-215 by p53 and the mechanism for positive feedback by miR-215 could not be replicated in our hands.

By combining the bioinformatics predictions of miR-215 targeting with prior knowledge of pathways likely to be affected by CDX1, we were able to generate a list of candidate miR-215 targets. The 3'UTRs of all 5 of these targets were directly repressed by miR-215 in luciferase reporter assays. This experiment often includes mutagenesis of miRNA binding sites within the target 3'UTRs to test for specificity, but such controls have become less common as the 3'UTR assay has become one of the most trusted ways to identify miRNA targets. Several of the targets are most well known in the contexts of hematology or development, and given the importance of CDX1 in the developing embryo, particularly in patterning the expression of *HOX* genes(Subramanian et al., 2013), this may indicate a need for further research into the role of miR-215 in development.

The most provocative of the miR-215 targets is *BMI1*, which is a very important and well-studied gene in the context of colonic stem cells and colorectal cancer. *BMI1* expression is though to be essential for the maintenance of a low-turnover population of crypt base stem cells that can repopulate the crypt after injury (Yan et al., 2012; Tian et

al., 2011). The Cancer and Immunogenetics laboratory has also identified a negative relationship between BMI1 and CDX1 across a large panel of cell lines, which corresponds to the degree of stemness or differentiation exhibited by cell lines *in vitro* (Ghandi's Thesis 2011). The importance of *BMI1* expression for maintaining stemness *in vitro* has also been supported by experiments involving the culture of primary murine intestinal epithelial cells in a Wnt-dependent niche (Ootani et al., 2009). BMI1 expression has also been found to correlate with progression and poor prognosis in colon cancer (Li et al., 2009; Kim et al., 2004; Tateishi et al., 2006), likely due the promotion of a less-differentiated cancer with a higher proportion of cancer stem cells. Recently, BMI1 inhibition via small-molecules was shown to correspond to a reduction in several malignant phenotypes, including proliferation, invasion, and metastasis in colorectal cancer cell lines and xenograft models (Kreso et al., 2014). In the following chapter, we will investigate the functional consequences of miR-215 expression and attempt to draw comparisons, bearing in mind the targets through which these functions are mediated.

CHAPTER SIX

MiR-215 Negatively Regulates Clonogenicity

CHAPTER 6: miR-215 Negatively regulates clonogenicity and stemness

6.1 Introduction

In the previous chapter, we showed that miR-215 regulates the expression of a set of genes associated with proliferation and stemness and that it is necessary for carrying out transcriptomic changes associated with its upstream regulator CDX1. The remaining questions regarding the role of miR-215 as a downstream effector of CDX1 are: what are the functional effects of miR-215 expression, and is miR-215 required for the phenotypic effects of CDX1 on differentiation, colony formation and proliferation?

In this chapter, we endeavor to address those questions using a variety of functional assays. From our previous data, we can generate several hypotheses regarding the functions of miR-215. Firstly, we know that miR-215 is a direct target of CDX1. Because CDX1 is a well-studied regulator of differentiation in the colorectum (Chan et al., 2009; Yeung et al., 2010; 2011; Wong et al., 2004) and correlates directly with tumor differentiation in both primary adenocarcinoma and colorectal cancer cell lines (Ashley et al., 2013; Guo et al., 2004) as well as precancerous metaplasia (Wong et al., 2005; Kang et al., 2011), we expect miR-215 to be an important mediator of differentiation. Secondly, our results and the work of several other groups has shown that miR-215 expression activates p53 (Georges et al., 2008; Pichiorri et al., 2010), so we can hypothesize that miR-215 is involved in promoting growth arrest in response to stress. However, we have also gathered evidence showing that previous studies of miR-215 and p53 have been

incomplete or inconsistent with our data, suggesting that there may be other roles for miR-215 regulation of cell growth outside the p53 pathway. Finally, we know that miR-215 directly represses the mRNAs of several genes associated with stemness in the colorectum, most notably including *BMI1*. Previous work by our lab and others has implicated *BMI1* in self renewal, stemness, and surrogates for malignancy such as *in vitro* migration and colony formation (Ghandi's thesis, 2011) (Kreso et al., 2014; Sangiorgi and Capecchi, 2008; Tateishi et al., 2006). Therefore, we can hypothesize that miR-215 will negatively regulate these cellular traits. To investigate these hypotheses, we employ fluorescent activated cell sorting (FACS) enrichment of stem cells from cell lines, cell cycle analysis, and colony formation assays.

6.2 Results

6.2.1 Correlation of miR-215 with stem cell marker expression

6.2.1.1 miR-215 expression is depleted in CD24+/CD44+ cells

Previous work in the Cancer Immunogenetics Laboratory and by others has identified the cell surface antigens CD24 and CD44, which are thought to be involved in cell-cell adhesion and migration, to be reliable markers for the enrichment of colorectal cancer stem cells (Ghandi 2011) (Yeung et al., 2010; Subramaniam et al., 2007). CDX1 has long been suspected to play a role in the differentiation of both normal and cancer stem cells, and its expression level increases from a minimum in the crypt-base stem cells to a maximum in terminally differentiated colon cells. It stands to reason that, as a

downstream target and potential effector of CDX1, miR-215 would share a similar expression pattern. The CDX1(+), differentiating cell lines SW1222 and LS180 were immunostained using fluorescent antibodies against the stem cell markers CD24 and CD44 and were then flow-cytometrically sorted according to fluorescent intensity. The top 10% of CD24/CD44 double-positive cells were collected, and total RNA was isolated **(Fig. 6.1 A)**. qRT-PCR quantitation of miR-215 expression in this stem-cell enriched population reveals a nearly 5-fold decrease in SW1222 CD24+/CD44+ cells relative to unsorted, and a nearly 10-fold decrease in the same subpopulation of LS180 **(Fig 6.1 B)**.

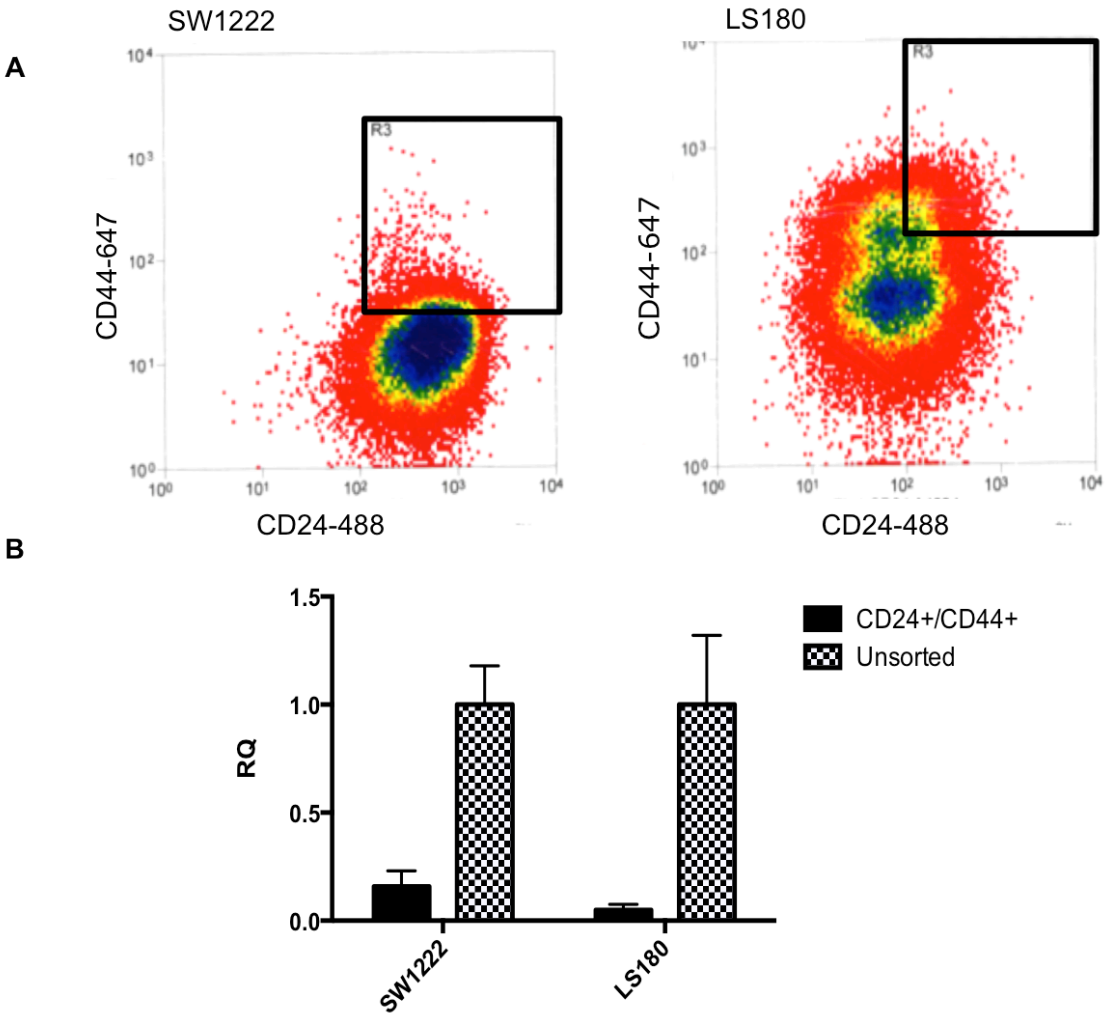

Figure 6.1
miR-215 expression is depleted in the cancer stem cell compartment
A) LS180 and SW1222 cell lines were co-stained with CD24-Alexafluor-488 and CD44-Alexafluor-647 antibody conjugates. Dead cells, debris, and doublets were excluded by gating on forward and side-scatter parameters. The top 10% of CD24/CD44 double positive cells were collected from SW1222 and LS180 by FACS. The gate on SW1222 was specifically drawn to include a spur of CD44+ cells with intermediate CD25 expression.
B) As determined by TaqMan qRT-PCR, miR-215 expression in these stem cell-enriched populations was depleted 5-fold in SW1222 and nearly 10-fold in LS180.

6.2.1.2 miR-215 knockdown affects the expression of stem cell markers

After finding that miR-215 correlates expression correlates inversely to the expression of cell-surface markers used to enrich for colorectal cancer stem cells, we hypothesized that miR-215 plays a role in regulating the process of differentiation downstream of the master regulator CDX1. By this reasoning, inhibition of miR-215 would cause decrease in the proportion of differentiated cells in a population. We transfected the cell line LS174T with miR-215 sponge (Chapter 5) and measured the distribution of CD24 and CD44 expression by flow cytometry. miR-215 knockdown caused a slight, yet detectable increase in the proportion of double positive cells. LS174T normally expresses very high levels of miR-215 (Chapter 4), and antagonizing miR-215 expression with the sponge construct causes a 14% increase in the CD24+/CD44+ subpopulation with a concomitant 14% decrease in the CD24-/CD44- subpopulation (**Fig 6.2 A**). This difference is due exclusively to an increase in the proportion of CD44+ cells. A univariate histogram of the intensity of CD44 staining shows the same 14% increase (**Fig 6.2 B**) as gate drawn on the bivariate CD24/CD44 plot.

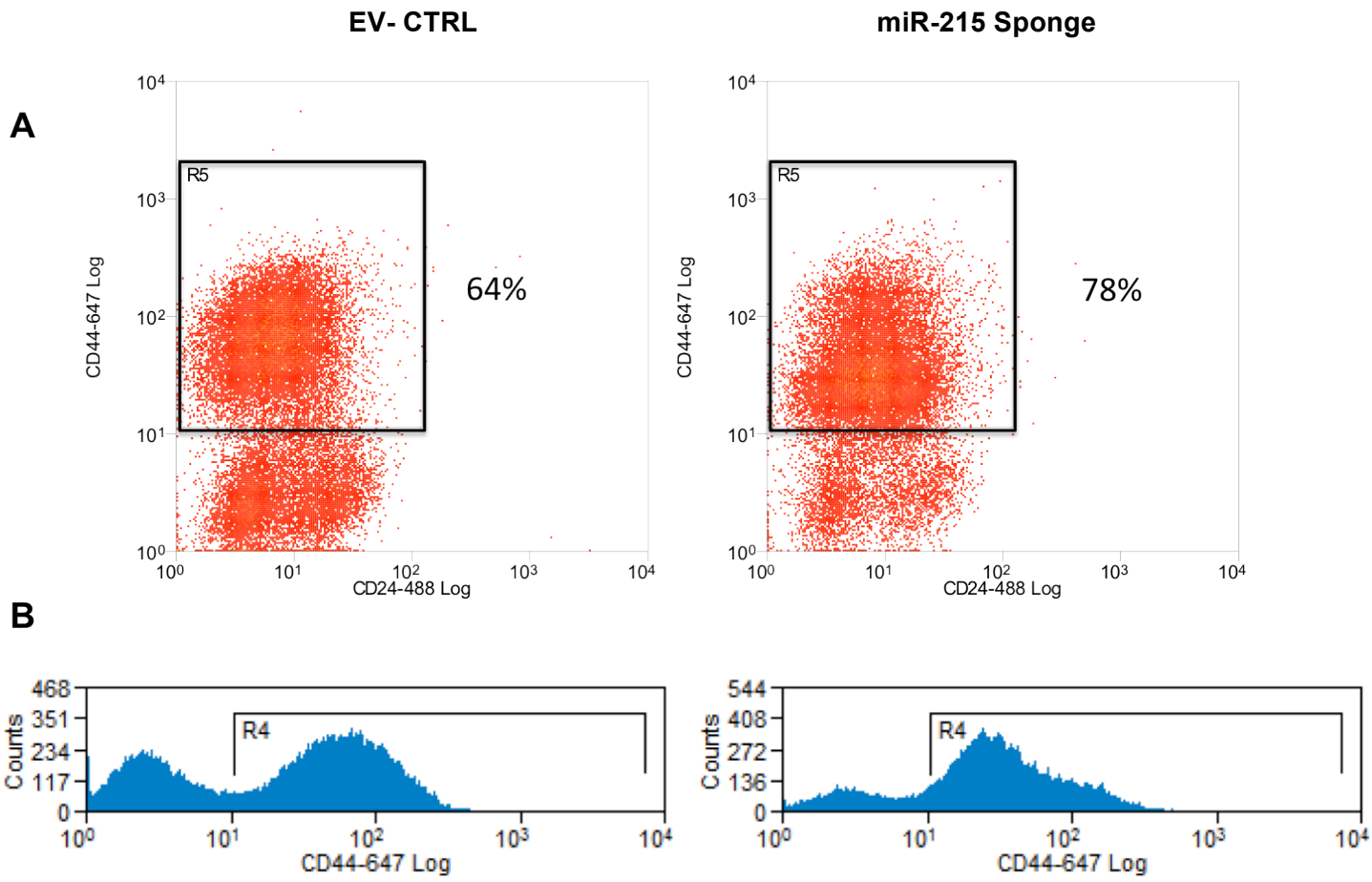

Figure 6.2
miR-215 knockdown increases the proportion of CD44+ cells
A) The LS174T cell line was transiently transfected with the miR-215 sponge construct described in chapter 5. The cells were then subjected to a live stain with CD44 and CD24 antibodies, conjugated to Alexafluor 647 and 488, respectively. miR-215 knockdown caused an approximately 14% reduction in the number of CD24-/CD44- cells. B) Univariate projection of the distribution of CD44 staining shown in (A). The same 14% reduction is observed when CD44 staining is examined independently of CD24.

6.2.2 miR-215 opposes colony formation and proliferation

6.2.2.1 Introduction of miR-215 to HCT116 induces changes in morphology and growth on plastic

Although the results of FACS analysis of the distribution of miR-215 expression in differentiating cell lines suggests a functional role for miR-215 in regulating stem cell dynamics and phenotypic heterogeneity *in vitro*, they do not, in themselves, point to a clear molecular function. Combined with the results of Chapter 5 however, in which we observed that miR-215 overexpression activates the cyclin-dependent kinase inhibitor p21 and inhibits the expression of a number of genes involved in self-renewal, particularly *BMI1*, we can hypothesize that miR-215 expression has anti-proliferative effects. To test this, we transfected HCT116 with miR-215 mimics or control mimics (cel-miR-67) and observed the cells' behavior on plastic. After 48 hours, a clear morphological change was apparent, with the normally adherent, polygonal, epithelial characteristics of HCT116 giving way to loosely attached, rounded cells (**Fig 6.3 A**). The transfectants were also less confluent than would be expected after 48 hours without passage, further suggesting an effect of miR-215 on cell growth.

To further assay the effects of miR-215 expression on cell growth, we seeded HCT116 cells transfected with miR-215 at a low density and measured the formation of colonies after 2 weeks. Although the cells were only transiently transfected, we detected a profound, 3-fold reduction in the number of colonies formed on plastic in miR-215 transfectants compared to control transfectants (**Fig 6.3 B**).

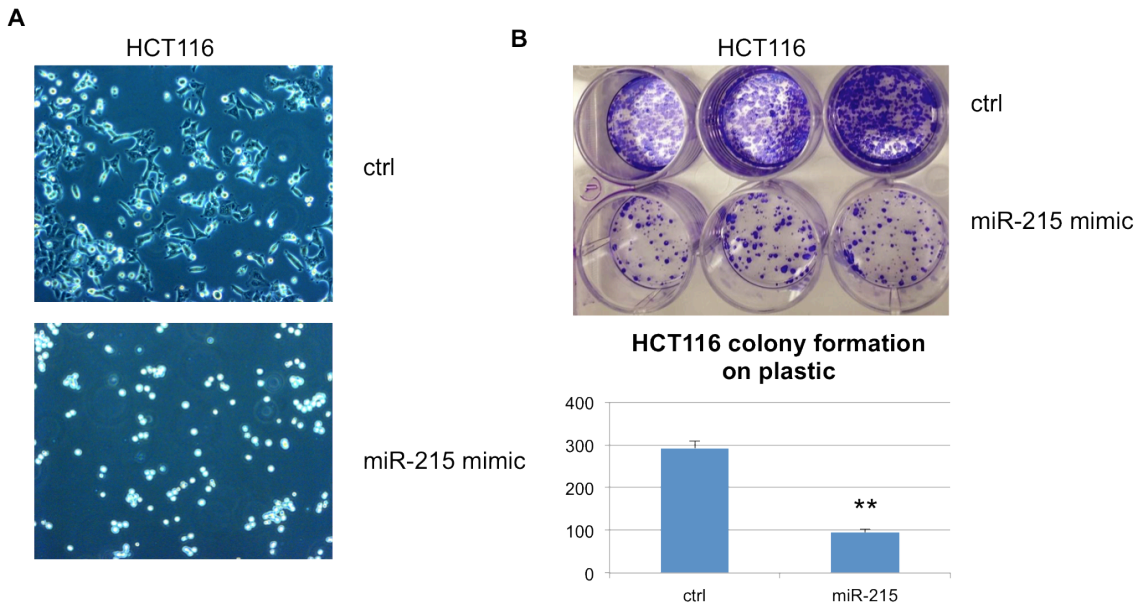

Figure 6.3
miR-215 transfection affects HCT116 morphology and proliferation
A) Light micrograph (5X) of HCT116 cells 48 hours after reverse transfection with miR-215 mimic shows loss of attachment, decreased cell density, and altered morphology compared to control.
B) *Upper panel*- HCT116 cells were seeded at a 1000 cells/well density 48 hours after miR-215 mimic reverse transfection. After 2 weeks, colonies were stained with crystal violet. *Lower panel*- Quantitation of stained colonies on plastic. Error bars represent s.e.m. of three technical replicates, although this experiment was repeated twice. Representative data are shown. ** $p<0.001$

6.2.2.2 Promotion of colony formation by miR-215 knockdown

As we showed in chapter 5, miR-215 mimic transfection results in physiological levels of mimic incorporation into the RNA-induced silencing pathway. However, it may be that the gain-of-function approach using mimic transfection into the CDX1/miR-215-low HCT116 does not accurately reflect the physiological roles of miR-215. If miR-215 overexpression inhibits colony formation on plastic, we would hypothesize the opposite effect would be caused by miR-215 knockdown in CDX1-miR-215 high cell lines. To test this hypothesis, we transfected the miR-215 sponge construct or pMSCV-PIG empty vector into LS174T and SW1222 and conducted colony formation assays on plastic as above. As expected, miR-215 knockdown causes a nearly symmetrical increase in the colony formation of the CDX1-high cell lines as miR-215 overexpression does in the CDX1-low HCT116. The magnitude of the change is not as pronounced as in the case of miR-215 overexpression, but increases are significant (**Figure 6.4**).

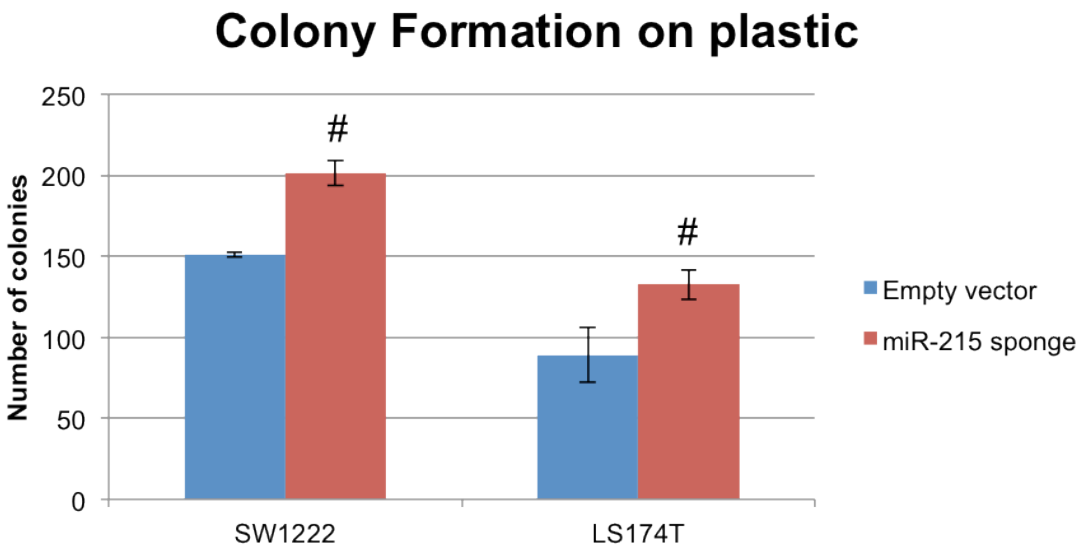

Figure 6.4
miR-215 antagonization potentiates colony formation on plastic
The CDX1-high cell lines SW1222 and LS174T were transiently transfected with either the miR-215 sponge construct or pMSCV-PIG empty vector, and seeded at low density in 12-well plates. After 10 days, the colonies were fixed and stained as in figure 6.3. #p<0.05.

6.2.2.3 Inhibition of transwell migration by miR-215

To further investigate potential functions mediated by miR-215, we conducted a cell invasion assay by transfecting HCT116 cells with miR-215 or control mimics and seeding the transfectants on the upper surface of a cell-permeable membrane coated with a thin layer of Matrigel. After 2 days, the membranes were fixed and stained with crystal violet, which revealed that orders of magnitude more control-transfected HCT116 cells had penetrated the Matrigel and crossed through the membrane than miR-215 transfected cells (**Fig 6.5**). This result suggests that miR-215 overexpression may inhibit cell migration and invasion. However, we cannot discount the possibility that proportionally equal numbers of control or miR-215 transfectants infiltrate the transwell chamber and that the difference in final cell number is due to inhibition of proliferation by miR-215 rather than inhibition of initial cell migration and invasion.

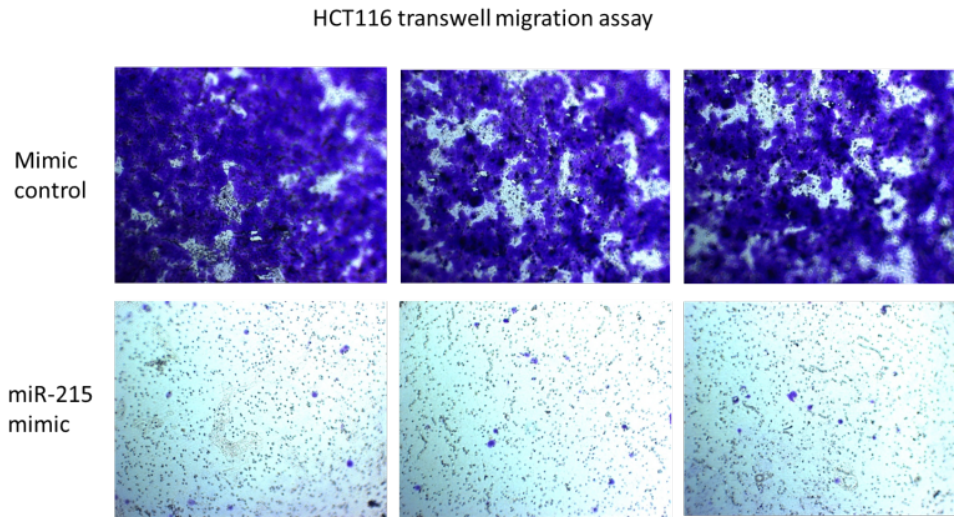

Figure 6.5
Introduction of miR-215 inhibits invasion *in vitro*
HCT116 cells were reverse transfected with miR-215 mimic and incubated for 24 hours, after which they were seeded onto the upper layer of a cell-permeable membrane and submerged in culture medium. After 48 hours, the membranes were fixed and stained with crystal violet. Experiment was repeated twice, representative images shown.

6.2.2.4 Induction of cell-cycle arrest by miR-215 expression

Given the data in chapter 5 indicating the activation of p53 signaling by miR-215, we suspected that the initial functional effects of miR-215 in inhibiting colony formation and migration may be confounded by inhibition of proliferation via p21-mediated cell-cycle arrest. To test this hypothesis, we conducted propidium iodide staining of the p53-wild type parental HCT116 and isogenic HCT116-p53KO cell lines transfected with miR-215 mimic or control. Propidium iodide (PI) quantitatively stains DNA in fixed cells, such that cells in fixed in pre-S-phase emit a signal of at half the intensity of cells fixed in post-S-phase (Fried et al., 1976). The intensity of PI staining was measured by flow cytometry. The PI profiles of both cell lines were similar under control conditions. Interestingly, transfection of miR-215 caused an increase in the size of the G2 peak in both cell lines, though this was accompanied by a decrease in the number of G1/G0-phase cells in HCT116 p53KO, and a decrease in the number of S-phase cells in HCT116-parental (**Fig. 6.6**). These data suggest that there are both p53-dependent and p53-independent mechanisms by which miR-215 effects cell cycle arrest.

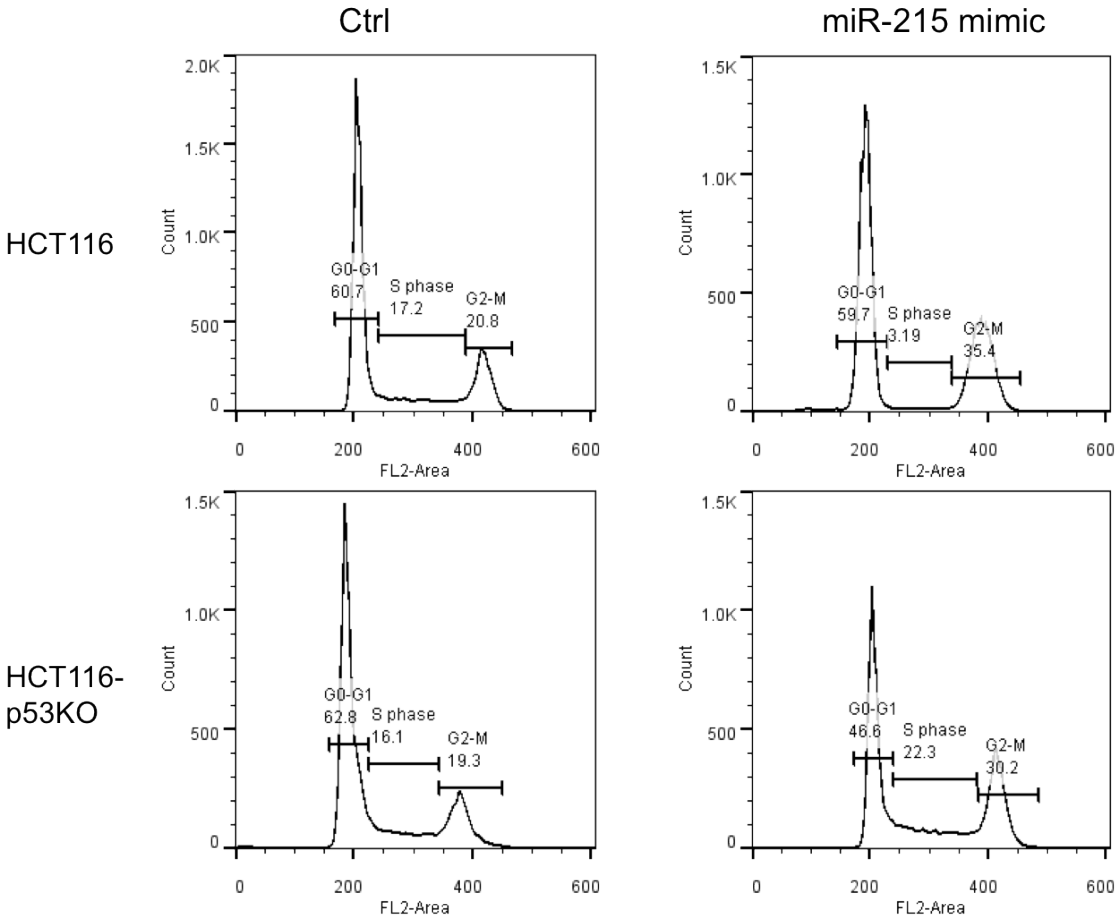

Figure 6.6
miR-215 expression induces a p53-independent G2 arrest
HCT116 parental or isogenic p53 knockout (HCT116-p53KO) cell lines were reverse transfected with miR-215 mimic or control. After 48 hours, the cells were fixed and stained with propidium iodide (PI). The proportion of PI stain incorporated into single cells was measured as by flow cytometry. Amount of PI stain is shown along the Y-axis of the histograms, with cells in G2 containing 2x the amount of stain as cells in G1.

6.2.3 Effects of miR-215 on clonogenicity and morphology in 3-Dimensional cell culture

Cell culture in 2 dimensions on plastic is an artificial system, and while comparisons can be made between different treatments on plastic, a more accurate model of cell growth and differentiation is given by cell culture in a 3-dimensional matrix containing vital components of the extracellular microenvironment. This is the principle behind cell culture in Matrigel™, in which we and others have observed cell lines to exhibit highly organized patterns of multilineage differentiation that are not observed on plastic (Ashley et al., 2013; Ootani et al., 2009). We reasoned that, because the effects of CDX1 on differentiation are most noticeable in Matrigel, the function of its downstream effector miR-215 may also be more pronounced in 3D culture.

6.2.3.1 miR-215 inhibits clonogenicity independently of p53 status

We and others have shown miR-215 to activate the p53 signaling pathway, yet the results presented in this chapter indicate effects of miR-215 on cell growth independent of p53. To investigate this relationship *in vitro*, we selected three CDX1-low, undifferentiated cell lines with differing p53 status. We transfected the p53-wild type HCT116 , HCT116-p53KO, and the p53 mutant DLD1 cell lines with miR-215 mimic to investigate the effects of miR-215 on cell growth and differentiation in Matrigel, and to evaluate the dependence of these effects on the presence of wild-type p53. We found that the

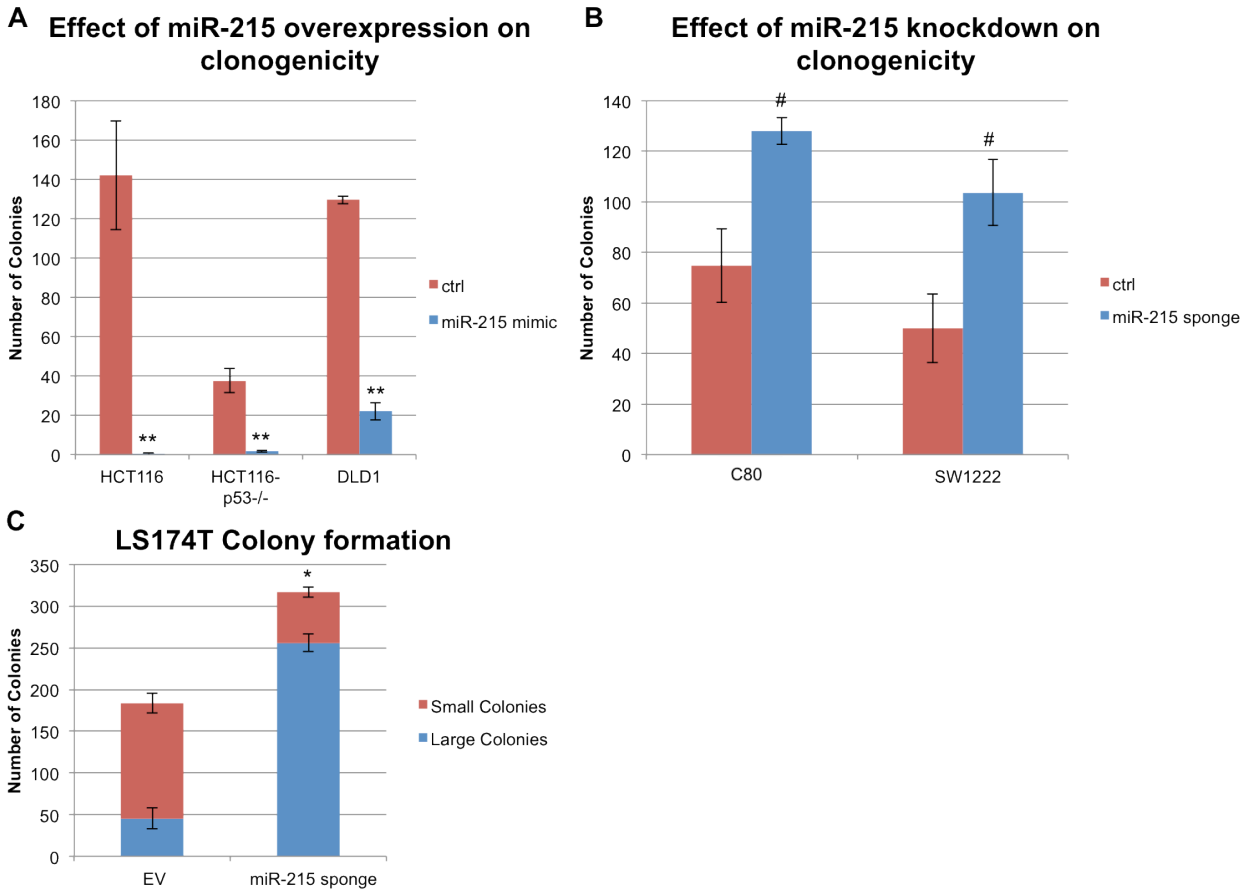

Figure 6.7
Inhibition of colony formation in 3-dimensional cell culture by miR-215
A) The CDX1/miR-215 low cell lines HCT116, HCT116-p53-/-, and the p53-mutant DLD1 cell lines were reverse transfected with miR-215 mimic for 24 hours, then seeded in Matrigel diluted 1:1 with DMEM. The colonies were grown for 2 weeks and counted under a light microscope. B) The CDX1-high cell lines C80 and SW1222 were subjected to forward transfection with miR-215 sponge, seeded in Matrigel and counted as in (A). C) The CDX1-high cell line was transfected with miR-215 sponge and seeded in Matrigel as in (B). After 2 weeks' incubation, a clear division could be noticed between large and small colonies. These subpopulations were counted under a light microscope and tallied. #$p<0.05$, *$p<0.01$, **$p<0.001$.

clonogenicity of all three cell lines was profoundly reduced by transfection with miR-215. Although the effect was strongest in HCT116, in which virtually zero colonies formed after miR-215 transfection, the colony formation of HCT116-p53 KO and DLD1 were reduced by nearly 5-fold (**Fig 6.7 A**).

6.2.3.2 miR-215 knockdown enhances clonogenicity in differentiating cell lines

In a loss-of-function approach similar to the gain of function experiment described in §6.3.3.2, we transfected the well-differentiated cell lines C80, SW1222, and LS174T with miR-215 sponge or empty vector. Although we have little evidence that miR-215 knockdown inhibits baseline p53 activity, and we might expect miR-215 loss of function phenotypes to be less contingent on p53 than the gain-of-function effect, we selected two p53 mutant cell lines (C80, SW1222) and one p53-wild type cell line to enable comparison of loss-of-function effects between p53 mutation statuses. After transfection with miR-215 sponge and 2 weeks culture in Matrigel, we observed significantly more colonies derived from C80 and SW1222 cells transfected with miR-215 sponge than those transfected with empty vector (**Fig 6.7 B**). Although neither increase was of the same magnitude as the reduction seen in Figure 6.7A, this may be due to the comparative inefficiency of the knockdown or the differential sensitivity of the transcriptome to perturbation via miRNA overexpression versus knockdown.

In LS174T, we also observed a significant, nearly 2-fold increase in the number of total colonies (**Fig 6.7 C**). Strikingly, the proportion of two morphologically distinct types of colonies was also significantly altered by miR-215 knockdown. In normal conditions, the

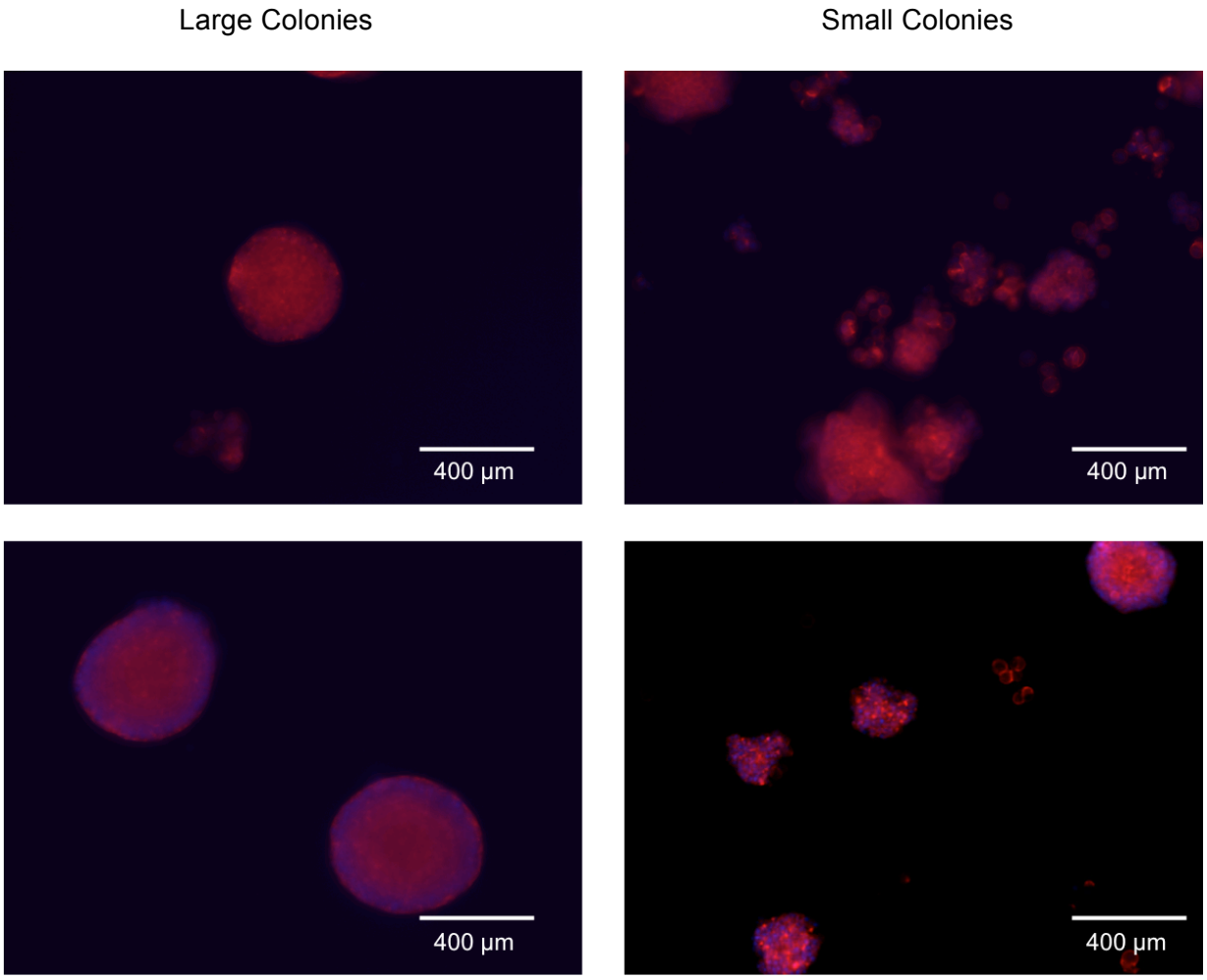

Figure 6.8
Colony morphology of LS174T in 3-Dimensional culture after miR-215 knockdown
LS174T cells were transfected with miR-215 sponge or empty vector and cultured in Matrigel as in Figure 6.7. After two weeks, the colonies were fixed in paraformaldehyde and stained for filamentous actin with phalloidin-TRITC (red) and for DNA with DAPI (blue). Stained colonies were imaged under a 20X fluorescent inverted microscope. The large vs. small colony classification refers to the chart in Figure 6.7 C.

majority of LS174T colonies are small and loose with irregular borders. Staining for filamentous actin, a reliable marker of lumen formation and therefore complex differentiation, does not show a central lumen in these small colonies but rather several small f-actin foci (**Fig 6.8**). A minority of colonies, in contrast, are large and dense with well-defined, regular borders. These colonies have diffuse, negative f-actin staining patterns with no foci or lumens (**Fig 6.8**). miR-215 knockdown resulted in a dramatic increase in the number of large, dense colonies and an absolute decrease in the number of small, loose colonies (**Fig 6.7 C**). Not only did miR-215 knockdown increase the clonogenicity of LS174T, it also significantly altered the ratio of two extant subpopulations, clearly favoring the large, dense colonies.

6.2.3.3 Knockdown of miR-215 antagonizes the effects of CDX1 in vitro

Of the three cell lines used in § 6.3.3.1 for miR-215 transfection, we reasoned that DLD1 would be best suited to further morphological study. Neither HCT116 nor HCT116-p53KO formed many colonies following miR-215 mimic transfection, so it would be difficult to study the morphology of transfected colonies. To investigate the role of miR-215 in CDX1-associated differentiation *in vitro*, we transfected DLD1 with either CDX1+pMSCV-PIG-empty vector, or CDX1+miR-215 sponge. Transfection of empty vector did not alter the classical 3-D morphology of DLD1: round, dense colonies. F-actin staining with phalloidin-TRITC was diffuse without any foci or lumens. Transfection of CDX1 did not induce the formation of lumens or f-actin foci after 2 weeks, but it did result in a quite striking change in 3-D morphology: the normally

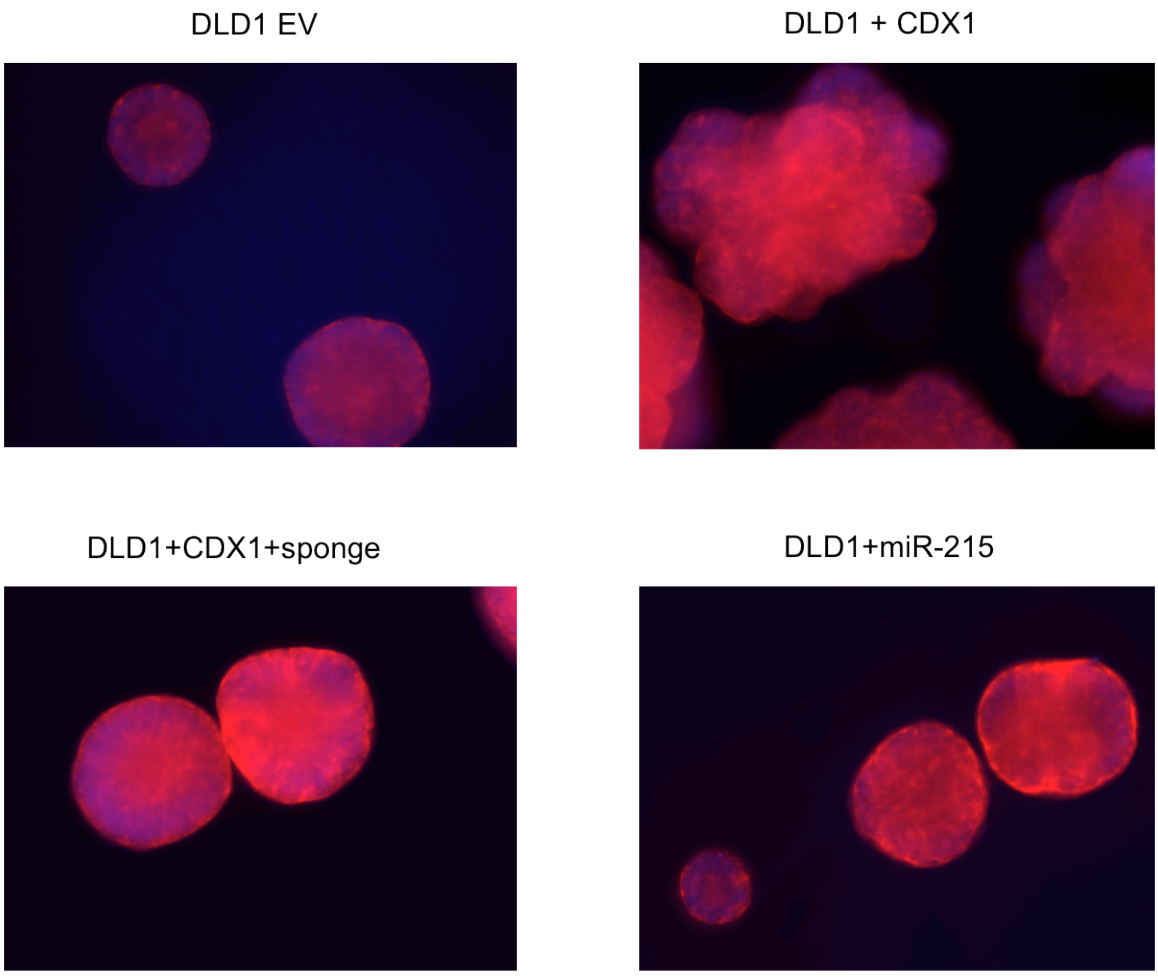

Figure 6.9
Antagonizing miR-215 prevents the promotion of complex morphology by CDX1
DLD1 cells were transfected with pRC-CMV-CDX1 in combination with either miR-215 sponge or pMSCV-PIG-empty vector. 24 hours after transfection, single cell suspensions were embedded in a 1:1 Matrigel-DMEM dilution as above. After 2 weeks, colonies were fixed and stained for filamentous actin with phalloidin-TRITC (red) and for DNA with DAPI (blue). Co-transfection of CDX1 and miR-215 sponge prevented the formation of complex, lobular morphologies seen after transfection with CDX1 alone.

rounded DLD1 colonies took on a lobular appearance with noticeable ridges and protrusions around the colony borders (**Fig 6.9**). This is consistent with the results reported in Ghandi's thesis (2011) and those observed for other cell lines in Yeung, *et al* (Yeung et al., 2010). No significant alteration in the clonogenicity was observed. When CDX1 was co-transfected with the miR-215 sponge construct, the lobular morphology was not observed, and the resulting colonies were morphologically indistinguishable from the empty vector control (**Fig 6.9**). Interestingly, DLD1 cells transfected with miR-215 alone underwent a reduction in clonogenicity (**Fig 6.9**), yet their morphology remained unchanged (**Fig 6.9**) This implies that CDX1 controls the expression of other genes besides miR-215 which are necessary to bring about the complex morphological changes associated with differentiation in 3-D culture.

6.3 Discussion

In this chapter, we have investigated the functional consequences of miR-215 expression on cell growth and clonogenicity. In previous chapters, we have characterized miR-215 as a downstream target of the transcription factor CDX1. miR-215 serves as a link between CDX1 expression and the down-regulation of stem cell genes, in particular *BMI1*, a PRC2 component that is important for maintaining a reserve stem cell population. Therefore, we suspected that the functions of miR-215 would be consistent with its role as a downstream effector of CDX1 and that miR-215 would promote a phenotype consistent with differentiation, cell-cycle arrest, and decreased stemness.

As noted above, previous work in the Cancer and Immunogenetics Laboratory has developed a method for the enrichment of cancer stem cells, i.e. a subpopulation of cells capable of forming colonies *in vitro* and xenograft tumors *in vivo*, from cancer cell lines by FACS selection of CD24/CD44 double positive cells (Yeung et al., 2010). Different colorectal cancer cell lines have intrinsically different capacities for differentiation, analogous to the histological grade of a primary adenocarcinoma, such that stem cells from some cell lines differentiate into organized, lumen-containing colonies in 3-D culture, while stem cells from other cell lines proliferate without full differentiation, giving rise to dense, undifferentiated colonies (Ghandi's thesis, 2011) (Ashley et al., 2013; 2014).

Although miR-215 expression is consistently higher than average in differentiating cell lines (see Chapter 4), we found that miR-215 expression was depleted in the FACS-enriched cancer stem cell compartment of the differentiating lines LS180 and SW1222 relative to the bulk population, as defined by CD24/CD44 immunostaining. Conversely, inhibition of miR-215 in LS174T increased the proportion of CD24/CD44 double positive cells, primarily by elevating the number of CD44-positive cells. miR-215 knockdown in other differentiating cell lines had little effect, but this discrepancy is likely due to the fact that miR-215 expression in LS174T was higher than any other cell we assayed by at least a factor of 3 (see Chapter 4). It is logically consistent that the effect of a knockdown would be more pronounced in a cell line with higher baseline expression, because miR-215 would play a greater role in transcriptomic regulation at high expression levels. Therefore knocking down miR-215 in LS174T would perturb the

transcriptome to a greater extent than in cell lines with lower baseline levels of miR-215 expression. Together, these results suggest that miR-215 is causally involved in inhibiting stem cell traits in differentiated cells. As neither CD24 nor CD44 were identified as targets of miR-215 in Chapter 5, there likely remain some indirect mechanisms that mediate the inverse correlation between CD24/CD44 and miR-215. If further research implicates miR-215 in regulating the expression of CD44, this would represent a significant functional similarity with another p53-regulated miRNA, miR-34a, which has also been reported to repress CD44 expression (Liu et al., 2011). Because CD44 has, as a cell-surface protein, been implicated in malignant phenotypes (Subramaniam et al., 2007), identifying therapeutic modalities to interfere with its expression is an important translational effort.

Over-expresion of miR-215 against a CDX1/miR-215-low background in HCT116 resulted in a change of morphology, inhibition of cell migration, cell cycle arrest, and inhibition of colony formation on plastic and in Matrigel. Although previous functional studies of the miR-215-192 family have focused on its activation of the p53 tumor suppressor pathway (Georges et al., 2008; Braun et al., 2008; Pichiorri et al., 2010), we found evidence for a growth inhibitor effect of miR-215 even in p53-null and p53-mutant cell lines. In particular, the inhibition of colony formation caused by miR-215 mimic transfection was striking. It must be noted that HCT116 does, in fact, carry a mutation in the CDKN2A locus ($p16^{INK4A}$/$p14^{ARF}$), which makes our interpretation of functional cell cycle arrest in response to miR-215 difficult to generalize to other cell lines. However, it is clear that p53 is not necessary for growth arrest in response to miR-215 expression.

It is unlikely that the magnitude of the effects of miR-215 overexpression is due to supra-physiological levels of miRNA mimic transfection, as the results of Chapter 5 indicate that miR-215 mimics are incorporated into the RNA-induced silencing pathway at physiological levels. However, it may be that over-expression of a miRNA represents a more profound transcriptomic perturbation than knockdown of a miRNA and may cause a greater deviation from a cell line's homeostatic baseline. This explanation is supported by the observation that miR-215 knockdown caused an opposite yet smaller effect in potentiating colony formation in CDX1/miR-215-high, differentiating cell lines. In other words, introduction of an exogenous miRNA can reduce the expression of myriad target mRNAs, yet knockdown of an endogenous miRNA may not result in the restored expression of those same target mRNAs, especially if their expression is simultaneously regulated by redundant or intersecting pathways. See, for instance, the significant yet attenuated effects of miR-215 sponge transfection on miR-215 target expression in LS174T and SW1222 shown in Chapter 5.

No difference in colony morphology was observed pursuant to miR-215 mimic transfection. The main difference was in the striking reduction of colony number. However, miR-215 knockdown in LS174T caused a marked change in the proportion of two morphologically distinct subpopulations in 3-D culture. The small, loose colonies whose number diminished following miR-215 knockdown contain small f-actin foci, which broadly indicate cell polarization and organization consistent with a program of differentiation (Ashley et al., 2013). The large, dense colonies which predominated

following miR-215 knockdown strongly resemble the undifferentiated colonies normally seen in CDX1-miR-215 low cell lines such as DLD1 and HCT116. As with the results from flow cytometry, the unique response of LS174T to miR-215 knockdown is likely attributable to its remarkably high level of endogenous miR-215 expression, yet the transition *in vitro* from colonies containing multiple, small f-actin foci to large, a greater number of dense colonies is consistent with both a promotion of cell growth and inhibition of differentiation due to loss of miR-215 function. Moreover, the inverse relationship between miR-215 and colony formation observed in all cell lines is entirely consistent with previous reports showing that inhibition of BMI1 causes a reduction of in self-renewal and colony formation (Kreso et al., 2014). However, our claim that miR-215 inhibits stemness is also based on inference from the fact that miR-215 inhibits BMI1, given the previously reported roles for BMI1 in regulating self-renewal. To directly test the ability of miR-215 to inhibit self renewal, limiting dilution assays to determine the number of stem cells per million and serial transplantation assays would need to be performed, as in Kreso, et al.

Finally, we have shown that miR-215 constitutes a necessary link between CDX1 and the promotion of a differentiated phenotype *in vivo* using combinatorial transfections of CDX1 and miR-215 sponge expression vectors. When transfected with CDX1 and cultured in Matrigel, DLD1 undergoes a notable morphological change from rounded, dense colonies to lobular, reticulated colonies. Although these CDX1-associated changes do not include the formation of lumens, they are still consistent with the *in vitro* characteristics of more differentiated, CDX1-high cell lines (Ghandi's thesis, 2011)

(Yeung et al., 2010). It should be noted that CDX1 has been previously shown to be a driver of lumen formation *in vitro*, and it is clear from the fact that miR-215 transfection alone does not completely copy the morphological changes induced by CDX1, that other downstream factors aside from miR-215 are necessary to carry out the effects of CDX1. On the other hand, CDX1-associated changes were not observed *in vitro* when CDX1was co-transfected with the miR-215 sponge. As in chapter 5, where we showed the miR-215 sponge transfection abrogated CDX1-associated gene expression, here we show that miR-215 knockdown abrogates CDX1-associated morphological changes. These two effects are certainly related, yet further work will be necessary to understand exactly how inhibition of miR-215 target genes contributes to the acquisition of complex, differentiated traits. Taken together, we can now propose that miR-215 is a downstream effector of CDX1 that is necessary for differentiation, but it is not sufficient in and of itself to promote differentiation in the absence of CDX1.

CHAPTER SEVEN

Characterization of a Novel MiRNA in the p53 Pathway: the Killer MiR-3189

CHAPTER 7: CHARACTERIZATION OF A NOVEL MIRNA IN THE P53 PATHWAY: THE KILLER MIRNA-3189

7.1 Introduction

In the foregoing chapters, we have discussed the roles of miR-215 in relation to the transcription factors CDX1 and p53. We arrive at the conclusion that previous studies of miR-215 as a mediator of tumor suppression elide the nuances of its role in differentiation downstream of CDX1. Although we have discounted the importance of p53 in the regulation of differentiation by CDX1 and miR-215, p53 has been extensively studied as a regulator of miRNA expression (Jones and Lal, 2012; Hermeking, 2012). In this chapter, we describe a novel, p53-regulated miRNA. This chapter is presented by way of a coda to the miR-215 story: miR-3189 is, to our knowledge, unrelated to CDX1, yet it is, like miR-215, a new player in an important transcription factor-miRNA network. Many miRNAs are transcriptionally regulated by p53 and regulate cell proliferation, stress response, differentiation and a host of other programs associated with p53 activation (Leung and Sharp, 2010). For instance, p53 has been shown to transactivate miR-34a after DNA damage, and miR-34a, in turn, represses the expression of pro-proliferative genes including *MYC*, *CDK6*, *CCNA1*, and *HDM4* (Raver-Shapira et al., 2007; Chang et al., 2007; Okada et al., 2014).

Many miRNAs are embedded in the introns or exons of protein-coding genes and are frequently transcriptionally co-regulated with their host genes. There are several

examples of p53-responsive miRNAs, such as the miR-107/*PANK1* (Bohlig et al., 2011) and miR-29/*PINT* loci (Huarte et al., 2010; Park et al., 2009). Recent high-throughput RNA sequencing studies have provided evidence supporting the existence of another such miRNA, the putative miR-3189 (Persson et al., 2011), embedded in the intron of the p53-inducible (Cheng et al., 2011) TGF-β superfamily member (Bootcov et al., 1997) *GDF15* on chromosome 19p13.11. While these studies indicated the production of a short, non-coding transcript that aligns to the intron of *GDF15*, it is not clear if this transcript is a miRNA with a defined function.

The traditional argument supporting non-coding RNA function invokes evolutionary conservation to justify physiological relevance (Friedman et al., 2008), yet a growing number of poorly-conserved miRNAs have been functionally validated in human cells. In fact, ~30% of the miRNAs in the most recent version of miRBase (Release 20) are unique to primates. However, what proportion of these putative primate-specific miRNAs produce a mature miRNA remains to be seen. Among the few primate-specific miRNAs that have been studied so far, miR-4423 was recently shown to mediate airway epithelial differentiation in the lung and suppress tobacco-associated carcinogenesis (Perdomo et al., 2013). The miR-548 family is conserved only among primates (Piriyapongsa and Jordan, 2007), yet this study demonstrated significant effects of miR-548 on tumorigenicity and angiogenesis (Hu et al., 2014). Here, we identify miR-3189 as a miRNA produced through canonical miRNA biogenesis pathways and conserved between humans and old-world apes. Furthermore, we characterize miR-3189 as a novel

p53-regulated miRNA, an important component of the cellular response to DNA damage, and a potent effector of cell death in cancer cells independent of p53 mutation status.

7.2 Results

7.2.1 The putative miR-3189 is a poorly conserved miRNA in the intron of *GDF15*

In the results of an unpublished microarray study profiling gene expression following p53 activation by the pharmacological inhibition of its inhibitor MDM2 with nutlin-3a, the probe corresponding to an unvalidated miRNA was a highly significant hit. The putative miR-3189 had been annotated by previous deep sequencing studies and deposited into miRBase (**Fig 7.1 B**), but no biochemical experiments had actually validated its existence as a functional human miRNA. miR-3189 is located within the intron of the well-studied p53 target gene *GDF15* (**Fig 7.1 A**), so there is a strong likelihood *a priori* that it is co-regulated by p53 along with its host gene. A strong argument for the physiological significance of non-coding RNAs *en masse* rests on their phylogenetic conservation implying functional importance. To determine whether miR-3189 is conserved, we aligned its sequence with orthologous regions across animal phyla and found that it is conserved only among humans, primates, and old-world monkeys (**Fig 7.1 C**). Orthologous sequences in new-world monkeys and more distantly related phyla are not predicted to form stable miRNA-like secondary structures via thermodynamic folding analysis (data not shown).

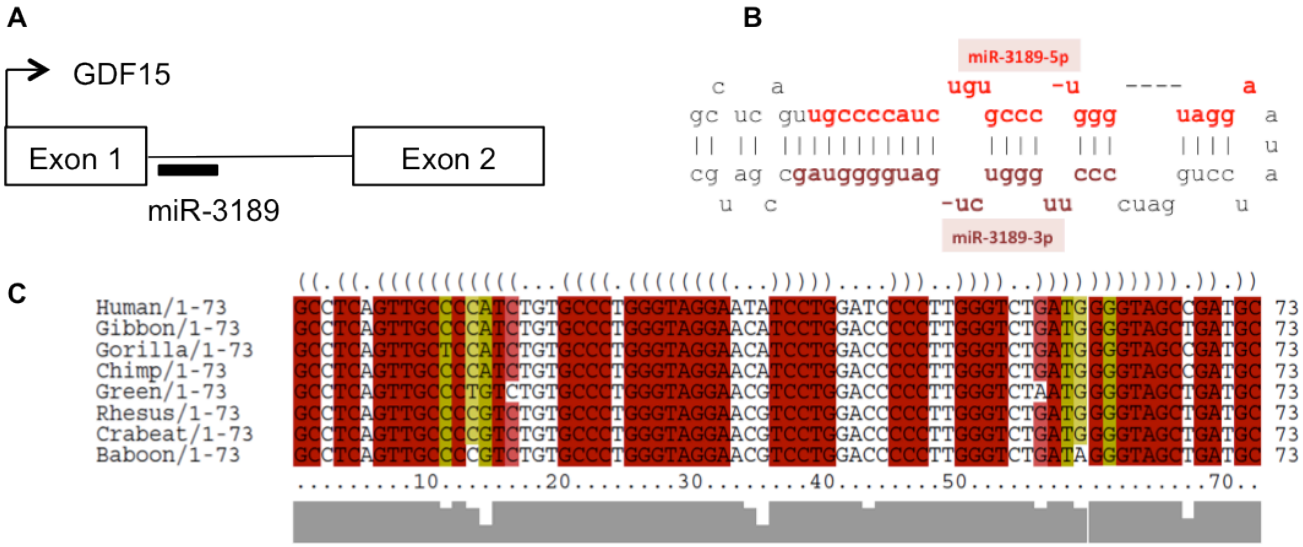

Figure 7.1
Locus, sequence, and multiple alignment of the novel miR-3189
A, B) The putative miR-3189 stem loop sequence is situated within the intron of the known p53-target gene GDF15. The miR-3189 hairpin sequence begins 95 bp downstream of the 5' splice site of *GDF15*. C) Multiple alignment and predicted consensus RNA secondary structure for miR-3189 candidate sequences in primates. Evolutionary analysis and a phylogenetic stochastic content-free grammar models for RNA evolution give a strong prediction that the miR-3189 precursors can fold into a stable conserved miRNA-like structure in apes and old-world monkeys. The optimal conserved secondary structure in dot-bracket notation is shown (dot= gap in secondary structure, bracket= paired nucleotide in secondary structure). Prediction of secondary structure is based on the multiple alignment of miR-3189 precursors in primates. Profile of similarity is shown below in grey. Highly conserved base-pairs in folding are shown in red; base-pairs, formed by several different combinations of nucleotides, are indicated by different colors. Sequence alignment and conservation analysis was performed by Svetlana Shabalina at the National Institute for Biotechnology Information, Bethesda, Maryland, USA.

7.2.2 miR-3189-3p is functionally incorporated into RISC in response to p53 activation

Because miR-3189 has never been experimentally confirmed to function as a miRNA, we sought to verify both the induction of a mature miRNA product by p53 and the involvement of this miRNA in the canonical miRNA-mediated gene silencing pathway. p53 activation with nutlin-3a treatment in the 3 p53-wild type cell lines HCT116, SW48 and RKO resulted in equivalent increases in both GDF15 mRNA and pri-mir-3189 expression (**Fig. 7.2 A**). The mature miRNA product from the 3' end of 3189 hairpin, miR-3189-3p, was significantly upregulated by either doxorubicin or nutlin-3a treatment of HCT116, albeit at slightly lower levels than the primary transcript. However, the induction of miR-3189-3p by p53 activation was consistent with that observed for the well-characterized p53-inducible miRNA miR-34a (**Fig 7.2 B**). The product from the 5' end of the hairpin, miR-3189-5p was also upregulated by p53 activation (data not shown). The incorporation of miR-3189-3p into RISC after p53 activation was assayed by Ago2 IP, as in Chapter 5. We found that, in HCT116, p53 activation by doxorubicin treatment corresponded with a nearly 6-fold enrichment of miR-3189-3p in RISC (**Fig 7.2 C**). miR-215 is included as a negative control for the Ago2 IP experiment, as the results of chapter 5 showed that it is not induced by doxorubicin treatment of HCT116, so we would not expect its enrichment in RISC following doxorubicin treatment.

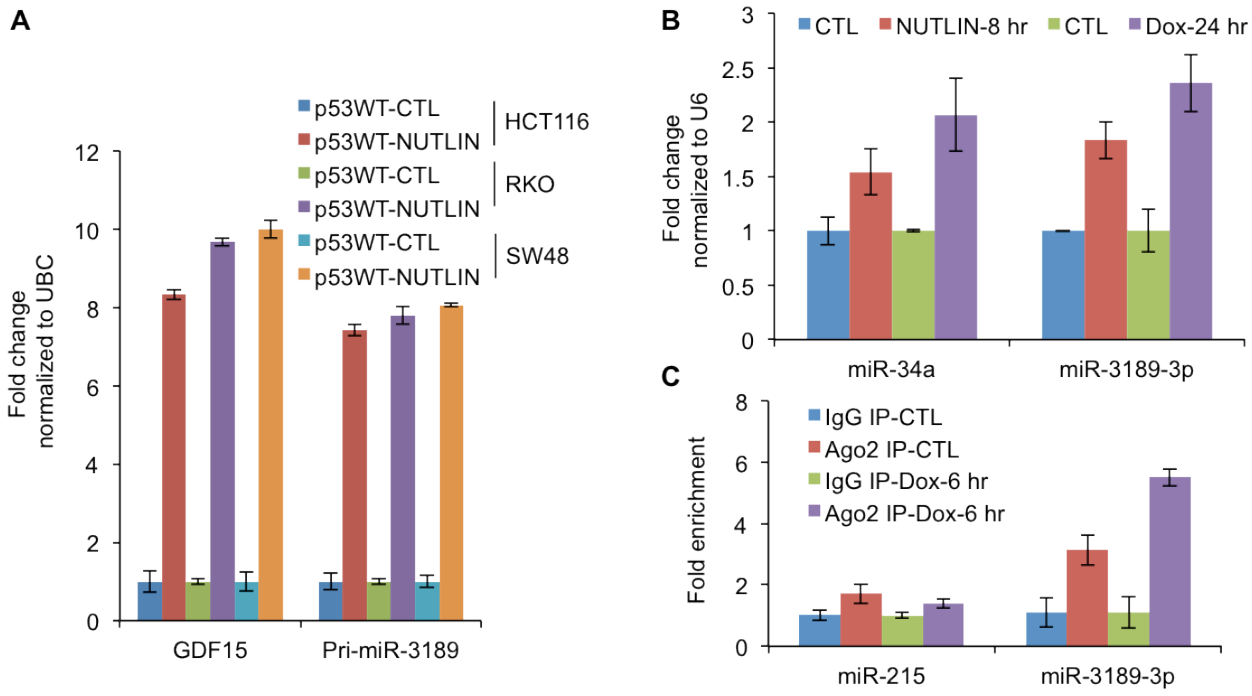

Figure 7.2
p53 activation induces miR-3189 expression
A) The p53-wild type cell lines HCT116, RKO and SW480 were treated with the MDM2-inhibitor nutlin-3a, RNA was isolated and the expression levels of GDF15 and pri-mir-3189 were assayed by SYBR-Green qRT-PCR. B) The induction of miR-3189-3p in response to either nutlin-3a or DNA-damage mediate p53 activation by doxorubicin was compared to the known p53-target miR-34a. HCT116 cells were treated for the indicated time, after which RNA was isolated and miRNA expression was assayed by TaqMan qRT-PCR. C) Incorporation of miR-3189-3p into RISC was measured after treatment with doxorubicin. miR-215 was included as a negative control, as the results of Chapter 4 indicated that it is not, in fact, induced by doxorubicin treatment.

7.2.3 miR-3189 is a necessary component of the p53-mediated response to DNA damage

If p53-wild type cells are treated with low to moderate doses of DNA damage, in the form of genotoxic agents or UV light, they undergo growth arrest while the damage is repaired but remain viable. We reasoned that knocking down an essential component of the p53 pathway would reduce the viability of cells in response to sub-lethal doses of doxorubicin. In the absence of DNA damage, miR-3189-3p knockdown using anti-miR chemistry resulted in a significant potentiation of cell growth over 4 days, as measured by MTT assay (**Fig 7.3 A**). We also attempted to knock down miR-3189-5p, but observed no effect on cell growth (data not shown). Importantly, we also determined that transfection of HCT116 the anti-miR-3189 oligo prevents induction of miR-3189-3p expression by doxorubicin and in fact causes a 2-fold reduction compared to the baseline level of expression (**Fig 7.3 B**). Treatment of HCT116 cells with a sub-lethal dose of doxorubicin in combination with anti-miR-3189-3p caused a significant reduction in the number of viable cells compared to control (**Fig 7.3 C**). These cells also formed significantly fewer colonies when cultured at low density on plastic for 10 days (**Fig. 7.3 D**), indicating that miR-3189 comprises a necessary constituent of the p53-mediated response to DNA damage.

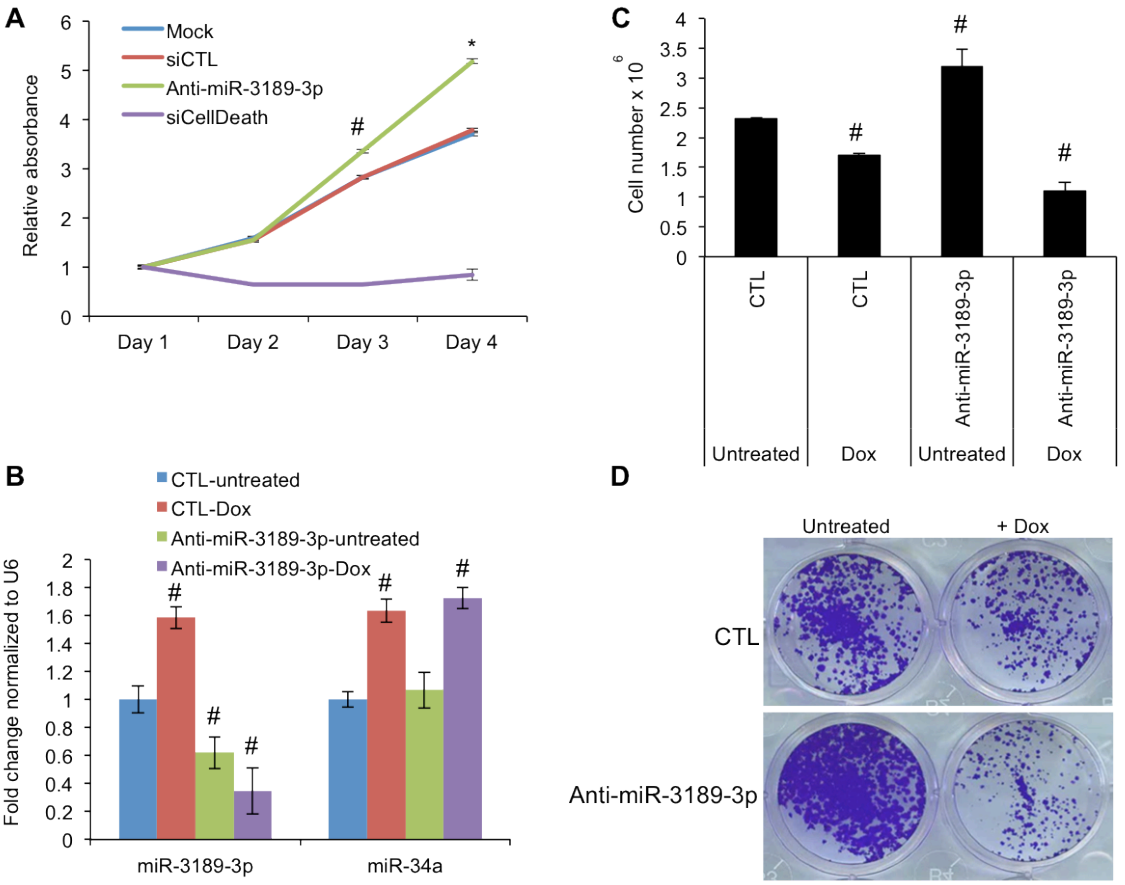

Figure 7.3
Inhibition of miR-3189-3p sensitizes HCT116 cells to genotoxic stress
A) HCT116 cells were transfected with miR-3189-3p, mock, control mimic, or siCell Death for 24 hours, and then re-seeded into 96-well plates. Cell proliferation was measured over 4 days by MTT assay. B) Transfection of synthetic Anti-miR against miR-3189 into HCT116 results in approximately 40% reduction of miR-3189-3p expression and prevents induction of miR-3189-3p by doxorubicin. miR-34a shown as negative control. C) HCT116 cells were transfected with anti-miR-3189-3p or control for 48 hours, then treated with doxorubicin for 6 hours, after which cells were counted. D) Equal numbers of the cells counted in (C) were seeded at low density in 12-well plates and allowed to grow for 10 days. Colonies were fixed and stained with crystal violet. #p<0.05, *p<0.01.

7.2.4 Effects of miR-3189 expression on cell growth and viability

7.2.4.1 Inhibition of cell proliferation by miR-3189-3p irrespective of p53 status

Because miR-3189-3p is a necessary component of the p53 pathway, we reasoned that miR-3189-3p function would be consistent with the overall effects of p53 signaling, namely cell cycle arrest, apoptosis, and tumor suppression. To test this hypothesis, we reverse transfected HCT116-p53WT with miR-3189-3p, -5p and control mimics. We also included HCT116-p53KO as a negative control under the assumption that miR-3189-3p effects would be p53-dependent. Surprisingly, miR-3189-3p mimic transfection reduced cell proliferation and viability as measured by MTT assay in both HCT116-p53WT and HCT116-p53KO cell lines (**Fig 7.4 A**). Consistent with previous results, miR-3189-5p had no detectable effect. In fact, the effect of miR-3189-3p on cell growth appears to depend on other factors to a greater extent than p53 status. We carried out MTT assays following miR-3189-3p or control mimic transfection in the p53 mutant MDA-MB-231 cell line and the p53-wild type SW480, and we found that the growth of the MDA-MB-231 cell line was inhibited to a much greater extent than SW480, though the growth of both cell lines was significantly reduced (**Fig 7.4 B**). When cultured over a longer time period at low density for colony formation on plastic, all cell lines transfected with miR-3189-3p mimic formed significantly fewer colonies than control, regardless of p53 status (**Fig 7.4 C**).

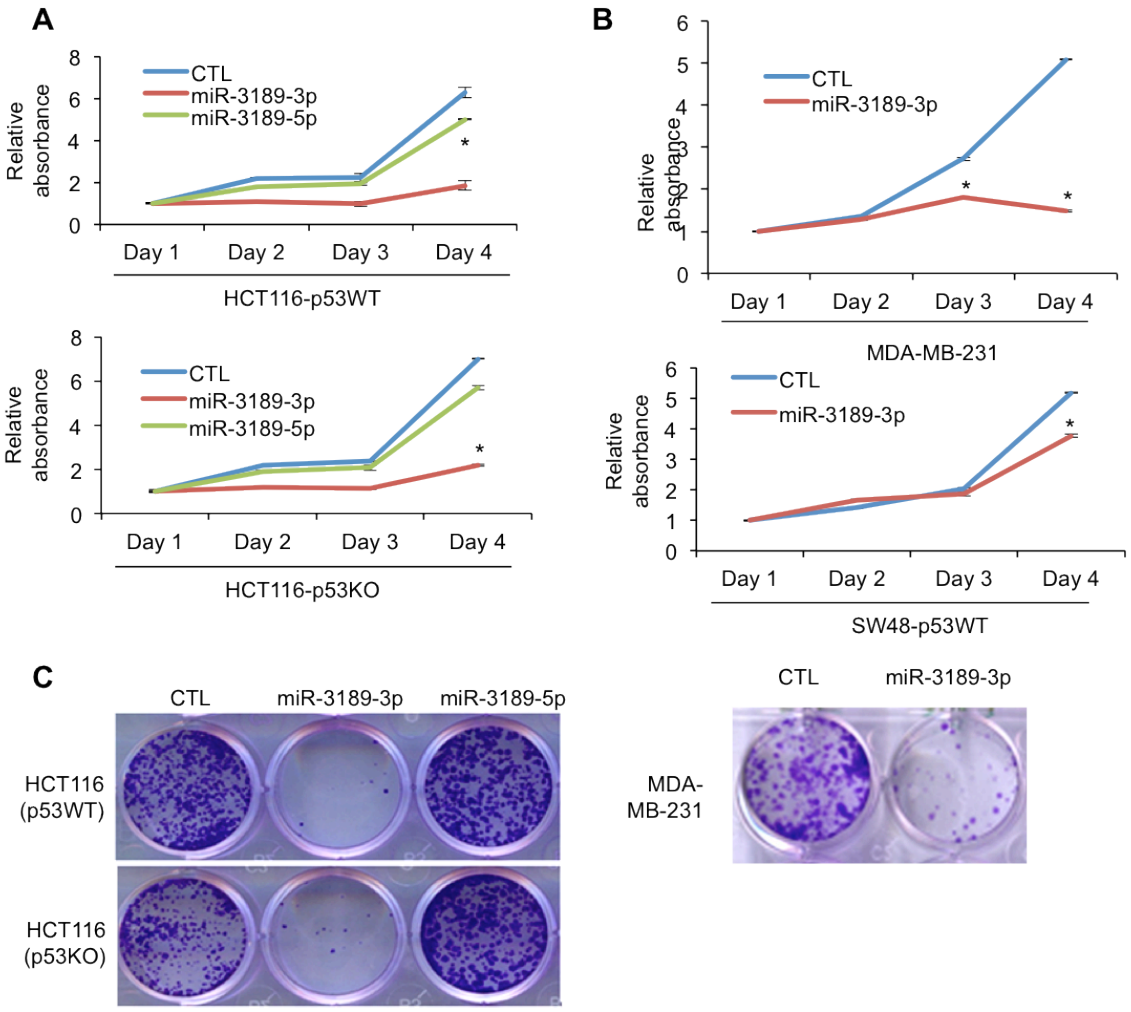

Figure 7.4
miR-3189-3p inhibits cell growth irrespective of p53 status
A) HCT116-p53WT and HCT116-p53KO were reverse transfected with miR-3189-3p, -5p or control mimics. After 48 hours, transfectants were re-seeded in 96 well plates and growth was assayed over 4 days by MTT assay. B) The p53-mutant breast cancer line MDA-MB-231 and the p53-WT colorectal cancer cell line SW480 were transfected as in (A) and MTT assays were conducted over 4 days. C) Cells transfected as in (A) and (B) were seeded at low density in 12-well plates and cultured for 10 days to allow colony formation. Colonies were fixed and stained with crystal violet.

7.2.4.2 p53-independent induction of apoptosis by miR-3189-3p

In light of the observation that miR-3189-3p overexpression causes sharp reduction in cell growth and viability, it is necessary to determine whether this effect is mediated by apoptosis, necrosis, senescence, growth arrest, or some other mechanism. We immediately suspected that that miR-3189-3p causes cell death rather than growth arrest, due mainly to the clearly visible presence of dead cells after visual inspection under the a microscope. We then began by testing for apoptosis, the most common type of programed cell death, in response to miR-3189-3p transfection by assaying DNA fragmentation and poly (ADP-ribose) polymerase (PARP) cleavage. Transfection of both HCT116-p53WT and HCT116-p53KO with miR-3189-3p resulted in a classically apoptotic DNA fragmentation pattern, with discreet bands present at roughly 150bp intervals (**Fig 7.5 A**). miR-3189-3p transfected cells also exhibited significantly increased levels of PARP cleavage (**Fig 7.5 B**) as determined by western immunoblot. There was little or no p53-dependent variation in the effect of miR-3189-3p on either DNA fragmentation or PARP cleavage.

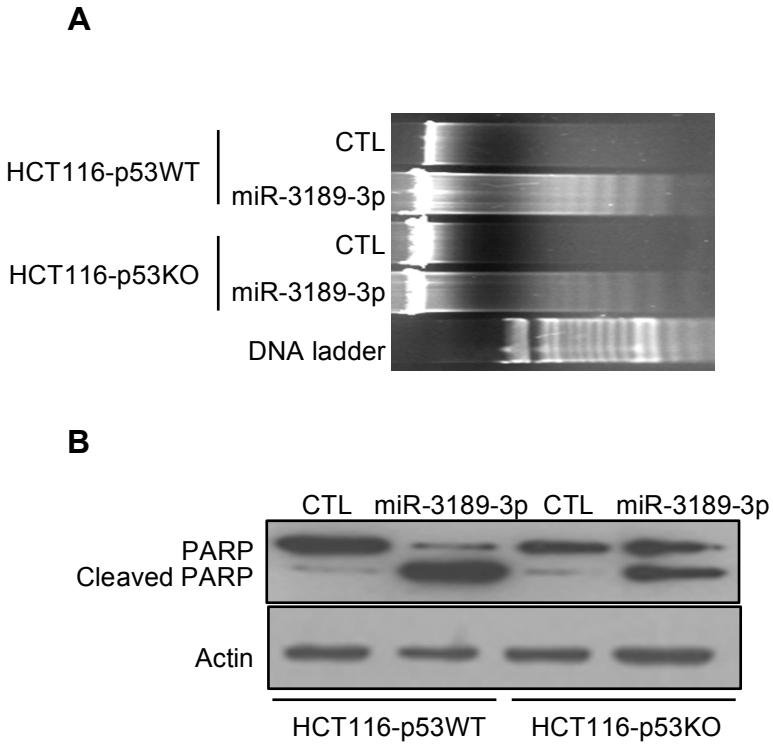

Figure 7.5
miR-3189-3p induces apoptotic cell death
A) Apoptotic DNA fragmentation assay. HCT116-p53WT or p53KO cells were reverse transfected with miR-3189-3p or CTL mimic for 48 hours. Genomic DNA was isolated and electrophoresed on a 2% agarose gel. B) Western immunblot for total and cleaved PARP. Cells were transfected as in A and protein was isolated after 48 hours. β-actin shown as loading control.

7.2.5 miR-3189 regulates the expression of genes controlling cell cycle and chromatin remodeling

7.2.5.1 Microarray expression profiling identifies miR-3189-3p effects on the transcriptome

In order to identify target mRNAs that mediate the pro-apoptotic effects of miR-3189, we conducted microarray expression profiling using a similar strategy as that deployed in chapter 5 for miR-215. Because there is such phenotypic similarity between the miR-3189 transfected p53WT and p53KO HCT116 cell lines, we profiled the gene expression of both cell lines after transfection with miR-3189-3p mimic. Further results of the microarray are given in **Appendix II**. As we expected, there was a high amount of ove--rlap between the genes differentially expressed in response to miR-3189-3p in HCT116-p53WT and HCT116-p53KO ($p<10^{-30}$) (**Fig 7.6 A**). A subset of genes downregulated by at least 2-fold and with Bonferroni-adjusted p-value<0.05 in both cell lines were selected for validation by qRT-PCR. All of the selected genes were also significantly downregulated in the qRT-PCR experiment (**Fig 7.6 B**), indicating that the microarray accurately detected differential expression across the transcriptome.

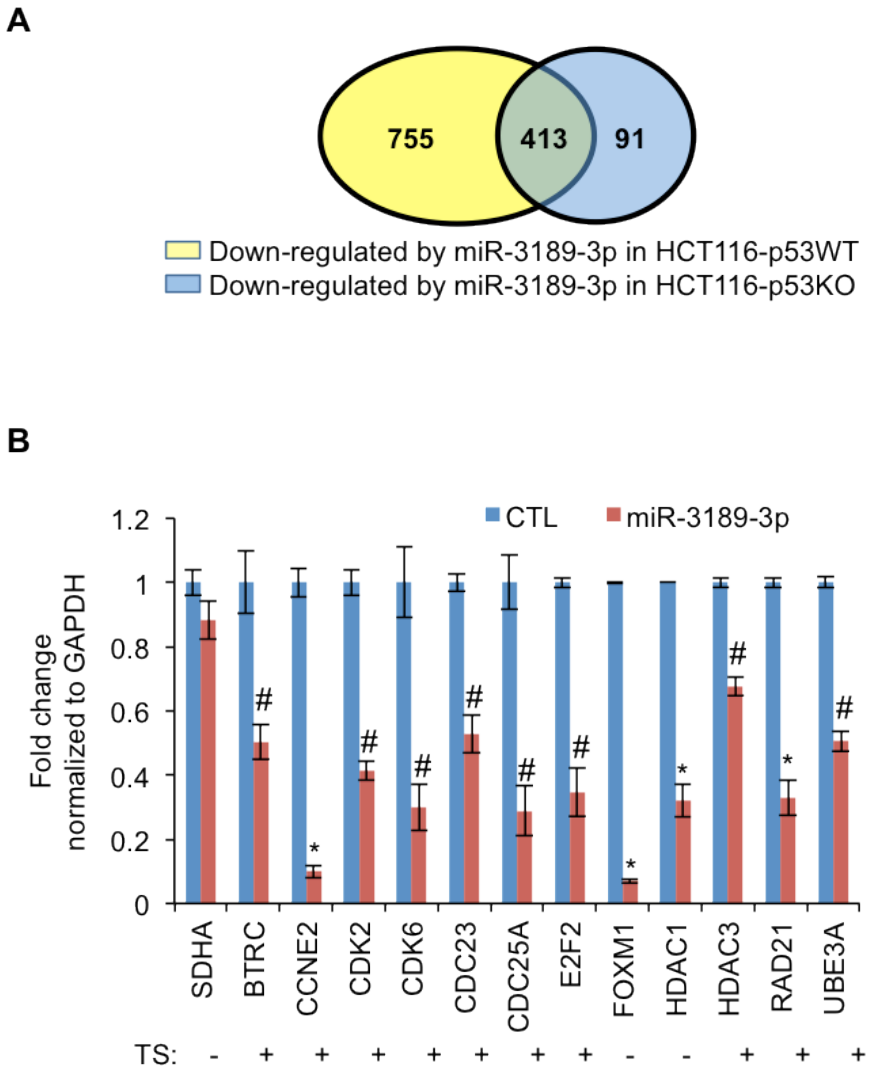

Figure 7.6
Transcriptomic impact of miR-3189-3p expression
A) Venn diagram showing the intersection of genes downregulated by miR-3189-3p in HCT116-p53WT and –p53KO cell lines. Cells were transfected with miR-3189-3p or control mimics and subjected to microarray gene expression profiling as described in chapter 4. B) SYBR-Green qRT-PCR of genes significantly down-regulated in the intersection of (A). SDHA expression shown as negative control. TS=TargetScan predicted miR-3189-3p target mRNA. #p<0.05, *p<0.01.

7.2.5.2 Identification of direct miR-3189-3p target mRNAs

Consequent to our previous observation that miR-3189-3p is a potent effector of apoptosis, we manually investigated the intersection of downregulated gene sets between HCT116-p53WT and HCT116-p53KO microarrays for genes with potential roles in cell cycle progression and cell survival. We found that the cyclins CCNA2 and CCNE2, the cyclin-dependent kinase CDK2, the mitotic polo-like kinases CDC23, CDC25A, and CDC25B, the forkhead-box transcription factor FOXM1, and the histone deacetylase HDAC3 were all bioinformatically predicted miR-3189-3p targets that were also downregulated in both HCT116-p53WT and HCT116-p53KO. As described in Chapter 5, the 3'UTRs of these genes were cloned into a heterologous luciferase reporter construct such that repression of the 3'UTR would be detected via a loss of luciferase activity. We found that the 3'UTRs of all of these genes, with the exception of CCNE2, were significantly repressed by miR-3189-3p mimic transfection, indicating that this genes are direct targets of post-transcriptional repression by miR-3189-3p (**Fig 7.7A**).

Additionally, we validated the down-regulation of HDAC1, HDAC3, and CDK2 at the protein level by western immunoblot. Importantly, the repression of these genes by miR-3189-3p was not dependent on p53 status, as they were consistently down-regulated in HCT116-p53KO as well as HCT116-p53WT (**Fig 7.7 B**). It should, however, be noted, that HDAC3 was not predicted as a direct target of miR-3189-3p, nor was its 3'UTR repressed in luciferase reporter assays, so it is likely that downregulation of HDAC3 occurs via an indirect mechanism.

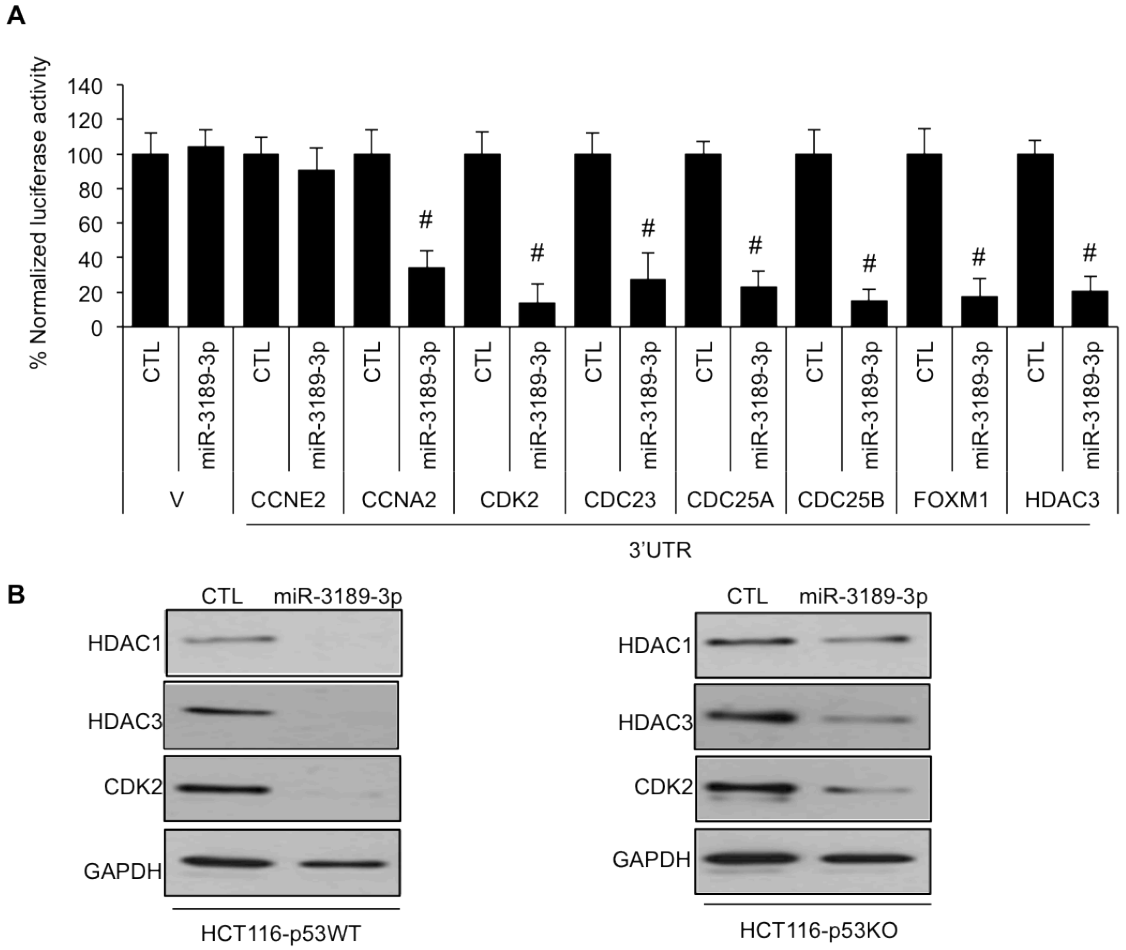

Figure 7.7
Identification and validation of direct miR-3189-3p target genes
A subset of genes from the intersection of downregulated gene sets from HCT116-p53WT and HCT116-p53KO microarray experiments (Fig 7.7A) were selected for 3'UTR luciferase assays. Full-length 3'UTRs were cloned downstream of the *Renilla* luciferase ORF in psiCHECK2. 3'UTR constructs were co-transfected into HCT116 cells with either miR-3189 mimic or control. B) Downregulation of direct miR-3189 targets from (A) was validated at the protein level by western immunoblot following miR-3189 mimic or control transfection of HCT116-p53WT or –p53KO cell lines. GAPDH used as loading control. #p<0.05

7.2.6 miR-3189 inhibits tumorigenicity *in vitro* and *in vivo*.

In addition to its effects on cell proliferation on plastic, we observed that in HCT116-p53WT and isogenic p53KO cells, miR-3189-3p mimics inhibited anchorage independent growth on soft agar (**Fig 7.8**). Because soft agar colony formation is often taken as a measure of tumorigenic potential, we hypothesized that miR-3189-3p also inhibits tumorigenicity in a xenograft model. Therefore, we subcutaneously injected NOD-SCID mice with HCT116-p53WT or HCT116-p53KO cells transfected with CTL or miR-3189-3p mimic. MiR-3189-3p over-expression dramatically reduced the rate of tumor growth over 4 weeks in both cell lines (**Fig 7.9 A**). The average tumor volume after 4 weeks was ~2000-fold greater in mice injected with either of the CTL-transfected lines than in mice injected with miR-3189-3p-transfected cells (**Fig 7.9 B**). Taken together, the results from this study suggest that miR-3189-3p is a novel p53-regulated miRNA that plays a role in cell survival during the DNA damage response, while introduction of exogenous miR-3189-3p strongly induces apoptosis even in cells lacking wild-type p53.

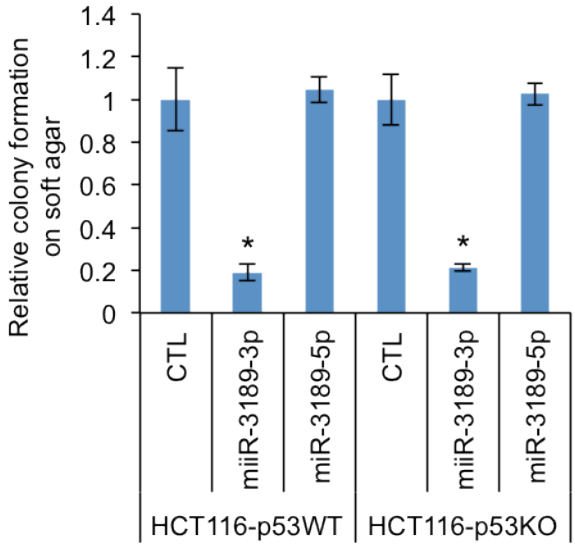

Figure 7.8
miR-3189-3p inhibits colony formation *in vitro*
Either HCT116-p53WT or HCT116-p53KO were transfected with miR-3189-3p or -5p mimics for 48 hours, then embedded in soft agar. Colonies were counted after 10 days. *p<0.01

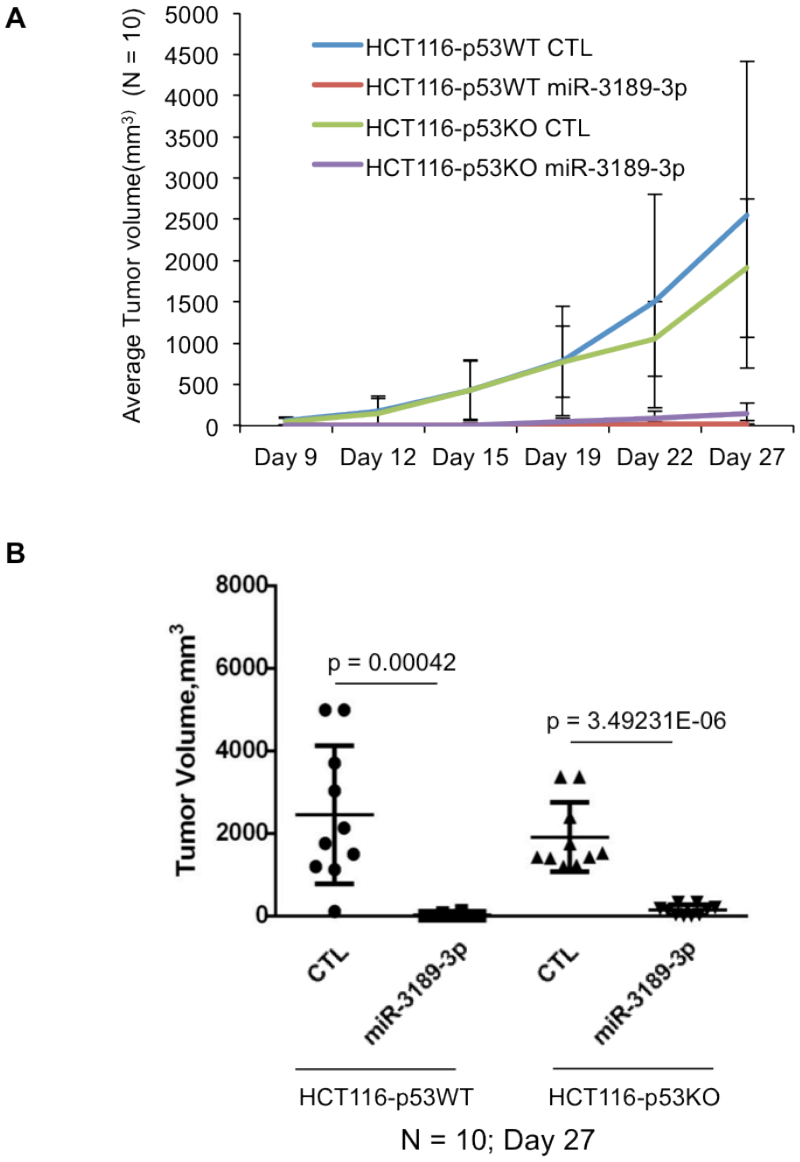

Figure 7.9
p53-independent inhibition of xenograft growth by miR-3189-3p
HCT116-p53WT or –p53KO were transfected with miR-3189-3p mimics, and equal number of cells were injected into the flanks of NOD-SCID mice after 48 hours.
Upper panel- growth curve of tumors measured by semi-daily caliper assessment.
Lower panel- after 4 weeks, mice were sacrificed, tumors were excised and measured.

7.3 Discussion

This study combined gene expression profiling in the context of p53 activation with loss- and gain-of-function experiments to characterize the biogenesis and function of a novel, primate-specific miRNA, miR-3189. Previous RNA-seq studies indicated the existence of a mature miRNA that maps to the intron of GDF15. Our work represents the first validation and functional study of miR-3189. When cloned into a lentiviral expression vector, the putative miR-3189 stem-loop sequence produces a functional mature miRNA. Furthermore, we established that miR-3189-3p, the mature miRNA from the 3'-end of pre-miR-3189, is more abundant, preferentially incorporated into RISC and required for cell viability following DNA damage. We could not detect a role of miR-3189-5p in cell cycle regulation or cell survival.

Many miRNAs are produced from loci within in an intron of a protein-coding host gene or even a spliced non-coding transcript (Wightman et al., 1993; Kim et al., 2009; Rearick et al., 2011).Although these intronic miRNAs may be regulated independently of their host genes by discrete promoters (Subramanian et al., 2014; Monteys et al., 2010), there are also instances in which the embedded miRNA is transcriptionally co-regulated with its host (Xiao et al., 2011).*GDF15* and miR-3189 have similar expression patterns across panels of both healthy tissues and in colorectal cancer patient samples (TCGA, data not shown). Our results indicate that *GDF15* and miR-3189-3p are transcriptionally co-regulated by p53. However, in order to establish that they are both directly transactivated by p53, further experiments will be necessary. Studies on the roles of *GDF15* (also

known as Macrophage Inhibitory Cytokine 1; *MIC1*, or NSAID activated gene; *NAG1*) have produced conflicting reports, and it has been implicated in a wide range of cellular processes (Mimeault and Batra, 2010). *GDF15* has been reported by multiple studies to be a target of p53 in response to both DNA damage and pharmacological p53 induction by Nutlin-3 treatment(Djuranovic et al., 2011; Esteller, 2011; Lujambio and Lowe, 2012; Kumar et al., 2009; Cheng et al., 2011; Li et al., 2000), and these and other results have attributed growth-inhibitory and tumor-suppressive functions to *GDF15* (Jones and Lal, 2012; Hermeking, 2012; Leung and Sharp, 2010; Raver-Shapira et al., 2007; Okada et al., 2014; Kelly et al., 2009; Yang et al., 2003). However, other studies have found elevated expression of *GDF15* in many human cancers(Bohlig et al., 2011; Brown et al., 2003; Xue et al., 2010; Karan et al., 2003), and high levels of *GDF15* expression correspond to increased metastasis in both mouse models and human patients (Huarte et al., 2010; Park et al., 2009; Persson et al., 2011; Stark et al., 2010; Cheng et al., 2011; Xue et al., 2010; Senapati et al., 2010).

Although it is possible that *GDF15* exerts pleiotropic effects on the growth of cancer cells, we believe that many of these prior studies have conflated the function of GDF15 with the function of the embedded miR-3189. For example, p53-independent up-regulation of *GDF15* by the long non-coding RNA MEG3 causes growth arrest in HCT116-p53KO cells (Bootcov et al., 1997; Zhou et al., 2007), which conflicts with earlier reports regarding GDF15 function (Friedman et al., 2008; Perdomo et al., 2013; Piriyapongsa and Jordan, 2007; Lim et al., 2007; Baek et al., 2001), yet is completely consistent with our results showing the p53-independent effects of the GDF15-embedded

miR-3189. It is known that GDF15 expression is also regulated by other cancer associated transcription factors, including HIF1α (Hu et al., 2014; Krieg et al., 2010), NF-κB (Okada et al., 2014; Park et al., 2009; Shim and Eling, 2005), and EGR1 (Baek et al., 2001). Further research will be needed to determine whether miR-3189 is co-regulated by these transcription factors and how the expression of miR-3189 contributes to the associated physiological contexts of hypoxia and inflammation. Our study has established miR-3189-3p as integral to the cellular response to genotoxic stress, and it may be that miR-3189-3p is also involved in hypoxic and inflammatory stress responses.

Our results have identified miR-3189-3p as miRNA that can kill cancer cells independently of p53. miR-34a, the most extensively studied p53-regulated miRNA, is involved in positive feedback loops with p53 by repressing the p53 inhibitors SIRT1 (Yamakuchi et al., 2008) and HDM4 (Okada et al., 2014), but its effects, unlike miR-3189-3p, are dependent on the presence of wild-type p53 (Okada et al., 2014; Chang et al., 2007; Hermeking, 2009), Our results indicate that miR-3189-3p does, indeed, mediate a positive feedback loop in which p53 activation is sustained by down-regulation of the well known p53 inhibitors HDAC1 and HDAC3 (Xiao et al., 2011; Murphy et al., 1999; Juan et al., 2000). We found that miR-3189-3p knockdown increases cell death following DNA damage. We reason that this effect is consistent with its essential role in the DNA damage response: without miR-3189-3p, cells are ill-equipped to recover from genotoxic stress. Re-introduction of miR-3189-3p into p53-null cancer cell lines caused a strong apoptotic response and the up-regulation of a subset of p53 target genes including *GADD45A* and *GDF15*. Because p53 is the most frequently mutated gene in human

cancers, a miRNA that circumvents mutant p53 to induce apoptosis offers significant promise for cancer therapy. Over the past 5 years, much research has focused on developing methods to target oncogenic miRNAs and restore tumor suppressive miRNAs for cancer therapy (Mimeault and Batra, 2010; Kasinski and Slack, 2011; Broderick and Zamore, 2011). The efficacy of any new cancer therapy must be rigorously tested in animal models, most commonly murine, before it can be applied to human patients, which presents the problem: how can a primate-specific miRNA be tested in a non-primate model? Although our results demonstrate that pre-treatment of cancer cells with synthetic miR-3189-3p greatly reduces xenograft tumor growth, further *in vivo* work using xenotransplantation of human tissue may facilitate validation of miR-3189-3p as a potential therapeutic molecule, but it remains to be seen if miR-3189-3p would have an effect on a transgenic mouse model of autochthonous tumor growth or whether systemic delivery of miR-3189-3p mimic would specifically and effectively target preformed tumors. However, miR-3189-3p over-expression represents an attractive tool to either kill cancer cells by directly introducing a miRNA mimic or to sensitize cells to genotoxic chemotherapy by antagomiR inhibition.

CHAPTER EIGHT

General Discussion & Future Directions

CHAPTER 8: GENERAL DISCUSSION & FUTURE DIRECTIONS

8.1 MiR-215 is a direct target of CDX1 in colorectal cancer cell lines

The work presented in this thesis implicates miR-215 in the transcriptional network regulated by CDX1. By profiling miRNA expression in cell lines with modulated CDX1 expression, we identified several miRNAs that were either up- or downregulated in response to CDX1. A key method used in the identification of miR-215 as an important target of CDX1 was profiling candidate miRNA expression in 10 colorectal cell lines with varying CDX1 expression. While many studies characterize transcriptional regulation in only one or two cell lines, we were able to detect a robust relationship that is maintained across cell lines with varying mutation and gene expression landscapes. However, the use of a greater number of cell lines may have allowed for the detection of a greater number of significant CDX1-miRNA correlations. A simple thought experiment illustrates how greater sample size can power detection of less robust correlations: doubling all of the numbers in **Table 4.3** while retaining the same ratios would have resulted in the inclusion of miR-99a and miR-193-3p as significant miRNA targets of CDX1. Despite the robust association between miR-215 and *CDX1* in cell lines, it would be a valuable addition to assay miR-215 and *CDX1* expression levels in primary tumor samples, which may also be compared with publicly available tumor data such as The Cancer Genome Atlas.

We used several standard biochemical and molecular biology techniques to verify the transactivation of miR-215 by CDX1. Chromatin immunoprecipitation, in particular, demonstrated that CDX1 appears to bind as strongly to the miR-215 promoter as to a previously characterized, protein-coding CDX1 target gene, *KRT20* (Chan et al., 2009). This result is consistent with our proposal in Chapter 3 that miRNA targets of CDX1 may be equally important as mediators of the effects of CDX1 compared to protein coding genes. In order to fully characterize the binding patterns of CDX1 across the genome, it would be beneficial to conduct chromatin immunoprecipitation followed by high-throughput sequencing, or ChIP-seq. This would facilitate the genome-wide annotation of CDX1 target genes and would surely cast new light on the downstream functional effects of CDX1. A major hurdle that must be surmounted for the success of this experiment would be the validation of our in-house CDX1 monoclonal antibody. The successful preparation of a ChIP-seq library requires a high-avidity antibody with specificity for formaldehyde fixed, DNA-bound protein. Although our antibody was suitable for ChIP-PCR, it may be sub-optimal for the preparation of large-scale sequencing libraries. Given the repeated unsuccessful attempts at this experiment by the author of this thesis and others in the Cancer Immunogenetics laboratory, it seems likely that this is the case. Another possible solution to this problem could entail fusing the coding sequence of CDX1 to an HA tag, and performing ChIP using an anti-HA antibody.

It would also be worthwhile to conduct ChIP-seq to map the binding sites of CDX2. This would allow us to discern the differences between the effects of CDX1 and CDX2 regulating differentiation in the gut. The respective effects of CDX1 versus CDX2 are a

topic which has long been the subject of some disagreement in the field (Savory et al., 2009; Mutoh et al., 2009). Moreover, it would be of great interest to compare the regulation of miRNAs by CDX2 to that of CDX1. Given the reported functional redundancy between the CDX family members, we might expect some overlap, but CDX1 and CDX2 seem to be responsible for driving distinct cell fate decisions, with CDX2 implicated in goblet cell differentiation while CDX1 is associated with epithelial lineages (Yamamoto et al., 2003; Chan et al., 2009). As a further example, the structural protein *KRT20* is a target of CDX1 but not CDX2 (Chan's thesis, 2009 and Chan, et al. 2010). Therefore, we might expect that CDX1 and CDX2 induce distinct sets of miRNAs. A recent finding has even suggested that miRNAs induced by CDX1 repress CDX2, hinting at a negative feedback mechanism between these homeobox genes (Tagawa et al., 2012). However, that study was only conducted in one cell line, and we found no evidence that miR-215 targets CDX2.

Outside of the gut, *CDX1* has been characterized as an essential factor in the anterior-posterior patterning of vertebrae in the developing embryo through its regulation of the *Hox* gene family (Subramanian et al., 1995). Interestingly, we have found that miR-215 represses *HOXA10* expression downstream of CDX1. This result provides only the first suggestion that miR-215 may be involved in embryonic development, but it may also be the case that the CDX1-miR-215 axis is significant for embryogenesis. Constitutive *Cdx1* knockout mice display normal guts due to functional compensation by *Cdx2*, but they do show homeotic fusions of the vertebrae and other skeletal abnormalities (Subramanian et al., 1995). It would be interesting to determine whether loss of miR-215 expression is

implicated in this phenotype. Knockout models of miR-215 would be a valuable tool to study its involvement in (a) normal gut function and (b) embryogenesis. It is possible that the closely related miR-192 would compensate for loss of miR-215, but we did not detect any relationship between miR-192 and *CDX1* in this thesis.

Although previous studies of miR-215 have grouped it together with the related cluster of miR-192-194-2, our data did not suggest that *CDX1* regulates the transcription of this cluster. This observation suggests previously undetected diversity of function in this miRNA family. Although this may seem unexpected given the paralogous relationship between those miRNAs, it is not unprecedented. Many protein-coding paralogs are not truly redundant, as they have evolved different upstream regulatory mechanisms and may have quite divergent patterns of expression and functions (Gu et al., 2002; Li et al., 2005). As total duplication of function is potentially disruptive to molecular pathways sensitive to dosage (Conrad et al., 2007), of which the canonical miRNA pathway could surely be considered an example, it is not unreasonable to suppose that paralogous miRNA clusters may be differentially regulated at the transcriptional level.

8.2 miR-215 is a downstream effector of CDX1 function

We have identified miR-215 as an effector of CDX1 function. Perhaps the most compelling evidence for this conclusion stems from a modified rescue experiment in which CDX1 was introduced into CDX1-low cell lines with or without a miR-215 sponge. Loss of miR-215 prevented many of the transcriptional and phenotypic changes

associated with CDX1 from taking place. Interestingly, there was a striking correspondence between the effects on 3-D morphology of miR-215 knockdown in LS174T and CDX1 overexpression in DLD1. Antagonizing miR-215 in CDX1-transfected DLD1 caused a reversion from a reticulated, lobular colony morphology resembling something like the differentiated colon to a dense, undifferentiated colony morphology. Similarly, miR-215 knockdown in LS174T causes a shift from loose colonies with polarized, f-actin foci to dense colonies that strongly resemble those in the CDX1-low cell lines DLD1 or HCT116. These results indicate that, although miR-215 expression alone is not sufficient to induce lumen formation and differentiation *in vitro*, loss of miR-215 interferes with the induction of differentiation by CDX1.

The functional results described above indicate that miR-215 is necessary but not sufficient for epithelial differentiation downstream of *CDX1*. This conclusion is supported by the microarray analysis of gene expression following miR-215 and *CDX1* expression. Introduction of miR-215 alone does not fully replicate the transcriptomic changes associated with CDX1, nor would we expect such a degree of overlap because CDX1 has direct transcriptional targets other than miR-215. However, there is a highly significant degree of overlap between the genes down-regulated by miR-215 and those down-regulated by CDX1. In fact, as CDX1 has previously been shown to upregulate mainly enterocyte differentiation proteins (**Fig 8.1)** (Staloch et al., 2005; Chan et al., 2009; Arango et al., 2012,), which are unlikely to mediate further gene expression changes. The downregulation of stem cell genes in response to *CDX1* expression is, therefore, a necessary but previously unexplained phenomenon. By again using co-

transfection of *CDX*1 and the miR-215 sponge, we have confirmed that CDX1-associated downregulation of several genes is, in fact, mediated by miR-215. However, these experiments have been performed in a handful of cell lines, and to truly understand the dependence of *CDX1* function on miR-215, they will need to be repeated in a wider range of cell lines.

In light of the well-documented roles for CDX1 in regulating differentiation in the normal colonic crypt, it may be that miR-215 is also necessary for mediating differentiation of normal enterocytes. However, it is important to note that the data presented here were gathered exclusively in cancerous tissues, which, despite their functional differentiation, cannot necessarily be assumed to reflect normal physiology. CDX1 has previously been shown by immunohistochemistry in normal tissue to stain epithelial cells lining the colonic lumen and extending some way into the middle, transit amplifying portion of the crypt (Chan et al., 2009). One of the first steps to demonstrating the importance of miR-215 in the normal colon would be to use fluorescent miRNA *in situ* hybridization to test whether miR-215 is expressed in a similar pattern.

8.3 MiR-215 represses stem cell genes, including *BMI1*

Previous studies on the effects of CDX1, including unpublished microarray gene expression profiles from 110 colorectal cancer cell lines in the Cancer and Immunogenetics Laboratory, have shown a robust negative association between *CDX1* and *BMI1* expression (Ghandi's thesis, 2011; Chan's thesis 2009) (Yeung et al., 2010;

Yeung et al., 2011). This negative correlation is thought to be tied to the role of CDX1 as a regulator of differentiation in the colon and to the role of *BMI1* as a marker and a regulator of a crypt-base stem cell population (Yan et al., 2012). Our previous conception of the roles of *CDX1* and *BMI1* in the regulation of stem cells was that in cancers with methylated *CDX1*, *BMI1* expression was high, which corresponded to incomplete differentiation, a high proportion of cancer stem cells, and a more aggressive growth profile. Conversely, *CDX1* expression correlates with low *BMI1* expression, a well-differentiated tumor, and a less aggressive phenotype. The mechanism underlying this correlation has proven elusive, as CDX1 is, canonically, a transcriptional activator, so a direct, negative interaction between CDX1 and *BMI1* would seem counterintuitive. Until the work presented in this thesis, there was little evidence of a link mediating this negative correlation. We have shown, here, that miR-215 acts as precisely such a link. We therefore hypothesize that miR-215 acts as part of a CDX1-mediated differentiation switch. As cells migrate upwards along the crypt through the transit amplifying zone, CDX1 expression is activated, which represses BMI1 through miR-215. Previous studies on the roles of miRNAs in regulating differentiation have indicated that they act as such switches, for example miR-489 regulating the transition from muscle stem cell quiescence to proliferation (Cheung et al., 2013) or miR-34a regulating cell-fate decisions in the intestinal crypt by repressing Notch signaling (Bu et al., 2014). As cells reach the steady state of terminal differentiation, miR-215 may be less important for maintaining the "off" state of stem cell genes–chromatin modification would seem a more efficient type of stable repression repression–but the feedback loop defined by CDX1-miR-215-BMI1 (**Fig. 8.1**) is surely important for enforcing the gene expression

changes necessary for the conversion from undifferentiated to differentiated cellular states. Further study will be necessary to determine whether miR-215 or some other mechanism, for example histone deacetylation near regulatory loci, is required for preventing the re-acquisition of stemness by terminally differentiated enterocytes.

In order to solidify the conclusion that the effects of miR-215 depend on *BMI1* repression, it will be necessary to perform rescue experiments. In such an experiment, a *BMI1* expression construct lacking a miR-215 binding site would be co-transfected into a cell line or panel of cell lines along with miR-215 or *CDX1*. We would expect, given our current data, that this BMI1 construct, immune to repression by miR-215, would counteract the effects we have observed on clonogenicity, cell cycle, and colony morphology. Indeed, a previous study on the pharmacological inhibition of BMI1 has shown results that concur with our observations of reduced clonogenicity and cell growth (Kreso et al., 2014), suggesting that a large portion of the functional effects of miR-215 expression may be explained by *BMI1* inhibition. However, it must be noted that miRNAs regulate *networks* of genes, not just individual genes in isolation. It may not be realistic to expect that all of the effects of miR-215 may be rescued by de-repression of a single target gene.

miR-215 acts to reduce the expression of other genes which may be connected to stem cell traits, yet which have not been explicitly linked to CDX1 in the literature. We have shown that *RUNX1*, for example, is a direct target of miR-215. *RUNX1* has long since been characterized as an important transcription factor in hematopoietic stem cells which

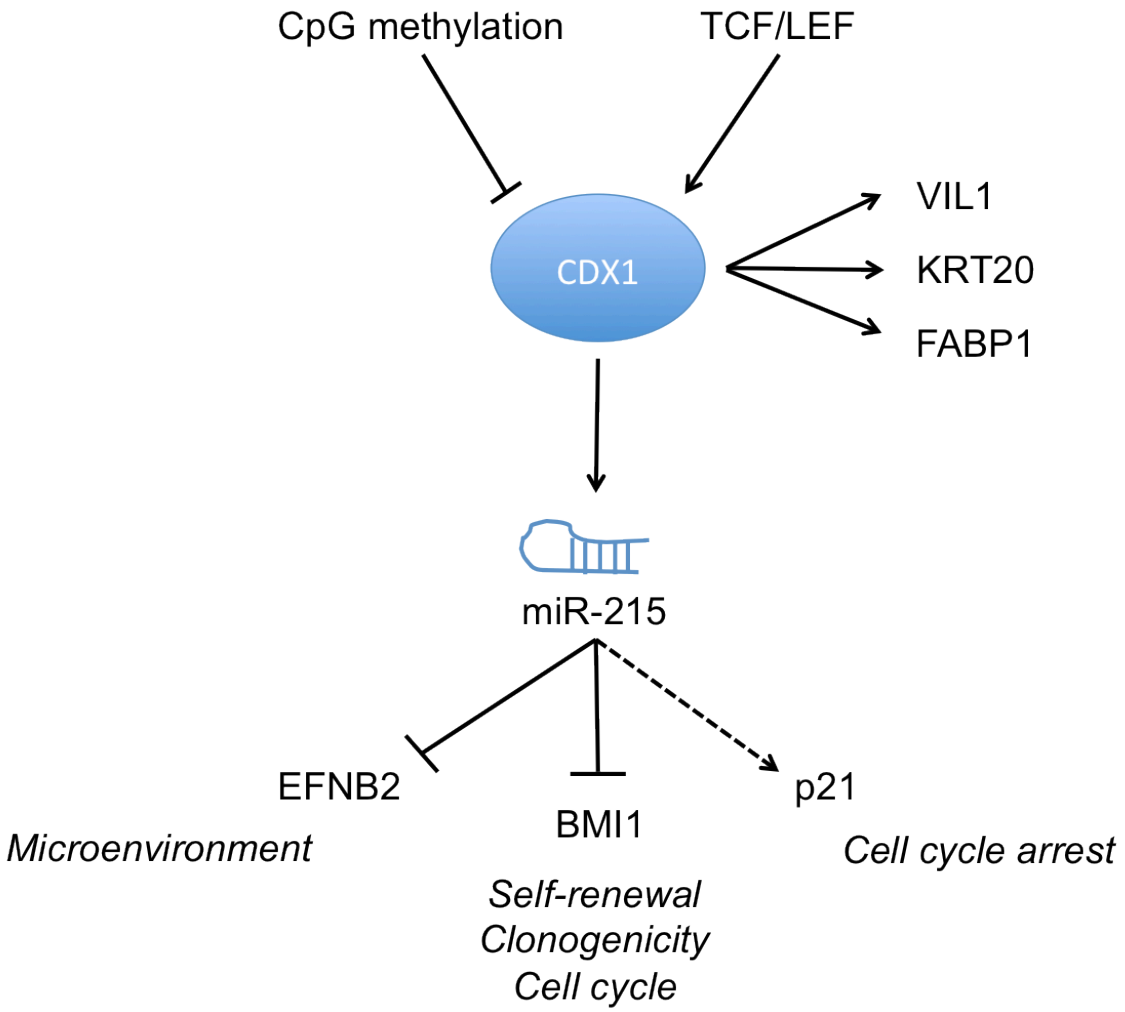

Figure 8.1
Model of the CDX1-miR-215 regulatory axis
An schema integrating the work of this thesis and previous studies on CDX1. Dotted line indicates indirect effect. Italicized labels indicate the processes impacted by miR-215 mediated gene regulation.

is also involved in hematopoietic malignancies as a cancer stem cell gene (Mangan et al., 2011). Recently, RUNX1 expression was also found to be important for both normal and cancerous epithelial stem cells by stimulating cell growth through STAT3 (Osorio et al., 208; Scheitz et al., 2012). Certain SNPs in *RUNX1* also confer an increased risk of colorectal cancer (Slattery et al., 2011). There is a lack of in depth studies of RUNX1 in the colonic stem cell niche, but its presence in the CDX1-miR-215 axis will hopefully incentivize further inquiry along these lines.

Another interesting miR-215 target is ephrin B2 (*EFNB2*), a secreted factor which has been implicated in maintaining a mesenchymal stem cell niche in bone, blood, and mammary tissue (Diercke et al., 2011; Kaenel et al., 2012; Tierny et al., 2013). Other ephrin ligands and receptors have been linked to colonic stem cells (Merlos-Suarez et al., 2011), and the connection between CDX1-miR-215 and *EFNB2* may offer a prospective link between *EFNB2*, colon stem cells, and colorectal cancer.

8.4 p53 is an important regulator of miRNA expression

There is a voluminous literature, including a review written by the author of this thesis (Jones and Lal, 2012), dedicated to uncovering the roles played by miRNAs in p53 signaling and cancer. miR-215 has previously been reported in that literature as a target of p53 (Georges et al., 2008; Braun et al., 2008) and a mediator of a positive feedback loop via repression of *MDM2* (Chan et al., 2009; Pichiorri et al., 2010). However, our results call these prior studies into question. A miRNA may certainly be regulated by

more than one upstream transcription factor, and regulation by CDX1 does not necessarily preclude regulation by p53. In fact, our reporter assay results for the miR-215 promoter suggest a permissive role for p53 in the transactivation of miR-215 by CDX1. However, we were unable to repeat previous results showing induction of miR-215 by DNA-damage mediated p53 induction. Nor did we observe any downregulation of *MDM2* expression consequent of miR-215 overexpression. This may be due to the fact that our miRNA mimic dosage for transfections was lower than those used in the previously cited studies by a factor of 5. We believe that this lower concentration more faithfully recapitulates physiological levels of miRNA expression, and we have supported this by using Ago2 immunoprecipitation to compare the amount of exogenous mimic incorporated into RISC with that of an endogenous miRNA.

On the other hand, we did observe up-regulation of a novel yet previously annotated pri-miRNA transcript in response to p53 activation in a microarray experiment using 3 p53-wild type cell lines. We characterized this miRNA as miR-3189-3p, an intronic miRNA embedded in the known p53 target gene *GDF15* (Savory et al., 2009; Yang et al., 2003; Mutoh et al., 2009). We found that this miRNA is regulated concurrently with its host gene, which is an important discovery as it implies that previous reports on the function of *GDF15* may have been confounded by the unrecognized activity of a miRNA encoded by the same locus. Some studies have shown pro-proliferative effects for *GDF15* (Xue et al., 2010), while others have reported anti-proliferative effects which seem more consistent with the function of the embedded miR-3189-3p (Tagawa et al., 2012; Tan et al., 2000; Yang et al., 2003).

We have shown in this thesis that both miR-215 and miR-3189 induce the expression of genes in the canonical p53 signaling pathway, yet these effects do not depend on the presence of wild-type p53. A simple explanation of miR-215-mediated growth arrest and miR-3189-3p-mediated apoptosis would invoke p53 activation, yet we observed that the respective functional effects of both miRNAs are nearly equivalent in p53 mutant or p53 knockout cell lines as in p53 wild-type cell lines. These effects will need to be tested in a much wider range of cell lines, yet the initial data are quite striking. This observation underscores the robustness of miRNA networks: although p53 is an important node, it may also be circumvented to achieve growth arrest and apoptosis. Clinically, miRNA-derived therapeutics offer an attractive method to, for example, induce growth arrest in p53-mutant tumors. Reconstitution of defective p53 signaling has been an area of fervent research in gene therapy for cancer, with prospective methods running the gamut from *MDM2* inhibition (Subramanian et al., 1995; Wade et al., 2013) to nanoparticle-mediated reintroduction of wild-type p53 (Li et al., 2005; Senzer et al., 2013; Gu et al., 2002). Similar nanoparticle delivery systems have been successfully used for therapeutic administration of miRNAs (Conrad and Antonarakis, 2007; Kasinski and Slack, 2011). However, the multifactorial mechanisms of miRNAs seem to offer a more robust alternative to specifically targeted gene therapies. We believe that both miR-215 or miR-3189-3p should be included in the new wave of miRNAs *en route* to the clinic (Broderick and Zamore, 2011).

8.5 Summary

We have outlined the effects of miR-215 as a mediator of CDX1 function. In this chapter, we have focused on trying to explain its effects in terms of a small number of target genes (**Fig. 8.1**). However, the great promise of miRNAs in cancer lies not in the ability to specifically inhibit a single gene, but rather to influence pathways and networks of genes. We have shown that miR-215 and miR-3189 are, albeit in distinct ways, potent inhibitors of cancer growth *in vitro*. miR-215 is an effector of CDX1 which can effectively promote growth arrest and downregulate stem-cell transcripts in colorectal cancer. These results offer novel insight into the physiology of the colorectal crypt and the means by which differentiation is controlled at a molecular level, and they also elucidate the mechanisms underlying the heterogeneous patterns of differentiation in colon cancer.

References

REFERENCES

Aigner, F., and H. Fritsch. 2010. Anorectal and Colonic Anatomy. *In* Anorectal and Colonic Diseases. Springer Berlin Heidelberg, Berlin, Heidelberg. 3–17.

Al-Hajj, M., M.S. Wicha, A. Benito-Hernandez, S.J. Morrison, and M.F. Clarke. 2003. Prospective identification of tumorigenic breast cancer cells. *Proc. Natl. Acad. Sci. U.S.A.* 100:3983–3988. doi:10.1073/pnas.0530291100.

Altschul, S.F., T.L. Madden, A.A. Schäffer, J. Zhang, Z. Zhang, W. Miller, and D.J. Lipman. 1997. Gapped BLAST and PSI-BLAST: a new generation of protein database search programs. *Nucleic Acids Research*. 25:3389–3402.

Altuvia, Y., P. Landgraf, G. Lithwick, N. Elefant, S. Pfeffer, A. Aravin, M.J. Brownstein, T. Tuschl, and H. Margalit. 2005. Clustering and conservation patterns of human microRNAs. *Nucleic Acids Research*. 33:2697–2706. doi:10.1093/nar/gki567.

Ambros, V., B. Bartel, D.P. Bartel, C.B. Burge, J.C. Carrington, X. Chen, G. Dreyfuss, S.R. Eddy, S. Griffiths-Jones, M. Marshall, M. Matzke, G. Ruvkun, and T. Tuschl. 2003. A uniform system for microRNA annotation. *RNA*. 9:277–279.

Ameres, S.L., and P.D. Zamore. 2013. Diversifying microRNA sequence and function. *Nat Rev Mol Cell Biol*. 14:475–488. doi:10.1038/nrm3611.

Anokye-Danso, F., C.M. Trivedi, D. Juhr, M. Gupta, Z. Cui, Y. Tian, Y. Zhang, W. Yang, P.J. Gruber, J.A. Epstein, and E.E. Morrisey. 2011. Highly Efficient miRNA-Mediated Reprogramming of Mouse and Human Somatic Cells to Pluripotency. *Cell Stem Cell*. 8:376–388. doi:10.1016/j.stem.2011.03.001.

Arango, D., S. Al-Obaidi, D.S. Williams, H. Dopeso, R. Mazzolini, G. Corner, D.S. Byun, A.A. Carr, C. Murone, L. Tögel, N. Zeps, L.A. Aaltonen, B. Iacopetta, and J.M. Mariadason. 2012. Villin Expression Is Frequently Lost in Poorly Differentiated Colon Cancer. *AJPA*. 180:1509–1521. doi:10.1016/j.ajpath.2012.01.006.

Armitage, P., and R. Doll. 1954. The age distribution of cancer and a multi-stage theory of carcinogenesis. *British Journal of Cancer*. 8:1–12. doi:10.1038/sj.bjc.6602297.

Ashley, N., T.M. Yeung, and W.F. Bodmer. 2013. Stem cell differentiation and lumen formation in colorectal cancer cell lines and primary tumors. *Cancer Research*. 73:5798–5809. doi:10.1158/0008-5472.CAN-13-0454.

Baek, D., J. Villén, C. Shin, F.D. Camargo, S.P. Gygi, and D.P. Bartel. 2008. The impact of microRNAs on protein output. *Nature*. 455:64–71. doi:10.1038/nature07242.

Baek, S.J., K.S. Kim, J.B. Nixon, L.C. Wilson, and T.E. Eling. 2001. Cyclooxygenase inhibitors regulate the expression of a TGF-beta superfamily member that has proapoptotic and antitumorigenic activities. *Mol. Pharmacol.* 59:901–908.

Bao, S., Q. Wu, R.E. McLendon, Y. Hao, Q. Shi, A.B. Hjelmeland, M.W. Dewhirst, D.D. Bigner, and J.N. Rich. 2006. Glioma stem cells promote radioresistance by preferential activation of the DNA damage response. *Nature*. 444:756–760. doi:10.1038/nature05236.

Barbolina, M.V., B.P. Adley, E.V. Ariztia, Y. Liu, and M.S. Stack. 2007. Microenvironmental regulation of membrane type 1 matrix metalloproteinase activity in ovarian carcinoma cells via collagen-induced EGR1 expression. *J. Biol. Chem.* 282:4924–4931. doi:10.1074/jbc.M608428200.

Barker, N., J.H. van Es, J. Kuipers, P. Kujala, M. van den Born, M. Cozijnsen, A. Haegebarth, J. Korving, H. Begthel, P.J. Peters, and H. Clevers. 2007. Identification of stem cells in small intestine and colon by marker gene Lgr5. *Nature*. 449:1003–1007. doi:10.1038/nature06196.

Barker, N., R.A. Ridgway, J.H. van Es, M. van de Wetering, H. Begthel, M. van den Born, E. Danenberg, A.R. Clarke, O.J. Sansom, and H. Clevers. 2009. Crypt stem cells as the cells-of-origin of intestinal cancer. *Nature*. 457:608–612. doi:10.1038/nature07602.

Barreau, C., S. Dutertre, L. Paillard, and H.B. Osborne. 2006. Liposome-mediated RNA transfection should be used with caution. *RNA*. 12:1790–1793. doi:10.1261/rna.191706.

Barretina, J., G. Caponigro, N. Stransky, K. Venkatesan, A.A. Margolin, S. Kim, C.J. Wilson, J. Lehár, G.V. Kryukov, D. Sonkin, A. Reddy, M. Liu, L. Murray, M.F. Berger, J.E. Monahan, P. Morais, J. Meltzer, A. Korejwa, J. Jané-Valbuena, F.A. Mapa, J. Thibault, E. Bric-Furlong, P. Raman, A. Shipway, I.H. Engels, J. Cheng, G.K. Yu, J. Yu, P. Aspesi, M. de Silva, K. Jagtap, M.D. Jones, L. Wang, C. Hatton, E. Palescandolo, S. Gupta, S. Mahan, C. Sougnez, R.C. Onofrio, T. Liefeld, L. MacConaill, W. Winckler, M. Reich, N. Li, J.P. Mesirov, S.B. Gabriel, G. Getz, K. Ardlie, V. Chan, V.E. Myer, B.L. Weber, J. Porter, M. Warmuth, P. Finan, J.L. Harris, M. Meyerson, T.R. Golub, M.P. Morrissey, W.R. Sellers, R. Schlegel, and L.A. Garraway. 2012. The Cancer Cell Line Encyclopedia enables predictive modelling of anticancer drug sensitivity. *Nature*. 483:603–607. doi:10.1038/nature11003.

Bingham, S., and E. Riboli. 2004. Diet and cancer--the European Prospective Investigation into Cancer and Nutrition. *Nature Reviews Cancer*. 4:206–215. doi:10.1038/nrc1298.

Bodmer, W. 1999. Familial adenomatous polyposis (FAP) and its gene, APC. *Cytogenet. Cell Genet.* 86:99–104.

Bohlig, L., M. Friedrich, and K. Engeland. 2011. p53 activates the PANK1/miRNA-107 gene leading to downregulation of CDK6 and p130 cell cycle proteins. *Nucleic Acids Research*. 39:440–453. doi:10.1093/nar/gkq796.

Bohnsack, M.T., K. Czaplinski, and D. Görlich. 2004. Exportin 5 is a RanGTP-dependent dsRNA-binding protein that mediates nuclear export of pre-miRNAs. *RNA*. 10:185–191. doi:10.1261/rna.5167604.

Bommer, G.T., I. Gerin, Y. Feng, A.J. Kaczorowski, R. Kuick, R.E. Love, Y. Zhai, T.J. Giordano, Z.S. Qin, B.B. Moore, O.A. MacDougald, K.R. Cho, and E.R. Fearon. 2007. p53-Mediated Activation of miRNA34 Candidate Tumor-Suppressor Genes. *Current Biology*. 17:1298–1307. doi:10.1016/j.cub.2007.06.068.

Bonnet, D., and J.E. Dick. 1997. Human acute myeloid leukemia is organized as a hierarchy that originates from a primitive hematopoietic cell. *Nature Medicine*. 3:730–737.

Bootcov, M.R., A.R. Bauskin, S.M. Valenzuela, A.G. Moore, M. Bansal, X.Y. He, H.P. Zhang, M. Donnellan, S. Mahler, K. Pryor, B.J. Walsh, R.C. Nicholson, W.D. Fairlie, S.B. Por, J.M. Robbins, and S.N. Breit. 1997. MIC-1, a novel macrophage inhibitory cytokine, is a divergent member of the TGF-beta superfamily. *Proc. Natl. Acad. Sci. U.S.A.* 94:11514–11519.

Borovski, T., F. De Sousa E Melo, L. Vermeulen, and J.P. Medema. 2011. Cancer Stem Cell Niche: The Place to Be. *Cancer Research*. 71:634–639. doi:10.1158/0008-5472.CAN-10-3220.

Braun, C.J., X. Zhang, I. Savelyeva, S. Wolff, U.M. Moll, T. Schepeler, F.T. Ørntroft, C.L. Andersen, P.S. Linsley, M.A. Cleary, B.N. Chau, and M. Dobbelstein. 2008. p53-Responsive MicroRNAs 192 and 215 Are Capable of Inducing Cell Cycle Arrest. *Cancer Research*. 68:10094–10104. doi:10.1158/0008-5472.CAN-08-1569.

Broderick, J.A., and P.D. Zamore. 2011. MicroRNA therapeutics. *Gene Ther.* 18:1104–1110. doi:10.1038/gt.2011.50.

Brown, D.A., R.L. Ward, P. Buckhaults, T. Liu, K.E. Romans, N.J. Hawkins, A.R. Bauskin, K.W. Kinzler, B. Vogelstein, and S.N. Breit. 2003. MIC-1 serum level and genotype: associations with progress and prognosis of colorectal carcinoma. *Clin. Cancer Res.* 9:2642–2650.

Bruggeman, S.W.M., D. Hulsman, E. Tanger, T. Buckle, M. Blom, J. Zevenhoven, O. van Tellingen, and M. van Lohuizen. 2007. Bmi1 controls tumor development in an Ink4a/Arf-independent manner in a mouse model for glioma. *Cancer Cell*. 12:328–341. doi:10.1016/j.ccr.2007.08.032.

Bu, P., K.-Y. Chen, J.H. Chen, L. Wang, J. Walters, Y.J. Shin, J.P. Goerger, J. Sun, M. Witherspoon, N. Rakhilin, J. Li, H. Yang, J. Milsom, S. Lee, W. Zipfel, M.M. Jin, Z.H. Gümüş, S.M. Lipkin, and X. Shen. 2013. A microRNA miR-34a-Regulated Bimodal Switch Targets Notch in Colon Cancer Stem Cells. *Cell Stem Cell*. 12:602–615. doi:10.1016/j.stem.2013.03.002.

Buczacki, S.J.A., H.I. Zecchini, A.M. Nicholson, R. Russell, L. Vermeulen, R. Kemp,

and D.J. Winton. 2013. Intestinal label-retaining cells are secretory precursors expressing Lgr5. *Nature*. 495:65–69. doi:10.1038/nature11965.

Burri, N., P. Shaw, H. Bouzourene, I. Sordat, B. Sordat, M. Gillet, D. Schorderet, F.T. Bosman, and P. Chaubert. 2001. Methylation silencing and mutations of the p14ARF and p16INK4a genes in colon cancer. *Lab Invest*. 81:217–229.

Calin, G.A., C. Sevignani, C.D. Dumitru, T. Hyslop, E. Noch, S. Yendamuri, M. Shimizu, S. Rattan, F. Bullrich, M. Negrini, and C.M. Croce. 2004. Human microRNA genes are frequently located at fragile sites and genomic regions involved in cancers. *Proc. Natl. Acad. Sci. U.S.A.* 101:2999–3004. doi:10.1073/pnas.0307323101.

Chan, C.W.M., N.A. Wong, Y. Liu, D. Bicknell, H. Turley, L. Hollins, C.J. Miller, J.L. Wilding, and W.F. Bodmer. 2009. Gastrointestinal differentiation marker Cytokeratin 20 is regulated by homeobox gene CDX1. *Proceedings of the National Academy of Sciences*. 106:1936–1941. doi:10.1073/pnas.0812904106.

Chang, C.-J., C.-H. Chao, W. Xia, J.-Y. Yang, Y. Xiong, C.-W. Li, W.-H. Yu, S.K. Rehman, J.L. Hsu, H.-H. Lee, M. Liu, C.-T. Chen, D. Yu, and M.-C. Hung. 2011. p53 regulates epithelial–mesenchymal transition and stem cell properties through modulating miRNAs. *Nature Cell Biology*. 13:317–323. doi:10.1038/ncb2173.

Chang, T.-C., E.A. Wentzel, O.A. Kent, K. Ramachandran, M. Mullendore, K.H. Lee, G. Feldmann, M. Yamakuchi, M. Ferlito, C.J. Lowenstein, D.E. Arking, M.A. Beer, A. Maitra, and J.T. Mendell. 2007. Transactivation of miR-34a by p53 Broadly Influences Gene Expression and Promotes Apoptosis. *Molecular Cell*. 26:745–752. doi:10.1016/j.molcel.2007.05.010.

Charafe-Jauffret, E., C. Ginestier, F. Iovino, J. Wicinski, N. Cervera, P. Finetti, M.H. Hur, M.E. Diebel, F. Monville, J. Dutcher, M. Brown, P. Viens, L. Xerri, F. Bertucci, G. Stassi, G. Dontu, D. Birnbaum, and M.S. Wicha. 2009. Breast Cancer Cell Lines Contain Functional Cancer Stem Cells with Metastatic Capacity and a Distinct Molecular Signature. *Cancer Research*. 69:1302–1313. doi:10.1158/0008-5472.CAN-08-2741.

Chen, L., C. Li, R. Zhang, X. Gao, X. Qu, M. Zhao, C. Qiao, J. Xu, and J. Li. 2011a. miR-17-92 cluster microRNAs confers tumorigenicity in multiple myeloma. *Cancer Letters*. 309:62–70. doi:10.1016/j.canlet.2011.05.017.

Chen, Q.-R., L.-R. Yu, P. Tsang, J.S. Wei, Y.K. Song, A. Cheuk, J.-Y. Chung, S.M. Hewitt, T.D. Veenstra, and J. Khan. 2011b. Systematic proteome analysis identifies transcription factor YY1 as a direct target of miR-34a. *J. Proteome Res.* 10:479–487. doi:10.1021/pr1006697.

Cheng, J.-C., H.-M. Chang, and P.C.K. Leung. 2011. Wild-type p53 attenuates cancer cell motility by inducing growth differentiation factor-15 expression. *Endocrinology*. 152:2987–2995. doi:10.1210/en.2011-0059.

Cheung, T.H., N.L. Quach, G.W. Charville, L. Liu, L. Park, A. Edalati, B. Yoo, P. Hoang, and T.A. Rando. 2013. Maintenance of muscle stem-cell quiescence by microRNA-489. *Nature*. 482:524–528. doi:10.1038/nature10834.

Chin, L.J., E. Ratner, S. Leng, R. Zhai, S. Nallur, I. Babar, R.-U. Muller, E. Straka, L. Su, E.A. Burki, R.E. Crowell, R. Patel, T. Kulkarni, R. Homer, D. Zelterman, K.K. Kidd, Y. Zhu, D.C. Christiani, S.A. Belinsky, F.J. Slack, and J.B. Weidhaas. 2008. A SNP in a let-7 microRNA complementary site in the KRAS 3' untranslated region increases non-small cell lung cancer risk. *Cancer Research*. 68:8535–8540. doi:10.1158/0008-5472.CAN-08-2129.

Choi, Y.J., C.-P. Lin, J.J. Ho, X. He, N. Okada, P. Bu, Y. Zhong, S.Y. Kim, M.J. Bennett, C. Chen, A. Ozturk, G.G. Hicks, G.J. Hannon, and L. He. 2011. miR-34 miRNAs provide a barrier for somatic cell reprogramming. *Nature Cell Biology*. 13:1–10. doi:10.1038/ncb2366.

Christensen, B.C., B.J. Moyer, M. Avissar, L.G. Ouellet, S.L. Plaza, M.D. McClean, C.J. Marsit, and K.T. Kelsey. 2009. A let-7 microRNA-binding site polymorphism in the KRAS 3' UTR is associated with reduced survival in oral cancers. *Carcinogenesis*. 30:1003–1007. doi:10.1093/carcin/bgp099.

Clarke, M.F., J.E. Dick, P.B. Dirks, C.J. Eaves, C.H.M. Jamieson, D.L. Jones, J. Visvader, I.L. Weissman, and G.M. Wahl. 2006. Cancer stem cells--perspectives on current status and future directions: AACR Workshop on cancer stem cells. 9339–9344.

Clevers, H. 2011. The cancer stem cell: premises, promises and challenges. *Nature Medicine*. 1–7. doi:10.1038/nm.2304.

Clevers, H. 2013. Stem Cells: A unifying theory for the crypt. *Nature*. 495:7–8. doi:10.1038/nature11958.

Conrad, B., and S.E. Antonarakis. 2007. Gene duplication: a drive for phenotypic diversity and cause of human disease. *Annu. Rev. Genom. Human Genet.* 8:17–35. doi:10.1146/annurev.genom.8.021307.110233.

Creighton, C.J., J.G. Reid, and P.H. Gunaratne. 2009. Expression profiling of microRNAs by deep sequencing. *Briefings in Bioinformatics*. 10:490–497. doi:10.1093/bib/bbp019.

Crosnier, C., D. Stamataki, and J. Lewis. 2006. Organizing cell renewal in the intestine: stem cells, signals and combinatorial control. *Nat Rev Genet*. 7:349–359. doi:10.1038/nrg1840.

Dalerba, P., S.J. Dylla, I.-K. Park, R. Liu, X. Wang, R.W. Cho, T. Hoey, A. Gurney, E.H. Huang, D.M. Simeone, A.A. Shelton, G. Parmiani, C. Castelli, and M.F. Clarke. 2007. Phenotypic characterization of human colorectal cancer stem cells. *Proc. Natl. Acad. Sci. U.S.A.* 104:10158–10163. doi:10.1073/pnas.0703478104.

de Lau, W., N. Barker, T.Y. Low, B.-K. Koo, V.S.W. Li, H. Teunissen, P. Kujala, A. Haegebarth, P.J. Peters, M. van de Wetering, D.E. Stange, J. van Es, D. Guardavaccaro, R.B.M. Schasfoort, Y. Mohri, K. Nishimori, S. Mohammed, A.J.R. Heck, and H. Clevers. 2012. Lgr5 homologues associate with Wnt receptors and mediate R-spondin signalling. *Nature*. 476:293–297. doi:10.1038/nature10337.

Denli, A.M., B.B. Tops, R.H. Plasterk, R.F. Ketting, and G.J. Hannon. 2004. Processing of primary microRNAs by the Microprocessor complex. *Nature*. 432:231–235.

Diederichs, S., and D.A. Haber. 2006. Sequence variations of microRNAs in human cancer: alterations in predicted secondary structure do not affect processing. *Cancer Research*. 66:6097–6104. doi:10.1158/0008-5472.CAN-06-0537.

Diehn, M., R.W. Cho, N.A. Lobo, T. Kalisky, M.J. Dorie, A.N. Kulp, D. Qian, J.S. Lam, L.E. Ailles, M. Wong, B. Joshua, M.J. Kaplan, I. Wapnir, F.M. Dirbas, G. Somlo, C. Garberoglio, B. Paz, J. Shen, S.K. Lau, S.R. Quake, J.M. Brown, I.L. Weissman, and M.F. Clarke. 2009. Association of reactive oxygen species levels and radioresistance in cancer stem cells. *Nature*. 458:780–783. doi:10.1038/nature07733.

Diercke, K., A. Kohl, C.J. Lux, and R. Erber. 2011. Strain-dependent up-regulation of ephrin-B2 protein in periodontal ligament fibroblasts contributes to osteogenesis during tooth movement. *Journal of Biological Chemistry*. 286:37651–37664. doi:10.1074/jbc.M110.166900.

Ding, L., T.J. Ley, D.E. Larson, C.A. Miller, D.C. Koboldt, J.S. Welch, J.K. Ritchey, M.A. Young, T. Lamprecht, M.D. McLellan, J.F. McMichael, J.W. Wallis, C. Lu, D. Shen, C.C. Harris, D.J. Dooling, R.S. Fulton, L.L. Fulton, K. Chen, H. Schmidt, J. Kalicki-Veizer, V.J. Magrini, L. Cook, S.D. McGrath, T.L. Vickery, M.C. Wendl, S. Heath, M.A. Watson, D.C. Link, M.H. Tomasson, W.D. Shannon, J.E. Payton, S. Kulkarni, P. Westervelt, M.J. Walter, T.A. Graubert, E.R. Mardis, R.K. Wilson, and J.F. DiPersio. 2012. Clonal evolution in relapsed acute myeloid leukaemia revealed by whole-genome sequencing. *Nature*. 481:506–510. doi:10.1038/nature10738.

Djuranovic, S., A. Nahvi, and R. Green. 2011. A Parsimonious Model for Gene Regulation by miRNAs. *Science*. 331:550–553. doi:10.1126/science.1191138.

Dvinge, H., A. Git, S. Gräf, M. Salmon-Divon, C. Curtis, A. Sottoriva, Y. Zhao, M. Hirst, J. Armisen, E.A. Miska, S.-F. Chin, E. Provenzano, G. Turashvili, A. Green, I. Ellis, S. Aparicio, and C. Caldas. 2013. The shaping and functional consequences of the microRNA landscape in breast cancer. *Nature*. 497:378–382. doi:10.1038/nature12108.

Easow, G., A.A. Teleman, and S.M. Cohen. 2007. Isolation of microRNA targets by miRNP immunopurification. *RNA*. 13:1198–1204. doi:10.1261/rna.563707.

Ebert, M.S., J.R. Neilson, and P.A. Sharp. 2007. MicroRNA sponges: competitive inhibitors of small RNAs in mammalian cells. *Nat Meth*. 4:721–726. doi:10.1038/nmeth1079.

Edgar, R.C. 2004. MUSCLE: a multiple sequence alignment method with reduced time and space complexity. *BMC Bioinformatics*. 5:113. doi:10.1186/1471-2105-5-113.

Erhard, F., J. Haas, D. Lieber, G. Malterer, L. Jaskiewicz, M. Zavolan, L. Dölken, and R. Zimmer. 2014. Widespread context dependency of microRNA-mediated regulation. *Genome Research*. 24:906–919. doi:10.1101/gr.166702.113.

Esteller, M. 2011. Non-coding RNAs in human disease. *Nat Rev Genet*. 12:861–874. doi:10.1038/nrg3074.

Evers, B.M., T.C. Ko, J. Li, and E.A. Thompson. 1996. Cell cycle protein suppression and p21 induction in differentiating Caco-2 cells. *Am. J. Physiol.* 271:G722–7.

Fearon, E.R., and B. Vogelstein. 1990. A genetic model for colorectal tumorigenesis. *Cell*. 61:759–767.

Ferlay, J., E. Steliarova-Foucher, J. Lortet-Tieulent, S. Rosso, J.W.W. Coebergh, H. Comber, D. Forman, and F. Bray. 2013. Cancer incidence and mortality patterns in Europe: estimates for 40 countries in 2012. *Eur. J. Cancer*. 49:1374–1403. doi:10.1016/j.ejca.2012.12.027.

Fevr, T., S. Robine, D. Louvard, and J. Huelsken. 2007. Wnt/ -Catenin Is Essential for Intestinal Homeostasis and Maintenance of Intestinal Stem Cells. *Molecular and Cellular Biology*. 27:7551–7559. doi:10.1128/MCB.01034-07.

Filipowicz, W., S.N. Bhattacharyya, and N. Sonenberg. 2008. Mechanisms of post-transcriptional regulation by microRNAs: are the answers in sight? *Nat Rev Genet*. 2008:102–114. doi:10.1038/nrg2290.

Fodde, R., J. Kuipers, C. Rosenberg, R. Smits, M. Kielman, C. Gaspar, J.H. van Es, C. Breukel, J. Wiegant, R.H. Giles, and H. Clevers. 2001. Mutations in the APC tumour suppressor gene cause chromosomal instability. *Nature Cell Biology*. 3:433–438. doi:10.1038/35070129.

Frazer, K.A., L. Pachter, A. Poliakov, E.M. Rubin, and I. Dubchak. 2004. VISTA: computational tools for comparative genomics. *Nucleic Acids Research*. 32:W273–9. doi:10.1093/nar/gkh458.

Fre, S., M. Huyghe, P. Mourikis, S. Robine, D. Louvard, and S. Artavanis-Tsakonas. 2005. Notch signals control the fate of immature progenitor cells in the intestine. *Nature*. 435:964–968. doi:10.1038/nature03589.

Fried, J., A.G. Perez, and B.D. Clarkson. 1976. Flow cytofluorometric analysis of cell cycle distributions using propidium iodide. Properties of the method and mathematical analysis of the data. *The Journal of Cell Biology*. 71:172–181.

Friedman, R.C., K.K.H. Farh, C.B. Burge, and D.P. Bartel. 2008. Most mammalian mRNAs are conserved targets of microRNAs. *Genome Research*. 19:92–105.

doi:10.1101/gr.082701.108.

Gautier-Stein, A., C. Domon-Dell, A. Calon, I. Bady, J.-N. Freund, G. Mithieux, and F. Rajas. 2003. Differential regulation of the glucose-6-phosphatase TATA box by intestine-specific homeodomain proteins CDX1 and CDX2. *Nucleic Acids Research*. 31:5238–5246.

Geibel, J.P. 2005. SECRETION AND ABSORPTION BY COLONIC CRYPTS. *Annu. Rev. Physiol.* 67:471–490. doi:10.1146/annurev.physiol.67.031103.153530.

Georges, S.A., M.C. Biery, S.-Y. Kim, J.M. Schelter, J. Guo, A.N. Chang, A.L. Jackson, M.O. Carleton, P.S. Linsley, M.A. Cleary, and B.N. Chau. 2008. Coordinated Regulation of Cell Cycle Transcripts by p53-Inducible microRNAs, miR-192 and miR-215. *Cancer Research*. 68:10105-10112

Git, A., H. Dvinge, M. Salmon-Divon, M. Osborne, C. Kutter, J. Hadfield, P. Bertone, and C. Caldas. 2010. Systematic comparison of microarray profiling, real-time PCR, and next-generation sequencing technologies for measuring differential microRNA expression. *RNA*. 16:991–1006. doi:10.1261/rna.1947110.

Gray, H. 2010. Gray's Anatomy: With original illustrations by Henry Carter - Henry Gray - Google Books. G. Davidson, editor. Arcturus Publishing, Ltd., London.

Gregorieff, A., D. Pinto, H. Begthel, O. Destrée, M. Kielman, and H. Clevers. 2005. Expression pattern of Wnt signaling components in the adult intestine. *YGAST*. 129:626–638. doi:10.1016/j.gastro.2005.06.007.

Gregory, P.A., A.G. Bert, E.L. Paterson, S.C. Barry, A. Tsykin, G. Farshid, M.A. Vadas, Y. Khew-Goodall, and G.J. Goodall. 2008. The miR-200 family and miR-205 regulate epithelial to mesenchymal transition by targeting ZEB1 and SIP1. *Nature cell Biology*. 10:593–601. doi:10.1038/ncb1722.

Griffiths-Jones, S. 2004. The microRNA Registry. *Nucleic Acids Research*. 32:109D–111. doi:10.1093/nar/gkh023.

Grosswendt, S., A. Filipchyk, M. Manzano, F. Klironomos, M. Schilling, M. Herzog, E. Gottwein, and N. Rajewsky. 2014. Unambiguous Identification of miRNA:Target Site Interactions by Different Types of Ligation Reactions. *Molecular Cell*. 54:1042–1054. doi:10.1016/j.molcel.2014.03.049.

Gu, Z., D. Nicolae, H.H.-S. Lu, and W.-H. Li. 2002. Rapid divergence in expression between duplicate genes inferred from microarray data. *Trends Genet.* 18:609–613.

Guo, H., N.T. Ingolia, J.S. Weissman, and D.P. Bartel. 2010. Mammalian microRNAs predominantly act to decrease target mRNA levels. *Nature*. 466:835–840. doi:10.1038/nature09267.

Guo, R.-J., E. Huang, T. Ezaki, N. Patel, K. Sinclair, J. Wu, P. Klein, E.R. Suh, and J.P.

Lynch. 2004. Cdx1 inhibits human colon cancer cell proliferation by reducing beta-catenin/T-cell factor transcriptional activity. *J. Biol. Chem.* 279:36865–36875. doi:10.1074/jbc.M405213200.

Guo, R.-J., E.R. Suh, and J.P. Lynch. 2004. The role of Cdx proteins in intestinal development and cancer. *Cancer Biology & Therapy*. 3:593–601.

Gupta, P.B., C.M. Fillmore, G. Jiang, S.D. Shapira, K. Tao, C. Kuperwasser, and E.S. Lander. 2011. Stochastic state transitions give rise to phenotypic equilibrium in populations of cancer cells. *Cell*. 146:633–644. doi:10.1016/j.cell.2011.07.026.

Hardwick, J.C., L.L. Kodach, G.J. Offerhaus, and G.R. van den Brink. 2008. Bone morphogenetic protein signalling in colorectal cancer. *Nature Reviews Cancer*. 8:806–812. doi:10.1038/nrc2467.

He, L., J.M. Thomson, M.T. Hemann, E. Hernando-Monge, D. Mu, S. Goodson, S. Powers, C. Cordon-Cardo, S.W. Lowe, G.J. Hannon, and S.M. Hammond. 2005. A microRNA polycistron as a potential human oncogene. *Nature*. 435:828–833. doi:10.1038/nature03552.

He, L., X. He, S.W. Lowe, and G.J. Hannon. 2007. microRNAs join the p53 network--another piece in the tumour-suppression puzzle. *Nature Reviews Cancer*. 7:819–822. doi:10.1038/nrc2232.

Hermann, P.C., S.L. Huber, T. Herrler, A. Aicher, J.W. Ellwart, M. Guba, C.J. Bruns, and C. Heeschen. 2007. Distinct populations of cancer stem cells determine tumor growth and metastatic activity in human pancreatic cancer. *Cell Stem Cell*. 1:313–323. doi:10.1016/j.stem.2007.06.002.

Hermeking, H. 2009. The miR-34 family in cancer and apoptosis. *Cell Death and Differentiation*. 17:193–199. doi:10.1038/cdd.2009.56.

Hermeking, H. 2012. MicroRNAs in the p53 network: micromanagement of tumour suppression. *Nature Reviews Cancer*. 12:613–626. doi:10.1038/nrc3318.

Horwich, M.D., and P.D. Zamore. 2008. Design and delivery of antisense oligonucleotides to block microRNA function in cultured Drosophila and human cells. *Nat Protoc*. 3:1537–1549. doi:10.1038/nprot.2008.145.

Hryniuk, A., S. Grainger, J.G.A. Savory, and D. Lohnes. 2012. Cdx function is required for maintenance of intestinal identity in the adult. *Developmental Biology*. 363:426–437. doi:10.1016/j.ydbio.2012.01.010.

Hu, B., X. Ying, J. Wang, J. Piriyapongsa, I.K. Jordan, J. Sheng, F. Yu, P. Zhao, Y. Li, H. Wang, W.L. Ng, S. Hu, X. Wang, C. Wang, X. Zheng, W. Li, W.J. Curran, and Y. Wang. 2014. Identification of a Tumor Suppressive Human Specific MicroRNA within the FHIT Tumor Suppressor Gene. *Cancer Research*. doi:10.1158/0008-5472.CAN-13-3279.

Huang, E.H., M.J. Hynes, T. Zhang, C. Ginestier, G. Dontu, H. Appelman, J.Z. Fields, M.S. Wicha, and B.M. Boman. 2009. Aldehyde Dehydrogenase 1 Is a Marker for Normal and Malignant Human Colonic Stem Cells (SC) and Tracks SC Overpopulation during Colon Tumorigenesis. *Cancer Research*. 69:3382–3389. doi:10.1158/0008-5472.CAN-08-4418.

Huang, J.C., T. Babak, T.W. Corson, G. Chua, S. Khan, B.L. Gallie, T.R. Hughes, B.J. Blencowe, B.J. Frey, and Q.D. Morris. 2007. Using expression profiling data to identify human microRNA targets. *Nat Meth*. 4:1045–1049. doi:10.1038/nmeth1130.

Huarte, M., M. Guttman, D. Feldser, M. Garber, M.J. Koziol, D. Kenzelmann-Broz, A.M. Khalil, O. Zuk, I. Amit, M. Rabani, L.D. Attardi, A. Regev, E.S. Lander, T. Jacks, and J.L. Rinn. 2010. A large intergenic noncoding RNA induced by p53 mediates global gene repression in the p53 response. *Cell*. 142:409–419. doi:10.1016/j.cell.2010.06.040.

Humphries, A., and N.A. Wright. 2008. Colonic crypt organization and tumorigenesis. *Nature Reviews Cancer*. 8:415–424. doi:10.1038/nrc2392.

Hutvagner, G. 2001. A Cellular Function for the RNA-Interference Enzyme Dicer in the Maturation of the let-7 Small Temporal RNA. *Science*. 293:834–838. doi:10.1126/science.1062961.

Ilyas, M., I.P. Tomlinson, A. Rowan, M. Pignatelli, and W.F. Bodmer. 1997. Beta-catenin mutations in cell lines established from human colorectal cancers. *Proc. Natl. Acad. Sci. U.S.A.* 94:10330–10334.

Itzkovitz, S., A. Lyubimova, I.C. Blat, M. Maynard, J. van Es, J. Lees, T. Jacks, H. Clevers, and A. van Oudenaarden. 2011. Single-molecule transcript counting of stem-cell markers in the mouse intestine. *Nature Cell Biology*. 14:106–114. doi:10.1038/ncb2384.

Jacobs, B., W. De Roock, H. Piessevaux, R. Van Oirbeek, B. Biesmans, J. De Schutter, S. Fieuws, J. Vandesompele, M. Peeters, J.-L. Van Laethem, Y. Humblet, F. Pénault-Llorca, G. De Hertogh, P. Laurent-Puig, E. Van Cutsem, and S. Tejpar. 2009. Amphiregulin and epiregulin mRNA expression in primary tumors predicts outcome in metastatic colorectal cancer treated with cetuximab. *J. Clin. Oncol.* 27:5068–5074. doi:10.1200/JCO.2008.21.3744.

Jahid, S., J. Sun, R.A. Edwards, D. Dizon, N.C. Panarelli, J.W. Milsom, S.S. Sikandar, Z.H. Gumus, and S.M. Lipkin. 2012. miR-23a Promotes the Transition from Indolent to Invasive Colorectal Cancer. *Cancer Discovery*. 2:540–553. doi:10.1158/2159-8290.CD-11-0267.

Ji, H., D.W. Greening, T.W. Barnes, J.W. Lim, B.J. Tauro, A. Rai, R. Xu, C. Adda, S. Mathivanan, W. Zhao, Y. Xue, T. Xu, H.-J. Zhu, and R.J. Simpson. 2013. Proteome profiling of exosomes derived from human primary and metastatic colorectal cancer cells reveal differential expression of key metastatic factors and signal transduction

components. *Proteomics*. 13:1672–1686. doi:10.1002/pmic.201200562.

Jiang, L., F. Schlesinger, C.A. Davis, Y. Zhang, R. Li, M. Salit, T.R. Gingeras, and B. Oliver. 2011. Synthetic spike-in standards for RNA-seq experiments. *Genome Research*. 21:1543–1551. doi:10.1101/gr.121095.111.

Jiang, S., H.-W. Zhang, M.-H. Lu, X.-H. He, Y. Li, H. Gu, M.-F. Liu, and E.-D. Wang. 2010. MicroRNA-155 functions as an OncomiR in breast cancer by targeting the suppressor of cytokine signaling 1 gene. *Cancer Research*. 70:3119–3127. doi:10.1158/0008-5472.CAN-09-4250.

Johnston, M.D., C.M. Edwards, W.F. Bodmer, P.K. Maini, and S.J. Chapman. 2007. Mathematical modeling of cell population dynamics in the colonic crypt and in colorectal cancer. *Proceedings of the National Academy of Sciences*. 104:4008–4013. doi:10.1073/pnas.0611179104.

Jones, M., and A. Lal. 2012. MicroRNAs, wild-type and mutant p53: more questions than answers. *RNA Biol*. 9:781–791.

Juan, L.J., W.J. Shia, M.H. Chen, W.M. Yang, E. Seto, Y.S. Lin, and C.W. Wu. 2000. Histone deacetylases specifically down-regulate p53-dependent gene activation. *J. Biol. Chem.* 275:20436–20443. doi:10.1074/jbc.M000202200.

Kaenel, P., M. Antonijevic, S. Richter, S. Küchler, N. Sutter, C. Wotzkow, R. Strange, and A.-C. Andres. 2012. Deregulated ephrin-B2 signaling in mammary epithelial cells alters the stem cell compartment and interferes with the epithelial differentiation pathway. *Int. J. Oncol.* 40:357–369. doi:10.3892/ijo.2011.1238.

Kai, K., O. Nagano, E. Sugihara, Y. Arima, O. Sampetrean, T. Ishimoto, M. Nakanishi, N.T. Ueno, H. Iwase, and H. Saya. 2009. Maintenance of HCT116 colon cancer cell line conforms to a stochastic model but not a cancer stem cell model. *Cancer Science*. 100:2275–2282. doi:10.1111/j.1349-7006.2009.01318.x.

Kang, J.M., B.H. Lee, N. Kim, H.S. Lee, H.E. Lee, J.H. Park, J.S. Kim, H.C. Jung, and I.S. Song. 2011. CDX1 and CDX2 Expression in Intestinal Metaplasia, Dysplasia and Gastric Cancer. *J Korean Med Sci*. 26:647–653. doi:10.3346/jkms.2011.26.5.647.

Karaayvaz, M., T. Pal, B. Song, C. Zhang, P. Georgakopoulos, S. Mehmood, S. Burke, K. Shroyer, and J. Ju. 2011. Prognostic Significance of miR-215 in Colon Cancer. *CLCC*. 10:340–347. doi:10.1016/j.clcc.2011.06.002.

Karan, D., S.-J. Chen, S.L. Johansson, A.P. Singh, V.M. Paralkar, M.-F. Lin, and S.K. Batra. 2003. Dysregulated expression of MIC-1/PDF in human prostate tumor cells. *Biochemical and Biophysical Research Communications*. 305:598–604.

Karolchik, D., G.P. Barber, J. Casper, H. Clawson, M.S. Cline, M. Diekhans, T.R. Dreszer, P.A. Fujita, L. Guruvadoo, M. Haeussler, R.A. Harte, S. Heitner, A.S. Hinrichs, K. Learned, B.T. Lee, C.H. Li, B.J. Raney, B. Rhead, K.R. Rosenbloom,

C.A. Sloan, M.L. Speir, A.S. Zweig, D. Haussler, R.M. Kuhn, and W.J. Kent. 2014. The UCSC Genome Browser database: 2014 update. *Nucleic Acids Research*. 42:D764–70. doi:10.1093/nar/gkt1168.

Karpala, A.J., T.J. Doran, and A.G.D. Bean. 2005. Immune responses to dsRNA: implications for gene silencing technologies. *Immunol. Cell Biol.* 83:211–216. doi:10.1111/j.1440-1711.2005.01331.x.

Kasinski, A.L., and F.J. Slack. 2011. MicroRNAs en route to the clinic: progress in validating and targeting microRNAs for cancer therapy. *Nature Reviews Cancer*. 11:849–864. doi:10.1038/nrc3166.

Kelly, J.A., M.S. Lucia, and J.R. Lambert. 2009. p53 controls prostate-derived factor/macrophage inhibitory cytokine/NSAID-activated gene expression in response to cell density, DNA damage and hypoxia through diverse mechanisms. *Cancer Letters*. 277:38–47. doi:10.1016/j.canlet.2008.11.013.

Kertesz, M., N. Iovino, U. Unnerstall, U. Gaul, and E. Segal. 2007. The role of site accessibility in microRNA target recognition. *Nature Genetics*. 39:1278–1284. doi:10.1038/ng2135.

Khvorova, A., A. Reynolds, and S.D. Jayasena. 2003. Functional siRNAs and miRNAs exhibit strand bias. *Cell*. 115:209–216.

Kim, H., J. Jen, B. Vogelstein, and S.R. Hamilton. 1994. Clinical and pathological characteristics of sporadic colorectal carcinomas with DNA replication errors in microsatellite sequences. *AJPA*. 145:148–156.

Kim, J.H., S.Y. Yoon, C.-N. Kim, J.H. Joo, S.K. Moon, I.S. Choe, Y.-K. Choe, and J.W. Kim. 2004. The Bmi-1 oncoprotein is overexpressed in human colorectal cancer and correlates with the reduced p16INK4a/p14ARF proteins. *Cancer Letters*. 203:217–224. doi:10.1016/j.canlet.2003.07.009.

Kim, K.-A., M. Kakitani, J. Zhao, T. Oshima, T. Tang, M. Binnerts, Y. Liu, B. Boyle, E. Park, P. Emtage, W.D. Funk, and K. Tomizuka. 2005. Mitogenic influence of human R-spondin1 on the intestinal epithelium. *Science*. 309:1256–1259. doi:10.1126/science.1112521.

Kim, T., A. Veronese, F. Pichiorri, T.J. Lee, Y.J. Jeon, S. Volinia, P. Pineau, A. Marchio, J. Palatini, S.S. Suh, H. Alder, C.G. Liu, A. Dejean, and C.M. Croce. 2011. p53 regulates epithelial-mesenchymal transition through microRNAs targeting ZEB1 and ZEB2. *Journal of Experimental Medicine*. 208:875–883. doi:10.1084/jem.20110235.

Kim, V.N., J. Han, and M.C. Siomi. 2009. Biogenesis of small RNAs in animals. *Nat Rev Mol Cell Biol*. 10:126–139. doi:10.1038/nrm2632.

Kim, Y.-K., G. Wee, J. Park, J. Kim, D. Baek, J.-S. Kim, and V.N. Kim. 2013. TALEN-based knockout library for human microRNAs. *nature structural & Molecular*

Biology. 20:1458–1464. doi:10.1038/nsmb.2701.

Kimura, M. 1968. Evolutionary rate at the molecular level. *Nature*. 217:624–626.

Kleinman, H.K., and G.R. Martin. 2005. Matrigel: basement membrane matrix with biological activity. *Semin. Cancer Biol.* 15:378–386. doi:10.1016/j.semcancer.2005.05.004.

Kluiver, J., I. Slezak-Prochazka, K. Smigielska-Czepiel, N. Halsema, B.-J. Kroesen, and A. van den Berg. 2012a. Generation of miRNA sponge constructs. *Methods*. 58:113–117. doi:10.1016/j.ymeth.2012.07.019.

Kluiver, J., J.H. Gibcus, C. Hettinga, A. Adema, M.K.S. Richter, N. Halsema, I. Slezak-Prochazka, Y. Ding, B.-J. Kroesen, and A. van den Berg. 2012b. Rapid generation of microRNA sponges for microRNA inhibition. *PLoS ONE*. 7:e29275. doi:10.1371/journal.pone.0029275.

Knudson, A.G. 1971. Mutation and cancer: statistical study of retinoblastoma. *Proc. Natl. Acad. Sci. U.S.A.* 68:820–823.

Kong, W., L. He, E.J. Richards, S. Challa, C.-X. Xu, J. Permuth-Wey, J.M. Lancaster, D. Coppola, T.A. Sellers, J.Y. Djeu, and J.Q. Cheng. 2014. Upregulation of miRNA-155 promotes tumour angiogenesis by targeting VHL and is associated with poor prognosis and triple-negative breast cancer. *Oncogene*. 33:679–689. doi:10.1038/onc.2012.636.

Kong, W., L. He, M. Coppola, J. Guo, N.N. Esposito, D. Coppola, and J.Q. Cheng. 2010. MicroRNA-155 regulates cell survival, growth, and chemosensitivity by targeting FOXO3a in breast cancer. *Journal of Biological Chemistry*. 285:17869–17879. doi:10.1074/jbc.M110.101055.

Korpal, M., E.S. Lee, G. Hu, and Y. Kang. 2008. The miR-200 family inhibits epithelial-mesenchymal transition and cancer cell migration by direct targeting of E-cadherin transcriptional repressors ZEB1 and ZEB2. *J. Biol. Chem.* 283:14910–14914. doi:10.1074/jbc.C800074200.

Kozomara, A., and S. Griffiths-Jones. 2014. miRBase: annotating high confidence microRNAs using deep sequencing data. *Nucleic Acids Research*. 42:D68–73. doi:10.1093/nar/gkt1181.

Kreso, A., P. van Galen, N.M. Pedley, E. Lima-Fernandes, C. Frelin, T. Davis, L. Cao, R. Baiazitov, W. Du, N. Sydorenko, Y.-C. Moon, L. Gibson, Y. Wang, C. Leung, N.N. Iscove, C.H. Arrowsmith, E. Szentgyorgyi, S. Gallinger, J.E. Dick, and C.A. O'Brien. 2014. Self-renewal as a therapeutic target in human colorectal cancer. *Nature Medicine*. 20:29–36. doi:10.1038/nm.3418.

Krieg, A.J., E.B. Rankin, D. Chan, O. Razorenova, S. Fernandez, and A.J. Giaccia. 2010. Regulation of the histone demethylase JMJD1A by hypoxia-inducible factor 1 alpha

enhances hypoxic gene expression and tumor growth. *Molecular and Cellular Biology*. 30:344–353. doi:10.1128/MCB.00444-09.

Kumar, M.S., R.E. Pester, C.Y. Chen, K. Lane, C. Chin, J. Lu, D.G. Kirsch, T.R. Golub, and T. Jacks. 2009. Dicer1 functions as a haploinsufficient tumor suppressor. *Genes & Development*. 23:2700–2704. doi:10.1101/gad.1848209.

Ladewig, E., K. Okamura, A.S. Flynt, J.O. Westholm, and E.C. Lai. 2012. Discovery of hundreds of mirtrons in mouse and human small RNA data. *Genome Research*. 22:1634–1645. doi:10.1101/gr.133553.111.

Lee, R.C., R.L. Feinbaum, and V. Ambros. 1993. The C. elegans heterochronic gene lin-4 encodes small RNAs with antisense complementarity to lin-14. *Cell*. 75:843–854.

Lee, Y., M. Kim, J. Han, K.-H. Yeom, S. Lee, S.H. Baek, and V.N. Kim. 2004. MicroRNA genes are transcribed by RNA polymerase II. *The EMBO Journal*. 23:4051–4060. doi:10.1038/sj.emboj.7600385.

Leung, A.K.L., and P.A. Sharp. 2010. MicroRNA Functions in Stress Responses. *Molecular Cell*. 40:205–215. doi:10.1016/j.molcel.2010.09.027.

Li, D.-W., H.-M. Tang, J.-W. Fan, D.-W. Yan, C.-Z. Zhou, S.-X. Li, X.-L. Wang, and Z.-H. Peng. 2009. Expression level of Bmi-1 oncoprotein is associated with progression and prognosis in colon cancer. *J Cancer Res Clin Oncol*. 136:997–1006. doi:10.1007/s00432-009-0745-7.

Li, H., and R. Durbin. 2009. Fast and accurate short read alignment with Burrows-Wheeler transform. *Bioinformatics*. 25:1754–1760. doi:10.1093/bioinformatics/btp324.

Li, H., S. Dai, T. Zhen, H. Shi, F. Zhang, Y. Yang, L. Kang, Y. Liang, and A. Han. 2014a. Clinical and biological significance of miR-378a-3p and miR-378a-5p in colorectal cancer. *Eur. J. Cancer*. 50:1207–1221. doi:10.1016/j.ejca.2013.12.010.

Li, P.X., J. Wong, A. Ayed, D. Ngo, A.M. Brade, C. Arrowsmith, R.C. Austin, and H.J. Klamut. 2000. Placental transforming growth factor-beta is a downstream mediator of the growth arrest and apoptotic response of tumor cells to DNA damage and p53 overexpression. *J. Biol. Chem.* 275:20127–20135. doi:10.1074/jbc.M909580199.

Li, W.-H., J. Yang, and X. Gu. 2005. Expression divergence between duplicate genes. *Trends Genet.* 21:602–607. doi:10.1016/j.tig.2005.08.006.

Li, X.L., T. Hara, Y. Choi, M. Subramanian, P. Francis, S. Bilke, R.L. Walker, M. Pineda, Y. Zhu, Y. Yang, J. Luo, L.M. Wakefield, T. Brabletz, B.H. Park, S. Sharma, D. Chowdhury, P.S. Meltzer, and A. Lal. 2014b. A p21-ZEB1 complex inhibits epithelial-mesenchymal transition through the microRNA 183-96-182 cluster. *Molecular and Cellular Biology*. 34:533–550. doi:10.1128/MCB.01043-13.

Liaw, H.-H., C.-C. Lin, H.-F. Juan, and H.-C. Huang. 2013. Differential microRNA regulation correlates with alternative polyadenylation pattern between breast cancer and normal cells. *PLoS ONE*. 8:e56958. doi:10.1371/journal.pone.0056958.

Lim, J.H., J.-W. Park, D.S. Min, J.-S. Chang, Y.H. Lee, Y.B. Park, K.S. Choi, and T.K. Kwon. 2007. NAG-1 up-regulation mediated by EGR-1 and p53 is critical for quercetin-induced apoptosis in HCT116 colon carcinoma cells. *Apoptosis*. 12:411–421. doi:10.1007/s10495-006-0576-9.

Linsen, S.E.V., E. de Wit, G. Janssens, S. Heater, L. Chapman, R.K. Parkin, B. Fritz, S.K. Wyman, E. de Bruijn, E.E. Voest, S. Kuersten, M. Tewari, and E. Cuppen. 2009. Limitations and possibilities of small RNA digital gene expression profiling. *Nat Meth*. 6:474–476. doi:10.1038/nmeth0709-474.

Liu, C., K. Kelnar, B. Liu, X. Chen, T. Calhoun-Davis, H. Li, L. Patrawala, H. Yan, C. Jeter, S. Honorio, J.F. Wiggins, A.G. Bader, R. Fagin, D. Brown, and D.G. Tang. 2011. The microRNA miR-34a inhibits prostate cancer stem cells and metastasis by directly repressing CD44. *Nature Medicine*. 17:211–215. doi:10.1038/nm.2284.

Loewer, S., M.N. Cabili, M. Guttman, Y.-H. Loh, K. Thomas, I.H. Park, M. Garber, M. Curran, T. Onder, S. Agarwal, P.D. Manos, S. Datta, E.S. Lander, T.M. Schlaeger, G.Q. Daley, and J.L. Rinn. 2010. Large intergenic non-coding RNA-RoR modulates reprogramming of human induced pluripotent stem cells. *Nature Genetics*. 42:1113–1117. doi:10.1038/ng.710.

Lopez-Garcia, C., A.M. Klein, B.D. Simons, and D.J. Winton. 2010. Intestinal Stem Cell Replacement Follows a Pattern of Neutral Drift. *Science*. 330:822–825. doi:10.1126/science.1196236.

Lorentz, O., I. Duluc, A. De Arcangelis, P. Simon-Assmann, M. Kedinger, and J.-N. Freund. 1997. Key role of the Cdx2 homeobox gene in extracellular matrix–mediated intestinal cell differentiation. *The Journal of Cell Biology*. 139:1553–1565.

Lorenz, R., S.H. Bernhart, C. Höner Zu Siederdissen, H. Tafer, C. Flamm, P.F. Stadler, and I.L. Hofacker. 2011. ViennaRNA Package 2.0. *Algorithms Mol Biol*. 6:26. doi:10.1186/1748-7188-6-26.

Lu, J., G. Getz, E.A. Miska, E. Alvarez-Saavedra, J. Lamb, D. Peck, A. Sweet-Cordero, B.L. Ebert, R.H. Mak, A.A. Ferrando, J.R. Downing, T. Jacks, H.R. Horvitz, and T.R. Golub. 2005. MicroRNA expression profiles classify human cancers. *Nature cell Biology*. 435:834–838. doi:10.1038/nature03702.

Lujambio, A., and S.W. Lowe. 2012. The microcosmos of cancer. *Nature*. 482:347–355. doi:10.1038/nature10888.

Luo, D., and W.M. Saltzman. 2000. Synthetic DNA delivery systems. *Nature Biotechnology*. 18:33–37. doi:10.1038/71889.

Mangan, J.K., and N.A. Speck. 2011. RUNX1 mutations in clonal myeloid disorders: from conventional cytogenetics to next generation sequencing, a story 40 years in the making. *Crit Rev Oncog*. 16:77–91.

Marusyk, A., V. Almendro, and K. Polyak. 2012. Intra-tumour heterogeneity: a looking glass for cancer? *Nature Publishing Group*. 12:323–334. doi:10.1038/nrc3261.

Mayr, C., and D.P. Bartel. 2009. Widespread shortening of 3'UTRs by alternative cleavage and polyadenylation activates oncogenes in cancer cells. *Cell*. 138:673–684. doi:10.1016/j.cell.2009.06.016.

McKenzie, L., S. King, L. Marcar, S. Nicol, S.S. Dias, K. Schumm, P. Robertson, J.-C. Bourdon, N. Perkins, F. Fuller-Pace, and D.W. Meek. 2010. p53-dependent repression of polo-like kinase-1 (PLK1). *Cell Cycle*. 9:4200–4212.

Medema, J.P., and L. Vermeulen. 2011. Microenvironmental regulation of stem cells in intestinal homeostasis and cancer. *Nature*. 474:318–326. doi:10.1038/nature10212.

Meijer, H.A., Y.W. Kong, W.T. Lu, A. Wilczynska, R.V. Spriggs, S.W. Robinson, J.D. Godfrey, A.E. Willis, and M. Bushell. 2013. Translational repression and eIF4A2 activity are critical for microRNA-mediated gene regulation. *Science*. 340:82–85. doi:10.1126/science.1231197.

Menendez, D., A. Inga, and M.A. Resnick. 2009. The expanding universe of p53 targets. *Nature Reviews Cancer*. 1–14. doi:10.1038/nrc2730.

Merlos-Suárez, A., F.M. Barriga, P. Jung, M. Iglesias, M.V. Céspedes, D. Rossell, M. Sevillano, X. Hernando-Momblona, V. da Silva-Diz, P. Muñoz, H. Clevers, E. Sancho, R. Mangues, and E. Batlle. 2011. The Intestinal Stem Cell Signature Identifies Colorectal Cancer Stem Cells and Predicts Disease Relapse. *Stem Cell*. 8:511–524. doi:10.1016/j.stem.2011.02.020.

Mestdagh, P., E. Fredlund, F. Pattyn, J.H. Schulte, D. Muth, J. Vermeulen, C. Kumps, S. Schlierf, K. De Preter, N. Van Roy, R. Noguera, G. Laureys, A. Schramm, A. Eggert, F. Westermann, F. Speleman, and J. Vandesompele. 2010. MYCN/c-MYC-induced microRNAs repress coding gene networks associated with poor outcome in MYCN/c-MYC-activated tumors. *Oncogene*. 29:1394–1404. doi:10.1038/onc.2009.429.

Meyer, B.I., and P. Gruss. 1993. Mouse Cdx-1 expression during gastrulation. *Development*. 117:191–203.

Mimeault, M., and S.K. Batra. 2010. Divergent molecular mechanisms underlying the pleiotropic functions of macrophage inhibitory cytokine-1 in cancer. *J. Cell. Physiol.* 224:626–635. doi:10.1002/jcp.22196.

Miranda, K.C., T. Huynh, Y. Tay, Y.-S. Ang, W.-L. Tam, A.M. Thomson, B. Lim, and I. Rigoutsos. 2006. A pattern-based method for the identification of MicroRNA binding

sites and their corresponding heteroduplexes. *Cell*. 126:1203–1217. doi:10.1016/j.cell.2006.07.031.

Monteys, A.M., R.M. Spengler, J. Wan, L. Tecedor, K.A. Lennox, Y. Xing, and B.L. Davidson. 2010. Structure and activity of putative intronic miRNA promoters. *RNA*. 16:495–505. doi:10.1261/rna.1731910.

Montgomery, R.K., D.L. Carlone, C.A. Richmond, L. Farilla, M.E.G. Kranendonk, D.E. Henderson, N.Y. Baffour-Awuah, D.M. Ambruzs, L.K. Fogli, S. Algra, and D.T. Breault. 2011. Mouse telomerase reverse transcriptase (mTert) expression marks slowly cycling intestinal stem cells. *Proc. Natl. Acad. Sci. U.S.A.* 108:179–184. doi:10.1073/pnas.1013004108.

Mu, P., Y.-C. Han, D. Betel, E. Yao, M. Squatrito, P. Ogrodowski, E. de Stanchina, A. D'Andrea, C. Sander, and A. Ventura. 2009. Genetic dissection of the miR-17~92 cluster of microRNAs in Myc-induced B-cell lymphomas. *Genes & Development*. 23:2806–2811. doi:10.1101/gad.1872909.

Muramatsu, F., H. Kidoya, H. Naito, S. Sakimoto, and N. Takakura. 2013. microRNA-125b inhibits tube formation of blood vessels through translational suppression of VE-cadherin. *Oncogene*. 32:414–421. doi:10.1038/onc.2012.68.

Murphy, M., J. Ahn, K.K. Walker, W.H. Hoffman, R.M. Evans, A.J. Levine, and D.L. George. 1999. Transcriptional repression by wild-type p53 utilizes histone deacetylases, mediated by interaction with mSin3a. *Genes & Development*. 13:2490–2501.

Mutoh, H., S. Sakurai, K. Satoh, H. Osawa, Y. Hakamata, T. Takeuchi, and K. Sugano. 2004. Cdx1 induced intestinal metaplasia in the transgenic mouse stomach: comparative study with Cdx2 transgenic mice. *Gut*. 53:1416–1423.

Navin, N., J. Kendall, J. Troge, P. Andrews, L. Rodgers, J. McIndoo, K. Cook, A. Stepansky, D. Levy, D. Esposito, L. Muthuswamy, A. Krasnitz, W.R. McCombie, J. Hicks, and M. Wigler. 2011. Tumour evolution inferred by single-cell sequencing. *Nature*. 472:90–94. doi:10.1038/nature09807.

Novelli, M.R., A. Cossu, O. Dahmane, Q. Alberto, S. Lakhani, R. Poulsom, P. Sasieni, P. Carta, M. Contini, A. Pasca, G. Palmieri, W. Bodmer, F. Tanda, and N. Wright. 2003. X-inactivation patch size in human female tissue confounds the assessment of tumor clonality. *Proceedings of the National Academy of Sciences*. 100:3311–3314.

Novelli, M.R., J.A. Williamson, I.P. Tomlinson, G. Elia, S.V. Hodgson, I.C. Talbot, W.F. Bodmer, and N.A. Wright. 1996. Polyclonal origin of colonic adenomas in an XO/XY patient with FAP. *Science*. 272:1187–1190.

Nowell, P.C. 1976. The clonal evolution of tumor cell populations. *Science*. 194:23–28.

O'Loghlen, A., A.M. Muñoz-Cabello, A. Gaspar-Maia, H.-A. Wu, A. Banito, N.

Kunowska, T. Racek, H.N. Pemberton, P. Beolchi, F. Lavial, O. Masui, M. Vermeulen, T. Carroll, J. Graumann, E. Heard, N. Dillon, V. Azuara, A.P. Snijders, G. Peters, E. Bernstein, and J. Gil. 2012. MicroRNA regulation of Cbx7 mediates a switch of Polycomb orthologs during ESC differentiation. *Cell Stem Cell*. 10:33–46. doi:10.1016/j.stem.2011.12.004.

Ogurtsov, A.Y., S.A. Shabalina, A.S. Kondrashov, and M.A. Roytberg. 2006. Analysis of internal loops within the RNA secondary structure in almost quadratic time. *Bioinformatics*. 22:1317–1324. doi:10.1093/bioinformatics/btl083.

Okada, N., C.-P. Lin, M.C. Ribeiro, A. Biton, G. Lai, X. He, P. Bu, H. Vogel, D.M. Jablons, A.C. Keller, J.E. Wilkinson, B. He, T.P. Speed, and L. He. 2014. A positive feedback between p53 and miR-34 miRNAs mediates tumor suppression. *Genes & Development*. 28:438–450. doi:10.1101/gad.233585.113.

Ootani, A., X. Li, E. Sangiorgi, Q.T. Ho, H. Ueno, S. Toda, H. Sugihara, K. Fujimoto, I.L. Weissman, M.R. Capecchi, and C.J. Kuo. 2009. Sustained in vitro intestinal epithelial culture within a Wnt-dependent stem cell niche. *Nature Medicine*. 15:701–706. doi:10.1038/nm.1951.

Osorio, K.M., S.E. Lee, D.J. McDermitt, S.K. Waghmare, Y.V. Zhang, H.N. Woo, and T. Tumbar. 2008. Runx1 modulates developmental, but not injury-driven, hair follicle stem cell activation. *Development*. 135:1059–1068. doi:10.1242/dev.012799.

Paranjape, T., H. Heneghan, R. Lindner, F.K. Keane, A. Hoffman, A. Hollestelle, J. Dorairaj, K. Geyda, C. Pelletier, S. Nallur, J.W. Martens, M.J. Hooning, M. Kerin, D. Zelterman, Y. Zhu, D. Tuck, L. Harris, N. Miller, F. Slack, and J. Weidhaas. 2011. A 3'-untranslated region KRAS variant and triple-negative breast cancer: a case-control and genetic analysis. *Lancet Oncol.* 12:377–386. doi:10.1016/S1470-2045(11)70044-4.

Park, C.Y., Y.S. Choi, and M.T. McManus. 2010. Analysis of microRNA knockouts in mice. *Human Molecular Genetics*. 19:R169–75. doi:10.1093/hmg/ddq367.

Park, M.J., H.Y. Kim, K. Kim, and J. Cheong. 2009a. Homeodomain transcription factor CDX1 is required for the transcriptional induction of PPARγ in intestinal cell differentiation. *FEBS Letters*. 583:29–35. doi:10.1016/j.febslet.2008.11.030.

Park, S.-M., A.B. Gaur, E. Lengyel, and M.E. Peter. 2008. The miR-200 family determines the epithelial phenotype of cancer cells by targeting the E-cadherin repressors ZEB1 and ZEB2. *Genes & Development*. 22:894–907. doi:10.1101/gad.1640608.

Park, S.-Y., J.H. Lee, M. Ha, J.-W. Nam, and V.N. Kim. 2009b. miR-29 miRNAs activate p53 by targeting p85 alpha and CDC42. *Nature Structural & Molecular Biology*. 16:23–29. doi:10.1038/nsmb.1533.

Pasquinelli, A.E., B.J. Reinhart, F. Slack, M.Q. Martindale, M.I. Kuroda, B. Maller, D.C.

Hayward, E.E. Ball, B. Degnan, P. Müller, J. Spring, A. Srinivasan, M. Fishman, J. Finnerty, J. Corbo, M. Levine, P. Leahy, E. Davidson, and G. Ruvkun. 2000. Conservation of the sequence and temporal expression of let-7 heterochronic regulatory RNA. *Nature*. 408:86–89. doi:10.1038/35040556.

Peltomäki, P. 2001. Deficient DNA mismatch repair: a common etiologic factor for colon cancer. *Human Molecular Genetics*. 10:735–740.

Perdomo, C., J.D. Campbell, J. Gerrein, C.S. Tellez, C.B. Garrison, T.C. Walser, E. Drizik, H. Si, A.C. Gower, J. Vick, C. Anderlind, G.R. Jackson, C. Mankus, F. Schembri, C. O'Hara, B.N. Gomperts, S.M. Dubinett, P. Hayden, S.A. Belinsky, M.E. Lenburg, and A. Spira. 2013. MicroRNA 4423 is a primate-specific regulator of airway epithelial cell differentiation and lung carcinogenesis. *Proc. Natl. Acad. Sci. U.S.A.* 110:18946–18951. doi:10.1073/pnas.1220319110.

Persson, H., A. Kvist, N. Rego, J. Staaf, J. Vallon-Christersson, L. Luts, N. Loman, G. Jonsson, H. Naya, M. Hoglund, A. Borg, and C. Rovira. 2011. Identification of new microRNAs in paired normal and tumor breast tissue suggests a dual role for the ERBB2/Her2 gene. *Cancer Research*. 71:78–86. doi:10.1158/0008-5472.CAN-10-1869.

Pichiorri, F., S.-S. Suh, A. Rocci, L. De Luca, C. Taccioli, R. Santhanam, W. Zhou, D.M. Benson Jr, C. Hofmainster, H. Alder, M. Garofalo, G. Di Leva, S. Volinia, H.-J. Lin, D. Perrotti, M. Kuehl, R.I. Aqeilan, A. Palumbo, and C.M. Croce. 2010. Downregulation of p53-inducible microRNAs 192, 194, and 215 Impairs the p53/MDM2 Autoregulatory Loop in Multiple Myeloma Development. *Cancer Cell*. 18:367–381. doi:10.1016/j.ccr.2010.09.005.

Pierce, G.B., and W.C. Speers. 1988. Tumors as caricatures of the process of tissue renewal: prospects for therapy by directing differentiation. *Cancer Research*. 48:1996–2004.

Pilozzi, E., M.R. Onelli, V. Ziparo, P. Mercantini, and L. Ruco. 2004. CDX1 expression is reduced in colorectal carcinoma and is associated with promoter hypermethylation. *J. Pathol.* 204:289–295. doi:10.1002/path.1641.

Piriyapongsa, J., and I.K. Jordan. 2007. A family of human microRNA genes from miniature inverted-repeat transposable elements. *PLoS ONE*. 2:e203. doi:10.1371/journal.pone.0000203.

Ponder, B.A.J., G.H. Schmidt, M.M. Wilkinson, M.J. Wood, M. Monk, and A. Reid. 1985. Derivation of mouse intestinal crypts from single progenitor cells. *Nature*. 313:689–691. doi:10.1038/313689a0.

Powell, S.M., N. Zilz, Y. Beazer-Barclay, T.M. Bryan, S.R. Hamilton, S.N. Thibodeau, B. Vogelstein, and K.W. Kinzler. 1992. APC mutations occur early during colorectal tumorigenesis. *Nature*. 359:235–237. doi:10.1038/359235a0.

Psaila, B., and D. Lyden. 2009. The metastatic niche: adapting the foreign soil. *Nature Reviews Cancer*. 9:285–293. doi:10.1038/nrc2621.

Ratner, E., L. Lu, M. Boeke, R. Barnett, S. Nallur, L.J. Chin, C. Pelletier, R. Blitzblau, R. Tassi, T. Paranjape, P. Hui, A.K. Godwin, H. Yu, H. Risch, T. Rutherford, P. Schwartz, A. Santin, E. Matloff, D. Zelterman, F.J. Slack, and J.B. Weidhaas. 2010. A KRAS-variant in ovarian cancer acts as a genetic marker of cancer risk. *Cancer Research*. 70:6509–6515. doi:10.1158/0008-5472.CAN-10-0689.

Raver-Shapira, N., E. Marciano, E. Meiri, Y. Spector, N. Rosenfeld, N. Moskovits, Z. Bentwich, and M. Oren. 2007. Transcriptional Activation of miR-34a Contributes to p53-Mediated Apoptosis. *Molecular Cell*. 26:731–743. doi:10.1016/j.molcel.2007.05.017.

Rawat, V.P.S., S. Thoene, V.M. Naidu, N. Arseni, B. Heilmeier, K. Metzeler, K. Petropoulos, A. Deshpande, L. Quintanilla-Martinez, S.K. Bohlander, K. Spiekermann, W. Hiddemann, M. Feuring-Buske, and C. Buske. 2008. Overexpression of CDX2 perturbs HOX gene expression in murine progenitors depending on its N-terminal domain and is closely correlated with deregulated HOX gene expression in human acute myeloid leukemia. *Blood*. 111:309–319. doi:10.1182/blood-2007-04-085407.

Rearick, D., A. Prakash, A. McSweeny, S.S. Shepard, L. Fedorova, and A. Fedorov. 2011. Critical association of ncRNA with introns. *Nucleic Acids Research*. 39:2357–2366. doi:10.1093/nar/gkq1080.

Reinhart, B.J., F.J. Slack, M. Basson, A.E. Pasquinelli, J.C. Bettinger, A.E. Rougvie, H.R. Horvitz, and G. Ruvkun. 2000. The 21-nucleotide let-7 RNA regulates developmental timing in Caenorhabditis elegans. *Nature*. 403:901–906. doi:10.1038/35002607.

Riley, T., E. Sontag, P. Chen, and A. Levine. 2008. Transcriptional control of human p53-regulated genes. *Nat Rev Mol Cell Biol*. 9:402–412. doi:10.1038/nrm2395.

Ryan, B.M., A.I. Robles, and C.C. Harris. 2010. Genetic variation in microRNA networks: the implications for cancer research. *Nature Reviews Cancer*. 10:389–402. doi:10.1038/nrc2867.

Sachs, L. 1987. The molecular control of blood cell development. *Science*. 238:1374–1379.

Saegusa, M., M. Hashimura, T. Kuwata, M. Hamano, J. Watanabe, M. Kawaguchi, and I. Okayasu. 2008. Transcription factor Egr1 acts as an upstream regulator of beta-catenin signalling through up-regulation of TCF4 and p300 expression during trans-differentiation of endometrial carcinoma cells. *J. Pathol.* 216:521–532. doi:10.1002/path.2404.

Sakai, W., E.M. Swisher, B.Y. Karlan, M.K. Agarwal, J. Higgins, C. Friedman, E.

Villegas, C. Jacquemont, D.J. Farrugia, F.J. Couch, N. Urban, and T. Taniguchi. 2008. Secondary mutations as a mechanism of cisplatin resistance in BRCA2-mutated cancers. *Nature*. 451:1116–1120. doi:10.1038/nature06633.

Sangiorgi, E., and M.R. Capecchi. 2008. Bmi1 is expressed in vivo in intestinal stem cells. *Nature Genetics*. 40:915–920. doi:10.1038/ng.165.

Sarver, A.L., L. Li, and S. Subramanian. 2010. MicroRNA miR-183 functions as an oncogene by targeting the transcription factor EGR1 and promoting tumor cell migration. *Cancer Research*. 70:9570–9580. doi:10.1158/0008-5472.CAN-10-2074.

Sato, T., J.H. van Es, H.J. Snippert, D.E. Stange, R.G. Vries, M. van den Born, N. Barker, N.F. Shroyer, M. van de Wetering, and H. Clevers. 2011. Paneth cells constitute the niche for Lgr5 stem cells in intestinal crypts. *Nature*. 469:415–418. doi:10.1038/nature09637.

Sato, T., R.G. Vries, H.J. Snippert, M. van de Wetering, N. Barker, D.E. Stange, J.H. van Es, A. Abo, P. Kujala, P.J. Peters, and H. Clevers. 2009. Single Lgr5 stem cells build crypt-villus structures in vitro without a mesenchymal niche. *Nature*. 459:262–265. doi:10.1038/nature07935.

Savory, J.G.A., N. Pilon, S. Grainger, J.-R. Sylvestre, M. Béland, M. Houle, K. Oh, and D. Lohnes. 2009. Cdx1 and Cdx2 are functionally equivalent in vertebral patterning. *Developmental Biology*. 330:114–122. doi:10.1016/j.ydbio.2009.03.016.

Scheitz, C.J.F., T.S. Lee, D.J. McDermitt, and T. Tumbar. 2012. Defining a tissue stem cell-driven Runx1/Stat3 signalling axis in epithelial cancer. *The EMBO Journal*. 31(21):4124-39. doi:10.1038/emboj.2012.270.

Schug, J. 2008. Using TESS to predict transcription factor binding sites in DNA sequence. *Curr Protoc Bioinformatics*. Chapter 2:Unit 2.6. doi:10.1002/0471250953.bi0206s21.

Selbach, M., B. Schwanhäusser, N. Thierfelder, Z. Fang, R. Khanin, and N. Rajewsky. 2008. Widespread changes in protein synthesis induced by microRNAs. *Nature*. 455:58–63. doi:10.1038/nature07228.

Senapati, S., S. Rachagani, K. Chaudhary, S.L. Johansson, R.K. Singh, and S.K. Batra. 2010. Overexpression of macrophage inhibitory cytokine-1 induces metastasis of human prostate cancer cells through the FAK-RhoA signaling pathway. *Oncogene*. 29:1293–1302. doi:10.1038/onc.2009.420.

Senzer, N., J. Nemunaitis, D. Nemunaitis, C. Bedell, G. Edelman, M. Barve, R. Nunan, K.F. Pirollo, A. Rait, and E.H. Chang. 2013. Phase I study of a systemically delivered p53 nanoparticle in advanced solid tumors. *Mol. Ther.* 21:1096–1103. doi:10.1038/mt.2013.32.

Shah, N.P., B.J. Skaggs, S. Branford, T.P. Hughes, J.M. Nicoll, R.L. Paquette, and C.L.

Sawyers. 2007. Sequential ABL kinase inhibitor therapy selects for compound drug-resistant BCR-ABL mutations with altered oncogenic potency. *J. Clin. Invest.* 117:2562–2569. doi:10.1172/JCI30890.

Shim, M., and T.E. Eling. 2005. Protein kinase C-dependent regulation of NAG-1/placental bone morphogenic protein/MIC-1 expression in LNCaP prostate carcinoma cells. *J. Biol. Chem.* 280:18636–18642. doi:10.1074/jbc.M414613200.

Sikic, B.I. 2008. Natural and Acquired Resistance to Cancer Therapies. *In* The Molecular Basis of Cancer. J. Mendelsohn, P.M. Howley, M.A. Israel, J.W. Gray, and C.B. Thompson, editors. The Molecular Basis of Cancer, Philadelphia. 583–592.

Silberg, D.G., E.E. Furth, J.K. Taylor, T. Schuck, T. Chiou, and P.G. Traber. 1997. CDX1 protein expression in normal, metaplastic, and neoplastic human alimentary tract epithelium. *YGAST*. 113:478–486.

Slattery, M.L., A. Lundgreen, J.S. Herrick, B.J. Caan, J.D. Potter, and R.K. Wolff. 2011. Associations between genetic variation in RUNX1, RUNX2, RUNX3, MAPK1 and eIF4E and risk of colon and rectal cancer: additional support for a TGF- -signaling pathway. *Carcinogenesis*. 32:318–326. doi:10.1093/carcin/bgq245.

Slevin, M., and S. Payne. 2004. New treatments for colon cancer. *BMJ*. 329:124–126. doi:10.1136/bmj.329.7458.124.

Snippert, H.J., L.G. van der Flier, T. Sato, J.H. van Es, M. van den Born, C. Kroon-Veenboer, N. Barker, A.M. Klein, J. van Rheenen, B.D. Simons, and H. Clevers. 2010. Intestinal crypt homeostasis results from neutral competition between symmetrically dividing Lgr5 stem cells. *Cell*. 143:134–144. doi:10.1016/j.cell.2010.09.016.

Song, B., Y. Wang, M.A. Titmus, G. Botchkina, A. Formentini, M. Kornmann, and J. Ju. 2010. Molecular mechanism of chemoresistance by miR-215 in osteosarcoma and colon cancer cells. *Mol Cancer*. 9:96. doi:10.1186/1476-4598-9-96.

Spurgers, K.B., D.L. Gold, K.R. Coombes, N.L. Bohnenstiehl, B. Mullins, R.E. Meyn, C.J. Logothetis, and T.J. McDonnell. 2006. Identification of cell cycle regulatory genes as principal targets of p53-mediated transcriptional repression. *J. Biol. Chem.* 281:25134–25142. doi:10.1074/jbc.M513901200.

Staloch, L.J., J.K. Divine, J.T. Witten, and T.C. Simon. 2005. C/EBP and Cdx family factors regulate liver fatty acid binding protein transgene expression in the small intestinal epithelium. *Biochim. Biophys. Acta*. 1731:168–178. doi:10.1016/j.bbaexp.2005.08.014.

Stamatakis, A., A.J. Aberer, C. Goll, S.A. Smith, S.A. Berger, and F. Izquierdo-Carrasco. 2012. RAxML-Light: a tool for computing terabyte phylogenies. *Bioinformatics*. 28:2064–2066. doi:10.1093/bioinformatics/bts309.

Stark, M.S., S. Tyagi, D.J. Nancarrow, G.M. Boyle, A.L. Cook, D.C. Whiteman, P.G. Parsons, C. Schmidt, R.A. Sturm, and N.K. Hayward. 2010. Characterization of the Melanoma miRNAome by Deep Sequencing. *PLoS ONE*. 5:e9685. doi:10.1371/journal.pone.0009685.

Subramanian, M., P. Francis, S. Bilke, X.L. Li, T. Hara, X. Lu, M.F. Jones, R.L. Walker, Y. Zhu, M. Pineda, C. Lee, L. Varanasi, Y. Yang, L.A. Martinez, J. Luo, S. Ambs, S. Sharma, L.M. Wakefield, P.S. Meltzer, and A. Lal. 2014. A mutant p53/let-7i-axis-regulated gene network drives cell migration, invasion and metastasis. *Oncogene*. doi:10.1038/onc.2014.46.

Subramanian, V., B.I. Meyer, and P. Gruss. 1995. Disruption of the murine homeobox gene Cdx1 affects axial skeletal identities by altering the mesodermal expression domains of Hox genes. *Cell*. 83:641–653.

Suh, E.R. 2002. DNA Methylation Down-regulates CDX1 Gene Expression in Colorectal Cancer Cell Lines. *Journal of Biological Chemistry*. 277:35795–35800. doi:10.1074/jbc.M205567200.

Sui, G., E.B. Affar, Y. Shi, C. Brignone, N.R. Wall, P. Yin, M. Donohoe, M.P. Luke, D. Calvo, S.R. Grossman, and Y. Shi. 2004. Yin Yang 1 is a negative regulator of p53. *Cell*. 117:859–872. doi:10.1016/j.cell.2004.06.004.

Tagawa, T., T. Haraguchi, H. Hiramatsu, K. Kobayashi, K. Sakurai, K.I. Inada, and H. Iba. 2012. Multiple microRNAs induced by Cdx1 suppress Cdx2 in human colorectal tumour cells. *Biochem. J.* 447:449–455. doi:10.1158/1078-0432.CCR-08-3257.

Takahashi, N., Y. Yamada, K. Furuta, Y. Honma, S. Iwasa, A. Takashima, K. Kato, T. Hamaguchi, and Y. Shimada. 2014. Serum levels of hepatocyte growth factor and epiregulin are associated with the prognosis on anti-EGFR antibody treatment in KRAS wild-type metastatic colorectal cancer. *British Journal of Cancer*. 110:2716–2727. doi:10.1038/bjc.2014.230.

Tam, W., and J.E. Dahlberg. 2006. miR-155/BIC as an oncogenic microRNA. *Genes Chromosomes Cancer*. 45:211–212. doi:10.1002/gcc.20282.

Tamura, K., D. Peterson, N. Peterson, G. Stecher, M. Nei, and S. Kumar. 2011. MEGA5: molecular evolutionary genetics analysis using maximum likelihood, evolutionary distance, and maximum parsimony methods. *Mol. Biol. Evol.* 28:2731–2739. doi:10.1093/molbev/msr121.

Tan, M., Y. Wang, K. Guan, and Y. Sun. 2000. PTGF-beta, a type beta transforming growth factor (TGF-beta) superfamily member, is a p53 target gene that inhibits tumor cell growth via TGF-beta signaling pathway. *Proc. Natl. Acad. Sci. U.S.A.* 97:109–114.

Tateishi, K., M. Ohta, F. Kanai, B. Guleng, Y. Tanaka, Y. Asaoka, M. Tada, M. Seto, A. Jazag, L. Lianjie, M. Okamoto, H. Isayama, M. Tada, H. Yoshida, T. Kawabe, and

M. Omata. 2006. Dysregulated expression of stem cell factor Bmi1 in precancerous lesions of the gastrointestinal tract. *Clin. Cancer Res.* 12:6960–6966. doi:10.1158/1078-0432.CCR-06-0449.

Thomson, D.W., C.P. Bracken, and G.J. Goodall. 2011. Experimental strategies for microRNA target identification. *Nucleic Acids Research*. 39:6845–6853. doi:10.1093/nar/gkr330.

Thomson, D.W., C.P. Bracken, J.M. Szubert, and G.J. Goodall. 2013. On measuring miRNAs after transient transfection of mimics or antisense inhibitors. *PLoS ONE*. 8:e55214. doi:10.1371/journal.pone.0055214.

Tian, H., B. Biehs, S. Warming, K.G. Leong, L. Rangell, O.D. Klein, and F.J. de Sauvage. 2011. A reserve stem cell population in small intestine renders Lgr5-positive cells dispensable. *Nature*. 478:255–259. doi:10.1038/nature10408.

Tierney, E.G., K. McSorley, C.L. Hastings, S.-A. Cryan, T. O'Brien, M.J. Murphy, F.P. Barry, F.J. O'Brien, and G.P. Duffy. 2013. High levels of ephrinB2 over-expression increases the osteogenic differentiation of human mesenchymal stem cells and promotes enhanced cell mediated mineralisation in a polyethyleneimine-ephrinB2 gene-activated matrix. *J Control Release*. 165:173–182. doi:10.1016/j.jconrel.2012.11.013.

Till, J.E., and E.A. McCulloch. 1961. A direct measurement of the radiation sensitivity of normal mouse bone marrow cells. *Radiat. Res.* 14:213–222.

Tomlinson, I.P., and W.F. Bodmer. 1995. Failure of programmed cell death and differentiation as causes of tumors: some simple mathematical models. *Proc. Natl. Acad. Sci. U.S.A.* 92:11130–11134.

Tomlinson, I.P., M.R. Novelli, and W.F. Bodmer. 1996. The mutation rate and cancer. *Proc. Natl. Acad. Sci. U.S.A.* 93:14800–14803.

Topley, G.I., R. Okuyama, J.G. Gonzales, C. Conti, and G.P. Dotto. 1999. p21(WAF1/Cip1) functions as a suppressor of malignant skin tumor formation and a determinant of keratinocyte stem-cell potential. *Proc. Natl. Acad. Sci. U.S.A.* 96:9089–9094.

Trang, P., J.F. Wiggins, C.L. Daige, C. Cho, M. Omotola, D. Brown, J.B. Weidhaas, A.G. Bader, and F.J. Slack. 2011. Systemic delivery of tumor suppressor microRNA mimics using a neutral lipid emulsion inhibits lung tumors in mice. *Mol. Ther.* 19:1116–1122. doi:10.1038/mt.2011.48.

van de Wetering, M., E. Sancho, C. Verweij, and W. De Lau. 2002. The β-Catenin/TCF-4 Complex Imposes a Crypt Progenitor Phenotype on Colorectal Cancer Cells. *Cell*. 111:241-250

van den Akker, E., S. Forlani, K. Chawengsaksophak, W. de Graaff, F. Beck, B.I. Meyer,

and J. Deschamps. 2002. Cdx1 and Cdx2 have overlapping functions in anteroposterior patterning and posterior axis elongation. *Development*. 129:2181–2193.

van Lohuizen, M., J.J.L. Jacobs, P. Keblusek, E. Robanus-Maandag, P. Kristel, M. Lingbeek, P.M. Nederlof, T. van Welsem, M.J. van de Vijver, E.Y. Koh, and G.Q. Daley. 2000. Senescence bypass screen identifies TBX2, which represses Cdkn2a (p19ARF) and is amplified in a subset of human breast cancers. *Nature Genetics*. 26:291–299. doi:10.1038/81583.

Ventura, A., A.G. Young, M.M. Winslow, L. Lintault, A. Meissner, S.J. Erkeland, J. Newman, R.T. Bronson, D. Crowley, J.R. Stone, R. Jaenisch, P.A. Sharp, and T. Jacks. 2008. Targeted Deletion Reveals Essential and Overlapping Functions of the miR-17~92 Family of miRNA Clusters. *Cell*. 132:875–886. doi:10.1016/j.cell.2008.02.019.

Vermeulen, L., F. De Sousa E Melo, M. van der Heijden, K. Cameron, J.H. de Jong, T. Borovski, J.B. Tuynman, M. Todaro, C. Merz, H. Rodermond, M.R. Sprick, K. Kemper, D.J. Richel, G. Stassi, and J.P. Medema. 2010. Wnt activity defines colon cancer stem cells and is regulated by the microenvironment. *Nature Cell Biology*. 12:468–476. doi:10.1038/ncb2048.

Verzi, M.P., H. Shin, L.L. Ho, X.S. Liu, and R.A. Shivdasani. 2011. Essential and Redundant Functions of Caudal Family Proteins in Activating Adult Intestinal Genes. *Molecular and Cellular Biology*. 31:2026–2039. doi:10.1128/MCB.01250-10.

Visvader, J.E. 2011. Cells of origin in cancer. *Nature*. 469:314–322. doi:10.1038/nature09781.

Wade, M., Y.-C. Li, and G.M. Wahl. 2013. MDM2, MDMX and p53 in oncogenesis and cancer therapy. *Nature Reviews Cancer*. 13:83–96. doi:10.1038/nrc3430.

Wang, E.T., R. Sandberg, S. Luo, I. Khrebtukova, L. Zhang, C. Mayr, S.F. Kingsmore, G.P. Schroth, and C.B. Burge. 2008. Alternative isoform regulation in human tissue transcriptomes. *Nature*. 456:470–476. doi:10.1038/nature07509.

Westholm, J.O., and E.C. Lai. 2011. Mirtrons: microRNA biogenesis via splicing. *Biochimie*. 93:1897–1904. doi:10.1016/j.biochi.2011.06.017.

White, N.M.A., H.W.Z. Khella, J. Grigull, S. Adzovic, Y.M. Youssef, R.J. Honey, R. Stewart, K.T. Pace, G.A. Bjarnason, M.A.S. Jewett, A.J. Evans, M. Gabril, and G.M. Yousef. 2011. miRNA profiling in metastatic renal cell carcinoma reveals a tumour-suppressor effect for miR-215. *British Journal of Cancer*. 105:1741–1749. doi:10.1038/bjc.2011.401.

Wightman, B., I. Ha, and G. Ruvkun. 1993. Posttranscriptional regulation of the heterochronic gene lin-14 by lin-4 mediates temporal pattern formation in C. elegans. *Cell*. 75:855–862.

Wijnhoven, B.P.L., D.J. Hussey, D.I. Watson, A. Tsykin, C.M. Smith, and M.Z. Michael. 2010. MicroRNA profiling of Barrett's oesophagus and oesophageal adenocarcinoma. *Br J Surg*. 97:853–861. doi:10.1002/bjs.7000.

Wilding, J.L., and W.F. Bodmer. 2014. Cancer cell lines for drug discovery and development. *Cancer Research*. 74:2377–2384. doi:10.1158/0008-5472.CAN-13-2971.

Wong, N., J.L. Wilding, S. Bartlett, Y. Liu, B.F. Warren, N. Maynard, J. Piris, R. Marshall, and W.F. Bodmer. 2005. CDX1 is an important molecular mediator of Barrett's metaplasia.

Wong, N., M.P. Britton, G.S. Choi, T.K. Stanton, D.C. Bicknell, J.L. Wilding, and W.F. Bodmer. 2004. Loss of CDX1 expression in colorectal carcinoma: promoter methylation, mutation, and loss of heterozygosity analyses of 37 cell lines. *Proc. Natl. Acad. Sci. U.S.A.* 101:574–579.

Wu, M., N. Jolicoeur, Z. Li, L. Zhang, Y. Fortin, D. L'Abbe, Z. Yu, and S.-H. Shen. 2008. Genetic variations of microRNAs in human cancer and their effects on the expression of miRNAs. *Carcinogenesis*. 29:1710–1716. doi:10.1093/carcin/bgn073.

Xiao, J., H. Lin, X. Luo, X. Luo, and Z. Wang. 2011. miR-605 joins p53 network to form a p53:miR-605:Mdm2 positive feedback loop in response to stress. *The EMBO Journal*. 30:524–532. doi:10.1038/emboj.2010.347.

Xue, H., B. Lü, J. Zhang, M. Wu, Q. Huang, Q. Wu, H. Sheng, D. Wu, J. Hu, and M. Lai. 2010. Identification of serum biomarkers for colorectal cancer metastasis using a differential secretome approach. *J. Proteome Res.* 9:545–555. doi:10.1021/pr9008817.

Yamakuchi, M., M. Ferlito, and C.J. Lowenstein. 2008. miR-34a repression of SIRT1 regulates apoptosis. *Proceedings of the National Academy of Sciences*. 105:13421–13426. doi:10.1073/pnas.0801613105.

Yamamoto, H., Y.Q. Bai, and Y. Yuasa. 2003. Homeodomain protein CDX2 regulates goblet-specific MUC2 gene expression. *Biochemical and Biophysical Research Communications*. 300:813–818.

Yan, K.S., L.A. Chia, X. Li, A. Ootani, J. Su, J.Y. Lee, N. Su, Y. Luo, S.C. Heilshorn, M.R. Amieva, E. Sangiorgi, M.R. Capecchi, and C.J. Kuo. 2012. The intestinal stem cell markers Bmi1 and Lgr5 identify two functionally distinct populations. *Proc. Natl. Acad. Sci. U.S.A.* 109:466–471. doi:10.1073/pnas.1118857109.

Yang, H., Z. Filipovic, D. Brown, S.N. Breit, and L.T. Vassilev. 2003. Macrophage inhibitory cytokine-1: a novel biomarker for p53 pathway activation. *Mol. Cancer Ther.* 2:1023–1029.

Yeung, T.M., S.C. Gandhi, and W.F. Bodmer. 2011. Hypoxia and lineage specification of

cell line-derived colorectal cancer stem cells. *Proc. Natl. Acad. Sci. U.S.A.* 108:4382–4387. doi:10.1073/pnas.1014519107/-/DCSupplemental/pnas.201014519SI.pdf.

Yeung, T.M., S.C. Gandhi, J.L. Wilding, R. Muschel, and W.F. Bodmer. 2010. Cancer stem cells from colorectal cancer-derived cell lines. *Proc. Natl. Acad. Sci. U.S.A.* 107:3722–3727. doi:10.1073/pnas.0915135107.

Zeki, S.S., T.A. Graham, and N.A. Wright. 2011. Stem cells and their implications for colorectal cancer. *Nature Reviews Gastroenterology & Hepatology*. 8:90–100. doi:10.1038/nrgastro.2010.211.

Zhang, H., W. Li, F. Nan, F. Ren, H. Wang, Y. Xu, and F. Zhang. 2011. MicroRNA expression profile of colon cancer stem-like cells in HT29 adenocarcinoma cell line. *Biochemical and Biophysical Research Communications*. 404:273–278. doi:10.1016/j.bbrc.2010.11.106.

Zhou, B.-B.S., H. Zhang, M. Damelin, K.G. Geles, J.C. Grindley, and P.B. Dirks. 2009. Tumour-initiating cells: challenges and opportunities for anticancer drug discovery. *Nat Rev Drug Discov*. 8:806–823. doi:10.1038/nrd2137.

Zhou, Y., Y. Zhong, Y. Wang, X. Zhang, D.L. Batista, R. Gejman, P.J. Ansell, J. Zhao, C. Weng, and A. Klibanski. 2007. Activation of p53 by MEG3 Non-coding RNA. *Journal of Biological Chemistry*. 282:24731–24742. doi:10.1074/jbc.M702029200.

Ziebarth, J.D., A. Bhattacharya, and Y. Cui. 2012. Integrative analysis of somatic mutations altering microRNA targeting in cancer genomes. *PLoS ONE*. 7:e47137. doi:10.1371/journal.pone.0047137.

APPENDIX I

Small RNA Sequencing Data

APPENDIX I: SMALL RNA SEQUENCING DATA

miRNA ID	HCT116 -CDX1	HCT116- vector	LS174T- vector	LS174T- siCDX1
hsa-miR-378a-3p@chr5:149112430-149112450:+	1513.32	1428.33	1587.48	1343.55
hsa-miR-140-3p@chr16:69967045-69967065:+	1502.3	1423.91	1579.85	1334.98
hsa-miR-30e-5p@chr1:41220043-41220064:+	1498.44	1420.26	1583.59	1338.05
hsa-miR-26b-5p@chr2:219267380-219267400:+	1501.04	1408.59	1573.37	1334.16
hsa-miR-3074-5p@chr9:97848345-97848365:-	1501.47	1415.48	1569.18	1328.76
hsa-miR-146b-5p@chr10:104196277-104196298:+	1492.26	1402.10	1571.41	1331.06
hsa-miR-3545-5p@chr14:104583805-104583826:-	1494.72	1407.32	1557.85	1322.29
hsa-miR-200b-3p@chr1:1102540-1102561:+	1486.53	1401.49	1557.75	1313.86
hsa-miR-7-5p@chr15:89155087-89155109:+	1485.92	1399.59	1548.09	1313.56
hsa-miR-7-5p@chr19:4770712-4770734:+	1483.97	1398.96	1547.21	1313.33
hsa-miR-200a-3p@chr1:1103296-1103317:+	1474.29	1391.52	1569.44	1307.42
hsa-miR-21-5p@chr17:57918634-57918655:+	1470.92	1398.41	1554.9	1305.92
hsa-miR-23b-3p@chr9:97847547-97847567:+	1482.97	1379.60	1544.59	1306.12
hsa-miR-141-3p@chr12:7073318-7073339:+	1480.24	1387.17	1546.37	1285.50
hsa-miR-17-3p@chr13:92002909-92002930:+	1473.46	1390.11	1534.61	1299.24
hsa-miR-148b-3p@chr12:54731062-54731083:+	1461.97	1385.93	1539.48	1298.44
hsa-miR-92a-3p@chr13:92003615-92003636:+	1460.39	1383.69	1535.9	1297.22
hsa-miR-29a-3p@chr7:130561507-130561528:-	1455	1372.96	1522.01	1289.86
hsa-miR-30c-5p@chr1:41222972-41222994:+	1453	1366.06	1529.59	1287.92
hsa-let-7b-5p@chr22:46509571-46509592:+	1452.23	1370.93	1524.07	1287.93
hsa-miR-210@chr11:568112-568133:-	1451.04	1369.68	1521.21	1289.01
hsa-miR-32-5p@chr9:111808552-111808573:-	1449.72	1371.13	1520.22	1288.36
hsa-miR-221-3p@chrX:45605608-45605630:-	1448.65	1370.61	1519.71	1287.69
hsa-miR-101-3p@chr1:65524125-65524145:-	1450.76	1369.01	1519.84	1286.52
hsa-miR-30c-5p@chr6:72086706-72086728:-	1448.25	1370.46	1519.64	1287.65
hsa-miR-148a-3p@chr7:25989542-25989563:-	1448.3	1370.37	1519.59	1287.65
hsa-let-7i-5p@chr12:62997471-62997492:+	1447.77	1369.32	1521.26	1287.01
hsa-let-7g-5p@chr3:52302352-52302373:-	1448.31	1369.94	1519.45	1287.54
hsa-miR-19b-3p@chrX:133303713-133303735:-	1448.06	1370.20	1519.42	1287.54
hsa-miR-182-5p@chr7:129410287-129410310:-	1448.14	1369.89	1519.73	1287.39
hsa-miR-27a-3p@chr19:13947261-13947281:-	1447.95	1370.15	1519.41	1287.12
hsa-miR-29b-3p@chr7:130562226-130562248:-	1447.86	1369.87	1519.26	1287.46
hsa-miR-30d-5p@chr8:135817162-135817183:-	1447.78	1369.79	1519.33	1287.43
hsa-miR-26a-5p@chr12:58218441-58218462:-	1447.94	1370.03	1519.07	1287.24

hsa-miR-96-5p@chr7:129414579-129414601:-	1447.5	1370.02	1519.35	1287.17
hsa-miR-106b-5p@chr7:99691666-99691686:-	1447.76	1369.94	1519.11	1287.21
hsa-miR-30b-5p@chr8:135812813-135812834:-	1447.8	1369.94	1518.96	1287.28
hsa-miR-31-5p@chr9:21512157-21512177:-	1447.86	1369.55	1519.49	1287.05
hsa-let-7f-5p@chrX:53584207-53584228:-	1447.76	1369.93	1519.01	1287.14
hsa-miR-340-5p@chr5:179442361-179442382:-	1447.61	1369.82	1519.16	1287.14
hsa-miR-25-3p@chr7:99691194-99691215:-	1447.69	1369.82	1519.07	1287.04
hsa-let-7a-5p@chr11:122017276-122017297:-	1447.27	1369.61	1519.31	1287.41
hsa-miR-29b-3p@chr1:207975795-207975817:-	1447.42	1369.82	1518.99	1287.29
hsa-miR-135b-5p@chr1:205417489-205417511:-	1448.06	1369.80	1518.83	1286.75
hsa-miR-374b-5p@chrX:73438422-73438443:-	1447.33	1369.69	1518.85	1287.07
hsa-miR-374c-3p@chrX:73438422-73438443:+	1447.33	1369.69	1518.85	1287.07
hsa-miR-1307-5p@chr10:105154098-105154118:-	1447.67	1369.47	1519.42	1286.34
hsa-miR-374a-3p@chrX:73507130-73507151:-	1447.76	1369.30	1518.61	1287.17
hsa-miR-186-5p@chr1:71533364-71533385:-	1447.51	1369.41	1518.97	1286.81
hsa-miR-15a-5p@chr13:50623303-50623324:-	1447.36	1368.75	1519.39	1286.67
hsa-miR-374a-5p@chrX:73507160-73507181:-	1447.35	1369.53	1518.44	1286.62
hsa-miR-93-5p@chr7:99691438-99691460:-	1447	1369.38	1518.52	1286.28
hsa-miR-222-3p@chrX:45606442-45606462:-	1446.52	1369.53	1518.57	1286.31
hsa-miR-16-5p@chr13:50623163-50623184:-	1446.74	1368.43	1518.4	1286.27
hsa-miR-151a-3p@chr8:141742686-141742706:-	1446.09	1366.49	1518.4	1285.73
hsa-miR-92a-3p@chrX:133303574-133303595:-	1445.58	1368.03	1517.37	1285.24
hsa-miR-191-5p@chr3:49058105-49058127:-	1445.37	1367.67	1516.42	1284.63
hsa-miR-34a-5p@chr1:9211794-9211815:-	1443.94	1366.99	1516.65	1284.09
hsa-miR-103a-3p@chr5:167987909-167987931:-	1445.04	1365.77	1515.64	1283.25
hsa-miR-103b@chr5:167987909-167987931:+	1445.04	1365.77	1515.64	1283.25
hsa-miR-103a-3p@chr20:3898188-3898210:+	1442.09	1365.97	1513.96	1281.18
hsa-miR-103b@chr20:3898188-3898210:-	1442.09	1365.97	1513.96	1281.18
hsa-miR-27b-3p@chr9:97847787-97847807:+	1443.5	1359.59	1516.96	1281.33
hsa-miR-185-5p@chr22:20020676-20020697:+	1437.1	1364.36	1515.36	1281.94
hsa-miR-23a-3p@chr19:13947409-13947429:-	1433.79	1362.05	1515.31	1283.49
hsa-miR-3184-3p@chr17:28444113-28444135:-	1435.69	1360.76	1513.14	1284.71
hsa-miR-423-5p@chr17:28444113-28444135:+	1435.69	1360.76	1513.14	1284.71
hsa-miR-130b-3p@chr22:22007643-22007664:+	1440.3	1359.67	1513.42	1279.50
hsa-miR-16-5p@chr3:160122542-160122563:+	1437.17	1358.05	1517.01	1279.43
hsa-miR-320a@chr8:22102488-22102509:-	1439.02	1360.96	1511.76	1279.86
hsa-miR-140-5p@chr16:69967006-69967027:+	1430.18	1357.22	1516.25	1281.38
hsa-miR-24-3p@chr19:13947103-13947124:-	1437.39	1355.72	1512	1279.72
hsa-miR-30e-3p@chr1:41220085-41220106:+	1433.89	1356.46	1508.01	1274.15

hsa-miR-24-3p@chr9:97848346-97848367:+	1435.72	1354.51	1505.43	1273.99
hsa-let-7a-5p@chr9:96938244-96938265:+	1435.47	1351.70	1507.01	1275.39
hsa-let-7e-5p@chr19:52196046-52196067:+	1438.98	1354.41	1501.7	1273.69
hsa-miR-425-5p@chr3:49057632-49057654:-	1438.01	1358.41	1499.86	1272.36
hsa-miR-590-5p@chr7:73605543-73605564:+	1430.9	1351.94	1509.76	1273.18
hsa-miR-203@chr14:104583806-104583827:+	1436.21	1355.65	1499.55	1274.28
hsa-let-7d-5p@chr9:96941123-96941144:+	1435.53	1351.97	1498.79	1271.51
hsa-let-7f-5p@chr9:96938635-96938656:+	1427.37	1344.64	1506.53	1273.23
hsa-miR-19a-3p@chr13:92003193-92003215:+	1428.9	1350.14	1504.55	1267.49
hsa-let-7a-5p@chr22:46508632-46508653:+	1429.83	1347.04	1503.87	1267.17
hsa-miR-1307-3p@chr10:105154058-105154079:-	1420.46	1346.19	1502.21	1272.75
hsa-miR-18a-5p@chr13:92003010-92003032:+	1429.43	1347.87	1492.95	1262.84
hsa-miR-7-5p@chr9:86584727-86584749:-	1434.8	1340.37	1491.53	1263.47
hsa-miR-19b-3p@chr13:92003499-92003521:+	1428.1	1328.01	1497.36	1266.06
hsa-miR-15b-5p@chr3:160122395-160122416:+	1421.33	1342.05	1489.34	1261.03
hsa-miR-3529-3p@chr15:89155087-89155110:-	1424.11	1340.95	1485.04	1259.69
hsa-miR-99b-5p@chr19:52195871-52195892:+	1420.66	1339.43	1488.28	1258.25
hsa-miR-17-5p@chr13:92002872-92002894:+	1415.97	1326.24	1499.75	1257.22
hsa-miR-10a-5p@chr17:46657266-46657288:-	1407.09	1340.77	1493.17	1251.72
hsa-miR-26a-5p@chr3:38010904-38010925:+	1424.67	1319.77	1485.17	1258.34
hsa-miR-590-3p@chr7:73605583-73605603:+	1337.39	1346.30	1520.08	1283.08
hsa-miR-301a-3p@chr17:57228510-57228532:-	1442.96	1363.99	1394.58	1284.20
hsa-miR-183-5p@chr7:129414807-129414828:-	1405.16	1326.85	1488.47	1251.70
hsa-miR-33a-5p@chr22:42296953-42296973:+	1424.51	1329.71	1460.91	1248.50
hsa-miR-429@chr1:1104435-1104456:+	1411.86	1337.27	1476.52	1235.81
hsa-miR-101-3p@chr9:4850345-4850365:+	1397.87	1328.27	1477.46	1242.13
hsa-miR-200c-3p@chr12:7072905-7072927:+	1393.68	1323.79	1473.22	1234.28
hsa-miR-22-3p@chr17:1617208-1617229:-	1230.92	1369.28	1518.99	1286.46
hsa-miR-20a-5p@chr13:92003326-92003348:+	1341.37	1271.58	1513.96	1275.98
hsa-miR-769-5p@chr19:46522219-46522240:+	1395	1313.88	1456.55	1234.00
hsa-miR-142-3p@chr17:56408606-56408628:-	1373.08	1323.00	1464.95	1238.38
hsa-miR-33b-5p@chr17:17717211-17717230:-	1447.57	1368.95	1292.97	1286.39
hsa-miR-192-5p@chr11:64658675-64658695:-	1319.88	1351.72	1458.6	1242.25
hsa-miR-107@chr10:91352513-91352535:-	1447.37	1369.11	1215.65	1286.19
hsa-miR-196b-5p@chr7:27209147-27209168:-	1136.2	1369.83	1519.13	1287.31
hsa-miR-21-3p@chr17:57918672-57918692:+	1495.25	1409.25	1032.95	1329.34
hsa-miR-452-5p@chrX:151128150-151128171:-	1389.77	1317.21	1356.9	1160.18
hsa-miR-423-3p@chr17:28444149-28444171:+	1422.41	1312.97	1164.51	1244.29
hsa-miR-98@chrX:53583260-53583281:-	1447.77	1369.86	964.461	1286.55
hsa-miR-3184-5p@chr17:28444146-28444169:-	1381.45	1280.50	1134.76	1215.11

hsa-miR-194-5p@chr11:64658876-64658897:-	910.33	1242.59	1519.57	1287.30
hsa-miR-28-3p@chr3:188406622-188406643:+	997.591	1375.44	1292.61	1290.05
hsa-miR-221-5p@chrX:45605649-45605670:-	1447.29	1365.23	844.726	1286.13
hsa-miR-29a-5p@chr7:130561545-130561566:-	1446.63	1368.01	820.974	1285.61
hsa-miR-28-5p@chr3:188406582-188406603:+	754.98	1356.53	1500.19	1276.71
hsa-miR-29c-3p@chr1:207975210-207975231:-	807.108	1265.20	1519.21	1286.66
hsa-miR-181a-5p@chr1:198828237-198828259:-	1445.43	597.42	1519.1	1286.83
hsa-miR-181a-5p@chr9:127454759-127454781:+	1434.3	600.88	1519.01	1282.84
hsa-miR-190a@chr15:63116170-63116191:+	740.278	1223.52	1543.27	1310.72
hsa-let-7d-3p@chr9:96941177-96941198:+	1425.03	1346.98	770.045	1266.49
hsa-miR-301b@chr22:22007314-22007336:+	1444.18	1364.82	550.672	1280.00
hsa-miR-744-5p@chr17:11985226-11985247:+	1398.26	1321.53	852.173	971.30
hsa-miR-532-5p@chrX:49767773-49767794:+	885.825	835.69	1505.41	1276.20
hsa-miR-194-5p@chr1:220291548-220291569:-	842.974	825.94	1519.42	1287.58
hsa-miR-378c@chr10:132760897-132760921:-	950.806	1155.28	1276.17	1093.08
hsa-miR-31-3p@chr9:21512120-21512141:-	1436.46	1358.58	452.36	1130.18
hsa-miR-215@chr1:220291258-220291278:-	1447.8	171.29	1484.55	1265.81
hsa-miR-193b-3p@chr16:14397874-14397895:+	1434.41	1349.81	481.038	1095.47
hsa-miR-141-5p@chr12:7073276-7073297:+	704.369	1113.94	1163.13	1270.72
hsa-miR-148b-5p@chr12:54731024-54731045:+	1463.06	1383.50	567.278	801.56
hsa-miR-95@chr4:8007039-8007060:-	266.151	1008.61	1516.26	1284.98
hsa-miR-345-5p@chr14:100774213-100774234:+	1073.97	892.74	807.263	1248.50
hsa-miR-9-5p@chr5:87962720-87962742:-	1435.44	1358.75	343.396	792.67
hsa-miR-335-5p@chr7:130135967-130135989:+	1391.75	1309.52	603.142	619.75
hsa-miR-9-3p@chr15:89911302-89911323:+	1446.28	1364.78	383.156	707.03
hsa-miR-9-5p@chr1:156390184-156390206:-	1435.12	1358.80	350.271	753.74
hsa-miR-9-5p@chr15:89911263-89911285:+	1412.59	1338.61	345.604	780.76
hsa-miR-15b-3p@chr3:160122433-160122454:+	1014.47	823.59	774.085	1245.14
hsa-miR-9-3p@chr5:87962684-87962705:-	1434.82	1351.77	356.377	687.28
hsa-miR-9-3p@chr1:156390146-156390167:-	1434.47	1351.48	368.623	660.69
hsa-miR-330-3p@chr19:46142267-46142289:-	1435.39	1216.82	394.641	758.64
hsa-miR-151a-5p@chr8:141742722-141742742:-	1025.77	1265.45	696.595	780.47
hsa-miR-222-5p@chrX:45606479-45606500:-	1510.13	1421.57	316.79	517.26
hsa-miR-361-5p@chrX:85158686-85158707:-	824.748	1062.72	840.921	968.12
hsa-miR-627@chr15:42491828-42491849:-	804.162	1088.66	563.988	1222.46
hsa-miR-27a-5p@chr19:13947301-13947322:-	824.671	1202.84	794.014	656.68
hsa-miR-197-3p@chr1:110141562-110141583:+	978.323	1220.21	644.697	634.73

hsa-miR-181b-5p@chr9:127456004-127456026:+	582.34	190.00	1408.74	1284.18
hsa-miR-24-2-5p@chr19:13947140-13947161:-	1163.84	1100.80	519.693	624.06
hsa-miR-125a-5p@chr19:52196521-52196544:+	873.512	564.30	837.899	1016.19
hsa-miR-200b-5p@chr1:1102504-1102525:+	259.742	356.21	1354.12	1259.06
hsa-miR-224-5p@chrX:151127103-151127123:-	526.937	353.10	938.758	1287.34
hsa-miR-181b-5p@chr1:198828054-198828076:-	485.611	153.75	1158.62	1277.32
hsa-miR-7-1-3p@chr9:86584686-86584707:-	947.711	806.52	380.571	925.07
hsa-miR-324-5p@chr17:7126661-7126683:-	1192.02	716.16	373.686	693.35
hsa-miR-19b-1-5p@chr13:92003461-92003483:+	777.739	961.71	362.341	811.26
hsa-miR-339-3p@chr7:1062591-1062613:-	541.7	756.58	767.49	845.17
hsa-miR-338-3p@chr17:79099687-79099708:-	114.014	473.68	1430.46	877.49
hsa-miR-3065-5p@chr17:79099686-79099708:+	113.946	473.65	1430.48	875.83
hsa-miR-577@chr4:115577930-115577950:+	657.477	374.08	765.615	1057.08
hsa-miR-130a-3p@chr11:57408725-57408746:+	1452.81	1376.28	0.569393	10.71
hsa-miR-100-5p@chr11:122022983-122023004:-	1447.54	1369.69	9.28201	4.35
hsa-miR-660-5p@chrX:49777864-49777885:+	227.606	253.57	1415.13	925.16
hsa-miR-125b-5p@chr11:121970517-121970538:-	1447.33	1369.64	1.89798	0.32
hsa-miR-424-5p@chrX:133680710-133680731:-	1447.51	1369.56	2.08777	0.00
hsa-miR-100-3p@chr11:122022948-122022969:-	1447.88	1369.69	0.189798	0.00
hsa-miR-106b-3p@chr7:99691625-99691646:-	808.693	569.73	495.688	932.68
hsa-miR-125b-5p@chr21:17962573-17962594:+	1438.84	1363.12	2.26853	0.64
hsa-miR-10b-5p@chr2:177015057-177015079:+	1388.13	1311.88	25.7693	76.76
hsa-miR-455-3p@chr9:116971767-116971787:+	1442.66	1346.92	0.597862	0.96
hsa-miR-126-5p@chr9:139565068-139565088:+	1424.13	1349.37	6.69037	6.75
hsa-miR-145-5p@chr5:148810224-148810246:+	1429.07	1339.70	0.560766	1.72
hsa-miR-126-3p@chr9:139565105-139565126:+	1419.45	1338.29	3.72365	1.74
hsa-miR-155-5p@chr21:26946295-26946317:+	0.180879	0.33	1476.29	1257.76
hsa-miR-188-5p@chrX:49768123-49768143:+	319.695	320.32	898.084	1114.01
hsa-miR-484@chr16:15737158-15737179:+	476.358	408.36	570.107	1188.68
hsa-miR-192-3p@chr11:64658631-64658652:-	11.6882	12.14	1358.63	1250.34
hsa-miR-331-3p@chr12:95702256-95702276:+	909.225	687.59	452.544	539.12
hsa-miR-148a-5p@chr7:25989580-25989601:-	262.283	217.55	1027.81	1056.81
hsa-miR-335-3p@chr7:130136003-130136024:+	629.519	939.20	538.817	397.73

hsa-miR-671-5p@chr7:150935535-150935557:+	355.214	1090.59	443.238	609.52
hsa-miR-30a-5p@chr6:72113298-72113319:-	517.478	798.13	195.519	919.27
hsa-miR-20a-3p@chr13:92003362-92003383:+	743.249	774.60	269.612	635.23
hsa-miR-5683@chr6:6169576-6169599:+	149.823	58.29	998.666	1184.15
hsa-miR-502-3p@chrX:49779257-49779278:+	275.763	227.16	831.033	948.52
hsa-miR-542-3p@chrX:133675394-133675415:-	831.036	1375.23	1.30147	0.16
hsa-miR-200a-5p@chr1:1103258-1103279:+	251.792	324.40	683.181	935.98
hsa-let-7c@chr21:17912158-17912179:+	542.749	722.47	271.881	624.00
hsa-miR-454-3p@chr17:57215148-57215170:-	490.897	382.90	519.916	738.47
hsa-miR-4741@chr18:20513370-20513392:+	13.4508	3.38	798.272	1220.88
hsa-miR-92b-3p@chr1:155165028-155165049:+	744.756	1150.81	3.52481	4.28
hsa-let-7b-3p@chr22:46509625-46509646:+	523.843	293.71	322.746	615.14
hsa-miR-505-3p@chrX:139006319-139006340:-	649.743	399.46	201.213	504.71
hsa-miR-132-3p@chr17:1953223-1953244:-	437.581	1104.10	100.511	94.37
hsa-miR-598@chr8:10892731-10892752:-	1.08527	0.00	729.564	996.70
hsa-miR-186-3p@chr1:71533325-71533346:-	419.717	496.01	273.318	514.09
hsa-miR-106a-5p@chrX:133304274-133304296:-	551.5	477.54	163.856	508.46
hsa-miR-34c-5p@chr11:111384176-111384198:+	640.904	267.70	195.932	588.61
hsa-miR-500a-3p@chrX:49773090-49773111:+	161.447	147.05	432.576	925.00
hsa-let-7a-3p@chr22:46508680-46508700:+	493.221	430.97	213.892	516.97
hsa-miR-362-5p@chrX:49773576-49773599:+	131.79	176.11	641.92	703.16
hsa-let-7a-3p@chr9:96938295-96938315:+	459.749	440.17	201.148	510.12
hsa-miR-183-3p@chr7:129414768-129414789:-	568.27	488.56	260.8	292.70
hsa-miR-362-3p@chrX:49773613-49773634:+	145.435	162.01	478.642	721.10
hsa-miR-125b-1-3p@chr11:121970477-121970498:-	992.259	513.11	0	0.00
hsa-miR-153@chr2:220158848-220158869:-	476.418	1009.41	5.31433	13.58
hsa-miR-149-5p@chr2:241395432-241395454:+	682.383	528.77	105.95	172.72
hsa-miR-375@chr2:219866370-219866391:-	430.449	699.15	222.434	136.57
hsa-miR-181a-3p@chr1:198828198-198828219:-	499.114	94.38	329.218	562.29
hsa-miR-153@chr7:157367041-157367062:-	456.987	999.40	6.82368	12.32
hsa-miR-532-3p@chrX:49767810-49767831:+	191.344	111.99	613.164	558.00
hsa-miR-365b-3p@chr17:29902497-29902518:+	297.348	836.88	118.027	209.05
hsa-miR-365a-3p@chr16:14403197-14403218:+	298.468	841.89	106.088	207.07
hsa-miR-128@chr2:136423016-136423036:+	267.764	478.54	281.214	424.30
hsa-miR-652-3p@chrX:109298617-109298637:+	287.381	367.71	298.03	479.28
hsa-miR-200c-5p@chr12:7072866-7072887:+	351.138	396.82	270.904	399.56

hsa-miR-574-3p@chr4:38869713-38869734:+	392.499	599.15	150.952	260.81
hsa-miR-3200-3p@chr22:31127597-31127618:+	756.737	516.17	34.2359	58.72
hsa-let-7f-1-3p@chr9:96938691-96938712:+	384.48	349.02	224.838	366.86
hsa-miR-16-2-3p@chr3:160122585-160122606:+	395.384	333.56	184.772	395.44
hsa-miR-4521@chr17:8090266-8090287:+	386.866	530.64	137.386	126.19
hsa-miR-33a-3p@chr22:42296993-42297014:+	285.35	316.40	215.176	362.20
hsa-miR-378d@chr8:94928307-94928326:-	289.387	246.70	158.931	454.50
hsa-miR-425-3p@chr3:49057592-49057613:-	225.763	337.15	200.092	354.79
hsa-miR-455-5p@chr9:116971729-116971750:+	424.825	684.65	0.189798	0.00
hsa-miR-128@chr3:35786019-35786039:+	226.614	353.48	207.677	318.92
hsa-miR-556-5p@chr1:162312351-162312372:+	287.865	518.53	114.8	180.03
hsa-miR-339-5p@chr7:1062626-1062648:-	201.031	156.50	385.108	342.25
hsa-miR-324-3p@chr17:7126627-7126646:-	453.083	278.18	124.317	227.70
hsa-miR-22-5p@chr17:1617246-1617267:-	113.006	447.34	287.182	234.17
hsa-miR-378d@chr4:5925006-5925025:-	275.222	232.30	149.491	423.12
hsa-miR-561-5p@chr2:189162244-189162265:+	171.146	453.52	190.846	262.44
hsa-miR-625-3p@chr14:65937871-65937892:+	206.59	280.19	220.572	359.17
hsa-miR-152@chr17:46114540-46114560:-	483.616	415.61	59.5205	80.53
hsa-miR-584-5p@chr5:148441936-148441957:-	106.934	862.87	40.2913	27.82
hsa-miR-1277-3p@chrX:117520403-117520424:+	232.206	388.38	139.456	274.70
hsa-miR-877-5p@chr6:30552109-30552128:+	494.276	313.22	66.7888	135.06
hsa-miR-378i@chr22:42319275-42319295:-	110.698	172.78	291.975	426.11
hsa-miR-625-5p@chr14:65937834-65937854:+	201.49	256.04	199.724	335.45
hsa-let-7a-2-3p@chr11:122017231-122017252:-	707.194	269.77	0.189798	0.00
hsa-let-7g-3p@chr3:52302296-52302316:-	233.533	344.09	143.316	236.79
hsa-miR-143-3p@chr5:148808541-148808561:+	614.328	304.23	12.204	13.12
hsa-miR-342-3p@chr14:100576052-100576074:+	559.763	350.41	1.34584	2.13
hsa-miR-30d-3p@chr8:135817122-135817143:-	172.938	369.69	149.768	187.74
hsa-miR-193a-3p@chr17:29887069-29887090:+	215.875	529.18	21.2121	103.00
hsa-miR-582-5p@chr5:58999492-58999514:-	6.02656	0.34	444.42	417.25
hsa-miR-3613-5p@chr13:50570601-50570622:-	21.249	31.26	231.047	542.06
hsa-miR-181a-2-3p@chr9:127454797-127454818:+	157.055	99.34	185.884	350.98
hsa-miR-501-3p@chrX:49774380-49774401:+	81.5161	78.11	263.828	366.51
hsa-miR-16-1-3p@chr13:50623121-50623142:-	168.149	180.88	157.396	281.76
hsa-miR-374b-3p@chrX:73438392-73438413:-	151.999	190.00	169.977	269.25
hsa-miR-500b@chrX:49775290-49775307:+	48.3585	61.58	370.027	300.51

hsa-miR-589-5p@chr7:5535504-5535525:-	160.474	224.13	171.686	218.74
hsa-miR-501-5p@chrX:49774343-49774364:+	69.9313	60.58	259.95	365.29
hsa-miR-582-3p@chr5:58999456-58999477:-	4.0827	0.66	396.948	351.54
hsa-miR-3074-3p@chr9:97848306-97848327:-	208.381	245.33	129.785	166.86
hsa-miR-24-1-5p@chr9:97848309-97848330:+	206.934	243.15	129.18	165.30
hsa-miR-4517@chr16:28969908-28969932:+	186.019	179.23	193.665	179.70
hsa-miR-331-5p@chr12:95702221-95702242:+	266.469	271.89	84.9299	108.67
hsa-let-7i-3p@chr12:62997527-62997548:+	155.298	235.84	105.473	226.02
hsa-miR-99a-5p@chr21:17911421-17911442:+	651.492	62.17	5.14261	1.72
hsa-miR-500a-5p@chrX:49773051-49773073:+	41.6844	55.54	334.259	265.63
hsa-miR-3158-5p@chr10:103361222-103361242:-	138.183	402.57	85.7506	68.12
hsa-miR-767-5p@chrX:151561953-151561975:-	2.33498	0.00	287.923	402.99
hsa-miR-3158-3p@chr10:103361184-103361205:-	133.48	391.84	78.2057	68.73
hsa-miR-576-5p@chr4:110409869-110409890:+	183.928	164.85	120.883	195.45
hsa-miR-3158-3p@chr10:103361223-103361244:+	131.482	382.02	81.5587	64.64
hsa-miR-29b-1-5p@chr7:130562266-130562289:-	194.005	200.07	65.7773	190.22
hsa-miR-1266@chr15:52569363-52569385:-	73.1738	42.09	247.591	279.94
hsa-miR-3158-5p@chr10:103361186-103361206:+	127.104	373.57	74.4861	65.55
hsa-miR-374c-5p@chrX:73438396-73438417:+	124.264	154.88	139.501	220.91
hsa-miR-1304-3p@chr11:93466857-93466878:-	277.503	149.58	99.8697	101.89
hsa-miR-27b-5p@chr9:97847745-97847766:+	84.393	179.89	171.071	181.82
hsa-miR-3607-3p@chr5:85916364-85916383:+	102.949	195.23	96.4971	214.95
hsa-miR-651@chrX:8095021-8095042:+	0.180879	247.43	169.941	176.75
hsa-miR-194-3p@chr11:64658840-64658861:-	7.04567	4.59	261.017	312.81
hsa-miR-196a-5p@chr12:54385546-54385567:+	219.182	309.27	14.8856	33.02
hsa-miR-93-3p@chr7:99691400-99691421:-	148.269	127.59	74.6808	209.25
hsa-miR-361-3p@chrX:85158646-85158668:-	144.391	76.90	185.225	153.24
hsa-miR-3545-3p@chr14:104583765-104583787:-	157.768	189.79	112.99	90.00
hsa-miR-326@chr11:75046152-75046171:-	124.112	70.00	133.917	219.10
hsa-miR-628-5p@chr15:55665189-55665210:-	52.0759	42.89	199.107	246.81
hsa-miR-18a-3p@chr13:92003051-92003073:+	200.028	104.44	61.0286	168.55
hsa-miR-130b-5p@chr22:22007605-22007625:+	160.087	99.20	79.7245	192.68
hsa-miR-34a-3p@chr1:9211752-9211773:-	112.05	133.21	102.138	183.43
hsa-miR-570-3p@chr3:195426331-195426352:+	146.056	179.26	59.8947	132.15
hsa-miR-641@chr19:40788510-40788533:-	139.851	103.86	71.661	193.98
hsa-miR-181d@chr19:13985724-13985746:+	284.26	162.46	30.7213	28.25

hsa-miR-378a-5p@chr5:149112392-149112413:+	94.7462	95.09	128.936	185.29
hsa-miR-1296@chr10:65132772-65132793:-	121.473	206.00	101.921	73.28
hsa-miR-551a@chr1:3477274-3477294:-	92.9537	169.47	4.29892	231.36
hsa-miR-10a-3p@chr17:46657226-46657247:-	123.368	49.80	69.9992	249.93
hsa-miR-629-5p@chr15:70371766-70371786:-	124.535	173.50	81.4991	108.48
hsa-miR-452-3p@chrX:151128106-151128127:-	114.109	81.16	119.048	171.84
hsa-miR-421@chrX:73438227-73438249:-	127.38	97.60	113.973	132.67
hsa-miR-338-5p@chr17:79099723-79099744:-	39.5694	208.14	136.347	86.52
hsa-miR-184@chr15:79502182-79502203:+	44.9872	39.40	87.7136	291.30
hsa-miR-3065-3p@chr17:79099726-79099748:+	40.3607	212.26	112.524	87.61
hsa-miR-935@chr19:54485616-54485638:+	168.966	278.25	0	0.00
hsa-miR-20b-5p@chrX:133303880-133303902:-	167.815	136.62	26.8132	112.77
hsa-miR-320b@chr1:224444751-224444772:-	62.1793	127.22	103.693	149.72
hsa-miR-3176@chr16:593336-593354:+	63.1569	115.72	139.364	118.23
hsa-miR-99b-3p@chr19:52195909-52195930:+	162.438	91.59	53.2337	126.42
hsa-miR-744-3p@chr17:11985283-11985304:+	116.521	194.48	41.9182	79.20
hsa-miR-181c-5p@chr19:13985539-13985560:+	259.165	142.49	13.1503	13.19
hsa-miR-33b-3p@chr17:17717171-17717192:-	103.73	135.85	73.6776	113.90
hsa-miR-196a-5p@chr17:46709894-46709915:-	165.754	233.97	3.22656	7.24
hsa-miR-142-5p@chr17:56408644-56408664:-	39.8476	66.14	149.75	151.92
hsa-miR-135b-3p@chr1:205417451-205417472:-	75.6333	171.52	61.9644	98.04
hsa-miR-320b@chr1:117214409-117214430:+	56.9424	110.08	93.5973	140.22
hsa-miR-139-5p@chr11:72326147-72326168:-	174.066	211.94	2.65717	4.95
hsa-miR-26a-2-3p@chr12:58218403-58218424:-	173.213	48.13	61.2414	108.94
hsa-miR-573@chr4:24521875-24521898:-	184.709	176.73	10.8762	18.17
hsa-let-7f-2-3p@chrX:53584157-53584178:-	105.444	150.41	34.6878	98.32
hsa-miR-4510@chr15:36219064-36219085:+	69.2767	71.95	31.7052	211.61
hsa-miR-548e@chr10:112748736-112748757:+	105.875	132.00	66.2846	78.78
hsa-miR-25-5p@chr7:99691233-99691253:-	138.969	99.12	41.9358	100.88
hsa-miR-664-3p@chr1:220373891-220373913:-	54.4035	109.44	100.946	103.56
hsa-miR-101-5p@chr1:65524160-65524181:-	60.5859	136.83	52.7457	110.56
hsa-miR-449c-5p@chr5:54468141-54468165:-	115.107	203.37	10.3756	21.55
hsa-miR-381@chr14:101512305-101512326:+	50.1207	293.40	2.04258	4.34
hsa-miR-32-3p@chr9:111808511-111808532:-	100.681	107.38	39.4146	97.97
hsa-miR-629-3p@chr15:70371726-70371747:-	106.279	102.24	41.403	87.57
hsa-miR-422a@chr15:64163188-64163209:-	74.815	90.56	35.4741	135.07
hsa-miR-105-5p@chrX:151562930-151562952:-	1.59502	0.48	133.842	199.70
hsa-miR-105-5p@chrX:151560737-151560759:-	1.08527	0.17	128.967	199.96
hsa-miR-4787-3p@chr3:50712561-50712584:+	146.087	166.89	2.44261	11.63

hsa-miR-1292@chr20:2633425-2633449:+	68.5607	108.49	75.4683	72.43
hsa-let-7e-3p@chr19:52196091-52196112:+	122.481	100.30	26.4361	72.91
hsa-miR-125a-3p@chr19:52196559-52196580:+	103.359	65.46	38.538	114.63
hsa-miR-103a-2-5p@chr20:3898151-3898173:+	97.6582	105.90	30.7903	82.92
hsa-miR-3689f@chr9:137742629-137742650:-	0	0.00	139.293	172.32
hsa-miR-1269a@chr4:67142608-67142629:+	0	0.00	59.253	242.58
hsa-miR-378f@chr1:24255611-24255630:+	94.3808	111.04	14.7143	81.34
hsa-miR-3934@chr6:33665929-33665950:+	92.722	103.58	48.1724	53.51
hsa-miR-1224-5p@chr3:183959193-183959211:+	180.346	111.49	0.200342	5.75
hsa-miR-29c-5p@chr1:207975248-207975269:-	56.2017	56.73	66.7455	110.10
hsa-miR-185-3p@chr22:20020711-20020732:+	63.945	128.22	36.6309	59.60
hsa-miR-150-5p@chr19:50004089-50004110:-	0.361758	0.67	238.774	38.67
hsa-miR-503@chrX:133680401-133680423:-	64.3436	202.81	0.353714	0.00
hsa-miR-3676-3p@chr17:8090552-8090571:+	54.5112	129.50	45.3317	36.19
hsa-miR-378e@chr5:169455549-169455567:+	78.5718	67.70	27.7737	91.23
hsa-miR-502-5p@chrX:49779221-49779241:+	19.2727	24.15	113.67	107.20
hsa-miR-1260b@chr11:96074611-96074629:+	24.278	78.54	96.6913	64.31
hsa-miR-1260a@chr14:77732574-77732591:+	24.8123	56.41	109.781	69.86
hsa-miR-4504@chr14:50766589-50766610:-	99.673	69.96	37.6251	48.65
hsa-miR-191-3p@chr3:49058064-49058085:-	79.4231	111.62	21.2844	42.78
hsa-miR-589-3p@chr7:5535465-5535488:-	35.4366	86.81	53.8117	77.20
hsa-miR-769-3p@chr19:46522258-46522280:+	67.731	106.27	25.1741	53.83
hsa-miR-18b-5p@chrX:133304114-133304136:-	76.9394	81.07	23.6816	70.28
hsa-miR-675-3p@chr11:2017998-2018017:-	15.1462	10.77	19.1596	205.68
hsa-miR-4664-5p@chr8:144815293-144815314:-	69.4834	71.86	56.9393	50.42
hsa-miR-151b@chr14:100575775-100575792:-	61.7649	116.93	28.6148	32.88
hsa-miR-1287@chr10:100155028-100155049:-	101.559	95.44	15.5453	21.93
hsa-miR-193b-5p@chr16:14397837-14397858:+	70.8271	113.52	16.6208	33.04
hsa-miR-1277-5p@chrX:117520364-117520387:+	33.9581	102.43	45.4111	49.62
hsa-miR-449a@chr5:54466414-54466435:-	61.3352	151.41	3.0458	12.04
hsa-miR-3676-5p@chr17:8090519-8090533:+	22.6745	83.93	19.5492	99.56
hsa-miR-561-3p@chr2:189162279-189162300:+	37.1663	98.57	30.5484	58.26
hsa-miR-296-5p@chr20:57392716-57392736:-	7.56074	10.11	65.5466	138.30
hsa-miR-378b@chr3:10371946-10371964:+	51.9424	53.17	13.4545	102.79
hsa-miR-30a-3p@chr6:72113257-72113278:-	55.0992	61.98	33.5128	69.71
hsa-miR-218-5p@chr4:20529922-20529942:+	94.7173	122.17	0.996437	1.16
hsa-miR-4704-3p@chr13:66792428-66792449:+	0.490957	0.49	80.0313	136.00

hsa-miR-652-5p@chrX:109298577-109298601:+	67.2192	47.04	37.0264	64.69
hsa-miR-449b-5p@chr5:54466534-54466555:-	62.4463	141.25	1.14782	11.03
hsa-miR-548k@chr11:70130092-70130113:+	86.8305	55.77	26.7344	44.98
hsa-miR-489@chr7:93113259-93113280:-	106.529	21.30	56.7585	23.95
hsa-miR-548d-3p@chr17:65467620-65467641:-	36.5376	114.02	15.9972	40.96
hsa-miR-548d-3p@chr8:124360289-124360310:-	34.1947	123.62	14.1896	35.42
hsa-miR-92a-1-5p@chr13:92003578-92003600:+	55.1105	54.94	36.1306	59.45
hsa-miR-30c-1-3p@chr1:41223011-41223032:+	48.3205	39.43	37.8511	79.90
hsa-miR-1304-5p@chr11:93466890-93466911:-	102.929	42.34	21.0766	34.54
hsa-miR-3928@chr22:31556048-31556069:-	49.8451	52.31	26.1559	68.62
hsa-miR-218-5p@chr5:168195216-168195236:-	79.0351	112.24	0.948988	0.80
hsa-miR-19a-5p@chr13:92003158-92003179:+	28.9234	61.31	43.5992	57.85
hsa-miR-491-3p@chr9:20716153-20716174:+	70.8271	57.29	24.6285	38.12
hsa-miR-450a-5p@chrX:133674594-133674615:-	49.5609	139.58	0.189798	0.00
hsa-miR-450a-5p@chrX:133674423-133674444:-	46.5031	138.44	0	0.00
hsa-miR-195-5p@chr17:6920986-6921006:-	84.5157	78.48	7.7817	13.19
hsa-miR-766-3p@chrX:118780726-118780747:-	63.1785	41.80	36.9202	41.60
hsa-miR-147b@chr15:45725296-45725317:+	37.4506	28.19	79.8958	37.68
hsa-miR-4802-3p@chr4:40504068-40504090:-	6.21566	5.53	84.6842	86.41
hsa-miR-1180@chr17:19247826-19247847:-	44.6599	61.22	40.9872	33.93
hsa-miR-1255a@chr4:102251522-102251544:-	48.2289	80.03	19.4197	30.24
hsa-miR-1306-5p@chr22:20073595-20073616:+	35.7279	34.24	46.4552	55.06
hsa-miR-3118@chr1:143424150-143424172:-	1.57858	0.00	62.1501	105.78
hsa-miR-330-5p@chr19:46142307-46142328:-	46.7874	34.01	52.6734	35.78
hsa-miR-3605-5p@chr1:33798050-33798072:-	31.1934	69.82	32.0931	35.96
hsa-miR-491-5p@chr9:20716119-20716140:+	44.6427	68.00	17.4704	33.82
hsa-miR-4446-3p@chr3:113313765-113313786:+	0	0.00	110.254	53.03
hsa-miR-3118@chr21:15017105-15017127:-	1.5868	0.17	66.9037	93.52
hsa-miR-145-3p@chr5:148810262-148810283:+	92.6359	67.81	0	0.00
hsa-miR-3611@chr10:35368537-35368557:-	30.1797	52.82	26.7615	50.01
hsa-miR-30b-3p@chr8:135812775-135812796:-	34.5221	55.33	21.8448	45.08
hsa-miR-26b-3p@chr2:219267415-219267436:+	52.5497	31.98	21.8629	50.36
hsa-miR-548o-3p@chr20:37145250-37145271:+	57.554	48.92	14.7319	34.53
hsa-miR-1301@chr2:25551520-25551543:-	77.3848	77.94	0	0.00
hsa-miR-320c@chr18:21901680-21901699:+	15.508	55.60	30.3377	53.61
hsa-miR-3615@chr17:72744802-72744822:+	17.0026	11.03	71.9713	53.88

hsa-miR-340-3p@chr5:179442319-179442340:-	44.1603	37.87	29.3373	42.14
hsa-miR-3118@chr1:142667332-142667354:+	0.863286	0.31	56.6115	95.00
hsa-miR-320c@chr18:19263520-19263539:+	15.8698	51.17	32.0458	52.84
hsa-miR-548o-3p@chr7:102046195-102046216:-	53.8417	51.31	16.3226	26.47
hsa-miR-3118@chr15:22049317-22049339:+	1.48814	0.00	56.5769	89.84
hsa-miR-3118@chr15:21038167-21038189:+	1.52103	0.00	53.799	91.90
hsa-miR-29b-2-5p@chr1:207975837-207975858:-	26.3136	33.82	25.7402	58.57
hsa-miR-3118@chr1:143163792-143163814:+	1.34837	0.00	53.3849	89.61
hsa-miR-301a-5p@chr17:57228548-57228569:-	79.1906	30.86	8.60416	25.55
hsa-miR-628-3p@chr15:55665152-55665172:-	8.50131	5.62	68.0519	60.89
hsa-miR-542-5p@chrX:133675430-133675452:-	61.2769	78.23	0	0.00
hsa-miR-942@chr1:117637277-117637298:+	37.6056	39.90	30.6116	31.08
hsa-miR-1247-3p@chr14:102026663-102026686:-	47.4768	89.13	0.379595	0.42
hsa-miR-1262@chr1:68649259-68649280:-	25.6159	65.27	11.2523	34.82
hsa-miR-146a-5p@chr5:159912379-159912400:+	63.8072	36.15	23.5439	9.01
hsa-miR-767-3p@chrX:151561919-151561941:-	0.180879	0.33	63.2457	68.31
hsa-miR-4326@chr20:61918170-61918189:+	18.2688	27.97	33.1546	52.08
hsa-miR-450b-5p@chrX:133674261-133674282:-	35.0044	94.95	0.0361519	0.00
hsa-miR-2110@chr10:115933910-115933931:-	33.4712	40.25	34.8324	20.13
hsa-miR-199b-5p@chr9:131007062-131007084:-	68.6189	59.61	0.189798	0.00
hsa-miR-3689b-5p@chr9:137742052-137742073:-	0	0.00	47.8109	79.13
hsa-miR-181b-3p@chr1:198828016-198828036:-	30.4058	11.75	34.9228	47.36
hsa-miR-3689e@chr9:137742460-137742481:-	0	0.00	47.9917	76.07
hsa-miR-96-3p@chr7:129414537-129414558:-	55.1336	35.23	9.57122	23.80
hsa-miR-941@chr20:62550848-62550870:+	30.7248	35.71	29.1426	27.96
hsa-miR-3689a-5p@chr9:137741380-137741401:-	0	0.00	45.5966	76.78
hsa-miR-23a-5p@chr19:13947444-13947465:-	33.2559	40.86	20.0282	27.61
hsa-miR-720@chr3:164059155-164059171:+	6.19511	35.56	42.5265	37.15
hsa-miR-941@chr20:62551155-62551177:+	27.9458	35.43	28.9528	27.60
hsa-miR-1827@chr12:100583710-100583727:+	25.5039	26.24	12.6383	55.20
hsa-miR-584-3p@chr5:148441897-148441918:-	9.65549	96.79	9.11932	3.80
hsa-miR-3171@chr14:28102452-28102475:-	0	0.00	47.7217	70.83
hsa-miR-181c-3p@chr19:13985577-13985598:+	75.082	36.37	1.49127	5.30
hsa-miR-2276@chr13:24736608-24736629:+	31.404	30.52	34.3082	21.76
hsa-miR-940@chr16:2321807-2321827:+	22.2933	39.45	26.9702	28.86

hsa-miR-671-3p@chr7:150935574-150935594:+	26.8877	44.60	18.8659	26.61
hsa-miR-182-3p@chr7:129410246-129410266:-	39.2236	38.85	9.70815	29.12
hsa-miR-1246@chr2:177465752-177465770:-	0.361758	14.03	41.6606	60.27
hsa-miR-545-5p@chrX:73506999-73507020:-	29.9139	40.25	21.167	24.51
hsa-miR-1252@chr12:79813041-79813062:+	44.5049	60.01	2.45833	8.26
hsa-miR-1305@chr4:183090496-183090517:+	0	0.18	44.9097	68.88
hsa-miR-642a-3p@chr19:46178236-46178257:+	44.3843	68.33	1.0936	0.00
hsa-miR-642b-5p@chr19:46178236-46178257:-	44.3843	68.33	1.0936	0.00
hsa-miR-643@chr19:52785110-52785131:+	21.2404	29.63	19.7932	41.85
hsa-miR-576-3p@chr4:110409908-110409929:+	34.746	23.71	20.1276	33.68
hsa-miR-624-5p@chr14:31483912-31483933:-	37.5712	39.07	12.4995	22.69
hsa-miR-642b-3p@chr19:46178199-46178220:-	53.3076	57.13	0.370557	0.00
hsa-miR-15a-3p@chr13:50623266-50623287:-	13.5659	22.16	25.5956	49.09
hsa-miR-642a-5p@chr19:46178201-46178222:+	53.1612	56.81	0.361519	0.00
hsa-miR-3194-5p@chr20:50069485-50069505:-	53.1151	55.34	0.569393	0.32
hsa-miR-26a-1-3p@chr3:38010943-38010964:+	32.9458	19.83	23.1824	32.20
hsa-miR-941@chr20:62551267-62551289:+	23.9582	30.08	24.32	28.49
hsa-miR-550b-3p@chr7:30329430-30329449:-	13.6611	36.02	20.7179	36.36
hsa-miR-549@chr15:81134334-81134354:-	2.81267	2.98	64.1041	36.55
hsa-miR-196a-3p@chr12:54385583-54385604:+	22.9027	83.50	0	0.00
hsa-miR-550b-3p@chr7:32772613-32772632:-	13.8896	32.44	20.8977	38.98
hsa-miR-376c@chr14:101506069-101506089:+	24.5453	78.44	1.1293	1.80
hsa-miR-550a-3p@chr7:30329470-30329491:+	18.5186	22.63	22.4594	39.94
hsa-miR-550b-2-5p@chr7:30329470-30329491:-	18.5186	22.63	22.4594	39.94
hsa-miR-1226-3p@chr3:47891098-47891119:+	38.9579	31.69	17.0456	15.35
hsa-miR-10b-3p@chr2:177015096-177015117:+	60.0949	41.49	0.189798	1.26
hsa-miR-550a-3p@chr7:32772653-32772674:+	12.9802	28.86	24.3212	36.29
hsa-miR-550b-2-5p@chr7:32772653-32772674:-	12.9802	28.86	24.3212	36.29
hsa-miR-550a-3p@chr7:29720364-29720385:-	14.5909	22.88	23.9778	39.43
hsa-miR-5699@chr10:687639-687660:-	48.6134	51.96	0	0.00
hsa-miR-3617@chr20:44333789-44333810:-	1.98967	97.80	0.569393	0.16
hsa-miR-365a-5p@chr16:14403157-14403179:+	30.4534	48.42	8.16992	12.90
hsa-miR-376b@chr14:101506834-101506855:+	20.9217	77.36	0.370557	0.80
hsa-miR-224-3p@chrX:151127056-151127078:-	10.6965	10.54	29.9794	47.42
hsa-miR-3912@chr5:170813682-170813702:-	18.7572	38.91	19.2645	21.48
hsa-miR-424-3p@chrX:133680674-133680694:-	26.5711	71.65	0	0.00

hsa-miR-550a-5p@chr7:30329431-30329453:+	12.752	33.49	18.8158	33.02
hsa-miR-615-3p@chr12:54427794-54427815:+	40.0604	55.59	0.352481	1.45
hsa-miR-550a-5p@chr7:32772614-32772636:+	12.9082	29.84	18.7727	35.65
hsa-miR-505-5p@chrX:139006355-139006376:-	31.9725	24.57	10.6377	28.45
hsa-miR-376a-5p@chr14:101507125-101507146:+	27.9243	65.56	1.08456	0.32
hsa-miR-1285-3p@chr7:91833341-91833362:-	16.2705	18.59	28.6143	30.51
hsa-miR-499a-5p@chr20:33578211-33578231:+	21.3528	51.47	10.7805	9.87
hsa-miR-3144-3p@chr6:120336372-120336393:+	0	0.00	23.6705	69.18
hsa-miR-3177-3p@chr16:1785039-1785059:+	22.9988	29.82	25.6132	13.77
hsa-miR-4704-5p@chr13:66792391-66792412:+	0	0.16	27.358	64.29
hsa-miR-499b-3p@chr20:33578209-33578230:-	20.7494	50.39	10.5473	9.61
hsa-miR-497-5p@chr17:6921298-6921318:-	43.6099	44.48	1.51838	1.61
hsa-miR-296-3p@chr20:57392681-57392702:-	5.22827	5.40	17.3891	63.11
hsa-miR-660-3p@chrX:49777900-49777920:+	9.09822	10.67	25.0248	46.00
hsa-miR-580@chr5:36148009-36148030:-	21.0853	26.15	20.227	23.02
hsa-miR-3691-5p@chr6:5148520-5148542:-	15.8845	31.49	18.9884	20.26
hsa-miR-3942-5p@chr15:35664522-35664543:-	22.3773	27.09	15.0573	21.69
hsa-miR-320d@chr13:41301964-41301982:-	8.50131	28.96	15.4474	33.09
hsa-miR-5580-3p@chr14:54415145-54415166:-	31.8003	34.87	10.1135	9.04
hsa-miR-1275@chr6:33967795-33967811:-	8.36565	39.87	16.7141	20.82
hsa-miR-328@chr16:67236230-67236251:-	38.2774	20.84	5.68489	20.52
hsa-miR-320d@chrX:140008337-140008355:-	7.88834	31.14	14.7304	29.65
hsa-miR-132-5p@chr17:1953259-1953280:-	21.3868	52.41	4.5461	4.83
hsa-miR-1247-5p@chr14:102026699-102026720:-	32.2395	50.47	0.189798	0.00
hsa-miR-5581-3p@chr1:37966536-37966557:-	15.1594	15.58	24.7912	26.74
hsa-miR-548a-3p@chr6:135560358-135560379:+	13.6434	27.60	14.5873	26.05
hsa-miR-193a-5p@chr17:29887035-29887056:+	12.9544	57.64	2.47641	8.80
hsa-miR-1291@chr12:49048277-49048300:-	34.0524	22.04	8.26857	16.87
hsa-miR-139-3p@chr11:72326110-72326131:-	26.3136	52.49	1.1659	0.66
hsa-miR-135a-5p@chr12:97957612-97957634:+	9.35638	54.85	6.52214	9.19
hsa-miR-483-5p@chr11:2155411-2155432:-	39.4661	39.63	0	0.16

Table A1
Normalized small RNA seq read counts
Number of reads as RPM (reads per million) for the 505 most highly expressed miRNAs across all four samples. The top 505 miRNAs account for 99% of all mapped reads.

APPENDIX II

Cell Line Panel: CDX1Expression

APPENDIX II: CELL LINE PANEL: CDX1 EXPRESSION

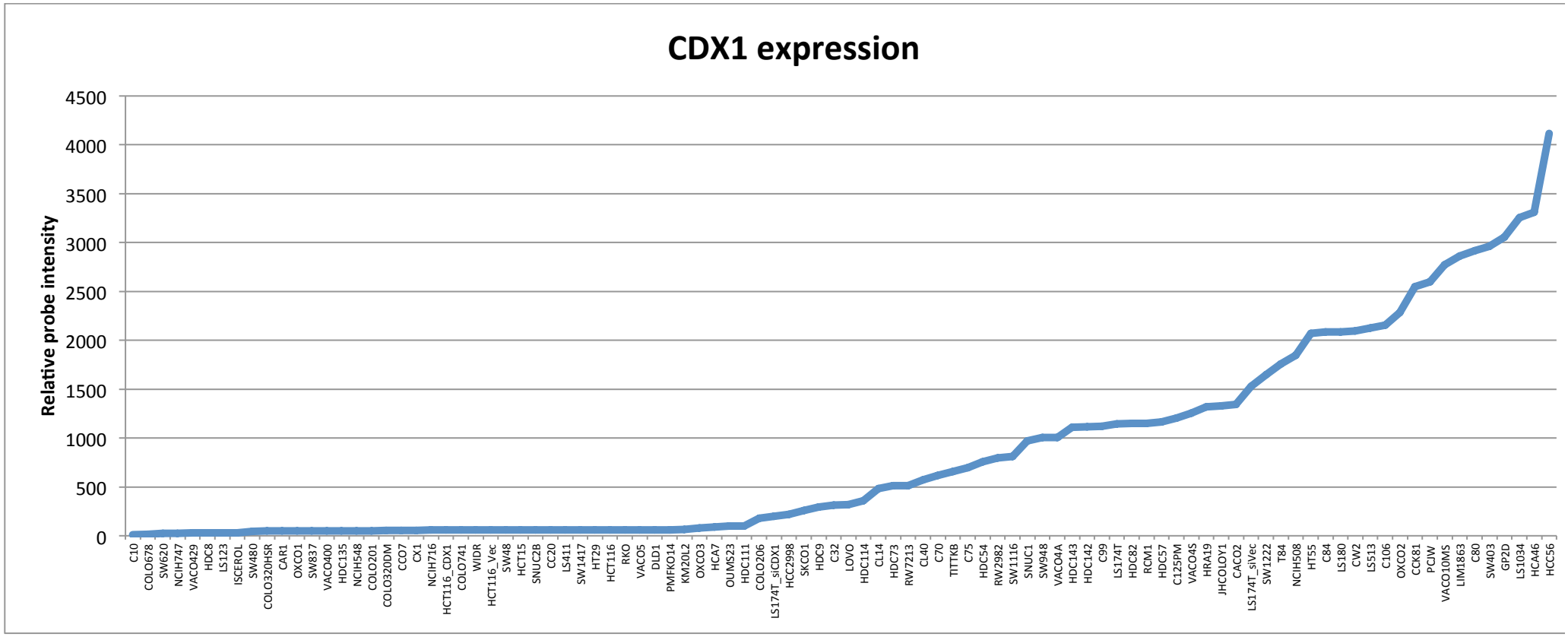

Figure A1
CDX1 Expression levels in 95 colorectal cancer cell lines
In an unpublished microarray study, the transcriptome-wide mRNA levels of 95 colorectal cancer cell lines were profiled. Here we display relative CDX1 probe intensity for these cell lines. Comparison with the results of Wong, et al., 2005 shows that the striking variation in CDX1 expression is likely to be due to CpG island methylation at the CDX1 promoter.

APPENDIX III

Microarray Data

APPENDIX III: MICROARRAY DATA

Gene Name	Accession No.	Illumina Probe ID	Chr.	Fold change	Adj. p-value
TMSB15A	NM_021992.2	1740291	X	0.077213665	0.000131
MGC39900	NM_194324.1	70270	X	0.077481731	0.000131
MGC39900	NM_194324.1	4200070	X	0.089871033	0.000199
PBK	NM_018492.2	3420554	8	0.093687475	0.000231
KIF20A	NM_005733.1	1050195	5	0.108292107	0.000199
DLGAP5	NM_014750.3	240221	14	0.10866807	0.000199
NEK2	NM_002497.2	4610669	1	0.112033337	0.000199
CCNB2	NM_004701.2	5360070	15	0.116145084	0.000199
HMMR	NM_012485.1	4060064	5	0.116790918	0.000199
HMMR	NM_012484.1	4050400	5	0.118175265	0.000371
DLGAP5	NM_014750.3	5220095	14	0.121329309	0.000231
MCM10	NM_018518.3	7570181	10	0.124481219	0.000242
BIRC5	NM_001168.2	1230682	17	0.127096834	0.000318
NCAPG	NM_022346.3	1450280	4	0.1301277	0.00038
NUSAP1	NM_018454.5	1500553	15	0.130398574	0.000231
BUB1	NM_004336.2	2070224	2	0.131214585	0.000231
TOP2A	NM_001067.2	3990619	17	0.133600749	0.000199
ASF1B	NM_018154.2	2630673	19	0.134157536	0.001184
CCNA2	NM_001237.2	2650608	4	0.13860008	0.000224
CDC2	NM_001786.2	1050706	10	0.139467415	0.000199
AURKB	NM_004217.2	6770026	17	0.140048652	0.000318
FBLN1	NM_006486.2	4830685	22	0.141414308	0.000242
LOC158345	XR_017130.1	3890747	9	0.143189737	0.000199
DEPDC1	NM_017779.3	6200201	1	0.144285677	0.00045
COCH	NM_004086.1	4120424	14	0.145188591	0.000683
CDC20	NM_001255.2	1500010	1	0.145894763	0.000242
TTK	NM_003318.3	5870725	6	0.145995924	0.000227
HMGB2	NM_002129.2	7610537	4	0.14629983	0.00026
GINS2	NM_016095.1	6020735	16	0.147624083	0.000199
BTF3L4	NM_152265.2	5490730	1	0.147828875	0.000231
FOXM1	NM_021953.2	540053	12	0.147931378	0.000242
ASPM	NM_018136.3	6130441	1	0.150308656	0.000673
CENPA	NM_001042426.1	2600392	2	0.151459083	0.000231
HJURP	NM_018410.3	3180367	2	0.157017798	0.000772
PRC1	NM_199413.1	2070494	15	0.160650792	0.000231
CDC25C	NM_022809.2	3460152	5	0.161768207	0.00036
HMGB2	NM_002129.2	5900482	4	0.162555018	0.000554
CKAP2L	NM_152515.2	6380324	2	0.162893394	0.000678
CDC25A	NM_001789.2	2480341	3	0.163006342	0.000336

UBE2C	NM_181800.1	4260368	20	0.163345657	0.000231
FAM64A	NM_019013.1	5870193	17	0.165167301	0.000231
CEP55	NM_018131.3	7510709	10	0.16539643	0.000305
BTF3L4	NM_152265.1	1170717	1	0.168170901	0.000285
MND1	NM_032117.2	7550730	4	0.168287509	0.000231
ANLN	NM_018685.2	6450669	7	0.168404197	0.000376
BRWD1	NM_001007246.1	5080066	21	0.168871761	0.000231
LOC400455	XR_018793.1	7000228		0.168988854	0.000231
CBFB	NM_001755.2	2600537	16	0.171110477	0.000231
KIF2C	NM_006845.2	1470647	1	0.171466661	0.000683
UBE2C	NM_181803.1	5310471	20	0.17206195	0.000242
KIF23	NM_004856.4	4120278	15	0.174101435	0.000267
KIF14	NM_014875.1	2810201	1	0.174584817	0.000875
CDCA5	NM_080668.2	1400673	11	0.175555609	0.000253
CCNB1	NM_031966.2	4590040	5	0.178006274	0.000231
FOXM1	NM_202003.1	2650364	12	0.178253215	0.001478
KIAA0101	NM_014736.4	5090754	15	0.180116219	0.000231
PPP1CA	NM_001008709.1	3990368	11	0.180241109	0.000231
LOC646688	XR_038043.1	6280370	1	0.182124889	0.000242
TRIP13	NM_004237.2	5700373	5	0.183137609	0.000231
RPL4	NM_000968.2	4250445	15	0.18351883	0.000231
POLQ	NM_199420.3	4060056	3	0.183773417	0.000351
MCM10	NM_018518.3	6580685	10	0.183773417	0.000365
TK1	NM_003258.2	4730196		0.185308376	0.000231
KIFC1	NM_002263.2	7330674	6	0.185436867	0.000365
FANCI	NM_018193.2	3170066	15	0.187115373	0.001771
SNORD13	NR_003041.1	7210035	8	0.187504874	0.00049
MYB	NM_005375.2	7380670	6	0.187504874	0.001594
NMU	NM_006681.1	7050220	4	0.193177637	0.000242
EGR1	NM_001964.2	870338	5	0.194117219	0.000242
ZWINT	NM_001005413.1	3800474	10	0.194521294	0.000393
SCARNA8	NR_003009.1	2600403	9	0.195738574	0.000267
MELK	NM_014791.2	2340392	9	0.197784325	0.000292
CDCA8	NM_018101.2	4830634	1	0.198333461	0.000515
NUSAP1	NM_018454.5	6350053	15	0.1986086	0.000231
PSRC1	NM_001032290.1	1070762	1	0.198746313	0.000242
CDCA3	NM_031299.3	6370474	12	0.199160024	0.000572
CENPF	NM_016343.3	4780129	1	0.199298119	0.000231
CDC45L	NM_003504.3	2320170	22	0.200684347	0.000231
CDCA2	NM_152562.2	2940398	8	0.202360554	0.002704
CCNE2	NM_057735.1	4760154	8	0.203063099	0.000318
B3GALNT1	NM_033168.2	2970040	3	0.203626891	0.000267

FEN1	NM_004111.4	1010719	11	0.203768083	0.000255
FEN1	NM_004111.4	3370703	11	0.203768083	0.000313
MELK	NM_014791.2	160097	9	0.204050762	0.000231
CENPA	NM_001042426.1	4760577	2	0.204475515	0.000527
CENPN	NM_018455.3	6550373	16	0.206040521	0.000615
TOR1AIP1	NM_015602.2	20403	1	0.206469416	0.001101
PRR11	NM_018304.2	2370072	17	0.208049684	0.000665
ACAT2	NM_005891.2	7330753	6	0.20891674	0.000242
CMTM6	NM_017801.2	1470520	3	0.211979991	0.000242
PTTG1	NM_004219.2	10414	5	0.213454429	0.00026
CDT1	NM_030928.2	2630433	16	0.215237297	0.00139
SNORA28	NR_002964.1	1780008	14	0.216884672	0.000318
MAD2L1	NM_002358.2	870546	4	0.21733614	0.000373
CDKN3	NM_005192.2	5260014	14	0.217637641	0.000242
RAD51AP1	NM_006479.3	4150196	12	0.21793956	0.00132
AURKA	NM_198434.1	5420309	20	0.219455449	0.000365
CGNL1	NM_032866.3	110100	15	0.219912269	0.000554
CDC25C	NM_001790.3	4200451	5	0.220217344	0.000434
GPSM2	NM_013296.3	1070292	1	0.223291463	0.000318
FBXO5	NM_012177.2	4010097	6	0.223446291	0.000242
LOC646688	XR_037673.1	5490202		0.223446291	0.000318
CDC2	NM_001786.2	2760603	10	0.225468845	0.00058
EREG	NM_001432.2	610170	4	0.226094844	0.000554
SMC4	NM_001002800.1	7380102	3	0.226408496	0.000458
KIF11	NM_004523.2	4060176	10	0.226722582	0.00167
NEK2	NM_002497.2	1570309	1	0.226879789	0.000554
CDCA4	NM_145701.1	290333	14	0.227194529	0.000365
PHF19	NM_001009936.1	5550402	9	0.228141372	0.001595
PTTG1	NM_004219.2	1510291	5	0.230366047	0.000536
C6orf173	NM_001012507.1	540215	6	0.230366047	0.001222
FAM72D	NM_207418.2	1090725	1	0.23116582	0.000667
LOC399942	XM_934471.1	1740673	11	0.231647015	0.000773
SPC25	NM_020675.3	1070411	2	0.232451236	0.000554
TROAP	NM_005480.2	4760646	12	0.233258248	0.000993
PHGDH	NM_006623.2	240086	1	0.233905874	0.000292
SNORA67	NR_002912.1	1240577	17	0.234717937	0.000318
KIAA1199	NM_018689.1	110181	15	0.234880687	0.000504
TOR1AIP1	NM_015602.2	6290524	1	0.235369616	0.000453
SGOL1	NM_138484.2	4610348	3	0.235532818	0.0017
PLK1	NM_005030.3	6130215	16	0.23618676	0.000612
KIF11	NM_004523.2	1110022	10	0.236514412	0.00127
ANKRD57	NM_023016.3	2510224	2	0.237171079	0.000613

KIAA1524	NM_020890.1	6280719	3	0.238820734	0.003236
TMPO	NM_003276.1	3400630	12	0.239317865	0.000544
KIF20B	NM_016195.2	5900433	10	0.23981603	0.00165
STIL	NM_003035.2	6220050	1	0.240648611	0.000524
DEPDC1B	NM_018369.1	2370441	5	0.240815474	0.000403
PTTG3P	NR_002734.1	5960224	8	0.240982452	0.000621
KDELC2	NM_153705.4	6110301	11	0.242490478	0.00037
LMNB1	NM_005573.2	3420593	5	0.242490478	0.002045
C11orf82	NM_145018.2	2570019	11	0.245024854	0.000673
SCARNA14	NR_004388.1	3140521	15	0.245194751	0.001636
PABPC4	NM_003819.2	5310278	1	0.246216611	0.000308
MND1	NM_032117.2	3870372	4	0.246558176	0.001541
GSG2	NM_031965.2	2900692	17	0.247929183	0.001225
UBXN2B	NM_001077619.1	4780731	8	0.24948068	0.000688
FAM83D	NM_030919.2	150543	20	0.25	0.000557
EXO1	NM_006027.3	1770646	1	0.25191344	0.000554
CENPV	NM_181716.2	1030026	17	0.25191344	0.000741
CENPK	NM_022145.3	5700086	5	0.25278802	0.002098
LMNB2	NM_032737.2	7570148	19	0.253138702	0.00036
OSBPL8	NM_001003712.1	3940358	12	0.254193668	0.000407
C13orf3	NM_145061.3	4180133	13	0.255253031	0.000857
SKA1	NM_145060.3	2030630	18	0.255607133	0.004411
NEIL3	NM_018248.1	1980039	4	0.257028457	0.00086
AURKA	NM_198436.1	4730605	20	0.257563488	0.000767
NRGN	NM_006176.1	6290747	11	0.25774208	0.000434
NUF2	NM_031423.3	2000458	1	0.258099634	0.000621
RACGAP1	NM_013277.2	2190010	12	0.258099634	0.00165
ESPL1	NM_012291.4	540224	12	0.258995691	0.001242
DEPDC1B	NM_018369.1	7330338	5	0.260977982	0.000875
SGOL2	NM_152524.3	3520754	2	0.26170257	0.003769
CENPE	NM_001813.2	2510639	4	0.261884032	0.005146
FAM129A	NM_052966.2	4230735	1	0.262247332	0.00093
DCK	NM_000788.1	5290703	4	0.264071406	0.00122
WDR51A	NM_015426.2	6660446	3	0.26425451	0.003745
GAS2L3	NM_174942.1	6400356	12	0.266277051	0.002704
MLF1IP	NM_024629.2	2120678	4	0.266646445	0.000554
DSCC1	NM_024094.1	3890372	8	0.266646445	0.001065
ZWINT	NM_001005413.1	3120307	10	0.267757706	0.000554
ADAM19	NM_033274.2	6900209	5	0.267943366	0.000665
SNORA63	NR_002586.1	4200711	3	0.268129154	0.000658
SMC4	NM_001002800.1	5910689	3	0.268315072	0.000995
HIBADH	NM_152740.2	2480136	7	0.268501118	0.000651

NCAPG2	NM_017760.5	1940632	7	0.269246594	0.000739
HMGB1L1	NM_001008735.1	6330039	20	0.269807059	0.000922
ITGAV	NM_002210.2	2690209	2	0.270931492	0.000615
UHRF1BP1	NM_017754.3	1240102	6	0.271872098	0.002027
PLK4	NM_014264.3	3190470	4	0.272249254	0.000697
FZD9	NM_003508.2	6200132	7	0.272249254	0.001709
SCARNA16	NR_003013.1	2030646	17	0.273005136	0.00052
SIX4	NM_017420.3	20653	14	0.273194435	0.000731
PRPS2	NM_001039091.1	7000521	X	0.273383864	0.001184
PRIM1	NM_000946.2	2140273	12	0.273763118	0.000613
RAD54L	NM_003579.2	1980291	1	0.273952942	0.001073
CTSL2	NM_001333.2	1430477	9	0.275476279	0.000683
BLM	NM_000057.2	2450717	15	0.275667291	0.001281
HADH	NM_005327.2	6290709	4	0.277008087	0.000651
CDC7	NM_003503.2	4900044	1	0.278355405	0.000731
SCARNA18	NR_003139.1	2750670	5	0.279321785	0.00102
ID3	NM_002167.2	7570324	1	0.280097304	0.000434
H2AFZ	NM_002106.3	2710292	4	0.281069731	0.00127
PPP1CA	NM_002708.3	4210414	11	0.281264621	0.00093
CLCC1	NM_015127.3	3610722	1	0.281654807	0.00058
ECT2	NM_018098.4	6840215	3	0.281850103	0.001184
HOXA10	NM_018951.3	510097	7	0.282241101	0.000554
PRPS2	NM_001039091.1	130619	X	0.283024726	0.000928
SCARNA23	NR_003007.1	2710427	X	0.283220971	0.005718
SPC24	NM_182513.1	5910349	19	0.283810526	0.001664
NDC80	NM_006101.1	1050470	18	0.284993318	0.003026
FANCG	NM_004629.1	4220612	9	0.285784584	0.000621
LIMS1	XM_938773.1	990358		0.287373712	0.000621
SNORA7B	NR_002992.2	7570110	3	0.287772373	0.000922
SCARNA20	NR_002999.2	1170497	17	0.287772373	0.001411
ERMP1	NM_024896.2	7380601	9	0.288371401	0.000554
ERCC6L	NM_017669.2	3370424	X	0.289372554	0.002309
UBA52	NM_003333.3	6550358	19	0.290175979	0.00088
LOC100132863	XR_036905.1	450546		0.292396916	0.000613
SLC40A1	NM_014585.3	730164	2	0.29259966	0.003767
TPX2	NM_012112.4	6290358	20	0.293005571	0.000621
OLFM1	NM_014279.4	2680072	9	0.293615493	0.000621
LOC729816	XR_042352.1	1850192	6	0.294226684	0.000685
CNTNAP2	NM_014141.4	1400520	7	0.295248165	0.000557
SNORA80	NR_002996.2	5260280	21	0.295248165	0.001242
E2F2	NM_004091.2	5340338	1	0.296273193	0.001225
LARP1B	NM_032239.2	5910164	4	0.296889917	0.001557

DONSON	NM_017613.2	990725	21	0.297095776	0.00104
	AK091091	510332	12	0.297301779	0.001043
CHAF1B	NM_005441.2	4610731	21	0.297507924	0.000928
PEG10	NM_001040152.1	7570630	7	0.297507924	0.000928
RRM1	NM_001033.2	2850575	11	0.298127218	0.000607
CENPV	NM_181716.2	10722	17	0.298127218	0.001184
SNORA79	NR_003021.2	1090196	14	0.298540797	0.002742
CCDC58	NM_001017928.2	3610300	3	0.298747801	0.000587
GTSE1	NM_016426.4	6980382	22	0.299577255	0.001483
ATAD2	NM_014109.2	1410242	8	0.299992846	0.000625
SNORA11B	NR_003709.1	3130278	14	0.299992846	0.000977
PRIM1	NM_000946.2	6200390	12	0.301451957	0.000896
IL17RB	NM_018725.3	1070152	3	0.304602566	0.001594
OGFRL1	NM_024576.3	2680079	6	0.304602566	0.001711
NBN	NM_002485.4	3610343	8	0.305660069	0.000922
MNS1	NM_018365.1	1090338	15	0.306296333	0.000802
INSIG1	NM_198336.1	360192	7	0.307572836	0.000965
SNORA42	NR_002974.1	6960438	1	0.307999518	0.002577
KAT2B	NM_003884.4	7200703	3	0.311434354	0.003217
FUBP1	NM_003902.3	20201	1	0.311650299	0.001222
RNY1	NR_004391.1	1010450	7	0.311650299	0.002014
CTHRC1	NM_138455.2	4860546	8	0.312082637	0.000631
ALS2CR4	NM_001044385.1	50348	2	0.312082637	0.000665
PHF19	NM_001009936.1	7650474	9	0.313600551	0.000878
SGK1	NM_005627.3	1410209	6	0.313600551	0.003329
TACC3	NM_006342.1	4390484	4	0.314907495	0.001829
SPC25	NM_020675.3	5860021	2	0.315125848	0.004948
RAB23	NM_016277.3	6020719	6	0.315563008	0.000793
ICK	NM_016513.3	4570524	6	0.315563008	0.000837
RAD54B	NM_012415.2	3190349	8	0.315563008	0.001594
	BG496257	2470450	8	0.317537746	0.001435
TERC	NR_001566.1	3420678	3	0.318198734	0.000708
CDKN2A	NM_058195.2	5550671	9	0.318198734	0.002269
LOC100130561	XM_001723189.1	2120377		0.318419369	0.000667
	AB074172	4010100	5	0.31930344	0.000837
CXorf57	NM_018015.4	6580626	X	0.320411981	0.00126
SRD5A1	NM_001047.2	1050278	5	0.321524371	0.00172
GPR177	NM_001002292.1	1570441	1	0.322640623	0.000802
CCNF	NM_001761.1	3130541	16	0.322864338	0.001148
SOX18	NM_018419.2	6100433	20	0.324434692	0.001012

ZDHHC2	NM_016353.3	2470243	8	0.324659651	0.005883
GMNN	NM_015895.3	4830373	6	0.325335464	0.000995
C6orf117	NM_138409.1	6040458	6	0.325561047	0.008837
FERMT2	NM_006832.1	1820328	14	0.325786787	0.000837
EXOC5	NM_006544.3	4250181	14	0.325786787	0.001576
RPL32	NM_001007074.1	6960220	3	0.326917837	0.001209
MCM7	NM_005916.3	730274	7	0.327371356	0.001165
NT5E	NM_002526.1	5960398	6	0.327371356	0.00136
KIF18A	NM_031217.2	2470035	11	0.327598351	0.001709
LIMCH1	NM_014988.1	1770754	4	0.328507907	0.001507
ELOVL5	NM_021814.3	4210129	6	0.32873569	0.000979
WEE1	NM_003390.2	2970332	11	0.329876978	0.001131
SGK1	NM_005627.3	2030324	6	0.329876978	0.003049
ORC6L	NM_014321.2	4830343	16	0.33010571	0.001677
CENPE	NM_001813.2	6100564	4	0.330563651	0.000928
SPAG5	NM_006461.3	4180709	17	0.332401777	0.003146
NUDT1	NM_198948.1	650347	7	0.332862903	0.000915
RHBDL3	NM_138328.2	3370725	17	0.332862903	0.003111
KCTD14	NM_023930.3	2940632	11	0.333093706	0.001237
SCARNA11	NR_003012.1	5310066	12	0.33401852	0.001912
LASS6	NM_203463.1	5690064	2	0.334481889	0.001148
FOXD1	NM_004472.2	3870500	5	0.334713814	0.001012
C13orf37	NM_001071775.2	3170187	13	0.334713814	0.001843
SCARA3	NM_016240.2	6420630	8	0.335410556	0.001974
TBL1X	NM_005647.2	2470070	X	0.335643126	0.001576
LHX2	NM_004789.3	5550142	9	0.336108749	0.001077
CCDC109B	NM_017918.3	1780259	4	0.336108749	0.001594
PSMC3IP	NM_016556.1	5960504	17	0.336808394	0.00132
C1orf112	NM_018186.2	940240	1	0.337509496	0.002413
CA8	NM_004056.4	1850097	8	0.337509496	0.003767
CKAP4	NM_006825.2	4490528	12	0.33985706	0.000837
RFC3	NM_002915.3	1780463	13	0.33985706	0.001248
C17orf58	NM_181656.3	3450176	17	0.340564509	0.000837
FANCD2	NM_001018115.1	2690240	3	0.341036959	0.000993
ID2	NM_002166.4	1260086	2	0.341273429	0.001261
POLA2	NM_002689.2	4920537	11	0.341746863	0.005612
B3GALNT1	NM_033167.2	1410370	3	0.342458245	0.013494
SNORA48	NR_002918.1	3360703	17	0.342695701	0.003964
RFC5	NM_007370.3	4890731	12	0.342933322	0.001086
NUP62CL	NM_017681.1	7100541	X	0.343647174	0.001716
PLOD1	NM_000302.2	60437	1	0.343647174	0.002892
C9orf100	NM_032818.2	6840039	9	0.343885455	0.006759

SKP2	NM_005983.2	4730674	5	0.3441239	0.001271
SLC1A3	NM_004172.3	4210403	5	0.344601288	0.001412
PRPF38A	NM_032864.3	4260184	1	0.345079338	0.00093
LOC100129342	XM_001718736.1	3310762	1	0.345318612	0.003317
NOXO1	NM_144603.2	20338	16	0.346037429	0.002816
ID2	NM_002166.4	1660296	2	0.346517471	0.000802
C1orf41	NM_016126.1	6450273	1	0.346757742	0.001597
GINS3	NM_022770.2	3060192	16	0.347238784	0.001983
03-Sep	NM_019106.4	4890021	22	0.347479555	0.00122
RFC4	NM_002916.3	7210435	3	0.347961598	0.00149
EML1	NM_004434.2	1170093	14	0.349654021	0.001186
CENPO	NM_024322.1	4560682	2	0.349654021	0.00515
NES	NM_006617.1	670278	1	0.349896466	0.009458
PSMC3IP	NM_016556.1	3990148	17	0.35013908	0.001201
NFE2	NM_006163.1	510468	12	0.35013908	0.001209
LOC653874	XM_936215.1	7330301		0.35013908	0.002791
DUT	NM_001025249.1	6330494	15	0.351354675	0.001636
KCNMB4	NM_014505.4	870468	12	0.351354675	0.001927
LOC647276	XR_017675.2	2810521	3	0.352086057	0.001594
PLS3	NM_005032.3	2190603	X	0.352330189	0.001257
10-Sep	NM_144710.2	3710386	2	0.352330189	0.001454
SNORD46	NR_000024.2	4210044	1	0.353308411	0.009485
SGK	NM_005627.2	4390450	6	0.353553391	0.003794
LOC653820	XM_930579.2	3440424	1	0.354289349	0.00139
GMPS	NM_003875.2	2480630	3	0.354535009	0.001441
STMN1	NM_203401.1	3460707	1	0.354535009	0.002212
CADPS2	NM_017954.9	7160102	7	0.354780839	0.004746
SNORA62	NR_002324.1	5870475	3	0.355273011	0.001383
NCALD	NM_032041.1	60093	8	0.355519353	0.013991
DNAJC9	NM_015190.3	50114	10	0.356259404	0.002327
NUDT21	NM_007006.2	3170446	16	0.356506429	0.001495
RECQL4	NM_004260.2	4250437	8	0.356753626	0.006796
PSRC1	NM_001032291.1	1510152	1	0.357000995	0.002098
AASDHPPT	NM_015423.2	7040717	11	0.357248535	0.001594
DYNLL2	NM_080677.1	3400551	17	0.357248535	0.002476
CKAP2	NM_001098525.1	1050672	13	0.357496247	0.001184
OSBPL8	NM_020841.4	3170274	12	0.357496247	0.003485
KLHDC5	NM_020782.1	4490273	12	0.357992185	0.00127
BMP6	NM_001718.4	6980064	6	0.357992185	0.009211
LOC730534	XR_015150.1	1450674		0.358737384	0.00149
B3GALNT1	NM_033167.2	5490672	3	0.358737384	0.030421
HMGN2	NM_005517.2	4050541	1	0.359484133	0.002704

LOC728715	XM_001128260.1	6770746	12	0.35998283	0.001849
COBLL1	NM_014900.3	5080601	2	0.35998283	0.004831
ERCC6L	NM_017669.2	5050181	X	0.35998283	0.021859
RPRML	NM_203400.1	7560497	17	0.360232437	0.001716
KIAA1618	NM_020954.2	7400743	17	0.360232437	0.003236
EPDR1	NM_017549.3	6400044	7	0.361483074	0.00163
RUNX1	NM_001754.3	7400368	21	0.361733721	0.011756
LOC731314	XM_001129173.1	4120538		0.361984543	0.001829
ARL2BP	NM_012106.3	2570523	16	0.361984543	0.001974
BMPR2	NM_001204.5	460730	2	0.361984543	0.004424
HMGB1L1	NM_001008735.1	3990202	20	0.362486708	0.003788
LOC653226	XM_927451.2	5390037	10	0.36298957	0.001344
KDELR3	NM_016657.1	540129	22	0.363493129	0.001304
LOC645058	XM_930423.1	1980600	1	0.363493129	0.001605
FOXA1	NM_004496.2	830056	14	0.363745171	0.00149
ITGB1	NM_033668.1	110440	10	0.363997387	0.002133
CEP78	NM_032171.1	4760091	9	0.365261095	0.00197
HIRIP3	NM_003609.2	1770717	16	0.365514362	0.00296
NUDT15	NM_018283.1	3450370	13	0.365767805	0.003045
TOP1P2	NR_001283.1	2230279	22	0.365767805	0.003584
FAM19A3	NM_182759.2	2100093	1	0.366021424	0.005088
ZCCHC12	NM_173798.2	2690279	X	0.366783336	0.002053
RAB11FIP2	NM_014904.1	4760630	10	0.367292158	0.002803
RAB23	NM_016277.3	3930047	6	0.367801686	0.006162
HAT1	NM_003642.2	3420068	2	0.368567304	0.002704
PBX3	NM_006195.4	2470634	9	0.368822864	0.003059
GINS4	NM_032336.1	3060433	8	0.369078601	0.002692
SLC39A8	NM_022154.5	3120543	4	0.369334516	0.00136
CPD	NM_001304.3	6020543	17	0.369334516	0.001729
TAF9L	NM_015975.3	610403	X	0.37035995	0.001504
CENPM	NM_001002876.1	1450192	22	0.37035995	0.001573
DLEU2	XR_001514.1	1500661	13	0.37035995	0.00287
STMN1	NM_005563.3	4260731	1	0.370616752	0.002048
RNASEH2A	NM_006397.2	4230068	19	0.37138823	0.001398
KIAA1467	NM_020853.1	1580333	12	0.371645746	0.001622
SCARA3	NM_182826.1	2190278	8	0.371903441	0.006205
CHM	NM_000390.2	780376	X	0.372161314	0.002617
EXO1	NM_006027.3	2690458	1	0.372161314	0.003113
RNASEL	NM_021133.2	110064	1	0.372419366	0.01149
SLC25A4	NM_001151.2	6840747	4	0.372677597	0.001974
BARD1	NM_000465.1	5080561	2	0.372677597	0.003158
SGOL1	NM_001012413.	7150128	3	0.373712312	0.011915

FAM54A	NM_001099286.1	4220544	6	0.3747499	0.010227
LAMP3	NM_014398.2	7320546	3	0.375009747	0.003436
SNX13	NM_015132.3	1500307	7	0.375529982	0.00172
TMEM194A	NM_015257.2	4610066	12	0.375529982	0.005815
RFC4	NM_181573.1	2030315	3	0.37579037	0.001949
SNORA27	NR_002575.1	6420647	13	0.37579037	0.003026
USP1	NM_001017416.1	1170689	1	0.376050938	0.001594
OAS3	NM_006187.2	990768	12	0.376050938	0.001597
RFC3	NM_002915.3	3890309	13	0.376050938	0.004093
EME1	NM_152463.1	1260398	17	0.377095019	0.00187
C8orf13	NM_053279.1	4010184	8	0.377095019	0.002941
C17orf58	NM_181656.3	3440703	17	0.377618146	0.001594
SCARNA21	NR_003000.1	2120370	17	0.377618146	0.002738
DLG5	NM_004747.3	6510215	10	0.377879982	0.003949
TMTC3	NM_181783.2	20273	12	0.378141999	0.001709
SCARNA22	NR_003004.1	5960176	4	0.378404198	0.003636
CDCA4	NM_145701.1	6520528	14	0.378929142	0.001829
LOC148915	XM_937758.1	3310392		0.379191886	0.001625
PDLIM3	NM_014476.1	6330008	4	0.379981214	0.001874
UBE2T	NM_014176.2	2480722	1	0.380244688	0.001594
LOC651816	XM_941060.1	1570746		0.380244688	0.002045
HOXA10	NM_153715.2	3290427	7	0.381036208	0.009813
TRMT5	NM_020810.1	5960253	14	0.381300413	0.001511
C17orf58	NM_181656.1	650168	17	0.381564802	0.001974
AP3M2	NM_006803.2	3420128	8	0.381829374	0.001677
GPR137C	NM_001099652.1	2640300	14	0.381829374	0.002098
BCL2L12	NM_001040668.1	7550753	19	0.382359069	0.001716
C1orf135	NM_024037.1	150129	1	0.382624192	0.002116
MPP1	NM_002436.2	5310554	X	0.383686524	0.00132
DUT	NM_001025248.1	6280242	15	0.383686524	0.009898
DICER1	NM_030621.2	5130091	14	0.384485208	0.01285
DHRS2	NM_182908.3	4890671	14	0.384751805	0.002026
CCDC5	NM_138443.2	2230681	18	0.385285554	0.003001
BMI1	NM_005180.5	1090292	10	0.385285554	0.004654
ERCC8	NM_001007234.1	160168	5	0.385820044	0.018593
MBOAT2	XM_001129292.1	5080468		0.386087567	0.012699
RASL11B	NM_023940.2	3370129	4	0.386355275	0.043414
EXOSC9	NM_001034194.1	6220142	4	0.387696603	0.001507
BCL2L12	NM_001040668.1	6420379	19	0.388234438	0.00191

PAX6	NM_001604.3	1740100	11	0.388234438	0.008777
MT1F	NM_005949.2	4220672	16	0.389312346	0.001636
SLC16A9	NM_194298.1	6290161	10	0.38958229	0.002205
SNORD16	NR_002440.1	1430427	15	0.38958229	0.004735
HIST1H4C	NM_003542.3	3890349	6	0.389852421	0.003491
FBLN1	NM_001996.2	580739	22	0.390934822	0.001829
GGH	NM_003878.1	2510338	8	0.391477148	0.001594
ENTPD7	NM_020354.2	3360382	10	0.392292049	0.002947
FAIM	NM_001033030.1	6110575	3	0.392292049	0.005805
ZAK	NM_016653.2	3360431	2	0.393108646	0.002045
MSRB3	NM_198080.2	4290088	12	0.393653988	0.001734
TIMELESS	NM_003920.2	4180050	12	0.394200087	0.002687
C6orf72	NM_138785.1	360017	6	0.394746943	0.003964
ANG	NM_001097577.1	3930392	14	0.395020656	0.002687
CAMTA1	NM_015215.1	3930411	1	0.395020656	0.003158
AASDHPPT	NM_015423.2	6060767	11	0.395568651	0.002135
PDE5A	NM_001083.3	1770333	4	0.395568651	0.013655
SNORA38B	NR_003706.2	380017	17	0.396666922	0.008601
HBXIP	NM_006402.2	6860653	1	0.396941965	0.002307
TGM2	NM_198951.1	2940446	20	0.3972172	0.002476
LOC100130932	XM_001726766.1	2570379	19	0.397492625	0.002791
TSPAN13	NM_014399.3	6660131	7	0.397768242	0.001945
ZAK	NM_133646.2	4670059	2	0.398044049	0.003566
DEF8	NM_017702.2	3130010	16	0.398320048	0.001636
SNORA9	NR_002952.1	2750523	7	0.398320048	0.04531
SLC39A8	NM_022154.5	2320358	4	0.398596238	0.001703
LOC100129267	XR_037397.1	5270551		0.39887262	0.001974
PHLDB2	NM_145753.1	3780441	3	0.399425958	0.0017
PAK6	NM_020168.3	2030735	15	0.399702915	0.01051
LOC729082	XR_040993.1	3400086		0.400257405	0.004464
MT1G	NM_005950.1	1170300	16	0.400257405	0.043341
MCM4	NM_005914.2	6020170	8	0.400534939	0.00195
C15orf42	NM_152259.3	5270402	15	0.400534939	0.004357
ORC1L	NM_004153.2	6660333	1	0.400534939	0.010315
CEP78	NM_001098802.1	5570142	9	0.401368694	0.00149
TSPAN13	NM_014399.3	3420452	7	0.401368694	0.00165
C12orf32	NM_031465.2	3180553	12	0.401646998	0.003317
HIATL1	NM_032558.2	4640427	9	0.402204185	0.001507
PPIH	NM_006347.3	5130241	1	0.402204185	0.00167
OIP5	NM_007280.1	7000161	15	0.402204185	0.002033
ERBB3	NM_001005915.1	3120608	12	0.402204185	0.003861

CYBRD1	NM_024843.2	2370300	2	0.402762146	0.002205
BRI3BP	NM_080626.5	6450474	12	0.402762146	0.002941
SEMA3A	NM_006080.2	6900114	7	0.403600537	0.003165
FAM71E1	NM_138411.1	1410470	19	0.403600537	0.00371
RHOBTB3	NM_014899.3	5870474	5	0.403880389	0.002613
MYT1	NM_004535.2	1450468	20	0.404440674	0.002694
EBP	NM_006579.1	4250156	X	0.404721108	0.001716
PLCE1	NM_016341.3	6220687	10	0.404721108	0.024715
TMEM45A	NM_018004.1	4610341	3	0.40584479	0.004075
NUP210	NM_024923.2	2320215	3	0.406126198	0.001636
BMPR2	NM_001204.5	6060475	2	0.406126198	0.002747
CUL5	NM_003478.3	6060025	11	0.406126198	0.005612
SNORA7A	NR_002582.1	4010193	3	0.406126198	0.008839
LOC389816	NM_001013653.1	2140541	9	0.406689599	0.001874
MDK	NM_001012333.1	7150437	11	0.406971593	0.002212
MRPL43	NM_032112.2	3060184	10	0.407253782	0.00165
CAMK2D	NM_001221.2	1110364	4	0.407253782	0.003329
ITGB1	NM_033669.1	650066	10	0.407818747	0.001684
ST3GAL6	NM_006100.2	5260440	3	0.407818747	0.006896
ROR1	NM_005012.2	3890132	1	0.408101523	0.001716
ACAA2	NM_006111.1	1450093	18	0.408101523	0.004388
MATN2	NM_002380.3	5810746	8	0.408101523	0.016792
LOC389662	XR_016813.2	4760544	8	0.408667664	0.002409
SORT1	NM_002959.4	160019	1	0.408667664	0.004045
MIS12	NM_024039.1	1050017	17	0.408951029	0.001949
SUV39H1	NM_003173.2	20195	X	0.409234591	0.002661
OGFRL1	NM_024576.3	6840347	6	0.409234591	0.002816
NCAPD2	NM_014865.2	2680497	12	0.409518349	0.001829
LRRC26	NM_001013653.2	7150270	9	0.409802304	0.003023
FAM171B	NM_177454.3	6060026	2	0.410086456	0.003236
ARSB	NM_000046.2	270215	5	0.410086456	0.005194
C17orf53	NM_024032.2	4570224	17	0.410370804	0.002062
SESTD1	NM_178123.3	670202	2	0.410370804	0.002409
LHX6	NM_199160.2	7550193	9	0.410370804	0.002661
TSPAN7	NM_004615.2	3840767	X	0.41065535	0.002572
MCM3	NM_002388.3	6290494	6	0.41065535	0.003785
GRP	NM_001012513.1	160500	18	0.41065535	0.010655
	AF131784	7040682	18	0.41065535	0.019476
GRRP1	NM_024869.2	1710270	1	0.410940094	0.011569
MAP6D1	NM_024871.1	2680538	3	0.411225034	0.002204
MAP3K1	NM_005921.1	4230373	5	0.411225034	0.003008
MCM3	NM_002388.3	6650053	6	0.411225034	0.003862

KDELR3	NM_006855.2	3360053	22	0.411510173	0.003008
SGK3	NM_170709.1	6510500	8	0.411795509	0.004458
GPER	NM_001039966.1	520463	7	0.412081042	0.005243
KCNK13	NM_022054.2	990112	14	0.412366774	0.014987

Table A2
500 most significantly downregulated genes in miR-215 microarray
Genes listed in ascending order by fold change. Fold change given as miR-215/control. P-value adjusted for multiple testing using the Bonferroni correction.

Gene Name	Accession No.	Illumina Probe ID	Chr.	Fold Change	Adj. p-value
TP53I3	NM_147184.1	1260020	2	6.935500508	0.000199
ORM1	NM_000607.1	2850315	9	6.87805189	0.000231
RPS23	NM_001025.4	380070	5	6.750526369	0.000231
LOC728285	XM_001127070.1	3940673	17	6.324712933	0.000199
LOC642934	XM_942991.2	7040482		5.775716782	0.000231
LOC644350	XM_927511.3	6370246	17	4.927992294	0.000242
	XM_059047	1660056		4.783279187	0.000554
TTYH3	NM_025250.2	770754	7	4.737086447	0.000683
NADSYN1	NM_018161.4	3370575	11	4.665397479	0.000393
ANKRD19	NM_001010925.2	2480040		4.610745387	0.000308
WBSCR27	NM_152559.2	2810326	7	4.553576116	0.000554
FCGBP	NM_003890.1	130609	19	4.487773922	0.000554
AGPAT4	NM_020133.2	3440025	6	4.392371255	0.000365
C20orf108	NM_080821.2	770561	20	4.325899054	0.000977
SYTL1	NM_032872.1	2760437	1	4.254530692	0.002582
TPMT	NM_000367.2	840014	6	4.236873339	0.000304
GDF15	NM_004864.1	5090671	19	4.225142501	0.000313
COL17A1	NM_000494.3	990372	10	4.169863043	0.001557
ORM2	NM_000608.2	450020	9	4.143931054	0.000631
ANO9	NM_001012302.2	5720373	11	4	0.001787
MYEOV	NM_138768.2	6100360	11	3.983399012	0.000515
SHISA5	NM_016479.3	160731	3	3.966866923	0.00045
C10orf46	NM_153810.4	4070598	10	3.950403446	0.000434
ASS1	NM_000050.4	110433	9	3.91768119	0.00046
UBE2G1	NM_003342.4	150630	17	3.874472757	0.000403
CBS	NM_000071.1	1230047	21	3.858392738	0.001709
CYP4F3	NM_000896.1	4290110	19	3.821131746	0.001605
KRT80	NM_182507.2	4830520	12	3.805273105	0.000769
ALOX5	XM_001127464.1	1780273		3.73471978	0.001159
CYCS	NM_018947.4	6200554	7	3.71921977	0.00093
TNFSF9	NM_003811.2	5420441	19	3.693529243	0.000554

MRPS35	NM_021821.2	7380270	12	3.688412472	0.000434
MFSD3	NM_138431.1	1510703	8	3.688412472	0.000537
IDUA	NM_000203.3	7400259	4	3.688412472	0.00149
APOBEC3H	NM_181773.2	160292	22	3.660396673	0.001014
NHP2L1	NM_001003796.1	2230491	22	3.655325801	0.000544
ATHL1	NM_025092.3	4070239	11	3.61751751	0.001411
C7orf41	NM_152793.2	1740458	7	3.600007719	0.000508
LOC100134226	XM_001721602.1	3440543		3.592529492	0.000767
KIFC2	NM_145754.2	4210561	8	3.572663409	0.000515
FBXO44	NM_001014765.1	1010427	1	3.567714078	0.000812
PROM2	NM_144707.1	4120193	2	3.543070076	0.000982
HIST1H2BD	NM_138720.1	290730	6	3.489450823	0.000736
MSLN	NM_013404.3	1230228	16	3.487032958	0.000741
ASS1	NM_054012.3	2640544	9	3.47256091	0.000683
LAMB2	NM_002292.3	7650189	3	3.45575275	0.000651
PTGES	NM_004878.3	1510181	9	3.434261746	0.000662
ABHD14B	NM_032750.1	150064	3	3.422380103	0.001462
NHP2L1	NM_005008.2	2360445	22	3.379945538	0.000554
HIST1H2BD	NM_138720.1	6200669	6	3.356598548	0.000782
LOC729580	XM_001130700.1	20450	20	3.356598548	0.001059
CD97	NM_078481.2	6960630	19	3.34962595	0.000697
PTRH1	NM_001002913.1	6370044	9	3.347304971	0.001242
CLDND2	NM_152353.1	610154	19	3.317278183	0.001336
CEACAM1	NM_001024912.1	5700753	19	3.30351066	0.001165
SELI	NM_033505.2	4280370	2	3.285242803	0.002045
LOC652097	XM_941428.1	2470347		3.262549973	0.001242
AHNAK2	NM_138420.2	5260594	14	3.21986455	0.001727
HIST3H2A	NM_033445.2	1500192	1	3.202059243	0.001462
LOC731042	XM_001128223.1	7000543		3.199840513	0.000802
CLEC11A	NM_002975.2	1940048	19	3.175535724	0.001148
HIST2H2AA3	NM_003516.2	610451	1	3.157975547	0.000689
PLEKHG4	NM_015432.2	2640014	16	3.149231906	0.000958
FAM113A	NM_022760.3	290296	20	3.140512475	0.001248
C14orf78	XM_001132404.1	3390551		3.138336392	0.001478
HIST2H2AA3	NM_003516.2	1820592	1	3.127478573	0.001383
LOC340274	XR_017256.2	1070121	7	3.12314597	0.000665
HMOX1	NM_002133.1	6660601	22	3.12314597	0.001054
RINL	NM_198445.2	2900474	19	3.11881937	0.001504
TPD52L2	NM_199361.1	5080577	20	3.108029075	0.001377
LOC392871	XR_018049.2	4560673	7	3.09298535	0.000802
CDKN1A	NM_000389.2	6660382	6	3.073750363	0.000896
FRMD8	NM_031904.3	6510408	11	3.073750363	0.000995
INO80B	NM_031288.2	460221	2	3.046177479	0.002667
C19orf33	NM_033520.1	630470	19	3.041957506	0.001248

LOC653458	XM_001714697.1	7320075	9	3.039849713	0.001077
	BG209440	3850709	4	3.018851937	0.001373
TXNRD1	NM_001093771.1	730286	12	3.014669819	0.000773
JUND	NM_005354.3	620280	19	3.008407503	0.000736
MBP	NM_001025100.1	3780681	18	3.004239854	0.002321
MZF1	NM_198055.1	1030053	19	2.993845974	0.001334
CD97	NM_001784.3	1470626	19	2.989698497	0.00126
C14orf147	NM_138288.3	1410050	14	2.985556767	0.001478
EWSR1	NM_005243.2	3370291	22	2.981420774	0.001086
NDRG4	NM_022910.1	7330739	16	2.975227525	0.001231
C6orf141	NM_153344.1	3450632	6	2.971105841	0.000993
C9orf23	NM_148178.1	5130414	9	2.971105841	0.001133
EEF1A1	NM_001402.5	3360504	6	2.962879596	0.000802
EBI3	NM_005755.2	2810767	19	2.962879596	0.001184
IPPK	NM_022755.4	3390136	9	2.954676127	0.006986
INPP5D	NM_005541.3	3130609	2	2.950582914	0.000846
LOC341230	XR_018617.1	2690538		2.942413492	0.001263
TRAFD1	NM_006700.1	1570129	12	2.924114897	0.001982
C8ORFK29	XR_017725.1	60270	8	2.920064021	0.001436
TPD52L2	NM_003288.2	6270241	20	2.916018758	0.001145
LOC791120	NR_015357.1	4920706		2.911979098	0.000875
RBM12	NM_006047.4	2810328	20	2.911979098	0.003113
FXYD4	NM_173160.2	7100040	10	2.90794503	0.00126
HIST1H2AC	NM_003512.3	6590594	6	2.905930099	0.004662
TULP4	NM_001007466.1	4200440	6	2.889860796	0.001664
TP53INP1	NM_033285.2	5420538	8	2.889860796	0.002417
LOC728312	XR_042486.1	7330372		2.887858391	0.001263
RPL34	NM_000995.2	2490379	4	2.879862637	0.001787
LOC100131512	XM_001722891.1	1400189		2.87786716	0.006826
	AK092751	4060242	9	2.865923301	0.002178
CDKN1A	NM_078467.1	5290475	6	2.865923301	0.003058
DCST2	NM_144622.2	5860553	1	2.86195304	0.009702
LOC644322	XM_933391.1	6980220	9	2.859969973	0.001052
CABC1	NM_020247.4	6220180	1	2.856007959	0.001164
PLCD3	NM_133373.3	7380241	17	2.850075228	0.001576
CLN8	NM_018941.3	5130066	8	2.836280071	0.004927
C8ORFK29	XR_015602.1	3140561		2.828427125	0.001336
WIPI2	NM_016003.3	1410075	7	2.826467288	0.001248
SNCG	NM_003087.1	7000669	10	2.826467288	0.003714
QTRT1	NM_031209.1	2100563	19	2.814736751	0.001429
AKR1B10	NM_020299.3	5310646	7	2.8108374	0.001625
MNAT1	NM_002431.2	2060564	14	2.806943452	0.001537
TRABD	NM_025204.2	270736	22	2.803054898	0.001436
OSBPL7	NM_145798.2	1440575	17	2.799171731	0.001242

URM1	NM_030914.1	60390	9	2.799171731	0.001588
ALDH1A3	NM_000693.2	2360551	15	2.795293944	0.001257
CES2	NM_003869.4	3520372	16	2.793357065	0.00102
TMC4	NM_144686.1	1450348	19	2.791421528	0.001511
ALS2CL	NM_147129.2	4570630	3	2.785622961	0.018611
ARTN	NM_057091.1	6560494	1	2.774061938	0.001052
C15orf52	NM_207380.1	2230156	15	2.774061938	0.00132
GOLSYN	NM_001099743.1	2690411	8	2.758721844	0.001248
LOC642282	XM_925818.1	150259	4	2.758721844	0.003291
MVP	NM_005115.3	3360646	16	2.756810306	0.0018
MVP	NM_017458.2	160291	16	2.754900093	0.001306
GJB4	NM_153212.1	3850341	1	2.754900093	0.009092
SFN	NM_006142.3	3710040	1	2.747272467	0.002305
SIX5	NM_175875.3	5810672	19	2.74156561	0.001242
KLK5	NM_012427.4	3170687	19	2.737767626	0.001184
PGAM5	XM_001126125.1	1050021		2.737767626	0.002941
GRIN2C	NM_000835.3	1300678	17	2.72829567	0.00132
KIAA0247	NM_014734.2	3170093	14	2.72829567	0.002829
COL7A1	NM_000094.2	2490593	3	2.720741705	0.00319
EPHA2	NM_004431.2	6510332	1	2.707572558	0.001436
NAT6	NM_012191.2	5910039	3	2.707572558	0.001483
LOC100131138	XM_001717925.1	3520280		2.701948169	0.00155
DPM3	NM_153741.1	7320435	1	2.70007597	0.003303
ZBTB5	NM_014872.1	2640184	9	2.692600139	0.001184
CEACAM1	NM_001024912.1	4150014	19	2.687006851	0.002748
LOC644100	XM_927327.1	3390082	5	2.67585511	0.001248
WDR5	NM_017588.2	4850079	9	2.67585511	0.002071
LOC100128430	XM_001721612.1	6200170	13	2.672148157	0.029521
LOC146517	XM_928464.1	1110286	16	2.670296607	0.001891
PRKX	NM_005044.2	70139		2.668446339	0.002632
CAPNS1	NM_001749.2	7550041	19	2.668446339	0.002824
KRT80	NM_182507.2	2340193	12	2.666597354	0.0153
PFKL	NM_002626.4	5570242	21	2.662903226	0.001656
S100A3	NM_002960.1	150100	1	2.662903226	0.002766
FLJ41484	XR_042107.1	6520538		2.662903226	0.004607
RRAGB	NM_006064.3	6940397	X	2.655530317	0.001236
MOAP1	NM_022151.4	270224	14	2.648177821	0.00207
POLDIP3	NM_178136.1	5700370	22	2.642676811	0.0017
TJP3	NM_014428.1	3450524	19	2.640845682	0.00322
LOC100134144	XM_001717999.1	5340088		2.635359903	0.003614
TMEM43	NM_024334.1	2510392	3	2.633533844	0.003157
SESN1	NM_014454.1	1240553	6	2.626242251	0.002026
KRTAP2-1	XM_926554.2	6020382	17	2.622604028	0.001358
DNER	NM_139072.3	4570669	2	2.622604028	0.002978

SP100	NM_001080391.1	4200240	2	2.622604028	0.003767
CEL	NM_001807.3	6650593	9	2.620786808	0.005705
C7orf59	NM_001008395.2	4590615	7	2.618970846	0.003662
NDUFA10	NM_004544.2	6040291	2	2.609909895	0.001734
SMARCD1	NM_003076.3	3400593	12	2.606294299	0.00176
MAFG	NM_002359.2	6290328	17	2.602683711	0.001734
CPNE7	NM_153636.1	6130543	16	2.602683711	0.002182
LOC100133747	XM_001719129.1	2260500		2.602683711	0.003866
ZNF580	NM_016202.2	2140392	19	2.597277205	0.008774
LOC389342	XM_945799.3	5090484		2.591881931	0.050934
TP53INP1	NM_033285.2	6660630	8	2.590085998	0.001594
NSUN5C	NM_149379.1	2970167	7	2.590085998	0.001912
MAN2C1	NM_006715.2	150241	15	2.582914701	0.003157
NHP2L1	NM_001003796.1	4230243	22	2.579336501	0.0017
FAM119B	NM_015433.2	870056	12	2.577549261	0.001462
C9orf169	NM_199001.1	6450162		2.575763259	0.002914
TMEM139	NM_153345.1	1850170	7	2.575763259	0.003217
WFDC3	NM_181522.1	4280048	20	2.573978495	0.002026
LOC644100	XM_937388.1	6960402		2.572194967	0.003201
LAMA5	NM_005560.3	4040176	20	2.570412675	0.00175
RPL37	NM_000997.3	4280743	5	2.561519723	0.003317
ELF3	NM_004433.3	1510300	1	2.559744828	0.002027
RHOB	NM_004040.2	3400332	2	2.554427518	0.001625
LOC730020	XR_041245.1	1510520	7	2.554427518	0.001627
FAS	NM_152877.1	3420026	10	2.545589871	0.001912
ANO9	NM_001012302.2	3400121	11	2.543826013	0.006986
SRRM2	NM_016333.2	7570551	16	2.542063379	0.00149
CCND1	NM_053056.2	5820601	11	2.540301965	0.002409
YWHAB	NM_139323.2	1340521	20	2.538541772	0.003421
TMEM88	NM_203411.1	540288	17	2.535025044	0.007367
VPS28	NM_016208.2	1190110	8	2.529759085	0.001636
N-PAC	NM_032569.2	7100424	16	2.528006197	0.005394
TTLL3	NM_015644.3	870500	3	2.514026749	0.005412
NRBP2	NM_178564.2	4490142	8	2.510543983	0.002867
WDR63	NM_145172.2	5560730	1	2.510543983	0.004511
BAX	NM_138765.2	3520092	19	2.505328877	0.004075
OSBPL2	NM_144498.1	4180717	20	2.50185816	0.002157
C12orf23	NM_152261.1	3290379	12	2.500124605	0.003344
CRIPAK	NM_175918.2	4210653	4	2.488023307	0.003794
ECE2	NM_014693.2	4230368	3	2.488023307	0.004276
	DN997246	2450435	10	2.482854983	0.001974
LOC100133019	XM_001715216.1	3170220		2.482854983	0.006255
YPEL5	NM_016061.1	2680097	2	2.4794154	0.001594
TXNRD1	NM_182743.1	2320133	12	2.4794154	0.001857

CPA4	NM_016352.2	520682	7	2.4794154	0.002098
GDI1	NM_001493.1	830653	X	2.4794154	0.002687
CAPNS1	NM_001003962.1	5290500	19	2.475980582	0.001605
HEMK1	NM_016173.3	3420767	3	2.474264957	0.00786
SPNS2	NM_001124758.1	1110537	17	2.465704651	0.002418
	AK094914	3400709	9	2.463996147	0.001656
S100A14	NM_020672.1	1240093	1	2.46058269	0.001734
GLI4	NM_138465.3	2750209	8	2.46058269	0.006759
KCTD13	NM_178863.2	2100189	16	2.458877735	0.001534
GOLT1A	NM_198447.1	460082	1	2.457173961	0.006826
ALDH1A3	NM_000693.1	4920148	15	2.45206972	0.003744
FAM84B	NM_174911.3	60014	8	2.446976082	0.002662
TPK1	NM_001042482.1	1050079	7	2.446976082	0.005506
C22orf29	NM_024627.5	6110246	22	2.441893025	0.003877
SLC12A9	NM_020246.2	110450	7	2.440201021	0.001983
CYP2S1	NM_030622.6	6770474	19	2.438510188	0.002914
CUL9	NM_015089.2	6580491	6	2.435132037	0.002855
DENND2A	NM_015689.2	6100072	7	2.435132037	0.00405
CANX	NM_001024649.1	5860477	5	2.433444717	0.00302
ACY1	NM_000666.1	1400341	3	2.42670712	0.002662
ARHGDIA	NM_004309.3	4760255	17	2.42670712	0.004976
HIST2H2AA4	NM_001040874.1	4290148	1	2.425025638	0.004194
LOC644132	XR_017532.2	1510673	17	2.421666168	0.001631
HIST1H1C	NM_005319.3	5570279	6	2.421666168	0.00355
TRAF4	NM_004295.3	2650477	17	2.414961183	0.005729
C1orf188	NM_173795.2	4810348	1	2.413287839	0.004453
CHP	NM_007236.3	6760192	15	2.408274762	0.0039
MAFG	NM_032711.2	6180148	17	2.406606052	0.00256
RETSAT	NM_017750.2	940477	2	2.403272099	0.001949
JARID2	NM_004973.2	2320286	6	2.399942765	0.002274
LOC147727	NR_024333.1	5340653	19	2.399942765	0.00533
OPLAH	NM_017570.2	5050537	8	2.386671486	0.002084
C17orf91	NM_001001870.1	5290161	17	2.386671486	0.017778
AGXT2L2	NM_153373.1	5690082	5	2.385017745	0.008847
RWDD4A	NM_152682.2	5670164	4	2.383365149	0.002704
C6orf52	XM_938497.2	6040156		2.380063393	0.002045
KLK8	NM_007196.2	3840010	19	2.37841423	0.006988
LOC100131139	XR_037336.1	4480528		2.375119332	0.004205
SLCO1B3	NM_019844.2	4850576	12	2.375119332	0.008129
DEPDC6	NM_022783.1	3800095	8	2.373473595	0.003101
NDUFA10	NM_004544.2	510725	2	2.371828999	0.002524
PSORS1C1	NM_014068.1	2450270	6	2.371828999	0.005723
LOC100128326	XR_038006.1	5570465		2.368543224	0.004436
ECE2	NM_032331.3	630674	3	2.365262	0.001985

C7orf10	NM_024728.1	2470102	7	2.363623094	0.004662
LOC100130914	XR_037646.1	4880630		2.358713185	0.002371
KLK5	NM_001077491.1	6660274	19	2.358713185	0.003008
C1orf86	NM_182533.2	1570564	1	2.357078816	0.003217
SLC19A1	NM_194255.1	4760014	21	2.355445579	0.007344
PIK3C2B	NM_002646.2	4610180	1	2.350552657	0.006153
SLC22A18	NM_002555.3	7400053	11	2.350552657	0.007859
FDXR	NM_024417.1	1400441	17	2.347296357	0.018296
TMBIM4	NM_016056.2	2680128	12	2.344044567	0.002742
PNPLA7	NM_152286.2	5050577	9	2.344044567	0.011025
GRB7	NM_001030002.1	5900243	17	2.342420362	0.004352
C9orf23	NM_148178.1	1770338	9	2.337554497	0.005272
TRAPPC6A	NM_024108.1	6860072	19	2.337554497	0.005377
C12orf76	NM_207435.1	2510181	12	2.334316204	0.00244
CANX	NM_001746.3	1070402	5	2.334316204	0.004637
NARS2	NM_024678.3	5860592	11	2.33269874	0.003785
GJB3	NM_001005752.1	3420446	1	2.331082396	0.00343
TATDN1	NM_032026.1	1110167	8	2.327853069	0.002393
PPPDE2	NM_015704.1	380541	22	2.326240083	0.003769
TSPAN10	NM_031945.3	3310097	17	2.324628215	0.005194
HINFP	NM_198971.1	1690324	11	2.321407829	0.003335
FTHL2	NR_002200.1	4060561	1	2.319799309	0.003145
SGSM1	NM_001039948.2	840364	22	2.319799309	0.003388
IP6K2	NM_001005911.1	6660682	3	2.319799309	0.004886
SYCE1L	NM_001129979.1	3870050	16	2.319799309	0.007831
CDK10	NM_001098533.1	6130762	16	2.318191904	0.003862
ZNRD1	NM_014596.4	4890112	6	2.316585612	0.003022
LY96	NM_015364.2	70167	8	2.316585612	0.007945
CLDN15	NM_014343.1	3780291	7	2.313376368	0.003216
PIAS3	NM_006099.2	4570201	1	2.310171569	0.008618
RFNG	XM_001132711.1	2070376		2.308570835	0.003471
TSC22D1	NM_183422.1	380689	13	2.308570835	0.004276
HYAL1	NM_153282.1	1070400	3	2.308570835	0.014899
ETF1	NM_004730.1	3170181	5	2.30697121	0.005444
LOC729009	XR_042330.1	2810463	2	2.305372694	0.005357
MGC52282	NM_178453.2	380437	16	2.303775285	0.004961
SPHK2	NM_020126.3	3800725	19	2.302178983	0.005728
ABCA1	NM_005502.2	4060358	9	2.300583787	0.016736
LOC642567	XR_038054.1	5090382		2.29739671	0.005545
HKDC1	NM_025130.2	870301	10	2.295804828	0.003217
C5orf28	NM_022483.3	6200300	5	2.294214048	0.0039
APOBEC3C	NM_014508.2	3120221	22	2.291035796	0.033124
LTB4R	NM_181657.1	4250136	14	2.289448321	0.006759
PRKX	NM_005044.1	1470367	X	2.289448321	0.007612

LOC650257	XM_944121.1	3190243		2.287861946	0.007744
LOC654103	XM_939368.1	7320707		2.286276671	0.003794
UBE2G2	NM_003343.4	2750750	21	2.286276671	0.004464
BTG2	NM_006763.2	1010487	1	2.284692494	0.003491
LOC144383	XM_938223.2	2230561		2.283109414	0.00345
PMAIP1	NM_021127.1	2750367	18	2.281527432	0.01107
MIR129-1	NR_029596.1	1500731		2.281527432	0.023719
DEPDC6	NM_022783.1	870390	8	2.279946545	0.004019
VPS13A	NM_001018038.1	5050349	9	2.279946545	0.021277
FXYD1	NM_005031.3	3850500	19	2.278366754	0.002748
DPM3	NM_018973.3	2850520	1	2.276788058	0.002204
PDLIM7	NM_213636.1	4560164	5	2.275210456	0.0039
	AK130294	2060014	X	2.275210456	0.004005
FTH1	NM_002032.2	5220240	11	2.27205853	0.00301
C16orf52	NM_173501.1	60243	16	2.270484204	0.008809
ASMTL	NM_004192.2	430376	Y	2.26891097	0.008813
	AL137257	4180612	1	2.267338826	0.003477
ISG20L2	NM_030980.1	2690224	1	2.267338826	0.003657
HIST1H2BK	NM_080593.1	5050402	6	2.267338826	0.005483
GOLGA8B	NM_001023567.2	5690671	15	2.267338826	0.00856
LOC728934	XM_001128836.2	4150148	17	2.265767771	0.004849
ACTA2	NM_001613.1	6480059	10	2.265767771	0.006915
DDX17	NM_030881.2	1780709	22	2.262628926	0.004575
SH2D3A	NM_005490.1	5490452	19	2.262628926	0.019349
FOXD4L1	NM_012184.4	3390563	2	2.261061134	0.007273
MEGF6	NM_001409.3	6590220	1	2.259494429	0.005653
HYAL1	NM_153283.1	1980300	3	2.25792881	0.007938
SEMA3B	NM_001005914.1	430181	3	2.256364275	0.014292
ATP6V0A1	NM_005177.3	1660215	17	2.254800824	0.003138
SULF2	NM_018837.2	7200242	20	2.254800824	0.006759
ACAD11	NM_032169.4	3370136	3	2.248557848	0.002694
PABPC1L	XM_001722078.1	5490301		2.248557848	0.004662
TM7SF3	NM_016551.1	2070474	12	2.248557848	0.005537
LAMB3	NM_000228.2	730040	1	2.246999806	0.0039
PQBP1	NM_005710.2	4810228	X	2.246999806	0.014944
BLOC1S2	NM_001001342.1	2630743	10	2.243886961	0.003329
LOC440957	NM_001124767.1	540240	3	2.243886961	0.005194
CYB5D2	NM_144611.2	2630333	17	2.242332156	0.008879
ABCC5	NM_001023587.1	7610050	3	2.240778428	0.005558
LOC100132324	XR_039314.1	1300358	20	2.240778428	0.011092
SFRS2B	NM_032102.2	4490133	11	2.239225777	0.003123
AGXT2L2	NM_153373.1	870139	5	2.239225777	0.013634
OTUB1	NM_017670.1	4780707	11	2.237674202	0.002803
DGAT1	NM_012079.2	3610039	8	2.237674202	0.003785

	XM_373666	1260356		2.234574276	0.00444
GPR141	NM_181791.1	5050647	7	2.234574276	0.004976
	AV737943	6020692	5	2.233025924	0.004725
LCN2	NM_005564.3	4390398	9	2.233025924	0.018296
ACP2	NM_001610.1	2480025	11	2.231478645	0.004093
LYPLA2	NM_007260.2	6480088	1	2.229932437	0.0039
MMP23B	NM_006983.1	2450110	1	2.226843236	0.009898
DGKA	NM_201554.1	3170020	12	2.223758315	0.003669
LOC644799	XM_934554.1	1980176	20	2.223758315	0.003785
TMEM97	NM_014573.2	3890561	17	2.220677667	0.006703
ZNF79	NM_007135.1	5390347	9	2.219138944	0.006083
MOGS	NM_006302.2	4230309	2	2.219138944	0.007329
KLHL28	NM_017658.3	7330575	14	2.217601287	0.004093
HIST1H3D	NM_003530.3	2140524	6	2.217601287	0.009084
C19orf4	NM_012109.1	6960035	19	2.212994706	0.008612
BAIAP2	NM_006340.1	70767	17	2.211461307	0.006986
POP5	NM_198202.1	4560528	12	2.20992897	0.004377
NCDN	NM_014284.2	5310458	1	2.20686748	0.010403
FSTL3	NM_005860.2	2360356	19	2.205338326	0.005969
MST1	NM_020998.2	3710202	3	2.205338326	0.009697
CD70	NM_001252.3	4220068	19	2.200757219	0.009365
DUSP8	NM_004420.2	4890041	11	2.199232299	0.005587
LOC653257	XM_932654.1	4150735	22	2.199232299	0.037239
PPHLN1	NM_016488.5	1430706	12	2.197708435	0.00724
RSAD1	NM_018346.1	540382	17	2.197708435	0.011338
DVL3	NM_004423.3	1070612	3	2.194663875	0.013421
WDR81	NM_152348.1	5130594	17	2.194663875	0.019522
ZMAT1	NM_032441.1	4830047	X	2.194663875	0.032493
ZNRD1	NM_170783.1	4050673	6	2.193143177	0.008474
TRIML2	NM_173553.1	510577	4	2.191623533	0.00322
PLEKHB2	NM_017958.1	1470341	2	2.190104942	0.035456
PTPRM	NM_002845.2	5860356	18	2.188587403	0.003506
TMCC1	NM_001017395.1	6760471	3	2.188587403	0.008816
LOC286512	XR_038196.1	770187		2.187070915	0.007938
RALGDS	NM_006266.2	2140735	9	2.185555478	0.003023
SUPT16H	NM_007192.2	780753	14	2.185555478	0.003154
ATXN1L	NM_001137675.2	4220133	16	2.185555478	0.003398
LOC728908	XR_015892.1	4230487	17	2.184041091	0.004261
DOM3Z	NM_005510.3	4150482	6	2.179504224	0.007315
C3orf52	NM_024616.1	3940079	3	2.176484883	0.004051
LOC400027	XM_931434.2	6650164	12	2.176484883	0.004332
SNORD35B	NR_001285.1	3190561	19	2.176484883	0.005922
SNORA61	NR_002987.1	3990497	1	2.176484883	0.007092
RGS16	NM_002928.2	1030102	1	2.174976782	0.004472

TOMM34	NM_006809.4	1190445	20	2.174976782	0.004627
WDR27	NM_182552.3	4830121	6	2.174976782	0.010475
C1orf116	NM_023938.5	730491	1	2.168954818	0.005587
DCAF16	NM_017741.3	5890707	4	2.167451934	0.013399
FTHL11	NR_002204.1	460164	8	2.165950091	0.003145
VPS28	NM_016208.2	5700348	8	2.165950091	0.004844
KDM6B	NM_001080424.1	3520239	17	2.165950091	0.005612
TRIP6	NM_003302.2	3130612	7	2.164449289	0.003506
LOC136143	XM_069734.5	4760431	7	2.162949527	0.004292
LETMD1	NM_001024668.1	4150575	12	2.162949527	0.007878
LOC643695	XM_929293.1	2650279	1	2.162949527	0.041725
POLD4	NM_021173.2	1050240	11	2.161450804	0.010244
VPREB3	NM_013378.1	4640768	22	2.161450804	0.01964
CYP4F12	NM_023944.2	6560239	19	2.158456473	0.00592
GDPD1	NM_182569.1	4780403	17	2.158456473	0.014899
PLEC1	NM_000445.2	1050500	8	2.15546629	0.003438
FTHL3	NR_002201.1	6450139	2	2.15546629	0.005733
LOC729660	XR_039044.1	4540577		2.150988781	0.007246
RPL13	NM_033251.1	1940743	16	2.150988781	0.007888
TRAK1	NM_014965.2	3140092	3	2.148008943	0.003817
TUSC2	NM_007275.1	4810072	3	2.148008943	0.008036
TNFRSF25	NM_148973.1	3990224	1	2.146520573	0.00444
PIGF	NM_002643.3	1450072	2	2.143546925	0.004844
ELMO3	NM_024712.3	4920121	16	2.142061646	0.004423
BCL3	NM_005178.2	6330725	19	2.142061646	0.006085
SYDE1	NM_033025.4	2370348	19	2.142061646	0.008849
CXCR4	NM_001008540.1	2600152	2	2.142061646	0.019202
ANKRD24	NM_133475.1	3460626	19	2.140577397	0.004238
HDHD2	NM_032124.4	6370477	18	2.140577397	0.005612
ETF1	NM_004730.1	650315	5	2.139094176	0.005507
EID2B	NM_152361.1	4900626	19	2.139094176	0.020114
SNIP1	NM_024700.2	2690270	1	2.137611982	0.00762
WDR45	NM_007075.3	50592	X	2.136130816	0.006176
FTHL8	NR_002203.1	1980594	X	2.134650676	0.003398
PPP1R13L	NM_006663.2	1240176	19	2.134650676	0.003567
LOC653778	XM_929667.1	830639	8	2.133171562	0.005828
OTUD4	NM_199324.1	3990201	4	2.131693472	0.00592
OR7E156P	NR_002171.1	3940201	13	2.130216407	0.007021
LOC727768	XR_042487.1	2640010		2.130216407	0.008104
MYPOP	NM_001012643.2	3140202	19	2.128740365	0.005705
ARL5A	NM_001037174.1	2630209	2	2.127265346	0.005045
ZDHHC8	NM_013373.2	4590154	22	2.127265346	0.009142
SLC39A10	NM_020342.1	5960332	2	2.124318373	0.004216
LYRM5	NM_001001660.2	10435	12	2.121375483	0.003636

ARMCX6	NM_019007.3	1690475	X	2.121375483	0.004436
BREA2	NR_015445.1	4590274	8	2.121375483	0.026803
ZNF791	NM_153358.1	3830192	19	2.119905567	0.012535
LOC641922	XR_037560.1	6380594	7	2.119905567	0.049942
CBLC	NM_012116.2	6840519	19	2.118436669	0.003761
CELSR3	NM_001407.2	6350437	3	2.11696879	0.003689
LOC100134634	XM_001726406.1	5960240	7	2.115501927	0.010056
TSC22D4	NM_030935.3	6200240	7	2.115501927	0.013071
BRWD2	NM_018117.10	5560136	10	2.114036081	0.011098
SIN3B	NM_015260.1	4290440	19	2.112571251	0.004366
FCHO1	NM_015122.1	4120703	19	2.112571251	0.004607
LOC144678	XM_945548.1	6760075		2.112571251	0.027101
MAP2K3	NM_002756.3	7160711	17	2.109644634	0.004994
LOC401357	NM_001013685.1	3370762	7	2.109644634	0.015354
SNHG9	NR_003142.2	1300608	16	2.108182847	0.013188
DGUOK	NM_080916.1	5090730	2	2.105262309	0.004899
C4orf16	NM_018569.2	1450239	4	2.105262309	0.033184
GAA	NM_001079804.1	1190634	17	2.103803558	0.003767
HEXDC	NM_173620.2	3840370	17	2.102345818	0.00741
LOC729231	XR_038105.1	7210133		2.100889088	0.016956
LOC643438	XR_015310.1	3180619	7	2.097978655	0.00741
GPNMB	NM_001005340.1	6840164	7	2.097978655	0.016354
LAMA3	NM_198129.1	6480592	18	2.096524951	0.047896
METTL2A	NM_181725.2	1240646	17	2.09216988	0.008234
DGKA	NM_201554.1	6940088	12	2.0907202	0.012155
LOC644033	XM_927280.1	3450722	8	2.089271526	0.004664
LOC646675	XM_929621.1	940446	22	2.089271526	0.013323
	BG496815	1030767	7	2.089271526	0.021941
FLJ14712	XM_371878.5	2570010	7	2.086377187	0.006205
LOC92249	NR_015353.1	50364	X	2.086377187	0.013621
ESPNL	NM_194312.1	70465	2	2.086377187	0.014466
MACROD1	NM_014067.2	2370279	11	2.084931522	0.005375
MLXIPL	NM_032952.2	5870010	7	2.084931522	0.006804
PLA2G4C	NM_003706.1	1990672	19	2.084931522	0.008716
	BU153693	3120670	2	2.084931522	0.020624
AEN	NM_022767.3	5090438	15	2.083486858	0.004803
ADAT2	NM_182503.2	2760725	6	2.083486858	0.005145
VCX2	XM_946075.1	4810609		2.083486858	0.006284
SPRYD4	NM_207344.2	3870113	12	2.083486858	0.006406
RBPJ	NM_203284.1	2450554	4	2.083486858	0.007633
STX12	NM_177424.2	6380743	1	2.082043195	0.007509
CDK5RAP3	NM_176095.1	4230228	17	2.07915887	0.005493
C13orf1	NM_020456.1	4010554	13	2.07915887	0.011008
C1orf216	NM_152374.1	4670608	1	2.077718207	0.008741

FAM173A	NM_023933.1	1470561	16	2.077718207	0.022453
NDUFB5	NM_002492.2	830762	3	2.074839873	0.005134
GCNT3	NM_004751.1	4610520	15	2.074839873	0.007933
FTHL12	NR_002205.1	3190133	9	2.073402202	0.005612
RAB17	NM_022449.1	3460739	2	2.073402202	0.007278
ATF6B	NM_004381.4	4640110	6	2.073402202	0.009522
LOC100134530	XM_001714618.1	1030707	7	2.069095163	0.008733
STK35	NM_080836.2	4230327	20	2.067661472	0.013655
C7orf11	NM_138701.1	2900047	7	2.067661472	0.013866
ISCU	NM_014301.2	6620397	12	2.066228775	0.00397
TGFBR3	NM_003243.2	3190379	1	2.066228775	0.004959
SDSL	NM_138432.2	3390021	12	2.064797071	0.004945
NTN5	NM_145807.1	6980228	19	2.064797071	0.020628
EXOSC5	NM_020158.3	2810241	19	2.060507907	0.003862
ZNF692	NM_017865.2	20431	1	2.060507907	0.009504
	AK093356	6980592	4	2.060507907	0.014632
AKR1A1	NM_153326.1	6130424	1	2.059080167	0.004516
MAP3K12	NM_006301.2	4920300	12	2.056227653	0.004559
IGFBP6	NM_002178.2	7380719	12	2.056227653	0.004997
	BX090843	2940341	12	2.056227653	0.005922
PRAF2	NM_007213.1	5270093	X	2.056227653	0.018301
LOC155060	NM_001004302.1	7200360	7	2.056227653	0.03955
HSD17B8	NM_014234.3	5700056	6	2.054802879	0.011602
N4BP1	NM_153029.3	2680561	16	2.054802879	0.013091
PLA2G4D	NM_178034.3	2230754	15	2.054802879	0.013929
CRYAA	NM_000394.2	6510068	21	2.054802879	0.016233
RPAIN	NM_001033002.2	730543	17	2.053379091	0.009813
CLN8	NM_018941.3	290661	8	2.053379091	0.010907
VHL	NM_198156.1	2490176	3	2.053379091	0.011092

Table A3
500 most significantly upregulated transcripts in miR-215 microarray
Genes in descending order by fold change. Fold change given as miR-215/control. P-value adjusted for multiple testing using the Bonferroni correction.

Symbol	Accession No.	Illumina Probe ID	Chr.	Fold Change	adj.P.Val
H1F0	NM_005318.2	630278	22	0.09	0.000153
LOC643031	XM_926402.1	4880477	5	0.10	0.000279
LOC400455	XR_018793.1	7000228		0.10	0.000153
LANCL1	NM_006055.1	4150138	2	0.11	0.000153
PABPC4	NM_003819.2	5310278	1	0.12	0.000153
TMED10	NM_006827.5	4070037	14	0.13	0.000153
GNAI2	NM_002070.2	1300730	3	0.13	0.000174
KIF20A	NM_005733.1	1050195	5	0.13	0.000256

TOP2A	NM_001067.2	3990619	17	0.14	0.000256
LANCL1	NM_006055.1	2450612	2	0.14	0.000256
C3orf21	NM_152531.3	3180408	3	0.15	0.000256
FLJ12684	NM_024534.4	3370377	4	0.15	0.000256
FOXM1	NM_021953.2	540053	12	0.15	0.000568
PPIL1	NM_016059.3	4200612	6	0.16	0.000256
NCAPD2	NM_014865.2	2680497	12	0.18	0.000256
ST6GAL1	NM_003032.2	1710630	3	0.18	0.000256
TXNDC12	NM_015913.2	7160274	1	0.19	0.000256
CHCHD10	NM_213720.1	940010	22	0.19	0.000256
LOC391019	XR_019605.1	2190630		0.19	0.000256
SSR2	NM_003145.3	4280041	1	0.19	0.000256
CTSB	NM_147780.2	240309	8	0.19	0.000256
FAM57A	NM_024792.1	5910600	17	0.19	0.000256
LOC652489	XM_941950.2	6650228		0.20	0.000256
TROVE2	NM_001042369.1	360259	1	0.20	0.000263
HDGF	NM_004494.1	6110474	1	0.20	0.000263
COMMD1	NM_152516.2	3360093	2	0.20	0.000457
CCNB2	NM_004701.2	5360070	15	0.20	0.000256
ID3	NM_002167.2	7570324	1	0.21	0.000256
KIFC1	NM_002263.2	7330674	6	0.21	0.000411
SCARNA8	NR_003009.1	2600403	9	0.21	0.00067
CEP55	NM_018131.3	7510709	10	0.22	0.000256
LOC647285	XR_019567.2	6040110		0.22	0.000256
SUMO2	NM_001005849.1	2600066	17	0.22	0.000256
LOC728820	XR_038223.1	4560669		0.22	0.000311
DCBLD2	NM_080927.3	60132	3	0.22	0.000256
PCGF2	NM_007144.2	3830296	17	0.22	0.000263
TESC	NM_017899.2	5050681	12	0.23	0.000425
DEPDC1	NM_017779.3	6200201	1	0.23	0.000425
CNPY3	NM_006586.3	10187	6	0.23	0.000256
SUMF1	NM_182760.2	5490626	3	0.23	0.000318
SLC25A23	NM_024103.2	6280092	19	0.23	0.000394
SH3KBP1	NM_031892.1	6020152	X	0.23	0.000264
DLGAP5	NM_014750.3	240221	14	0.23	0.000279
CPS1	NM_001875.2	6110044	2	0.23	0.000364
GAD1	NM_013445.3	1440477	2	0.23	0.000279
LOC728820	XR_038223.1	2320672		0.23	0.000318
KIF2C	NM_006845.2	1470647	1	0.23	0.000311
SUMO2	NM_001005849.1	520133	17	0.23	0.000311
CDC25C	NM_001790.3	4200451	5	0.23	0.001387

HJURP	NM_018410.3	3180367	2	0.24	0.000297
CORO1C	NM_014325.2	670025	12	0.24	0.000263
ASPM	NM_018136.3	6130441	1	0.24	0.000722
HABP4	NM_014282.1	6510689	9	0.24	0.000778
FOXM1	NM_202003.1	2650364	12	0.24	0.00094
NUSAP1	NM_018454.5	1500553	15	0.24	0.000364
FAM3C	NM_001040020.1	780332	7	0.24	0.000279
SNORD3D	NR_006882.1	380685	17	0.24	0.002228
CYBRD1	NM_024843.2	2370300	2	0.24	0.00065
LEMD1	NM_001001552.3	3180615	1	0.24	0.00043
KIF3B	NM_004798.2	450398	20	0.24	0.000358
UAP1	NM_003115.3	3460187	1	0.24	0.00061
CKAP2L	NM_152515.2	6380324	2	0.24	0.000752
ECH1	NM_001398.2	5360553	19	0.24	0.000318
RNFT2	NM_032814.3	730292	12	0.25	0.000312
NASP	NM_002482.2	4260682	1	0.25	0.000279
CCNA2	NM_001237.2	2650608	4	0.25	0.000411
KIF3B	NM_004798.2	2450037	20	0.25	0.000516
EXT2	NM_207122.1	6760070	11	0.25	0.001366
SRXN1	NM_080725.1	3780717	20	0.25	0.000568
FAM64A	NM_019013.1	5870193	17	0.25	0.000597
FAM3C	NM_001040020.1	1260767	7	0.25	0.000577
VCAN	NM_004385.2	5910113	5	0.25	0.00068
SCARNA11	NR_003012.1	5310066	12	0.25	0.000398
RNY1	NR_004391.1	1010450	7	0.25	0.000762
	AK026966	1940563	1	0.25	0.000411
EVL	NM_016337.2	6550754	14	0.25	0.00059
CENPA	NM_001042426.1	4760577	2	0.25	0.001152
SERPINH1	NM_001235.2	7650017	11	0.26	0.000411
GTSE1	NM_016426.4	6980382	22	0.26	0.000318
CDC25C	NM_022809.2	3460152	5	0.26	0.001121
CCNE2	NM_057735.1	4760154	8	0.26	0.000778
DSC2	NM_004949.2	2710400	18	0.26	0.000686
	D87470	2630601	11	0.26	0.000423
LOC100127918	XR_038502.1	4610754		0.26	0.000568
LOC390466	XM_372521.1	3710471	14	0.26	0.000704
NES	NM_006617.1	670278	1	0.26	0.000932
MYO1C	NM_033375.4	3710605	17	0.26	0.000318
ITFG3	NM_032039.1	6250553	16	0.26	0.000752
VPS24	NM_001005753.1	6200332	2	0.27	0.000411
TROAP	NM_005480.2	4760646	12	0.27	0.000457

AURKB	NM_004217.2	6770026	17	0.27	0.001695
VTI1B	NM_006370.1	3890136	14	0.27	0.002322
CPD	NM_001304.3	6020543	17	0.27	0.000568
	BC035116	4780187	3	0.27	0.000568
PANX2	NM_052839.2	4070300	22	0.27	0.000402
STS-1	NM_032873.3	1940524	11	0.27	0.000326
TMEM97	NM_014573.2	3420541	17	0.27	0.000319
CENPA	NM_001042426.1	2600392	2	0.27	0.000394
TPP1	NM_000391.3	670113	11	0.27	0.000536

Table A4
100 most significantly downregulated transcripts in miR-3189 p53 WT microarray
Genes in descending order by fold change. Fold change given as miR-3189/control. P-value adjusted for multiple testing using the Bonferroni correction.

Symbol	Accession No.	Ilumina Probe ID	Chr.	Fold Change	adj.P.Val
KRT80	NM_182507.2	4830520	12	13.43	0.000123
LOC645638	XR_040455.1	70121		11.20	0.000153
MIR1974	NR_031738.1	2260349		9.19	0.000153
KRT7	NM_005556.3	3800161	12	7.01	0.000153
C9orf169	NM_199001.1	6450162		6.96	0.000256
ATF3	NM_001040619.1	4780128	1	6.63	0.000256
SLC39A3	NM_213568.1	5670136	19	6.58	0.000153
LOC147727	NR_024333.1	5340653	19	5.88	0.000256
KRT81	NM_002281.2	430446	12	5.71	0.000279
MRPS35	NM_021821.2	7380270	12	5.52	0.000256
SFMBT1	NM_016329.2	1780152	3	5.03	0.000458
MSI2	NM_170721.1	7040369	17	4.84	0.000704
LOC100134018	XM_001715564.1	7560292		4.80	0.000394
GALNT5	NM_014568.1	4010138	2	4.77	0.000686
LOC389834	NM_001013655.1	1740239	4	4.68	0.000423
GDF15	NM_004864.1	5090671	19	4.63	0.000279
NUAK2	NM_030952.1	840356	1	4.61	0.000704
PMAIP1	NM_021127.1	2750367	18	4.60	0.000583
TP53I3	NM_147184.1	1260020	2	4.58	0.000256
OASL	NM_198213.1	7650097	12	4.57	0.000256
RPS23	NM_001025.4	380070	5	4.55	0.000279
SFMBT1	NM_001005158.1	2650433	3	4.51	0.000279
	XM_498568	4220184		4.42	0.000256

HMOX1	NM_002133.1	6660601	22	4.40	0.000423
RPL36A	NM_021029.4	6860671	X	4.29	0.000425
MRPS12	NM_021107.1	6980487	19	4.20	0.000695
TMEM33	NM_018126.1	6650382	4	4.08	0.002453
CYR61	NM_001554.3	3930605	1	4.06	0.000318
PIBF1	NM_006346.2	780184	13	4.05	0.001379
KRT18P28	XR_017689.1	2260068	1	4.03	0.000568
LOC642934	XM_942991.2	7040482		4.00	0.000318
LOC158160	NM_001031744.1	2030672	10	4.00	0.000425
C3orf52	NM_024616.1	3940079	3	4.00	0.000571
SERPINB1	NM_030666.2	3190112	6	3.95	0.000568
NHP2L1	NM_001003796.1	4230243	22	3.88	0.000307
RRAS2	NM_012250.3	620546	11	3.86	0.000568
LMAN2L	NM_030805.2	1190673	2	3.79	0.0004
CXorf40A	NM_178124.3	2480048	X	3.77	0.000318
LRRC26	NM_001013653.2	7150270	9	3.76	0.000425
C20orf24	NM_018840.2	7040176	20	3.71	0.000394
NARS2	NM_024678.3	5860592	11	3.70	0.000411
SLC25A3	NM_213611.1	4250204	12	3.69	0.000468
RAGE	NM_014226.1	1470348	14	3.68	0.000425
ATAD1	NM_032810.2	5340551	10	3.65	0.000411
CTGF	NM_001901.1	5690687	6	3.61	0.000597
LOC653108	XR_016129.1	1400543	21	3.61	0.000707
FLJ10996	NM_019044.2	2850392	2	3.61	0.000778
	AI458759	6450386	3	3.61	0.003252
RSPH1	NM_080860.2	6020451	21	3.58	0.000411
ZFAND2A	NM_182491.1	870379	7	3.54	0.000686
IL8	NM_000584.2	1980309	4	3.53	0.000853
UCRC	NM_013387.3	7550768	22	3.50	0.000568
FAM84B	NM_174911.3	60014	8	3.50	0.000778
	AK054902	6400390	1	3.48	0.001291
TMEM125	NM_144626.1	3780082	1	3.46	0.000808
SNRPD1	NM_006938.2	1510039	18	3.45	0.000526
SLC35A3	NM_012243.1	6660767	1	3.44	0.004091
TPMT	NM_000367.2	840014	6	3.44	0.001008
GAN	NM_022041.3	460600	16	3.43	0.000516
LOC729887	XR_040891.1	2470128	16	3.42	0.0009
NOSTRIN	NM_052946.2	7210113	2	3.42	0.000636
HINT3	NM_138571.4	2140279	6	3.39	0.001121
CXorf40B	NM_001013845.1	7150608	X	3.38	0.000944
FASTKD3	NM_024091.2	580053	5	3.36	0.000707

TPD52L2	NM_199361.1	5080577	20	3.32	0.000973
UPP1	NM_003364.2	7570673	7	3.29	0.000944
NDUFB5	NM_002492.2	830762	3	3.27	0.001062
PGF	NM_002632.4	1940438	14	3.26	0.000988
ATAD1	NM_032810.2	5260221	10	3.26	0.001859
LOC389816	NM_001013653.1	2140541	9	3.26	0.000636
NACC2	NM_144653.3	630706	9	3.25	0.000655
AMMECR1	NM_015365.2	2340601	X	3.23	0.000788
	AL137257	4180612	1	3.20	0.000704
TTYH1	NM_020659.2	50719	19	3.18	0.000688
LACTB2	NM_016027.1	4050711	8	3.18	0.001592
RRAS2	NM_012250.3	6350239	11	3.17	0.000921
ANKRA2	NM_023039.2	7400114	5	3.16	0.001605
UBL5	NM_024292.2	1440551	19	3.16	0.000725
C6orf35	NM_018452.3	3140121		3.16	0.003511
TIMM22	NM_013337.2	3390373	17	3.15	0.000797
TPD52L2	NM_003288.2	6270241	20	3.15	0.000557
BAIAP2	NM_017450.1	6590050	17	3.14	0.001647
FLJ40504	NM_173624.1	4880333	17	3.13	0.000725
LOC729086	XM_001129280.2	4480170	1	3.13	0.000725
NR2C2AP	NM_176880.4	3060563	19	3.12	0.001366
MLYCD	NM_012213.2	7330377	16	3.12	0.001387
LOC645166	XM_001129441.2	1090500	1	3.08	0.000778
NFKBIE	NM_004556.2	540139	6	3.05	0.002356
C1orf89	NM_030907.2	5670471	1	3.04	0.001058
LOC399965	XR_036921.1	3520333		3.03	0.000778
C19orf51	NM_178837.3	3520612	19	3.03	0.000762
RRM2B	NM_015713.3	7150224	8	3.03	0.001316
NEK6	NM_014397.3	5860463	9	3.01	0.001338
DUSP5	NM_004419.3	5390161	10	3.01	0.0008
CHMP6	XM_001132548.1	4480592		3.00	0.000762
ZNF816A	NM_001031665.1	780471	19	2.99	0.0008
IQCG	NM_032263.2	70551	3	2.99	0.000857
C1orf102	NM_145047.3	6550554	1	2.99	0.000654
ABLIM1	NM_006720.3	3610315	10	2.99	0.000943
DNAL1	NM_031427.1	2810500	14	2.98	0.000701

Table A5
100 most significantly upregulated transcripts in miR-3189 p53 WT microarray
Genes in descending order by fold change. Fold change given as miR-3189/control. P-value adjusted for multiple testing using the Bonferroni correction.

Symbol	Accession No.	ProbeID	Chr	FC 3189/ctl	adj.P.Val
TMED10	NM_006827.5	4070037	14	0.14	0.00103
PABPC4	NM_003819.2	5310278	1	0.14	0.00103
LOC400455	XR_018793.1	7000228		0.16	0.00108
GNAI2	NM_002070.2	1300730	3	0.18	0.00168
LANCL1	NM_006055.1	4150138	2	0.19	0.00119
LANCL1	NM_006055.1	2450612	2	0.19	0.00103
PPIL1	NM_016059.3	4200612	6	0.20	0.00119
CHCHD10	NM_213720.1	940010	22	0.20	0.00119
CYBRD1	NM_024843.2	2370300	2	0.23	0.00154
FAM57A	NM_024792.1	5910600	17	0.23	0.00166
CCNE2	NM_057735.1	4760154	8	0.23	0.00166
FLJ12684	NM_024534.4	3370377	4	0.23	0.00154
SUMF1	NM_182760.2	5490626	3	0.23	0.00341
SERPINH1	NM_001235.2	7650017	11	0.23	0.00278
CYBRD1	NM_024843.2	2450465	2	0.24	0.00135
CTSB	NM_147780.2	240309	8	0.24	0.00135
SUMO2	NM_001005849.1	520133	17	0.25	0.00166
C3orf21	NM_152531.3	3180408	3	0.25	0.00168
ANXA2	NM_001002857.1	770730	15	0.25	0.00135
H1F0	NM_005318.2	630278	22	0.25	0.00154
COMMD1	NM_152516.2	3360093	2	0.26	0.00166
ST6GAL1	NM_003032.2	1710630	3	0.26	0.00234
TCFL5	NM_006602.2	1510154	20	0.27	0.00166
RNY1	NR_004391.1	1010450	7	0.27	0.00294
CD44	NM_001001392.1	4560193	11	0.27	0.00312
HABP4	NM_014282.1	6510689	9	0.27	0.00278
MYO1C	NM_033375.4	3710605	17	0.27	0.00339
HDGF	NM_004494.1	6110474	1	0.27	0.00166
ITFG3	NM_032039.1	6250553	16	0.27	0.00321
MTPN	NM_145808.2	5890630	7	0.28	0.00229
TFDP1	NM_007111.3	3290435	13	0.28	0.00215
MTPN	NM_145808.1	4210128	7	0.28	0.00229
SLC6A10P	NR_003083.2	7610615	16	0.28	0.00401
TROVE2	NM_001042369.1	360259	1	0.28	0.00167
LOC391019	XR_019605.1	2190630		0.28	0.00636

ANXA2	NM_001002857.1	3520328	15	0.28	0.00165
SRD5A1	NM_001047.2	1050278	5	0.29	0.00278
SSR2	NM_003145.3	4280041	1	0.29	0.00215
VCAN	NM_004385.2	5910113	5	0.29	0.00215
HIST1H2BK	NM_080593.1	6110630	6	0.29	0.00199
TM4SF18	NM_138786.1	4830156	3	0.29	0.00339
TMEM97	NM_014573.2	3420541	17	0.29	0.00188
PCGF2	NM_007144.2	3830296	17	0.30	0.0023
LOC652489	XM_941950.2	6650228		0.30	0.00188
SCARNA8	NR_003009.1	2600403	9	0.30	0.00462
ECH1	NM_001398.2	5360553	19	0.30	0.00292
DCBLD2	NM_080927.3	60132	3	0.30	0.00374
TM4SF18	NM_138786.2	7400291	3	0.31	0.00278
HIST1H2BK	NM_080593.1	5050402	6	0.31	0.00234
SF3B2	NM_006842.2	3930070	11	0.31	0.00215
TOR1AIP1	NM_015602.2	6290524	1	0.31	0.0026
UBE2J1	NM_016021.2	5080020	6	0.31	0.00278
CDK6	NM_001259.5	670286	7	0.31	0.00401
PANX2	NM_052839.2	4070300	22	0.31	0.00339
FOXM1	NM_021953.2	540053	12	0.32	0.00316
TPP1	NM_000391.3	670113	11	0.32	0.00403
FAM3C	NM_001040020.1	780332	7	0.32	0.00366
	D87470	2630601	11	0.32	0.00234
EEF1A1	NM_001402.5	3360504	6	0.32	0.00278
CNPY3	NM_006586.3	10187	6	0.32	0.00278
NME4	NM_005009.2	2320079	16	0.32	0.00294
LOC728820	XR_038223.1	2320672		0.32	0.00346
ATP2A2	NM_001681.2	1940053	12	0.32	0.0026
ARL2	NM_001667.2	3290739	11	0.33	0.00276
LOC100129585	XM_001721365.1	6550093	X	0.33	0.00523
DCBLD2	NM_080927.3	830661	3	0.33	0.00227
LOC647000	XM_929980.2	3310288	13	0.33	0.00278
MTCP1	NM_014221.3	990615	X	0.33	0.00366
SUMO2	NM_001005849.1	2600066	17	0.33	0.00394
EXT2	NM_000401.2	6620682	11	0.33	0.00278
FAM3C	NM_001040020.1	1260767	7	0.33	0.00577
ZCRB1	NM_033114.3	1990639	12	0.33	0.00234
SRXN1	NM_080725.1	3780717	20	0.33	0.00339
KLK7	NM_005046.2	6020139	19	0.33	0.0043
STS-1	NM_032873.3	1940524	11	0.34	0.00339
RBMX	NM_002139.2	6180537	X	0.34	0.00286

LOC728820	XR_038223.1	4560669		0.34	0.00668
TFDP1	NM_007111.3	510487	13	0.34	0.00316
LOC390466	XM_372521.1	3710471	14	0.34	0.00425
UGDH	NM_003359.2	4780050	4	0.35	0.00646
TOR1AIP1	NM_015602.2	20403	1	0.35	0.00374
RNY4	NR_004393.1	1070079	7	0.35	0.00698
LOC100127918	XR_038502.1	4610754		0.35	0.00646
VTI1B	NM_006370.1	3890136	14	0.35	0.00774
TXNDC12	NM_015913.2	7160274	1	0.35	0.00646
SNTB1	NM_021021.2	3420739	8	0.35	0.00646
LOC100129585	XM_001720509.1	6100626		0.35	0.00316
LOC647285	XR_019567.2	6040110		0.35	0.00339
LOC100131735	XR_038716.1	3830246		0.35	0.00286
KIF3B	NM_004798.2	2450037	20	0.35	0.00338
EFTUD2	NM_004247.2	6980475	17	0.35	0.00408
NAV1	NM_020443.2	940685	1	0.36	0.01327
LOC100127922	XR_038410.1	5130403	5	0.36	0.03068
LOC643272	XM_926633.1	4040113	3	0.36	0.0119
ARPC1A	NM_006409.2	7610692	7	0.36	0.00366
	BC035116	4780187	3	0.36	0.00321
CPS1	NM_001875.2	6110044	2	0.36	0.00278
WBP11	NM_016312.2	5960278	12	0.36	0.00341
RNFT2	NM_032814.3	730292	12	0.36	0.00346
NXN	NM_022463.3	2140431	17	0.37	0.00383

Table A6
100 most significantly downregulated transcripts in miR-3189 p53 WT microarray
Genes in descending order by fold change. Fold change given as miR-3189/control. P-value adjusted for multiple testing using the Bonferroni correction.

Symbol	Accesion No.	Illumina ProbeID	Chr.	FC	adj.P.Val
MRPS35	NM_021821.2	7380270	12	4.39	0.00154
MSI2	NM_170721.1	7040369	17	4.30	0.00165
C3orf52	NM_024616.1	3940079	3	4.30	0.00134
RAGE	NM_014226.1	1470348	14	3.93	0.00166
KRT80	NM_182507.2	4830520	12	3.81	0.00294
SFMBT1	NM_001005158.1	2650433	3	3.74	0.00316
ATF3	NM_001040619.1	4780128	1	3.51	0.00234
TSC22D3	NM_004089.3	6350446	X	3.51	0.00227
TTC25	NM_031421.2	7550021	17	3.48	0.00278
SFMBT1	NM_016329.2	1780152	3	3.45	0.00227

DDIT3	NM_004083.4	830619	12	3.39	0.00339
ARHGAP19	NM_032900.4	6110332	10	3.34	0.00215
TPD52L2	NM_003288.2	6270241	20	3.22	0.00234
ANGPT2	NM_001147.1	3450066	8	3.20	0.00234
LMAN2L	NM_030805.2	1190673	2	3.20	0.00401
PPP1R15A	NM_014330.2	1340600	19	3.10	0.00278
GDF15	NM_004864.1	5090671	19	3.09	0.00341
MRPS12	NM_021107.1	6980487	19	3.03	0.00234
LOC389834	NM_001013655.1	1740239	4|NT_113889.1	3.03	0.00728
GADD45A	NM_001924.2	670255	1	3.02	0.00401
TSC22D3	NM_198057.2	6350632	X	3.00	0.00339
TPD52L2	NM_199361.1	5080577	20	2.99	0.00278
PDLIM7	NM_213636.1	4560164	5	2.94	0.00278
C9orf169	NM_199001.1	6450162		2.90	0.00921
RRAS2	NM_012250.3	620546	11	2.86	0.00374
LOC100134018	XM_001715564.1	7560292		2.86	0.00479
FLJ10996	NM_019044.2	2850392	2	2.82	0.00656
TCN1	NM_001062.3	1770603	11	2.80	0.03204
FAM46B	NM_052943.2	4180324	1	2.78	0.00339
EGR2	NM_000399.2	6020255	10	2.76	0.00881
LOC442427	XR_038544.1	4540553		2.76	0.01236
NFKBIE	NM_004556.2	540139	6	2.68	0.00366
NACC2	NM_144653.3	630706	9	2.66	0.00388
KIAA1370	NM_019600.1	4180142	15	2.65	0.0109
SERPINB1	NM_030666.2	3190112	6	2.65	0.00522
OVGP1	NM_002557.3	1820196	1	2.64	0.00995
HMOX1	NM_002133.1	6660601	22	2.64	0.00316
TRIM23	NM_001656.3	1440543	5	2.63	0.00316
AMMECR1	NM_015365.2	2340601	X	2.63	0.00401
YWHAB	NM_139323.2	1340521	20	2.62	0.00312
WDR79	NM_018081.1	2260630	17	2.61	0.00346
RPS23	NM_001025.4	380070	5	2.61	0.00339
RPL36A	NM_021029.4	6860671	X	2.61	0.00365
ANKRD37	NM_181726.2	240682	4	2.61	0.00881
DNAL1	NM_031427.1	2810500	14	2.59	0.00339
SYTL2	NM_206929.1	6760037	11	2.58	0.00346
UGCG	NM_003358.1	3800647	9	2.58	0.00885
DUSP5	NM_004419.3	5390161	10	2.58	0.00369
ATAD1	NM_032810.2	5260221	10	2.57	0.00462
CD97	NM_001784.3	1470626	19	2.56	0.00479

LMCD1	NM_014583.2	3830093	3	2.55	0.00738
LRP5L	NM_182492.1	540403	22	2.55	0.00377
UBE2H	NM_003344.2	6020736	7	2.55	0.00479
NDUFB5	NM_002492.2	830762	3	2.54	0.00462
BLOC1S2	NM_001001342.1	2630743	10	2.52	0.00755
C10orf10	NM_007021.2	2900747	10	2.52	0.00462
MBIP	NM_016586.1	6480041	14	2.52	0.00846
RALGPS2	NM_152663.2	6250630	1	2.50	0.007
C20orf24	NM_018840.2	7040176	20	2.50	0.00523
LRRC48	NM_031294.2	1230162	17	2.49	0.01387
TMEM93	NM_001014764.1	3140768	17	2.49	0.00422
DNAJC5	NM_025219.1	4040703	20	2.48	0.00462
SYNJ1	NM_203446.1	650020	21	2.48	0.00773
SLC39A3	NM_213568.1	5670136	19	2.47	0.00656
RRAS2	NM_012250.3	6350239	11	2.47	0.00507
MBIP	NM_016586.1	5360411	14	2.46	0.00479
CD97	NM_078481.2	6960630	19	2.45	0.00462
TRAK1	NM_014965.2	3140092	3	2.44	0.00458
AVPI1	NM_021732.1	990500	10	2.43	0.00679
CSTF1	NM_001033521.1	520754	20	2.43	0.0119
LOC147727	NR_024333.1	5340653	19	2.42	0.0109
ATAD1	NM_032810.2	5340551	10	2.41	0.00773
SLC7A6OS	NM_032178.1	2320601	16	2.41	0.012
SYTL2	NM_206928.1	5810278	11	2.41	0.00846
PRMT10	NM_138364.2	2450553	4	2.41	0.01862
LOC100129907	XM_001720756.1	5080630		2.38	0.01327
CSE1L	NM_177436.1	4920139	20	2.37	0.00604
MUC4	NM_018406.3	110471	3	2.37	0.00827
RHBDD2	NM_001040456.1	6650746	7	2.37	0.01011
TBC1D19	NM_018317.1	20475	4	2.36	0.00643
PHC3	NM_024947.2	240524	3	2.36	0.00845
TMEM79	NM_032323.1	520195	1	2.36	0.00897
C20orf24	NM_199483.1	4760537	20	2.35	0.00646
FASTKD3	NM_024091.2	580053	5	2.34	0.01564
ARID4A	NM_023001.2	7160440	14	2.34	0.00827
CRB3	NM_139161.2	7400524	19	2.33	0.00666
OKL38	NM_013370.2	4010086	16	2.33	0.0103
ELMOD2	NM_153702.1	2480373	4	2.33	0.0105
NDUFA10	NM_004544.2	510725	2	2.33	0.00646

MNAT1	NM_002431.2	2060564	14	2.33	0.00937
MT1F	NM_005949.2	4220672	16	2.32	0.00739
SLC25A25	NM_052901.2	10487	9	2.32	0.00698
	XM_498568	4220184		2.32	0.00603
SLC4A7	NM_003615.3	940035	3	2.32	0.00666
SNRPD1	NM_006938.2	1510039	18	2.32	0.01391
CPEB3	NM_014912.3	3610386	10	2.32	0.0065
TRIM15	NM_033229.1	5860470	6	2.31	0.01178
ARL5B	NM_178815.3	2340564	10	2.31	0.00646
C7orf53	NM_182597.1	5390497	7	2.31	0.00604
TRAFD1	NM_006700.1	1570129	12	2.29	0.01679

Table A7
100 most significantly upregulated transcripts in miR-3189 p53 KO microarray
Genes in descending order by fold change. Fold change given as miR-3189/control. P-value adjusted for multiple testing using the Bonferroni correction.